HOKKAIDO UNIVERSITY

Title	A Study on Catalytic Conversion of Non-Food Biomass into Chemicals
Author(s)	藪下, 瑞帆
Degree Grantor	北海道大学
Degree Name	博士(理学)
Dissertation Number	甲第11922号
Issue Date	2015-03-25
DOI	https://doi.org/10.14943/doctoral.k11922
Doc URL	https://hdl.handle.net/2115/63042
Type	doctoral thesis
File Information	Mizuho_Yabushita.pdf

Hokkaido University Collection of Scholarly and Academic Papers : HUSCAP

A Study on Catalytic Conversion of Non-Food Biomass into Chemicals

Mizuho Yabushita

Hokkaido University

2015

A Study on Catalytic Conversion of Non-Food Biomass into Chemicals

非可食バイオマスの触媒的変換に関する研究

Mizuho Yabushita

藪 下　瑞 帆

Hokkaido University

北海道大学

2015

Table of Contents

List of Abbreviations 1

Chapter 1. General Introduction 5

1.1. General background: Why non-food biomass? 6

1.2. Cellulose 6

1.2.1. Plant-derived biomass: Lignocellulose 6

1.2.2. Crystal structure of cellulose 8

1.2.3. Glucose and its derivatives 13

1.2.4. Hydrolysis of cellulose in homogeneous systems 18

1.2.5. Hydrolysis of cellulose by heterogeneous catalysts 22

1.2.6. Hydrolytic hydrogenation of cellulose to sorbitol 28

1.3. Chitin 32

1.3.1. Property of chitin 32

1.3.2. Transformation of chitin 34

1.4. Objectives of this work 37

1.5. Constitution of the thesis 38

References 39

Chapter 2. Hydrolysis of Cellulose to Glucose Using Carbon Catalysts 51

2.1. Introduction 52

2.2. Experimental 53

2.2.1. Reagents 53

2.2.2. Synthesis of mesoporous carbon CMK-3 55

2.2.3. Analysis of oxygenated functional groups on carbons 56

2.2.4. Analysis of components in bagasse kraft pulp 56

2.2.5. Ball-milling and mix-milling pre-treatment of cellulose 57

2.2.6. Catalytic reactions 58

2.2.7. Reuse experiments of mix-milled cellulose 60

2.3. Results and discussion 61

2.3.1. Screening of carbon catalysts for hydrolysis of cellulose 61

2.3.2. High-yielding production of glucose from cellulose 66

2.3.3. Effect of mix-milling pre-treatment 76

2.4. Conclusions 84

References 85

Chapter 3. Mechanistic Study of Cellulose Hydrolysis by Carbon Catalysts 89

3.1. Introduction 90

3.2. Experimental 91

3.2.1. Reagents 91

3.2.2. Heat-treatment of alkali-activated carbon K26 92

3.2.3. Characterization of carbon materials 93

3.2.4. Ball-milling pre-treatment and hydrolysis of cellulose 94

3.2.5. Hydrolysis of cellobiose by aromatic compounds 95

3.2.6. Adsorption of cellulosic molecules 95

3.2.7. Computational modeling of adsorption state 96

3.3. Results and discussion 97

3.3.1. Contributions of oxygenated functional groups on carbons for hydrolysis of cellulose 97

3.3.2. Hydrolysis of cellobiose by aromatic compounds as model reactions 101

3.3.3. Adsorption of cellulosic molecules onto alkali-activated carbon K26 107

3.3.4. Proposed mechanism of cellulose hydrolysis by carbon catalysts 121

3.3.5. Hydrolysis of cellulose by zeolite-templated carbon ZTC 122

3.4. Conclusions 124

References and note 124

4. Two-Step Depolymerization of Chitin to Monomers 129

4.1. Introduction 130

4.2. Experimental 131

4.2.1. Reagents 131

4.2.2. Mechanocatalytic hydrolysis of chitin 133

4.2.3. Methanolysis of chitin 134

4.2.4. Synthesis of MeGlcNAc 136

4.2.5. Hydrolysis of MeGlcNAc 136

4.3. Results and discussion 137

4.3.1. Mechanocatalytic depolymerization of chitin 137

4.3.2. Methanolysis of chitin oligomers 139

4.4. Conclusions 143

Appendices: LC/MS spectra, IR spectrum, and NMR spectra 144

References 149

Chapter 5. Dehydration of Sorbitol to 1,4-Sorbitan Catalyzed by Acid Catalysts 151

5.1. Introduction 152

5.2. Experimental 153

5.2.1. Reagents 153

5.2.2. Preparation of sulfated zirconia 154

5.2.3. Dehydration of sorbitol 154

5.2.4. Product identification 155

5.3. Results and discussion 157

5.3.1. Dehydration of sorbitol by acids 157

5.3.2. Kinetic study of sorbitol dehydration by H_2SO_4 160

5.3.3. Reaction mechanism for dehydration of sorbitol by H_2SO_4 164

5.4. Conclusions 167

Appendices: raw data for HPLC, LC/MS, and NMR 168

References 178

6. General Conclusions 181

List of Publications 187

Acknowledgements 193

List of Abbreviations

3A5AF	3-Acetamido-5-acetylfuran
3-HPA	3-Hydroxypropionic acid
5-HMF	5-Hydroxymethylfurfural
AC	Activated carbon
ACC	Aqueous counter collision
ADP	Adenosine diphosphate
AH1	Uncharacterized mono-anhydrohexitol 1
AH2	Uncharacterized mono-anhydrohexitol 2
APCI	Atmospheric pressure chemical ionization
ATP	Adenosine triphosphate
B3LYP	Becke 3-parameter Lee-Yang-Parr
BET	Brunauer-Emmett-Teller
[BMIM]Cl	1-Butyl-3-methylimidazolium chloride
CBH	Cellobiohydrolase
CNF	Carbon nanofiber
CNT	Carbon nanotube
COSY	Correlation spectroscopy
CP/MAS	Cross polarization/magic angle spinning
CP-SO_3H	Sulfonic chloromethyl polystyrene resin
CrI	Crystallinity index
CVD	Chemical vapor deposition
DEPT	Distortionless enhancement by polarization transfer
DFT	Density functional theory
DMAc	*N*,*N*-Dimethylacetamide
DMF	2,5-Dimethylfuran

DMSO	Dimethyl sulfoxide
DOE	Department of Energy
DP	Degree of polymerization
DRIFT	Diffuse reflectance infrared Fourier transform
DTGS	Deuterated triglycine sulfate
EDX	Energy dispersive X-ray spectroscopy
EG	Endoglucanase
FDCA	2,5-Furandicarboxylic acid
GC	Gas chromatography
GlcN	Glucosamine
GlcNAc	*N*-Acetylglucosamine
GO	Graphene oxide
HAADP	1-*O*-(2-Hydroxyethyl)-2-acetamido-2-deoxyglucopyranoside
HADP	1-*O*-(2-Hydroxyethyl)-2-amino-2-deoxyglucopyranoside
HMBC	Heteronuclear multiple bond correlation
HMQC	Heteronuclear multiple quantum coherence
HPA	Heteropoly acid
HPLC	High-performance liquid chromatography
ICP-AES	Inductivity coupled plasma atomic emission spectroscopy
IL	Ionic liquid
IR	Infrared
LC/MS	Liquid chromatography/mass spectroscopy
MC	Mesoporous carbon
MCT	Mercury-cadmium-telluride
MeGlc	1-*O*-Methylglucose
MeGlcNAc	1-*O*-Methyl-*N*-acetylglucosamine
m.p.	Melting point

NAD^+	Nicotinamide adenine dinucleotide
NADH	Reduced form of nicotinamide adenine dinucleotide
NLDFT	Nonlocal density functional theory
NMR	Nuclear magnetic resonance
OFG	Oxygenated functional group
PEIT	Polyethylene isosorbide terephthalate
PET	Polyethylene terephthalate
PTFE	Polytetrafluoroethylene
PVDF	Polyvinylidene difluoride
RI	Refractive index
S/C	Substrate/catalyst
SCRF	Self-consistent reaction field
SEM	Scanning electron microscope
SZ	Sulfated zirconia
TEM	Transmission electron microscope
TEOS	Tetraethyl orthosilicate
TOC	Total organic carbon
TOF	Turnover frequency
TON	Turnover number
TOSS	Total suppression of sidebands
UV	Ultraviolet
XAFS	X-ray absorption fine structure
XRD	X-ray diffraction
YAG	Yttrium-aluminium-garnet
ZTC	Zeolite-templated carbon

Chapter 1

General Introduction

Conversion of biomass to renewable and valuable chemicals has attracted global interest in order to build up sustainable society. Cellulose and chitin are the first and second most abundant biomass on earth and utilization of cellulose and chitin does not compete with food production. However, their low reactivity due to their rigid structures has hampered selective depolymerization to chemicals. Design of catalysts coupled with reaction engineering for transformation of cellulose and chitin has been expected to overcome this issue. Indeed, a number of reaction systems employing homo- and heterogeneous catalysts and enzymes have been reported to produce platform compounds such as glucose and *N*-acetylglucosamine, which can be further transformed into various kinds of valuable chemicals. In this chapter, the present situations in biorefinery, namely utilization of cellulose and chitin, are summarized and discussed.

1.1. General background: Why non-food biomass?

Our human civilization has been drastically progressed by consuming a huge amount of fossil fuels as sources of energy and chemicals since the Industrial Revolution in the 18–19th century. Meanwhile, the limitless consumption of fossil fuels has caused worldwide problems such as global warming by greenhouse gases and acid rain. The situation of energy production using nuclear energy has totally changed since March 11, 2011, when a tragic accident happened at a nuclear power plant in Fukushima Prefecture in Japan. Hence, development of new technologies employing safe, environmentally benign, and renewable resources is an enormous challenge to overcome the current issues of energy and chemical productions.

Biomass, organic compounds produced by animals and plants, is a promising alternative to petroleum owing to its renewability and large quantity. Biorefinery using biomass as resources of fuels and chemicals is an attractive technology to build up sustainable society and is required to be evolved. To date, a 10^7–10^8 tons of bioethanol has been annually manufactured from corn starch and sugar cane molasses in the United States and Brazil for a decade.[1] However, use of these edible crops as resources competes with food supply, and thus non-food biomass is more favorable feedstock in chemical industry. Especially, cellulose and chitin are attractive resources because of their abundance and potential transformation to various kinds of chemicals.[2–10] Hence, chemical transformation of cellulose and chitin is expected to be game-changing and beneficial technology to build sustainable society. In this thesis, the author has aimed the development of new catalytic systems for efficient utilization of both cellulose and chitin as chemical resources.

1.2. Cellulose

1.2.1. Plant-derived biomass: Lignocellulose

The major components of plant-derived biomass are cellulose (30–50%), hemicellulose (10–40%), and lignin (5–30%) (Figure 1.1).[11,12] These three polymers are intricately intertwined each other, so-called lignocellulose, and constitute cell walls in plants. Cellulose is a polymer of glucose units (Figure 1.2a) linked by β-1,4-glycosidic bonds. Hemicellulose is a copolymer of several kinds of sugar molecules, and a typical building block is β-xylose (Figure 1.2b). Arabinose (Figure 1.2c) is sometimes contained in hemicellulose. The detailed structure of hemicellulose depends on the plants. Lignin is a 3D network polymer and its

structure has remained unclear. It is suggested that three kinds of aromatic compounds, *i.e.*, *p*-coumaryl alcohol, coniferyl alcohol, and sinapyl alcohol (Figure 1.3), link with each other by ether bonds to form lignin.[13] Transformation of cellulose, hemicellulose, and lignin is a mainstream of the next-generation biorefinery. Indeed, many researchers have reported a variety of reactions to produce a variety of chemicals from lignocellulose, *e.g.*, pyrolysis, hydrolysis, hydrolytic hydrogenation, and hydrodeoxygenation.[8,14–16] However, the utilization of lignocellulose has still been a great challenge due to its recalcitrance. In this section, the author has focused on cellulose, the largest component in lignocellulose, and summarized its characteristics and reported catalytic systems for its transformation.

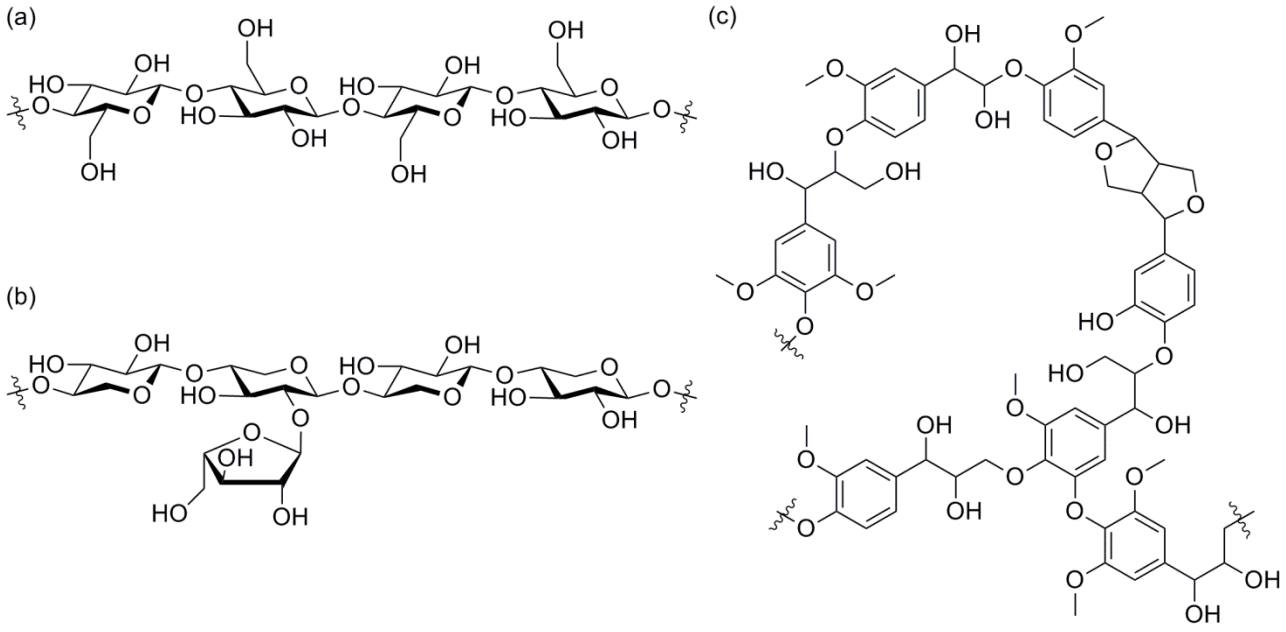


Figure 1.1. Structures of (a) cellulose, (b) hemicellulose, and (c) lignin.

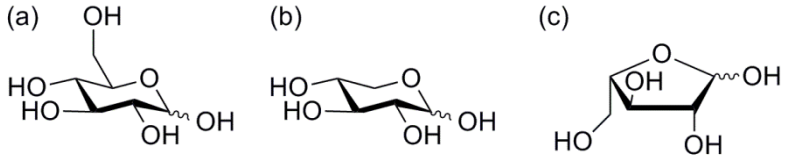


Figure 1.2. Building blocks of cellulose and hemicellulose: (a) glucose; (b) xylose; and (c) arabinose.

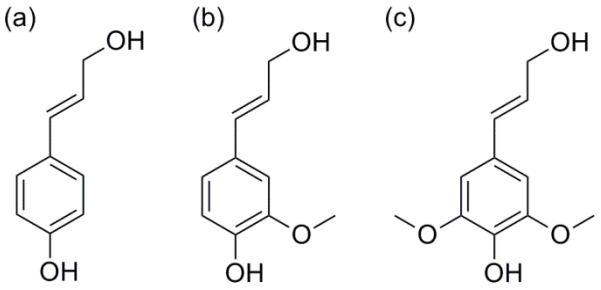


Figure 1.3. Structures of lignin components: (a) *p*-coumaryl alcohol; (b) coniferyl alcohol; and (c) sinapyl alcohol.

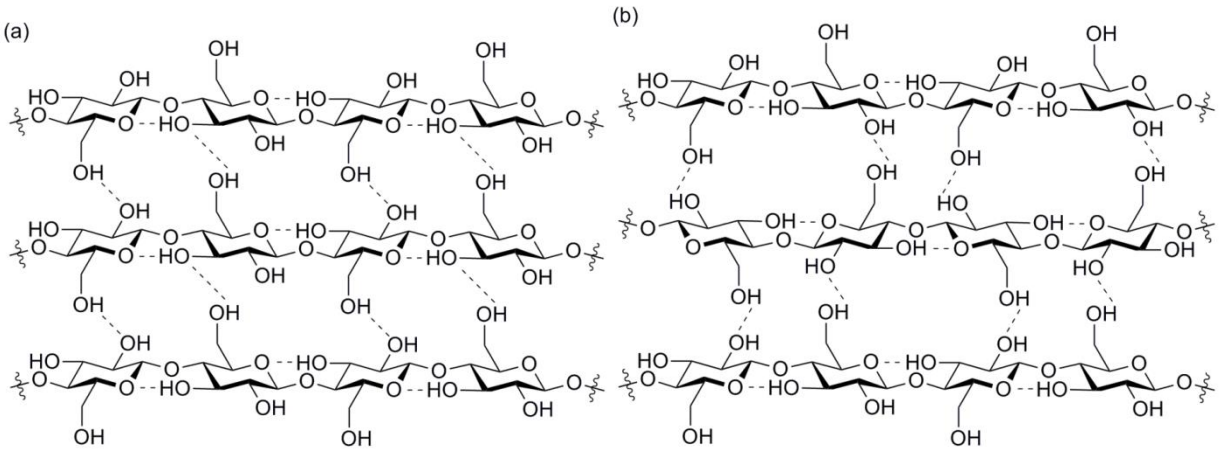


Figure 1.4. Packing manners of (a) cellulose I (parallel) and (b) cellulose II (anti-parallel).

1.2.2. Crystal structure of cellulose

A glucose unit in cellulose has three hydroxyl groups, which form inter- and intramolecular hydrogen bonds with those of other glucose residues. As a result, cellulose molecules are uniformly packed; in other words, crystal structure of cellulose is formed. Seven types of crystal structure (I_α, I_β, II, III_I, III_{II}, IV_I, and IV_{II}) are known for cellulose.[17,18] Plants synthesize cellulose I_β, and bacteria does cellulose I_α. The structure of cellulose I is based on parallel chain packing (Figure 1.4a),[17] and electron diffraction reveals that I_α and I_β are composed of one-chain triclinic and two-chain monoclinic unit cell, respectively.[19] Other types are artificially obtained by chemical treatments for cellulose I. The mercerization using concentrated NaOH produces the type II of crystalline cellulose from the type I,[20] and its structure is based on antiparallel chain packing (Figure 1.4b).[17] Cellulose III_I and III_{II} are obtained from type I and II, respectively, by treatment with liquid

ammonia.[21] The difference of type III_I and III_{II} appears to be parallel and anti-parallel packing reflected their respective original forms, namely type I and II.[17] Cellulose IV is prepared by treating cellulose III in glycerol at 533 K.[21] Although both powder X-ray diffraction (XRD) and ^{13}C nuclear magnetic resonance (NMR) cannot distinguish IV_I and IV_{II}, acetylation of cellulose enables to identify them. That is, cellulose triacetate with parallel packing is formed from cellulose IV_I, and that with anti-parallel packing is from cellulose IV_{II}.[17] The crystalline structures impart chemical and physical stability to cellulose. These properties enable us to use cellulose in a wide range of applications such as fibers (*e.g.*, rayon),[22] papers, food additives,[23] and catalyst supports.[24,25] In some cases, *cellulose nanofiber* is favorable for practical applications due to its high strength (equivalent to stainless steel) and five times lower density than steel.[26] The aqueous counter collision (ACC) method is useful for preparation of cellulose nanofiber. The method drastically diminished the length of cellulose particles from 100 μm to 100 nm and the width from 10 μm to 15 nm;[27] meanwhile the crystal structure of cellulose was maintained (see Figure 1.5).

In contrast to the use of cellulose as a polymer, the crystalline structure of cellulose hampers its chemical transformation in biorefinery because the robust feature limits the access of catalysts to reaction sites of cellulose.[28] Accordingly, crystallinity index (*CrI*) is a useful value to estimate reactivity of cellulose materials, and cellulose with low *CrI* is desirable for its transformation. *CrI* for a mixture of cellulose I and amorphous cellulose can be determined by XRD (eq. 1.1, Figure 1.5),[29] ^{13}C NMR (eq. 1.2, Figure 1.6),[30] and infrared spectroscopy (IR, eq. 1.3),[31] in which XRD and ^{13}C NMR are commonly used. ^{13}C NMR is the most reliable method since the peaks derived from crystalline and amorphous parts are clearly separated.[32]

$$CrI_{\mathrm{XRD}} = \frac{I_{22.5} - I_{18.5}}{I_{22.5}} \times 100 \qquad (1.1)$$

where $I_{22.5}$ and $I_{18.5}$ are intensities observed at 22.5° and 18.5° in XRD, respectively.

$$CrI_{\mathrm{NMR}} = \frac{A_{79\text{-}86}}{A_{86\text{-}92} + A_{79\text{-}86}} \times 100 \qquad (1.2)$$

where $A_{79\text{-}86}$ and $A_{86\text{-}92}$ are peak area from 79 to 86 ppm and from 86 to 92 ppm in ^{13}C NMR, respectively.

$$CrI_{\mathrm{IR}} = \frac{\alpha_{1372}}{\alpha_{2900}} \times 100 \qquad (1.3)$$

where α_{1372} and α_{2900} are intensities at 1372 cm^{-1} and 2900 cm^{-1} in IR, respectively.

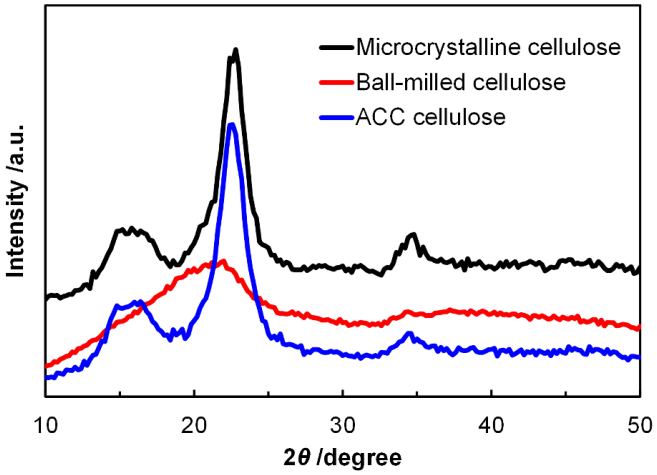


Figure 1.5. XRD patterns of various types of cellulose.

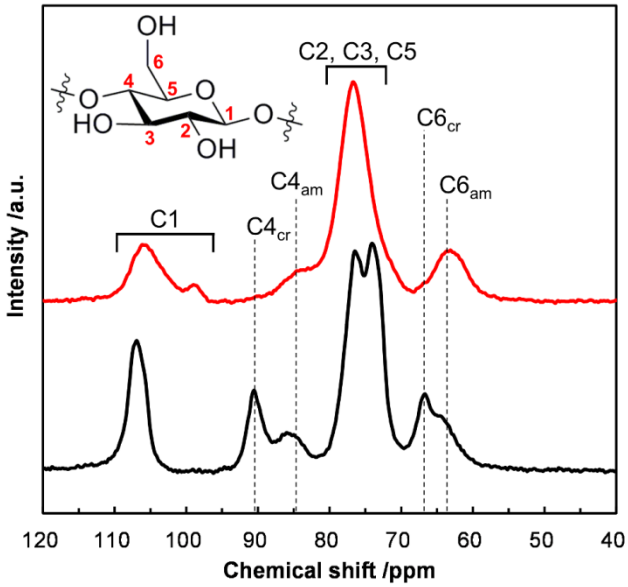


Figure 1.6. ^{13}C NMR spectra of microcrystalline cellulose (black) and amorphous cellulose (ball-milled cellulose, red). In the figure, $C4_{cr}$ and $C6_{cr}$ peaks are derived from crystal part, and $C4_{am}$ and $C6_{am}$ are from amorphous part.

Mechanical and chemical treatments can decrease *CrI* of cellulose. Milling methods such as ball-milling (Figure 1.7)[33] are typical mechanical techniques for disrupting the crystal structure of cellulose. For example, the ball-milling in a ceramic pot with ZrO_2 balls for 96 h decreased CrI_{XRD} from 80% to 10%, calculated from eq. 1.1 and the XRD patterns (Figure 1.5).[34] Additional effect of milling is the shrink of secondary particle sizes; the median diameter measured in H_2O by laser diffraction was reduced from 67 μm to 42 μm. Scanning electron microscope (SEM) images showed that the fibrous shape of cellulose particles turned into smaller spherical morphology by ball-milling (Figure 1.8). Degree of polymerization (DP) of cellulose became almost half by the milling; in other words, one dissociation for each cellulose chain happened. High-power milling processes such as rod-milling and planetary ball-milling (Figure 1.9) also convert crystalline cellulose into amorphous one in a shorter time (<1 h),[35,36] whereas *CrI* does not decrease by jet-milling.[35] In chemical methods, Wang *et al.* reported that *CrI* of cellulose decreased by treating it with H_3PO_4.[37] The parameter depended on the concentration of H_3PO_4 and the temperature and time of treatment. For example, the treatment in 43% H_3PO_4 at 298 K for 1 h decreased *CrI* from 85 to 79, and *CrI* of cellulose diminished to 33 by 85% H_3PO_4 at 323 K for 40 min. Note that cellulose is partially hydrolyzed during the treatment and DP decreased. Tsao *et al.* demonstrated that supercritical CO_2 reduced *CrI* to *ca.* 50% for 1 h.[38] Other physicochemical methods such as ammonia fiber explosion and SO_2-steam explosion are also effective for decreasing *CrI*.[39] The amorphous cellulose thus prepared is expected to show higher reactivity than crystalline one.[40]



Figure 1.7. Apparatus of ball-milling: pot (left) and balls (right).

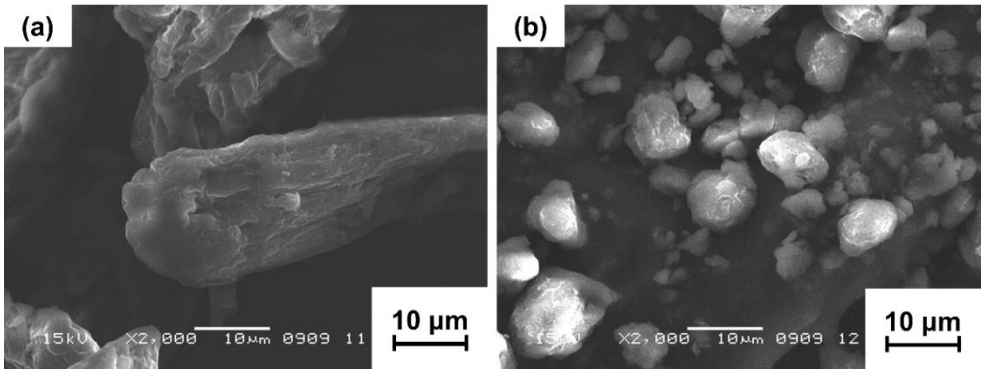


Figure 1.8. SEM images of (a) microcrystalline cellulose and (b) ball-milled one.

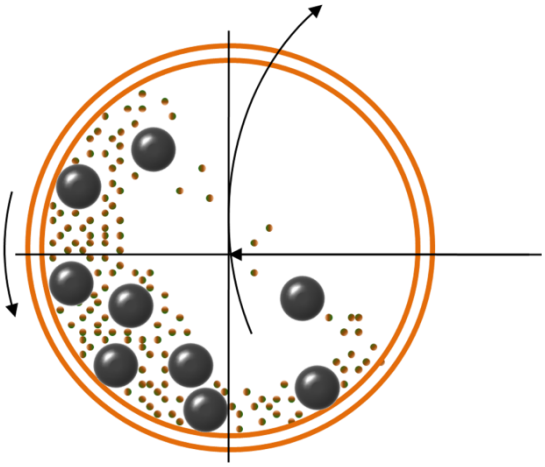


Figure 1.9. Diagram of planetary ball-milling, reproduced from a reference.[41]

Although cellulose is almost insoluble in H_2O[42] except for at high temperatures (>593 K),[43] solvents of cellulose have been explored to handle it as a soluble substrate and to increase reactivity.[44] Lithium chloride/*N*,*N*-dimethylacetamide (LiCl/DMAc) is well known to dissolve cellulose, where chloride ions cleave hydrogen bonds of cellulose.[45,46] Schweizer's reagent forms a complex with cellulose[47] and dissociates hydrogen bonds to dissolve cellulose. In recent years, ionic liquids (ILs) such as 1-butyl-3-methylimidazolium chloride ([BMIM]Cl) have received a significant attention as new solvents for cellulose,[48] because ILs are chemically and thermally stable and their physicochemical properties are tunable.[49] The dissolution mechanism of cellulose into ILs is almost the same as that into LiCl/DMAc.[49]

1.2.3. Glucose and its derivatives

A monomer of cellulose is glucose, produced by hydrolysis. Glucose is one of the energy sources for living things and is used as a sweetener and a medicine against hypoglycemia. In addition to the applications of itself, glucose is transformed into a variety of valuable chemicals as depicted in Figure 1.10.[34]

The present mainstream of glucose transformation is ethanol production by fermentation *via* catabolism, including the Embden-Meyerhof-Parnas pathway and successive ethanol fermentation (Figure 1.11).[50,51] During fermentation from pyruvate to ethanol, one-equivalent mole of CO_2 is emitted. Ethanol produced from crops is called bioethanol, and the annual production volume has gradually increased in the world.[1] Bioethanol is mainly used as an additive to gasoline, *e.g.*, E15 (including ethanol 15% and gasoline 85%),[52] and is now sold in the United States and European countries.

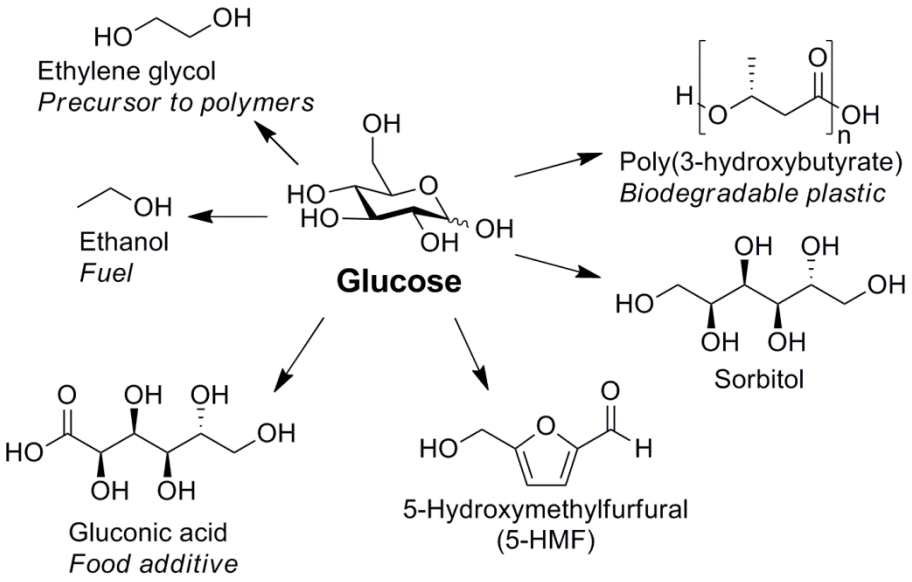


Figure 1.10. Chemicals derived from glucose. The derivatizations of sorbitol and 5-hydroxymethylfurfural (5-HMF) are depicted in Figures 1.13 and 1.14, respectively.

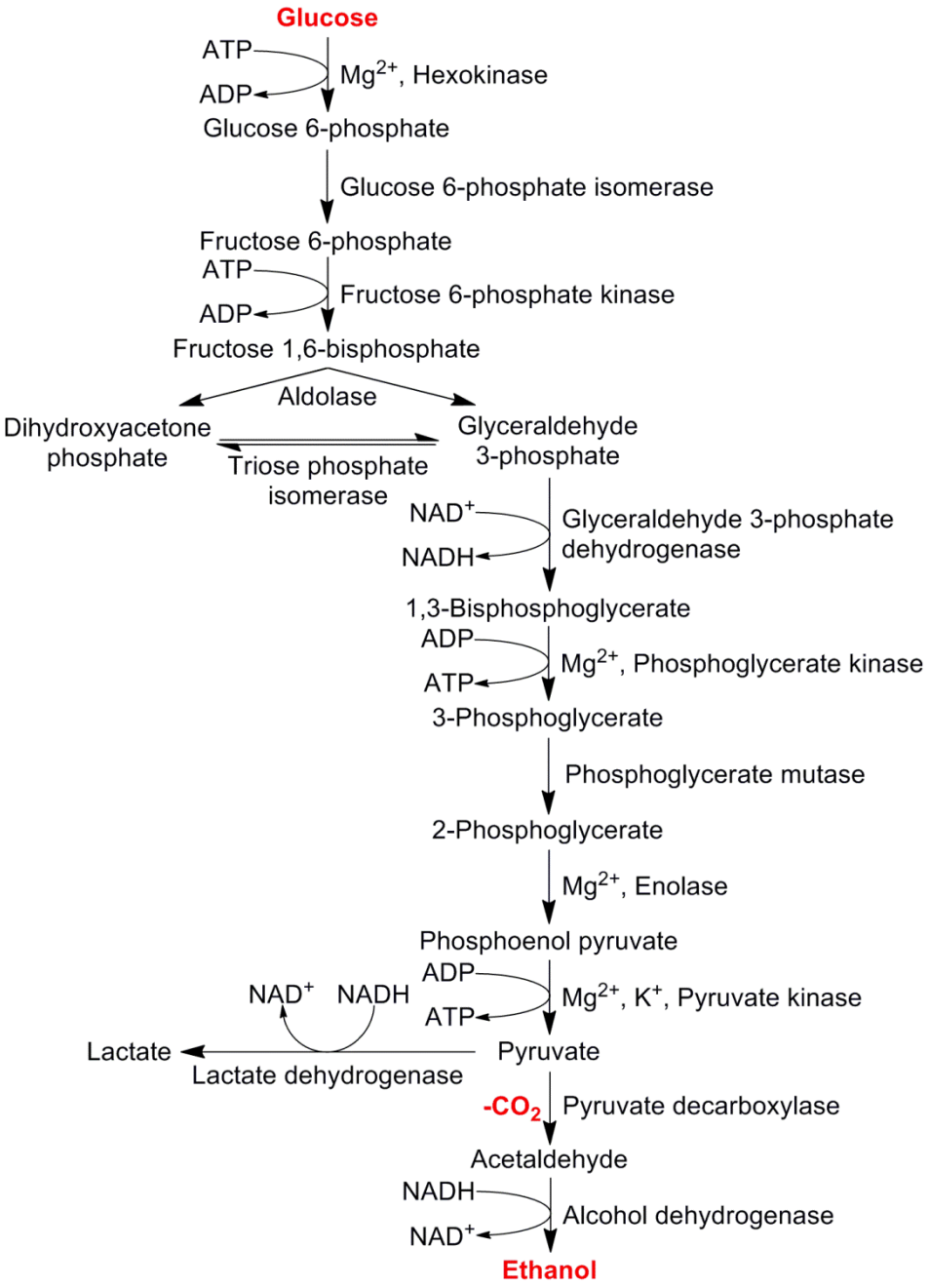


Figure 1.11. Embden-Meyerhof-Parnas pathway from glucose to pyruvate and successive fermentation from pyruvate to ethanol. Two pyruvate molecules are produced from one glucose molecule. Abbreviations: ATP = adenosine triphosphate, ADP = adenosine diphosphate, NAD^+ = nicotinamide adenine dinucleotide, and NADH = reduced form of NAD^+.

Glucose is hydrogenated to sorbitol by supported metal catalysts,[53–56] and this process has been established in chemical industries. Sorbitol is one of the top 12 building block chemicals produced from biomass resources (Figure 1.12), suggested by Department of Energy (DOE) in the United States.[57] Indeed, sorbitol is a good precursor to valuable chemicals as well as glucose (Figure 1.13).[58] For example, *n*-hexane and (*E*)-hexatriene are obtained by complete removal of hydroxyl groups.[59,60] Sorbitol undergoes dehydration in the presence of acid catalysts to give two useful products, 1,4-anhydrosorbitol (1,4-sorbitan) and 1,4:3,6-dianhydrosorbitol (isosorbide). 1,4-Sorbitan is a raw material for various environmentally benign surfactants, *e.g.*, fatty acid esters (Span) and polysorbates (Tween), which are extremely useful as emulsifiers, insecticides, and soft templates for material synthesis.[61] The emulsifiers can be used in food, cosmetic, and pharmaceutical industries owing to their low-toxicity to human being.[62] Isosorbide-based polymers are outstanding engineering plastics showing good transparencies and high glass transition temperatures, and Mitsubishi Chemical, Teijin, and Sabic provide isosorbide-based polycarbonates.[63–65] Other polymers such as polyethylene isosorbide terephthalate (PEIT) are also under consideration as an alternative to polyethylene terephthalate (PET).[66] Additionally, isosorbide and its nitrate esters are medicines for Meniere's disease and angina pectoris, respectively.[67] To date, the dehydration of sorbitol has been conducted by using H_2SO_4 in industrial processes.[68] H_2SO_4 can control the ratio of 1,4-sorbitan and isosorbide by changing reaction conditions. For example, 58% yield of 1,4-sorbitan and 18% yield of isosorbide is formed for 18 min (Table 1.1, entry 1), whereas isosorbide (66%) becomes the major product for 48 min (entry 2). Note that the details of the mechanism for sorbitol dehydration by H_2SO_4 have not yet been revealed. Recently, a variety of heterogeneous catalysts have been developed to produce isosorbide in a laboratory scale (Table 1.1, entries 3–11), *e.g.*, immobilized $H_3PW_{12}O_{40}$,[69] metal phosphate,[70] $CuSO_4$,[71] Ru modified Raney Cu,[72] sulfonated polystyrene resin (Amberlyst 35),[73] sulfonated oxides,[74,75] and zeolites.[76,77] H_2O is formed during the reaction, and thus low-pressure conditions are favorable to avoid coverage of acid sites on catalyst by H_2O molecules. Although the selective production of isosorbide by heterogeneous catalysts has been reported as shown above, that of 1,4-sorbitan is more difficult since 1,4-sorbitan readily undergoes subsequent dehydration to form isosorbide in the presence of acids. Takagaki *et al.* reported that layered niobium molybdate $HNbMoO_6$ provided *ca.* 40% yield of 1,4-sorbitan in the dehydration of sorbitol

(entry 12).[78] They have proposed that molecular recognition is the key to high yields of 1,4-sorbitan.

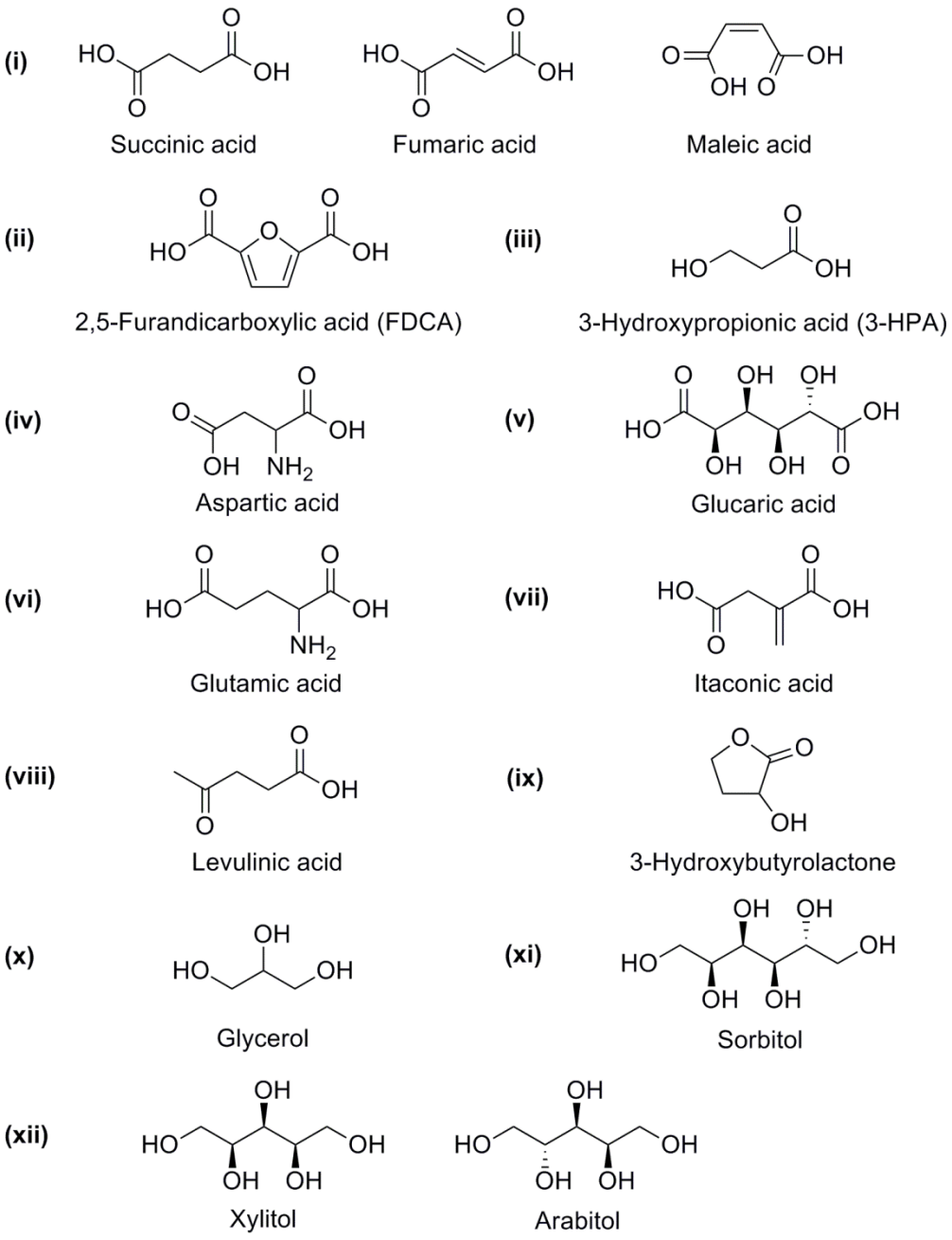


Figure 1.12. Top 12 building block chemicals produced from biomass resources, suggested by DOE in the United States.[57]

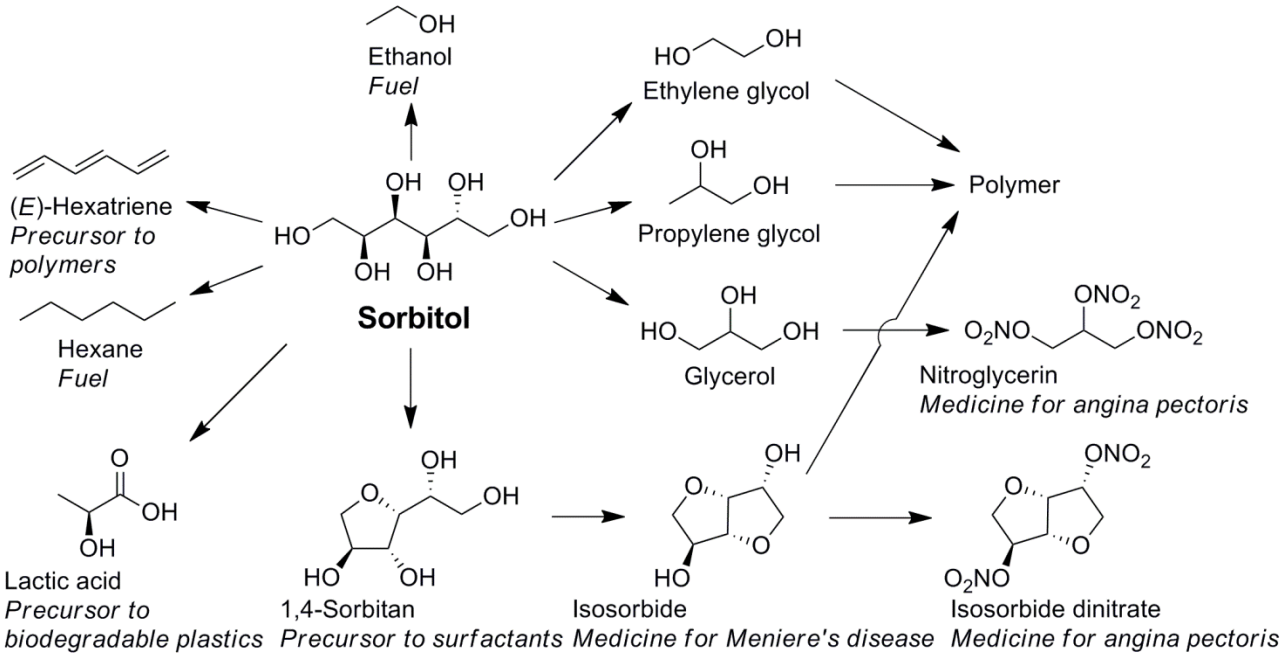


Figure 1.13. Chemicals derived from sorbitol.

Table 1.1. Dehydration of sorbitol to 1,4-sorbitan and isosorbide by acid catalysts.

Entry	Catalyst	*T* /K	Time /h	Conv. /%	Yield /%		Ref
					1,4-Sorbitan	Isosorbide	
1	H_2SO_4	453	0.3	98	58	18	68
2	H_2SO_4	453	0.8	100	0.1	66	68
3	$H_3PW_{12}O_{40}/SiO_2$	523	0.4	96	16	56	69
4	SnPO	573	2	72	24	47	70
5	$CuSO_4$	473	4	100	n.d.[a]	67	71
6	Ru-Raney Cu	533	4	n.d.[a]	7.5	51	72
7	Amberlyst 35	408	2	n.d.[a]	19	73	73
8	Sulfated ZrO_2	483	2	100	18	65	74
9	Sulfated TiO_2	503	4	100	13	75	75
10	H-MFI[b]	533	1	100	n.d.[a]	50	76
11	H-MOR[b]	523	5.8	85	n.d.[a]	40	77
12	$HNbMoO_6$	433	60	94	42	21	78

[a]No data. [b]Si/Al ratio was not shown.

5-Hydroxymethylfurfural (5-HMF) has attracted much attention as 5-HMF derivatives are applicable in a wide range of fields (Figure 1.14). The production of 5-HMF from glucose is still under consideration in laboratories, but high-yielding synthesis of 5-HMF has been reported. The reaction requires both Lewis and Brønsted acids since Lewis acids are necessary for epimerization of glucose to fructose[79] and Brønsted ones

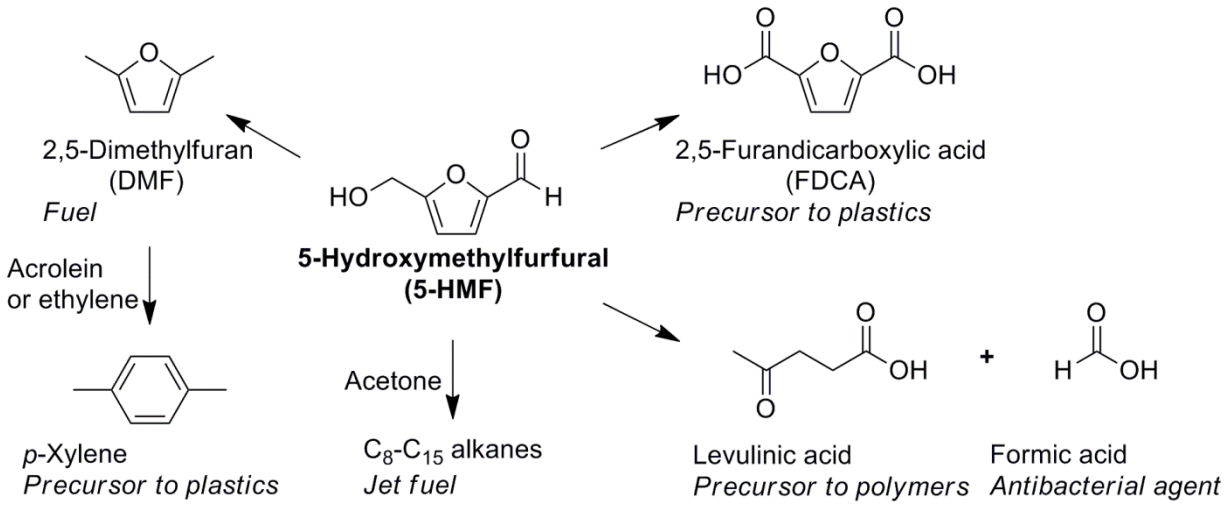


Figure 1.14. Chemicals derived from 5-hydroxymethylfurfural (5-HMF).

are for successive dehydration of fructose to 5-HMF.[80] Hara *et al.* synthesized 5-HMF from glucose in 81% yield in H_2O by using a bifunctional heterogeneous catalyst, phosphate/TiO_2.[81] 5-HMF can be derivatized to a variety of chemicals. The hydrodeoxygenated product of 5-HMF is 2,5-dimethylfuran (DMF),[2] high-octane number fuel with high energy density (30,000 kJ L^{-1}). DMF is further transformed into *p*-xylene, a precursor to PET, through Diels-Alder reaction with acrolein or ethylene.[82,83] The oxidation of 5-HMF over metal catalysts provides 2,5-furandicarboxylic acid (FDCA),[84,85] which can be a polymer-substrate alternative to terephthalic acid. 5-HMF also undergoes hydrolysis to form levulinic acid and formic acid.[86] Levulinic acid is a good precursor to polymers, lubricants, and medicines.[87] Furthermore, Dumesic *et al.* reported the production of C_8–C_{15} alkanes for jet fuels by hydrogenation and hydrodeoxygenation following condensation with acetone.[88]

1.2.4. Hydrolysis of cellulose in homogeneous systems

Production of glucose from cellulose is an attractive reaction in biorefinery due to wide applications of glucose as shown in Section 1.2.3. Hydrolysis of cellulose to glucose (Figure 1.15) is a challenge due to the recalcitrance of cellulose, and many researchers have tried to depolymerize cellulose using various kinds of catalytic systems.

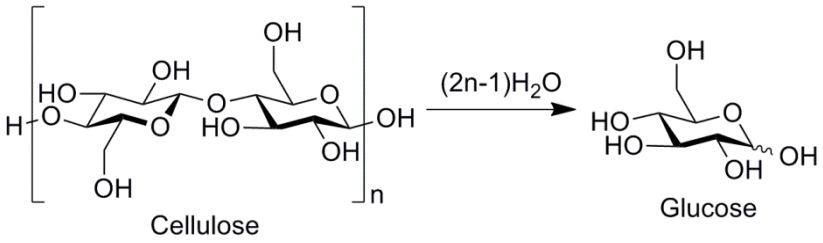


Figure 1.15. Hydrolysis of cellulose to glucose.

The typical catalysts for cellulose hydrolysis to glucose are H_2SO_4 and cellulase enzymes.[89,90] Industrial processes using H_2SO_4 are known as the Scholler process [diluted H_2SO_4 (0.5%)] developed in Germany[91] and Hokkaido process [concentrated H_2SO_4 (30–70%)] conducted in Japan, and the processes produced up to 90% yield of glucose. However, these processes are unprofitable due to equipment corrosion by H_2SO_4, complicated separation system, and acidic waste disposal; consequently, they have been suspended.

Recently, mechanocatalytic depolymerization of cellulose using acid catalysts, *e.g.*, kaolinite ($Al_2Si_2O_7 \cdot 2H_2O$) and H_2SO_4, without solvents has been reported. In a work by Blair *et al.*, cellulose and kaolinite were planetary ball-milled together at 350 rpm for 3 h, and 84% of cellulose was depolymerized into water-soluble products during the milling process.[92] Rinaldi *et al.* conducted the planetary ball-milling of H_2SO_4-impregnated cellulose at 350 rpm for 2 h, and cellulose was almost completely hydrolyzed into water-soluble oligosaccharides.[93] Beltramini *et al.* characterized the produced oligomers in detail by using 2D NMR and found the formation of branched polymers linked by α-1,6-glycosidic bonds, which improved solubility of the oligomers.[94] This result indicates that both hydrolysis and condensation of glucans occur during the milling process. No researchers have so far explained the origin of H_2O molecules, which react with the substrate and form hydroxyl groups. The author speculates that the substrate may undergo hydrolysis by physisorbed H_2O on the substrate or H_2O in atmosphere. The author knows that cellulose generally contains 5–10 wt% of physisorbed H_2O. For example, 1 g of the substrate with 10 wt% of H_2O contains 0.9 g of cellulose (equivalent to 5.6 mmol of glucose unit) and 0.1 g of H_2O (5.6 mmol); hence, the amount of physisorbed H_2O is sufficient to hydrolyze cellulose to oligomers and glucose. Owing to high solubility and reactivity of the oligomers, further transformation easily proceeds. Rinaldi *et al.* reported that a

91% yield of glucose and a 91% yield of sugar alcohols (sorbitol 86%, mannitol 5%) in a batch-type reactor were formed from the water-soluble oligosaccharides.[93,95] Beltramini *et al.* have also demonstrated the hydrolytic transfer-hydrogenation of the oligomers to produce sorbitol (see Figure 1.23) using Ru/C catalyst and 2-propanol as a hydrogen source in continuous production due to difficult control of flow of gaseous H_2 and liquid H_2O at the same time in a laboratory scale.[96] The remaining issue of these systems should be reusability of the catalyst, H_2SO_4.

Heteropoly acids (HPAs) work as homogeneous catalysts in H_2O, but they can be separated by extraction using organic solvents such as 2-propanol and diethyl ether. Some of HPAs have higher acidity than mineral acids. For example, the Hammet acidity function (H_0) of $H_5BW_{12}O_{40}$ (0.7 M at 298 K, *vide infra*) is –2.1 lower than those (*ca.* 0) of H_2SO_4 and HCl (0.7 M).[97] Hence, it is expected that HPAs are active and reusable catalysts for the hydrolysis instead of H_2SO_4. Shimizu *et al.* showed that the hydrolysis of cellobiose and cellulose in H_2O was promoted by HPAs such as $H_3PW_{12}O_{40}$, $H_4SiW_{12}O_{40}$, and $Sn_{0.75}PW_{12}O_{40}$.[98] The total yield of reducing sugars from cellulose was *ca.* 40% when using $Sn_{0.75}PW_{12}O_{40}$ at 423 K for 16 h. They also conducted the screening of counter cations of $PW_{12}O_{40}^{3-}$ for the hydrolysis of cellobiose and found that there was a volcano-type correlation between turnover frequencies (TOFs) for glucose formation and Lewis acidities. Thus, both Brønsted and Lewis acidities were important for the catalytic activity of HPAs, although the Lewis acidity was not evaluated in H_2O. Mizuno *et al.* found that $H_5BW_{12}O_{40}$ showed a good performance for the conversion of crystalline cellulose to give glucose in 77% yield, and $H_3PW_{12}O_{40}$ (glucose yield 8%) and $H_4SiW_{12}O_{40}$ (37%) were less active than $H_5BW_{12}O_{40}$.[97] They remarked that the acidity and the function of decreasing *CrI* were important for the catalytic activity of HPAs. In fact, the order of the H_0 function was $H_3PW_{12}O_{40} \geq H_4SiW_{12}O_{40} \geq H_5BW_{12}O_{40}$ in the same order of catalytic activity. According to their screening, HPAs containing highly negatively charged anions were preferable. The anions also dissociated hydrogen bonds between cellulose molecules to decrease *CrI*. Furthermore, protons of HPAs also weakened hydrogen bonds of cellulose, and a higher concentration of proton was suitable for this purpose. Thus, $H_5BW_{12}O_{40}$ worked as a highly active catalyst for the hydrolysis of cellulose. $H_5BW_{12}O_{40}$ can be recovered by extraction and recycled for 10 times.

In enzymatic hydrolysis of cellulose to glucose, three types of enzymes, *i.e.*, endoglucanase (EG),

exoglucanase (so-called cellobiohydrolase, CBH), and β-glucosidase, are simultaneously employed.[99] EG randomly cleaves β-1,4-glycosidic bonds of cellulose in amorphous parts to increase the number of reducing/non-reducing ends. Subsequently, CBH depolymerizes the polymer from the reducing/non-reducing ends in both crystalline and amorphous parts to form only cellobiose. β-Glucosidase works for the hydrolysis of soluble oligomers produced by EG and CBH to glucose. The functions of EG and CBH for the hydrolysis of cellulose are proposed as follows. First, enzymes adsorb onto the surface of cellulose through hydrophobic interactions derived from the binding domain composed of three exposed tyrosine residues.[100] In the second step, cellulose chains are introduced into a pocket (in the case of EG) or a tunnel (CBH, Figure 1.16), where there is an active site.[101] Then, a glycosidic bond in cellulose is cleaved by a pair of carboxylic acid and carboxylate, in which two types of mechanism, inverting and retaining ones, are presumed (Figure 1.17).[102]

Nowadays, cellulase enzymes can afford glucose in 75% yield from cellulose under moderate conditions (*e.g.*, 343 K, 1.5 days),[89,90] and some enzymatic systems have been extended to a commercial scale. Although adsorption process separates EG and CBH from a product solution after the reaction, β-glucosidase does not adsorb on the adsorbent and cannot be recovered.[103,104] Immobilization of cellulases has been considered for easy separation and recycle, and various reports have shown their reusability.[105–107] However, the immobilized cellulases are less active than *free* cellulases because of low accessibility.

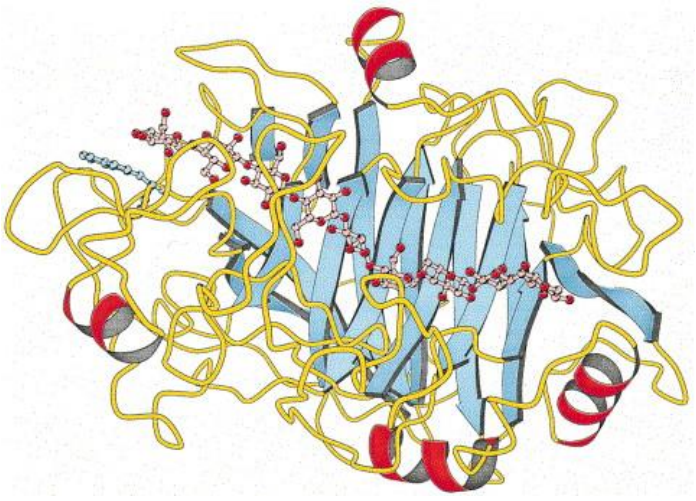


Figure 1.16. Schematic representation of catalytic domain of exoglucanase (CBH), in which a cellulosic molecule penetrates into the *tunnel*. This figure is reproduced from a reference.[108]

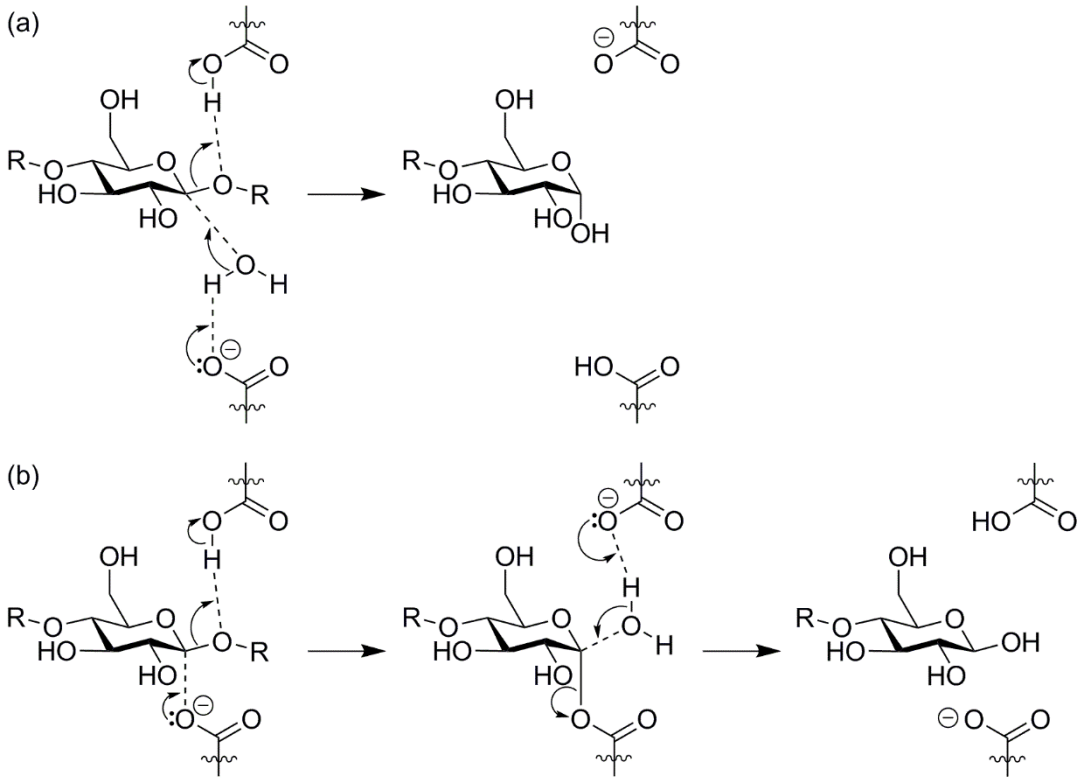


Figure 1.17. Proposed reaction mechanism for glycosidic bond cleavage by cellulase: (a) inverting mechanism and (b) retaining mechanism.

Reaction systems using only supercritical water as both solvent and reactant are tested in laboratories, and have produced glucose from cellulose in 24% yield.[109,110] However, a special reactor resisting harsh conditions is required and produced glucose readily undergoes the further degradation at such a high temperature (673 K). Gaseous water is also used for the hydrolysis of crystalline cellulose.[111] Water vapor penetrates interstices of cellulose molecules, weakens hydrogen bonds, and hydrolyzes glycosidic bonds. In this system, the glucose yield is only 17%.

1.2.5. Hydrolysis of cellulose by heterogeneous catalysts

Heterogeneous catalysis for cellulose hydrolysis has been investigated since heterogeneous catalysts are advantageous over homogeneous ones thanks to their ease of separation and reusability.

As mentioned in Section 1.2.2, cellulose is dissolved in ILs and is expected to show higher reactivity

than that in H_2O. Zhao *et al.* performed the hydrolysis of cellulose dissolved in [BMIM]Cl in the presence of H_2SO_4 at 373 K (Table 1.2, entry 13).[112] Schüth and co-workers employed a sulfonated polystyrene resin (Amberlyst 15DRY) instead of H_2SO_4 in [BMIM]Cl (entry 14).[113] Later it was found that H^+ species was released from SO_3H by ion-exchange with $[BMIM]^+$ to become a hydrolysis catalyst.[114] This was the reason for the deactivation of Amberlyst 15DRY catalyst after the reaction in ILs, although the catalytic activity of the resin was regenerated by washing with H_2SO_4. Furthermore, ILs-immobilized sulfonated char was easily separated from products (entry 15).[115] However, ILs are expensive and toxic, and a decisive advantage is necessary to use ILs as a solvent instead of H_2O.

Heterogeneous catalysts working under aqueous conditions have also been developed in recent years. Hara *et al.* synthesized a sulfonated carbon (Figure 1.18) by carbonization of cellulose at 723 K under N_2 followed by sulfonation using oleum at 353 K. This sulfonated carbon hydrolyzed cellulose to glucose (4% yield) and water-soluble oligosaccharides (64%) in H_2O at 373 K in a Pyrex test tube (entry 16).[116,125,126]

Table 1.2. Hydrolysis of cellulose to glucose.

Entry	Catalyst	Pre-treatment of cellulose	S/C[a]	*T* /K	Time /h	Conv. /%	Yield /%		Ref
							Glc[b]	Olg[c]	
13[d]	H_2SO_4	Microcrystalline	0.11	373	9	n.d.[h]	43	34[j]	112
14[d]	Amberlyst 15DRY	Microcrystalline	5.0	373	5	29	0.9	0.6[k]	113
15[e]	C-SO_3H-IL	Microcrystalline	2.0	363	2	n.d.[h]	33[i]	n.d.[h]	115
16	C-SO_3H	Microcrystalline	0.083	373	3	n.d.[h]	4	64	116
17	AC-SO_3H	Ball-milled	0.9	423	24	n.d.[h]	41	n.d.[h]	117
18	SiO_2-C-SO_3H	Ball-milled	1.0	423	24	61	50	2	118
19	CMK-3-SO_3H	Ball-milled	0.9	423	24	94	75	n.d.[h]	119
20	Fe_3O_4-SBA-SO_3H	[BMIM]Cl	0.7	423	3	n.d.[h]	50	n.d.[h]	120
21	Fe_3O_4-SBA-SO_3H	Microcrystalline	1.0	423	3	n.d.[h]	26	n.d.[h]	120
22	$CoFe_2O_4$/SiO_2-SO_3H	[BMIM]Cl	1.0	423	3	n.d.[h]	7.0	30[k]	121
23	CP-SO_3H	Microcrystalline	0.2	393	10	n.d.[h]	93	n.d.[h]	122
24	2.0 wt% Ru/CMK-3	Ball-milled	6.5	503	0.83[f]	56	24	16	123
25	CMK-3	Ball-milled	6.5	503	0.83[f]	54	16	5	123
26	MC	Ball-milled	3.3	518	0.75[g]	71	41	0.9[k]	119
27	GO	Not mentioned	0.9	423	24	59	50	4[k]	124

[a]Ratio of substrate and catalyst based on weight. [b]Glucose. [c]Oligosaccharides. [d]The reaction was conducted in [BMIM]Cl. [e]Microwave (350 W) was used. [f]Total time including heating and cooling. The keeping time at 503 K was less than 1 min. [g]The reaction mixture was heated from room temperature to 518 K in 45 min and rapidly cooled down to room temperature. [h]No data. [i]Total yield of reducing sugars. [j]Total yield of reducing sugars other than glucose. [k]Cellobiose.

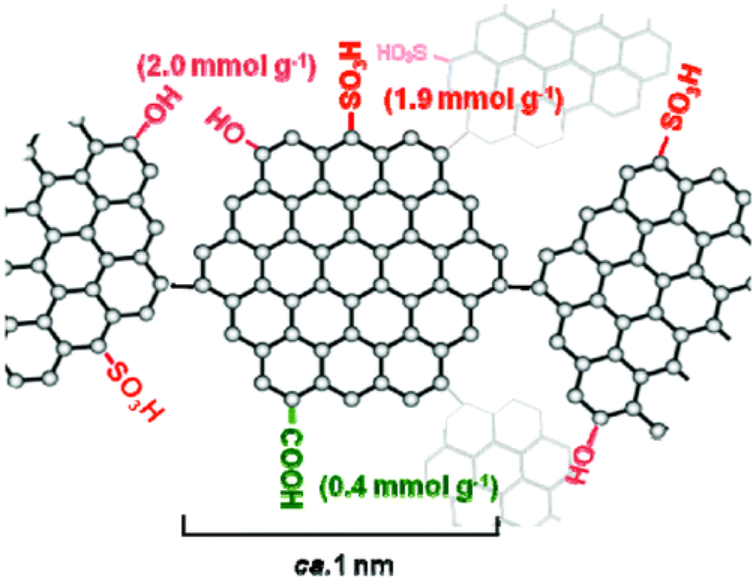


Figure 1.18. Proposed schematic structure of sulfonated carbon, reproduced from a reference.[116]

Sulfonic groups on large graphene sheets are usually decomposed in hot-compressed water,[127] but those on this material are stabilized by electron-withdrawing effect of carboxylic acids and small size of on graphene (*ca.* 1 nm). The sulfonated carbon maintained its catalytic activity in reuse runs more than 25 times. For the catalytic mechanism, they have proposed that neutral or weakly acidic OH groups such as phenolic groups on carbon adsorb β-1,4-glucans by hydrogen bonds, and then sulfonic groups cleave glycosidic bonds.[128,129] Later, Hara *et al.* also submitted a patent for a specific reactor equipped with a strong agitation wing grinding cellulose-catalyst slurry.[130] The author therefore speculates that mechanocatalytic process may be involved in their catalytic system in addition to thermal process giving a good performance in the hydrolysis of cellulose. Onda *et al.* demonstrated that a sulfonated carbon prepared from commercial activated carbon (denoted as AC-SO_3H) gave a 41% yield of glucose at 423 K for 24 h (entry 17).[117,131] After the hydrolysis of cellulose by AC-SO_3H, they performed hydrolysis of cellulose again using filtrate of the first run as a solvent without adding any solid catalysts. However, glucose yield was as low as that in a blank reaction without catalyst, indicating that the hydrolysis was not enhanced by soluble species derived from the catalyst. Furthermore, AC-SO_3H showed similar catalytic activity in repeated reactions. Hence, they concluded that AC-SO_3H worked as a durable solid catalyst under the reaction conditions. It is noteworthy that they pre-treated

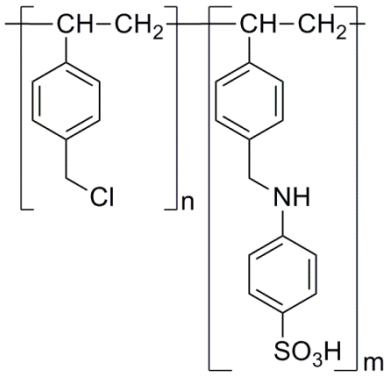


Figure 1.19. Structure of CP-SO_3H, which is synthesized from Merrifield's resin and sulfanilic acid, in which Cl groups and SO_3H groups are expected to be binding and active sites, respectively.[122]

AC-SO_3H in hot-compressed water at 473 K before the reaction at 423 K to remove weakly bonded sulfonic groups, and remaining sulfonic groups on AC were stable and reusable under the reaction conditions at 423 K. Only a small amount of sulfate ions [35 μM (1.2% of sulfonic groups in the catalyst), detected by ion chromatography] leached from the pre-treated AC-SO_3H, and the reported performance was almost reproduced.[34] In contrast, sulfuric acid leached from the catalyst without the pre-treatment at 473 K.

These reports motivated other researchers to develop sulfonic acid catalysts. A silica/carbon nanocomposite and a mesoporous carbon CMK-3, both of which were treated by H_2SO_4, yielded glucose in 50% (entry 18)[118] and 75% (entry 19),[119] respectively. Magnetic catalysts with sulfonic groups, *e.g.*, a sulfonated composite of mesoporous silica SBA-15 and Fe_3O_4[120,132] and sulfonated $CoFe_2O_4$-embedded silica,[121] were also used for the hydrolysis of cellulose (entries 20–22). They were easily separated from product cocktail by a magnet after the reactions. Fe_3O_4-SBA-SO_3H catalyst afforded glucose in 26% yield from microcrystalline cellulose at 423 K for 3 h, whereas levulinic acid became a major product (42% yield) by prolonging the reaction time to 12 h.[120] Pan *et al.* synthesized a sulfonic chloromethyl polystyrene resin (CP-SO_3H, Figure 1.19) to promote adsorption of cellulose onto CP-SO_3H by hydrogen bonds between Cl of the catalyst and OH groups of the substrate and subsequent hydrolysis of glycosidic bonds by SO_3H groups.[122] They reported that CP-SO_3H converted microcrystalline cellulose into glucose in 93% yield at 393 K for 10 h (entry 23). However, the base polymer chloromethyl polystyrene, so-called Merrifield's resin,

easily undergoes S_N2 reaction at a benzyl position as widely used for connecting peptides and proteins.[133] Indeed, in their synthetic scheme of CP-SO_3H, sulfanilic acid nucleophilically attacks a carbon atom at the benzyl position of Merrifield's resin to form a C–N covalent bond. Besides, leaching of both Cl^- and SO_4^{2-} species was detected by ion chromatography in the author's test possibly due to S_N2 reaction at the benzyl position of CP-SO_3H by H_2O molecules.[34] Hence, one should take care of the possibility of leaching of SO_3H and Cl in using sulfonated or chlorinated materials as catalysts in H_2O at high temperatures. More seriously, the author could not reproduce reported high yields of glucose. Back to their original concept, Cl^- ion exactly may have a good interaction with cellulose,[45,46] but one can hardly expect that covalently bonded Cl has a similar ability. Furthermore, the reactions by these sulfonic acid catalysts are typically conducted at S/C [substrate/catalyst (wt/wt)] ratios lower than 1; higher S/C ratios are favorable to improve the efficiency.

Supported metal catalysts have also been used for the hydrolysis of cellulose. Fukuoka *et al.* found that 2 wt% Ru/CMK-3 hydrolyzed cellulose (conversion 56%) to glucose (24% yield, 43% selectivity) in H_2O (entry 24), and TOF for the production of glucose was 18 h^{-1} per bulk Ru atom.[123,134] The yield of glucose was raised up to 31% by increasing the Ru loading to 10 wt%. This catalyst was reusable up to five times without loss of the activity or Ru leaching, checked by inductivity coupled plasma atomic emission spectroscopy (ICP-AES). The Ru species on CMK-3 was highly dispersed $RuO_2 \cdot 2H_2O$ characterized by X-ray absorption fine structure spectroscopy (XAFS) and XRD, and the high valent Ru species may work as a catalyst for hydrolysis. They have proposed that an empty site on Ru atom works as a Lewis acid and/or an H_2O molecule coordinating to Ru does as a Brønsted acid (Figure 1.20).

It is known that acids with a pK_a value larger than –3 are usually ineffective for the hydrolysis of cellulose.[135] Intriguingly, mesoporous carbons (MCs) and graphene oxide (GO) also catalyzed the hydrolysis of cellulose to glucose and that of xylan to xylose even in the absence of strong acidic groups or metals (entries 25–27).[119,123,124,134,136] The weakly acidic groups such as carboxylic acids and phenolic groups are proposed as active sites; however, the detailed structures and their catalysis remain unclear. Katz *et al.* also reported that even OH groups on SiO_2 and Al_2O_3 with very weak acidity (pK_a = *ca.* 7) were able to hydrolyze cellulosic molecules by inducing stressful conformations by forming ether bonds between SiO_2 (or Al_2O_3)

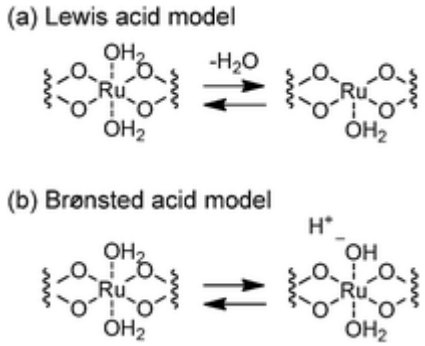


Figure 1.20. Speculated active sites on Ru/CMK-3 catalyst, reproduced from a reference.[8]

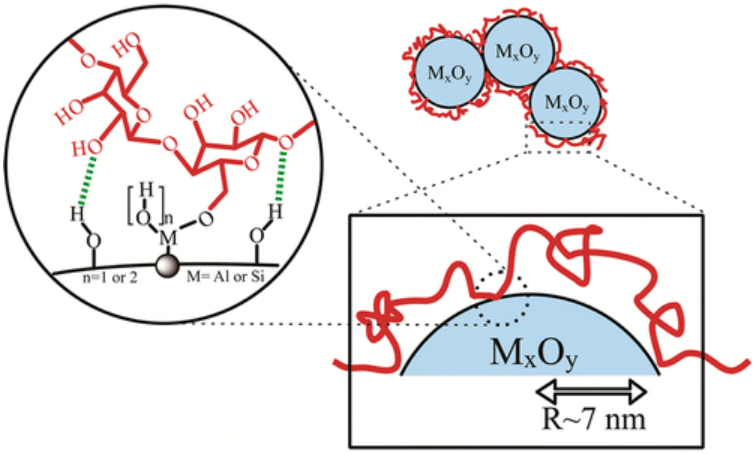


Figure 1.21. Schematic activation mechanism of glycosidic bonds in grafted cellulosic molecules, reproduced from a reference.[139]

and cellulosic molecules.[137–139] They proposed that the proximity of surface OH groups was important to hydrolyze the biomass-derived polymers. OH groups on SiO_2 (or Al_2O_3) captured the substrate by forming ether bonds with hydroxyl groups of the substrate, which kept neighboring other OH groups on catalyst close to the immobilized polymer. Then, the OH groups had the enhanced chances to activate glycosidic bonds (Figure 1.21). Note that both SiO_2 and Al_2O_3 could not hydrolyze glycosidic bonds without immobilization of the substrate. These results clearly suggest the importance of positioning of substrate and surface OH groups.

1.2.6. Hydrolytic hydrogenation of cellulose to sorbitol

Direct conversion of cellulose to platform chemicals other than glucose has also been investigated, and especially hydrolytic hydrogenation of cellulose to sorbitol (Figure 1.22) is an active area in biorefinery. The author therefore summarizes typical works in this section (Table 1.3).

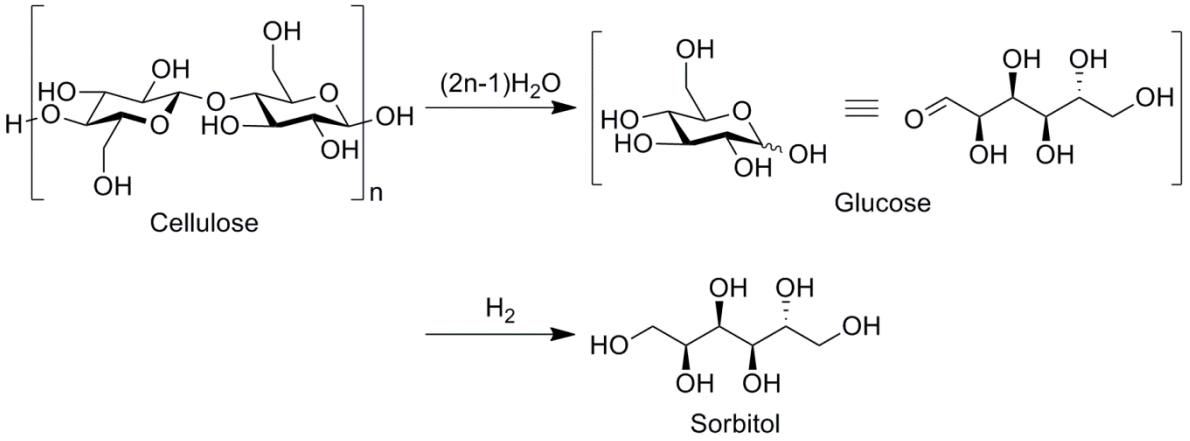


Figure 1.22. Hydrolytic hydrogenation of cellulose to sorbitol *via* glucose.

In the 1950s, Balandin *et al.* showed that Ru/C combined with H_2SO_4 gave sorbitol from cellulose under 7 MPa of H_2 (entry 28).[140,153] In this process, soluble H_2SO_4 hydrolyzes solid cellulose to glucose, and then soluble glucose is hydrogenated to sorbitol by solid Ru/C. In detail, formation of soluble oligosaccharides and their reduced alcohols are involved in the reaction;[154,155] however, they are omitted for better handling and easier understanding the reaction. Later, Jacobs and co-worker used a bifunctional catalyst Pt/FAU for the hydrolytic hydrogenation of starch, which is a water-soluble polymer composed of α-glucose.[156] Solid FAU zeolite hydrolyzes soluble starch to glucose and solid Pt hydrogenates glucose to sorbitol.[157] Hence, both are solid-liquid interfacial reactions and the degradation of solid cellulose by solid catalysts has remained an issue for a long period. In 2006, Fukuoka *et al.* reported the first hydrolytic hydrogenation of cellulose using only solid catalysts, in which Pt/γ-Al_2O_3 produced sorbitol and mannitol in 25% and 6% yields, respectively (entry 29).[141] Interestingly, the hydrolysis step is also accelerated by the solid catalyst regardless of relatively low acidity of γ-Al_2O_3 (pK_a = +3.3 ~ +6.8).[158] Although it was proposed

Table 1.3. Hydrolytic hydrogenation of cellulose to sugar alcohols.

Entry	Catalyst	Pre-treatment of cellulose	*T* /K	Time /h	*P*(H_2) /MPa	Conv. /%	Yield /%			Ref
							Sor[a]	Man[b]	Total[c]	
28	H_2SO_4, Ru/C	Sulfite[h]	433	2	7	n.d.[k]	n.d.[k]	n.d.[k]	82[l]	140
29	2.5 wt% Pt/γ-Al_2O_3	Microcrystalline	463	24	5.0	n.d.[k]	25	6	31	141
30	4.0 wt% Ru/C	Microcrystalline	518	0.5	6.0	86	30	10	39	142
31	1.0 wt% Ru/CNT	H_3PO_4	458	24	5.0	n.d.[k]	69	4	73	37
32	1.0 wt% Ru/CNT	Microcrystalline	458	24	5.0	n.d.[k]	36	4	40	37
33	2.0 wt% Pt/BP2000	Ball-milled	463	24	5.0	82	49	9	58	143
34	5.0 wt% Ru/C, $H_4SiW_{12}O_{40}$	Ball-milled	463	1	9.5	100	n.d.[k]	n.d.[k]	85	144
35	5.0 wt% Ru/C, $H_4SiW_{12}O_{40}$	Microcrystalline	463	1	9.5	77	n.d.[k]	n.d.[k]	36	144
36	16 wt% Ni_2P/AC	Microcrystalline	498	1.5	6.0	100	48	5	53	145
37	$Ni_{12}P_5$/AC[d]	Ball-milled	503	0.7	5.0	92	62	5	67	146
38	3.0 wt% Ni/CNF	Ball-milled	463	24	6.0	92	50	6	57	147
39	3.0 wt% Ni/CNF	Microcrystalline	483	24	6.0	87	30	5	35	147
40	7.5 wt% Ni/oxidized CNF	Ball-milled	463	24	6.0	93	64	7	71	148
41	4.0 wt% Ir-4.0 wt% Ni/MC	Microcrystalline	518	0.5	6.0	100	47	12	58	149
42	Pt/Ni/mesoporous Al_2O_3[e]	Microcrystalline	473	6	5.0	49	26	6	32	150
43	Pt/Ni/BEA[f]	Microcrystalline	473	6	5.0	51	34	3	37	150
44	2.0 wt% Ru/AC	Ball-milled	463	18	0.8	83	30	8	38	151
45	2.0 wt% Ru/AC	Mix-milled[i]	463	3	0.9	89	58	9	68	152
46	Pt, $H_4SiW_{12}O_{40}$[g]	Mercerization, ball-milled	333	24	0.7	n.d.[k]	54	n.d.[k]	n.d.[k]	97
47	2.0 wt% Ru/AC	Ball-milled	463	18	0.0[j]	74	34	9	43	151
48	2.0 wt% Ru/CMK-3	Ball-milled	463	18	0.0[j]	81	36	9	45	151

[a]Sorbitol. [b]Mannitol. [c]Total yield of sorbitol and mannitol. [d]Ni and P loadings were 10 wt% and 2.6%, respectively. [e]Ni/Pt ratio = 22. [f]Ni/Pt ratio = 22. Si/Al ratio of BEA = 75. [g]Pt amount was 24 mol% to cellulose and the concentration of $H_4SiW_{12}O_{40}$ was 0.70 M. [h]Substrate was treated by sulfurous acid to extract lignin, and resulting powder was used for the reaction. [i]Cellulose and catalyst were ball-milled together. [j]2-Propanol was used instead of H_2. [k]No data. [l]Monoanhydrides of sorbitol.

that the hydrolysis was accelerated by proton produced *via* heterolysis of H_2 over Pt,[141,159,160] this mechanism would be excluded.[161] How supported Pt catalysts promote the hydrolysis is still unclear. The residual Cl on the catalysts derived from catalyst precursors such as H_2PtCl_6 also affected the catalytic performance. The rates of cellulose hydrolysis and side reactions were enhanced by HCl or Al^{3+} species.[143,162] This problem can be avoided by using Cl-free precursors such as $Pt(NH_3)_2(NO_2)_2$ and carbon supports. In contrast, Liu *et al.* proposed that protons from hot-compressed water promoted the hydrolysis step,[142,163] because pK_w of H_2O $\left[-\log\left(a_{H^+}\cdot a_{OH^-}\right)\right]$ is down to 11.2 at 448 K.[164] However, its corresponding pH (5.6) is high enough to be free from acid-catalyzed hydrolysis of cellulose, and direct attack of H_2O molecule to glycosidic bonds may be more significant.[165] Major active species for the hydrolysis alters by catalysts and reaction conditions

employed.

Later, it was found that γ-Al_2O_3 support was transformed into boehmite [AlO(OH)] in hot water, and the catalytic activity reduced in repeated reactions.[143] Thus, the development of more active, selective, and durable catalysts has been a target. Carbon materials such as activated carbon (AC) and carbon nanotubes (CNTs) are known as heat- and water-tolerant supports. For this reason, carbon supported metal catalysts have been extensively studied. Liu *et al.* conducted the hydrolytic hydrogenation of cellulose by a durable Ru/C catalyst, which produced hexitols in 39% yield with 86% conversion (entry 30).[142] According to the results of ICP and transmission electron microscope (TEM) analyses, neither leaching nor sintering of Ru occurred. Wang *et al.* reported that the yield of sugar alcohols was improved to 73% by using Ru/CNT and H_3PO_4-pretreated cellulose (entry 31).[37] The Ru/CNT catalyst also yielded sugar alcohols in 40% yield from microcrystalline cellulose (entry 32). Fukuoka and co-workers used a carbon black BP2000 as a support, and Pt/BP2000 afforded sugar alcohols in 58–65% yields in reuse experiments (entry 33).[143] The rate-determining step of the hydrolytic hydrogenation is the hydrolysis of cellulose to glucose,[143] and a mixture of Ru/C and $H_4SiW_{12}O_{40}$ was used to enhance the hydrolysis.[144] This strategy gave an 85% yield of sugar alcohols from ball-milled cellulose (entry 34) and a 36% yield from crystalline cellulose (entry 35). Such high-yielding and selective production of sugar alcohols from cellulose is surprising since side reactions decrease their yields in typical catalytic reactions. Indeed, Palkovits *et al.* showed that in similar catalytic systems side reactions happened such as further transformation of sorbitol at a higher concentration of acids for longer reaction time, in which C2–C6 polyols such as erythritol, xylitol, sorbitan, and isosorbide were obtained as by-products.[166]

Recently, Ni catalysts have been studied instead of precious metals to reduce cost of catalysts. Microcrystalline cellulose was converted to sorbitol (48% yield) and mannitol (5%) by a Ni_2P catalyst supported on AC (entry 36).[145] Fukuoka *et al.* also reported that $Ni_{12}P_5$/AC produced sorbitol (62%) and mannitol (5%) from ball-milled cellulose (entry 37), and the high catalytic performance was attributed to an amorphous nickel phosphide phase generated during the reaction.[146] Although the nickel phosphide catalysts were active, they were not durable in hot water due to P leaching and Ni sintering. In contrast, it was reported that Ni species on carbon nanofibers (CNFs) was stable in H_2O for 24 h even at 483 K (entries 38

and 39), and Ni/CNF catalyst kept its activity in reuse experiments up to three times.[147] Ni/CNF was prepared by chemical vapor deposition (CVD) of carbon on Ni/γ-Al_2O_3 using methane as a carbon source, in which methane decomposed on Ni metal and CNF was produced. The method of catalyst preparation was modified by post-treatment for a better balance of hydrolysis and hydrogenation activities.[148] In detail, Ni/CNF was treated in concentrated HNO_3 at 383 K to oxidize CNF and to remove Ni species, and then Ni was again impregnated on the CNF. This three-step preparation including CVD, removing of Ni, and impregnation of Ni was complicated compared to the previous one (only CVD), but the dispersion of Ni on the oxidized CNF increased thanks to more oxygenated functional groups (OFGs) of the CNF. Ni supported on the oxidized CNF showed higher activity than the original Ni/CNF catalyst and gave sorbitol (64%) and mannitol (7%) with 93% conversion of cellulose (entry 40). Bimetallic catalysts containing Ni were also effective for the hydrolytic hydrogenation of cellulose to hexitols, and Ir-Ni supported on MC afforded 58% yield of sugar alcohols in repeated reactions for four times (entry 41).[149] Ir improves the thermal stability and catalytic activity, and MC enhanced dispersion of metals and adsorption of substrates onto the catalyst surface. According to a recent report about adsorption of substrates onto MC by Katz *et al.*, the longer the chain length of cellulosic molecules becomes, the easier the cellulosic molecules adsorb onto the surface of MC.[167] The adsorption occurred by the CH hydrogens in the cellulosic molecules and aromatic rings of the MC surface. A small amount of Pt were also loaded onto Ni catalyst (Pt/Ni ratio = 0.45) (entries 42 and 43), in which Pt species enhanced catalytic activity.[150]

All the catalytic reactions described above need H_2 pressure higher than 2 MPa. Fukuoka *et al.* demonstrated that a highly dispersed Ru/AC afforded sorbitol (30%) and mannitol (8%) under as low as 0.8 MPa of H_2 (entry 44).[151] Recently, the yield of sorbitol increased up to 58% even under low H_2 pressure (0.7–0.9 MPa) by optimizing pre-treatment and reaction conditions (entry 45).[152] It was also reported that the hydrolytic hydrogenation of cellulose was promoted under low H_2 pressure (0.7 MPa) using a high Pt loading (24 mol% to cellulose) catalyst in a concentrated $H_4SiW_{12}O_{40}$ solution (0.70 M) (entry 46).[97] Moreover, the hydrolytic transfer-hydrogenation of cellulose to sorbitol (Figure 1.23) was also promoted by Ru/AC catalyst (entries 47 and 48).[151] In contrast, Ru/TiO_2, Ru/ZrO_2, Ru/Al_2O_3, and various metals (Rh, Ir,

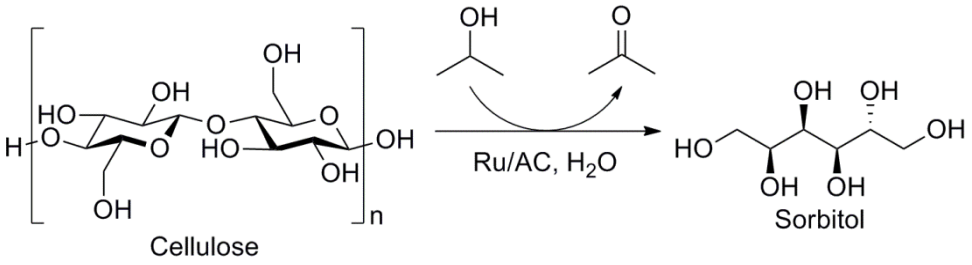


Figure 1.23. Hydrolytic transfer-hydrogenation of cellulose to sorbitol with 2-propanol.

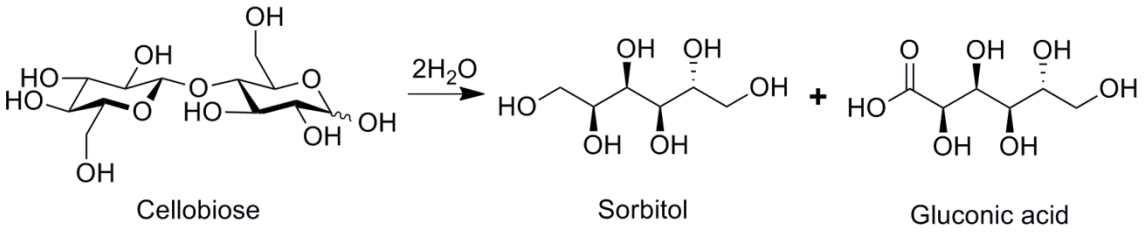


Figure 1.24. Simultaneous production of sorbitol and gluconic acid from cellobiose.

Pd, Pt, and Au) supported on AC were inactive for the hydrolytic transfer-hydrogenation. This reaction proceeds *via* the production of active hydrogen species from 2-propanol, in which the addition of H_2 gas is not necessary.

Recently, another type of reaction to produce sorbitol from β-glucan has been reported. Under Ar atmosphere, disproportionation including both reduction and oxidation of reducing ends in glucan molecules takes place over $Ru^{\delta+}$/AC, resulting in the simultaneous production of sorbitol and gluconic acid from cellobiose (Figure 1.24).[168] In this reaction, hydrogen species is provided by oxidation of a reducing end, and thus hydrogen sources such as H_2 gas and 2-propanol are not required.

1.3. Chitin

1.3.1. Property of chitin

Chitin is the most abundant *N*-containing biomass and 10^{11} tons of chitin is annually produced by crustaceans in the oceans.[169] The structure of chitin molecule is the same as that of cellulose molecule except for functional group at C2 position (Figure 1.25); C2 in chitin coordinates to an acetamido group instead of a

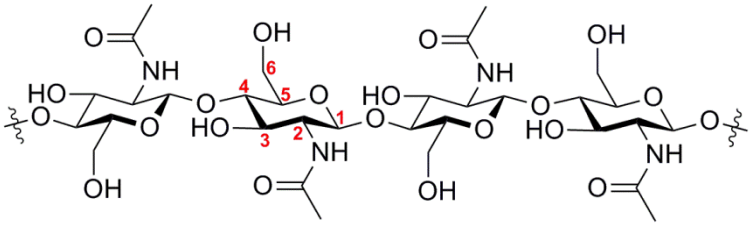


Figure 1.25. Structure of chitin.

hydroxyl group. The monomeric unit possessing acetamide is called *N*-acetylglucosamine (denoted as GlcNAc). Another *N*-containing polymer, chitosan, is also known as one of the ocean biomass resources and its building block is glucosamine (GlcN), which has an amino group at C2 position. Chitin has crystalline structures bearing a number of hydrogen bonds similar to cellulose, known as α-, β-, and γ-type, distinguished by packing manner. The molecules in α-chitin are assembled as antiparallel packing, those in β-chitin are parallel, and γ-chitin includes both packing senses.[170,171] Chitin itself is utilized in several areas, *e.g.*, biocompatible materials,[172] column packing materials for affinity chromatography,[173] catalyst supports owing to its high stability,[174] and source of *N*-doped carbons.[175]

In order to disrupt the crystal structure and improve reactivity of chitin, pre-treatment of chitin has been conducted as well as that of cellulose described in Section 1.2.2. Totani *et al.* reported that converge milling changed crystalline chitin to an amorphous form for 30 min, and *CrI* calculated from eq. 1.4[176] and the XRD patterns (Figure 1.26) decreased from 91% to 40%.[177]

$$CrI_{\mathrm{XRD}} = \frac{I_{20} - I_{16}}{I_{20}} \times 100 \qquad (1.4)$$

where I_{20} and I_{16} are diffraction intensities at 20° and 16° in XRD, respectively.

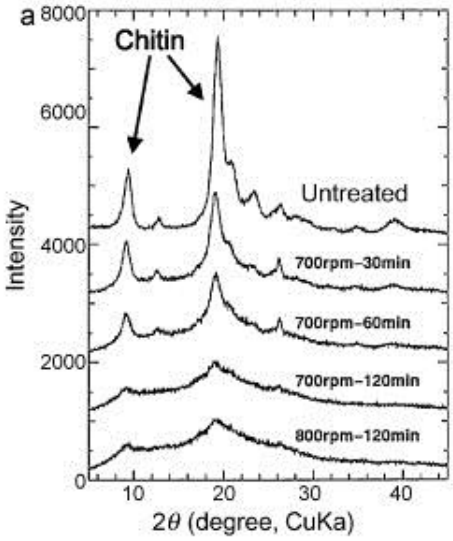


Figure 1.26. XRD patterns of converge milled crab chitin, reproduced from a reference.[177]

Osada *et al.* applied sub- and supercritical water to decompose crystal structure of chitin.[178] After supercritical water treatment at 673 K for 2 min, *CrI* decreased from 90% to 50%. The *d*-spacing determined from XRD slightly increased by the treatment. Both the decrease of *CrI* and increase of *d*-spacing may lead easy access of catalysts to chitin. They also demonstrated the combination of supercritical water treatment and converge milling.[179] *CrI* of the treated sample is 26%, clearly indicating that the combination is more effective than individual methods.

1.3.2. Transformation of chitin

Hydrolysis of chitin to GlcNAc (Figure 1.27) is a challenge since GlcNAc is a potential substrate as dietary supplements,[180] cosmetics,[9] and medicines against arthritic and inflammatory bowel diseases.[181] It is noteworthy that a deacetylated monomer GlcN is also used as dietary supplements but shows lower physiological activity and usability than GlcNAc.[182,183] Hence, the production of GlcNAc from chitin without deacetylation is favorable.

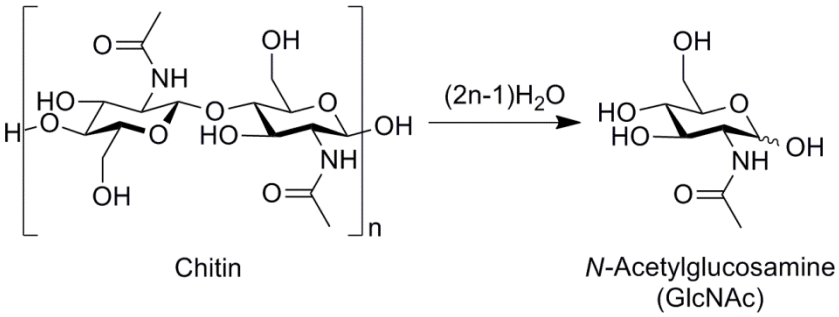


Figure 1.27. Hydrolysis of chitin to *N*-acetylglucosamine (GlcNAc).

Chitinase enzymes including endo- and exochitinase depolymerize crystalline chitin to GlcNAc in a high yield of 77%.[184] Although enzymes work under ambient conditions at 290 K, it takes 10 days to complete the reaction. Osada *et al.* drastically decreased the reaction time to 24 h by the supercritical water and converge milling pre-treatment as described in Section 1.3.1.[179] The resulting product was a dimer of GlcNAc, chitobiose, in 93% yield by using only endochitinase. Note that exochitinase or chitobiase is necessary for further depolymerization of chitobiose to GlcNAc. Chitinase enzymes recognize and selectively divide glycosidic bonds in chitin under mild conditions, in which chitin and products do not undergo deacetylation. Consequently, *N*-acetyl groups are completely preserved.

Hydrolysis of chitin in a concentrated HCl solution (15–36%) has also afforded GlcNAc in *ca.* 65% yield with preserving *N*-acetyl groups.[185,186] Intriguingly, the rate constant for hydrolysis of glycosidic bonds is >100 times larger than that of *N*-acetyl groups at 298–308 K in a 12 M of HCl solution. This large difference of reaction rates contributes to the high-yielding production of GlcNAc from chitin with suppressing deacetylation. However, this system suffers from several drawbacks including corrosive property of concentrated HCl and a huge amount of acidic waste.[9] In a diluted HCl solution (3 M), the ratio of the rate constants is only *ca.* 2 at 298–308 K, and both depolymerization and deacetylation happen.[186]

GlcNAc is derivatized to *N*-containing compounds (Figure 1.28) such as 3-acetamido-5-acetylfuran (3A5AF),[187,188] 2-acetamido-2,3-dideoxy-erythro-hex-2-enofuranose (Chromogen I),[189,190] 3-acetamido-5-(1,2-dihydroxyethyl)furan (Chromogen III),[189,190] *N*-acetylglucosaminic acid,[191] and 2-acetamido-2-deoxy-sorbitol,[192] which are biologically-active agents and potential precursors to medicines

and polymers. Recently, Yan and co-workers reported the direct production of 3A5AF from chitin by boric acid.[193] Boric acid gave a 3.6% yield of 3A5AF from crystalline chitin, and the additives of LiCl and HCl further increased the yield to 6.2%. They proposed that boric acid formed a bidentate complex with GlcNAc during the reaction. As a result, the substrate and intermediate easily underwent both activation and dehydration to form 3A5AF. Meanwhile, Cl^- species possibly disrupted hydrogen bonds in chitin and improved its reactivity; this function of Cl^- for chitin is the same as that for cellulose (see Section 1.2.2). Yan and co-workers also demonstrated the degradation of chitin in ethylene glycol in the presence of H_2SO_4 catalyst.[194] Both glycosidic bonds and *N*-acetamido groups were cleaved under their conditions, and the major product was 1-*O*-(2-hydroxyethyl)-2-amino-2-deoxyglucopyranoside (HADP, *ca.* 25%, Figure 1.29). The *N*-acetamido-groups-retaining product, 1-*O*-(2-hydroxyethyl)-2-acetamido-2-deoxyglucopyranoside (HAADP), was obtained in <10% yield.

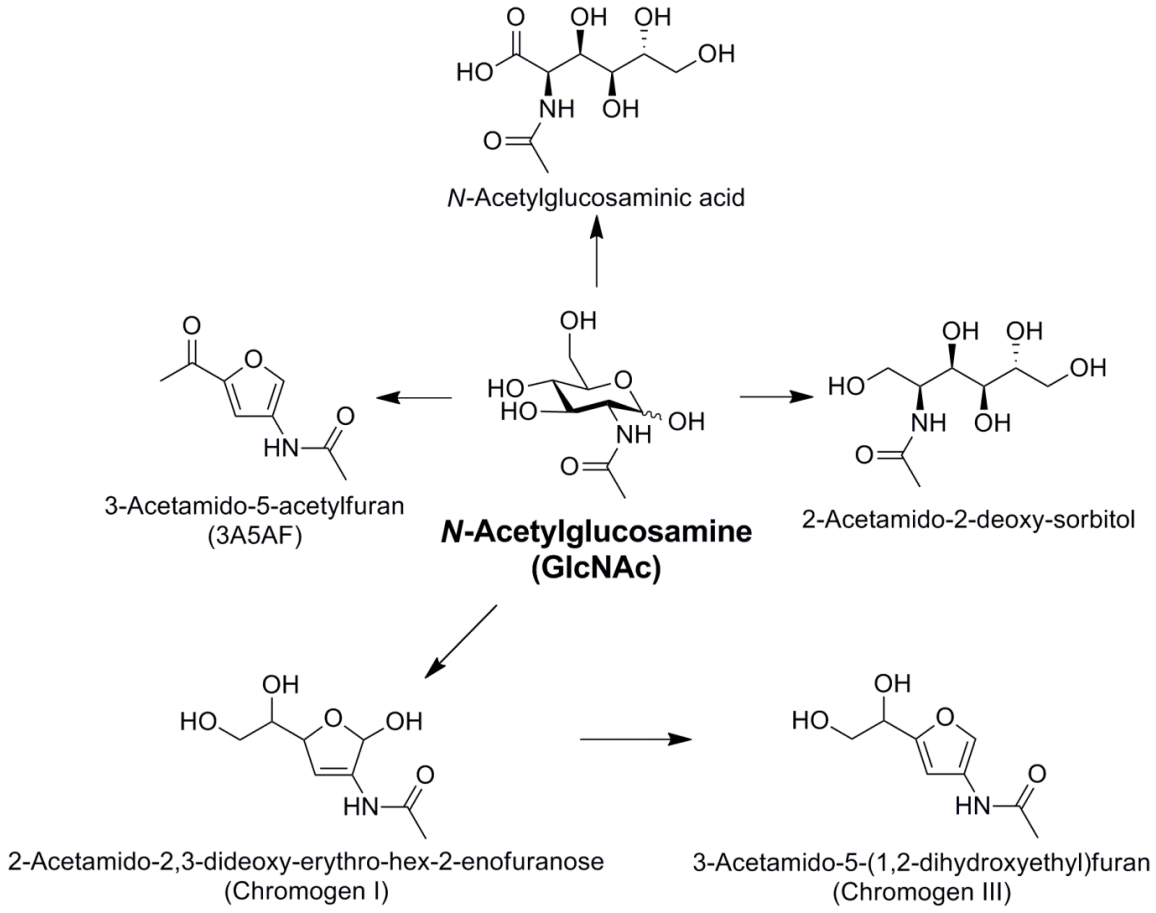


Figure 1.28. Derivatives of GlcNAc.

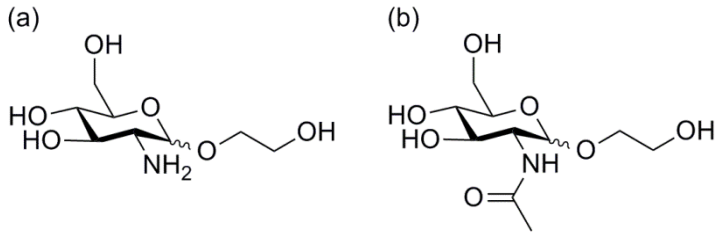


Figure 1.29. Structures of (a) 1-*O*-(2-hydroxyethyl)-2-amino-2-deoxyglucopyranoside (HADP) and (b) 1-*O*-(2-hydroxyethyl)-2-acetamido-2-deoxyglucopyranoside (HAADP).

1.4. Objectives of this work

As described above, the hydrolysis of cellulose to produce glucose is a challenge in biorefinery. H_2SO_4 and cellulase enzymes have been used for the depolymerization even in a commercial scale, but their complete recovery requires unprofitable processes. Hence, to date, heterogeneous catalysts have attracted great interests due to their ease of separation and reusability. In this area, most of researchers focused on strong acid catalysts, namely sulfonated materials, and indeed they efficiently hydrolyze pure cellulose to glucose in 75–92% yields as described in Section 1.2.5; however, their durability and S/C ratio are low in some cases. Additionally, for practical use, catalysts need to preserve their catalytic activity even in the presence of salts derived from raw biomass, but strong acids are easily deactivated by ion exchange. Interestingly, it has been found that unmodified carbons promote the hydrolysis of cellulose, and weakly acidic active sites are expected to resist ion exchange with salts. Hence, one of the objectives of this work is depolymerization of cellulose and raw biomass to sugars using carbon materials. In addition, the structure-activity correlation has been studied by physicochemical characterization, thermodynamics, kinetics, and model reactions.

Next, the author focuses on the efficient transformation of chitin with preserving acetyl groups, which is a grand challenge in ocean biomass refinery. The depolymerization of chitin without deacetylation has been achieved only using chitinase enzymes and concentrated HCl, and these systems suffer from several issues such as long reaction times, equipment corrosion by concentrated HCl, and a huge amount of acidic waste. Herein, the author has developed a new catalytic system to overcome these issues and depolymerize chitin to monomers without deacetylation.

The third target is selective production of 1,4-sorbitan from sorbitol, which is in high demand due to its wide applications. As described above, carbon catalysts hydrolyze cellulose to glucose, and glucose is easily hydrogenated to form sorbitol over supported metal catalysts even in an industrial scale. In contrast, the selective production of 1,4-sorbitan has been hampered by successive dehydration of 1,4-sorbitan. Hence, the author has investigated the dehydration of sorbitol using homo- and heterogeneous acids.

1.5. Constitution of the thesis

Chapter 1. General Introduction

The importance of biomass utilization in the current world situations is described. Subsequently, the chemical transformations of cellulose and chitin using catalysts and their remaining issues are discussed. Then, the goal of this research is stated.

Chapter 2. Hydrolysis of Cellulose to Glucose Using Carbon Catalysts

The objective in this chapter is high-yielding production of glucose from cellulose using carbon catalysts. The author demonstrates that alkali-activated carbons possessing significant catalytic activity for the hydrolysis of cellulose and a new pre-treatment method, named mix-milling, achieve one of the highest yields of glucose in any methods. The effects of mix-milling are investigated by characterization, model reactions, and kinetics.

Chapter 3. Mechanistic Study of Cellulose Hydrolysis by Carbon Catalysts

The catalysis of carbon materials for hydrolysis of glycosidic bonds is studied. The author proposes active sites on carbons and their catalysis from physicochemical characterization of carbons, model reactions, kinetics, and thermodynamics.

Chapter 4. Depolymerization of Chitin to Monomers with Preserving Acetyl Groups

The depolymerization of chitin to monomers with complete preservation of *N*-acetyl groups has been achieved. A combination of mechanocatalytic hydrolysis and solvolysis, hydrolysis and methanolysis,

provided monomers in good yields.

Chapter 5. Dehydration of Sorbitol to 1,4-Sorbitan Catalyzed by Acid Catalysts

The sorbitol dehydration catalyzed by H_2SO_4 is investigated in detail by product characterization and kinetics. The results represented here provide a blueprint of designing new solid catalysts for the selective synthesis of anhydropolyols.

Chapter 6. General Conclusions

This chapter summarizes all of the work and shows its significance in both scientific and social senses.

References

1. J. Goldemberg, *Science*, 2007, **315**, 808–810.
2. Y. Roman-Leshkov, C. J. Barrett, Z. Y. Liu, and J. A. Dumesic, *Nature*, 2007, **447**, 982–985.
3. J. N. Chheda, G. W. Huber, and J. A. Dumesic, *Angew. Chem. Int. Ed.*, 2007, **46**, 7164–7183.
4. A. Corma, S. Iborra, and A. Velty, *Chem. Rev.*, 2007, **107**, 2411–2502.
5. M. E. Himmel, S.-Y. Ding, D. K. Johnson, W. S. Adney, M. R. Nimlos, J. W. Brady, and T. D. Foust, *Science*, 2007, **315**, 804–807.
6. P. Gallezot, *ChemSusChem*, 2008, **1**, 734–737.
7. A. Fukuoka and P. L. Dhepe, *Chem. Rec.*, 2009, **9**, 224–235.
8. H. Kobayashi, H. Ohta, and A. Fukuoka, *Catal. Sci. Technol.*, 2012, **2**, 869–883.
9. J.-K. Chen, C.-R. Shen, and C.-L. Liu, *Mar. Drugs*, 2010, **8**, 2493–2516.
10. X. Chen and N. Yan, *Catal. Surv. Asia*, 2014, **18**, 164–176.
11. P. McKendry, *Bioresour. Technol.*, 2002, **83**, 37–46.
12. N. Mosier, C. Wyman, B. Dale, R. Elander, Y. Y. Lee, M. Holtzapple, and M. Ladisch, *Bioresour. Technol.*, 2005, **96**, 673–686.
13. J. Ralph, K. Lundquist, G. Brunow, F. Lu, H. Kim, P. Schatz, J. Marita, R. Hatfield, S. Ralph, J. Christensen, and W. Boerjan, *Phytochem. Rev.*, 2004, **3**, 29–60.

14. D. Meier and O. Faix, *Bioresour. Technol.*, 1999, **68**, 71–77.

15. D. Mohan, C. U. Pittman, and P. H. Steele, *Energy Fuels*, 2006, **20**, 848–889.

16. M. P. Pandey and C. S. Kim, *Chem. Eng. Technol.*, 2011, **34**, 29–41.

17. P. Zugenmaier, *Prog. Polym. Sci.*, 2001, **26**, 1341–1417.

18. R. Rinaldi and F. Schüth, *ChemSusChem*, 2009, **2**, 1096–1107.

19. J. Sugiyama, R. Vuong, and H. Chanzy, *Macromolecules*, 1991, **24**, 4168–4175.

20. P. Langan, Y. Nishiyama, and H. Chanzy, *Biomacromolecules*, 2001, **2**, 410–416.

21. J. Hayashi, A. Sufoka, J. Ohkita, and S. Watanabe, *J. Polym. Sci. Polym. Lett. Ed.*, 1975, **13**, 23–27.

22. N. Drisch and P. Herrbach, US Patent 2,705,184, 1955.

23. S. Kawano, K. Tajima, Y. Uemori, H. Yamashita, T. Erata, M. Munekata, and M. Takai, *DNA Res.*, 2002, **9** , 149–156.

24. K. R. Reddy, N. S. Kumar, P. S. Reddy, B. Sreedhar, and M. L. Kantam, *J. Mol. Catal. A: Chem.*, 2006, **252**, 12–16.

25. C. M. Cirtiu, A. F. Dunlop-Briere, and A. Moores, *Green Chem.*, 2011, **13**, 288–291.

26. H. Yano and S. Nakahara, US Patent 7,378,149, 2008.

27. K. Hayakawa, T. Kondo, M. Morita, and Y. Onda, US Patent 7,357,339, 2008.

28. H. Zhao, J. H. Kwak, Y. Wang, J. A. Franz, J. M. White, and J. E. Holladay, *Energy*, 2006, 807–811.

29. L. Segal, J. J. Creely, A. E. Martin Jr., and C. M. Conrad, *Text. Res. J.*, 1959, **29**, 786–794.

30. Y.-H. P. Zhang and L. R. Lynd, *Biotechnol. Bioeng.*, 2004, **88**, 797–824.

31. H. Wikberg and S. L. Maunu, *Carbohydr. Polym.*, 2004, **58**, 461–466.

32. S. Park, D. Johnson, C. Ishizawa, P. Parilla, and M. Davis, *Cellulose*, 2009, **16**, 641–647.

33. L. T. Fan, Y.-H. Lee, and D. R. Beardmore, *Biotechnol. Bioeng.*, 1981, **23**, 419–424.

34. M. Yabushita, H. Kobayashi, and A. Fukuoka, *Appl. Catal. B: Environ.*, 2014, **145**, 1–9.

35. T. Suzuki and H. Nakagami, *Eur. J. Pharm. Biopharm.*, 1999, **47**, 225–230.

36. R. Avolio, I. Bonadies, D. Capitani, M. E. Errico, G. Gentile, and M. Avella, *Carbohydr. Polym.*, 2012, **87**, 265–273.

37. W. Deng, X. Tan, W. Fang, Q. Zhang, and Y. Wang, *Catal. Lett.*, 2009, **133**, 167–174.

38. Y. Zheng, H.-M. Lin, and G. T. Tsao, *Biotechnol. Prog.*, 1998, **14**, 890–896.

39. P. Alvira, E. Tomás-Pejó, M. Ballesteros, and M. J. Negro, *Bioresour. Technol.*, 2010, **101**, 4851–4861.

40. V. S. Chang and M. T. Holtzapple, *Appl. Biochem. Biotechnol.*, 2000, **84–86**, 5–37.

41. A. Shrotri, H. Kobayashi, and A. Fukuoka, *J. Jpn. Petrol. Inst.*, 2015, **58**, 1–8.

42. J. Strachan, *Nature*, 1938, **141**, 332–333.

43. Z. Fang and J. A. Koziński, *Proc. Combust. Inst.*, 2000, **28**, 2717–2725.

44. H. Zhao, J. H. Kwak, Y. Wang, J. A. Franz, J. M. White, and J. E. Holladay, *Carbohydr. Polym.*, 2007, **67**, 97–103.

45. C. L. McCormick, P. A. Callais, and B. H. Hutchinson, *Macromolecules*, 1985, **18**, 2394–2401.

46. T. Röder, B. Morgenstern, N. Schelosky, and O. Glatter, *Polymer*, 2001, **42**, 6765–6773.

47. W. Burchard, N. Habermann, P. Klüfers, B. Seger, and U. Wilhelm, *Angew. Chem. Int. Ed.*, 1994, **33**, 884–887.

48. R. P. Swatloski, S. K. Spear, J. D. Holbrey, and R. D. Rogers, *J. Am. Chem. Soc.*, 2002, **124**, 4974–4975.

49. J. F. Brennecke and E. J. Maginn, *AIChE J.*, 2001, **47**, 2384–2389.

50. R. Lamed and J. G. Zeikus, *J. Bacteriol.*, 1980, **141**, 1251–1257.

51. Y. Lin and S. Tanaka, *Appl. Microbiol. Biotechnol.*, 2006, **69**, 627–642.

52. Y. Sun and J. Cheng, *Bioresour. Technol.*, 2002, **83**, 1–11.

53. P. Gallezot, N. Nicolaus, G. Flèche, P. Fuertes, and A. Perrard, *J. Catal.*, 1998, **180**, 51–55.

54. H. Li, W. Wang, and J. F. Deng, *J. Catal.*, 2000, **191**, 257–260.

55. H. Li, H. Li, and J.-F. Deng, *Catal. Today*, 2002, **74**, 53–63.

56. B. W. Hoffer, E. Crezee, F. Devred, P. R. M. Mooijman, W. G. Sloof, P. J. Kooyman, A. D. van Langeveld, F. Kapteijn, and J. A. Moulijn, *Appl. Catal. A: Gen.*, 2003, **253**, 437–452.

57. T. Werpy, G. Petersen, A. Aden, J. Bozell, J. Holladay, J. White, A. Manheim, D. Elliot, L. Lasure, S. Jones, M. Gerber, K. Ibsen, L. Lumberg, and S. Kelley, "Top Value Added Chemicals From Biomass Volume I: Results of Screening for Potential Candidates from Sugars and Synthesis Gas," http://www.dtic.mil/cgi-bin/GetTRDoc?Location=U2&doc=GetTRDoc.pdf&AD=ADA436528 (accessed Nov. 20, 2014).

58. J. Zhang, J. Li, S.-B. Wu, and Y. Liu, *Ind. Eng. Chem. Res.*, 2013, **52**, 11799–11815.

59. K. Chen, M. Tamura, Z. Yuan, Y. Nakagawa, and K. Tomishige, *ChemSusChem*, 2013, **6**, 613–621.

60. M. Shiramizu and F. D. Toste, *Angew. Chem. Int. Ed.*, 2012, **51**, 8082–8086.

61. H. Kobayashi and A. Fukuoka, *Green Chem.*, 2013, **15**, 1740–1763.

62. T. Yoshioka, B. Sternberg, and A. T. Florence, *Int. J. Pharm.*, 1994, **105**, 1–6.

63. M. Fuji, M. Akita, and T. Tanaka, US Patent 2010/0190953, 2010.

64. B. J. P. Jansen, J. H. Kamps, H. Looij, E. Kung, L. Prada, and W. J. D. Steendam, US Patent 7,666,972, 2009.

65. A. Oda, E. Kitazono, T. Miyake, M. Kinoshita, and M. Saito, US Patent 8,017,722, 2011.

66. R. M. Gohil, *Polym. Eng. Sci.*, 2009, **49**, 544–553.

67. F. Fenouillot, A. Rousseau, G. Colomines, R. Saint-Loup, and J.-P. Pascault, *Prog. Polym. Sci.*, 2010, **35**, 578–622.

68. M. A. Andrews, K. K. Bhatia, and P. J. Fagan, US Patent 6,689,892, 2004.

69. P. Sun, D. H. Yu, Y. Hu, Z. C. Tang, J. J. Xia, H. Li, and H. Huang, *Korean J. Chem. Eng.*, 2011, **28**, 99–105.

70. M. Gu, D. Yu, H. Zhang, P. Sun, and H. Huang, *Catal. Lett.*, 2009, **133**, 214–220.

71. J. Xia, D. Yu, Y. Hu, B. Zou, P. Sun, H. Li, and H. Huang, *Catal. Commun.*, 2011, **12**, 544–547.

72. C. Montassier, J. C. Ménézo, J. Moukolo, J. Naja, L. C. Hoang, J. Barbier, and J. P. Boitiaux, *J. Mol. Catal.*, 1991, **70**, 65–84.

73. K. M. Moore, A. J. Sanborn, and P. Bloom, US Patent 7,439,352, 2008.

74. N. A. Khan, D. K. Mishra, I. Ahmed, J. W. Yoon, J.-S. Hwang, and S. H. Jhung, *Appl. Catal. A: Gen.*, 2013, **452**, 34–38.

75. I. Ahmed, N. A. Khan, D. K. Mishra, J. S. Lee, J.-S. Hwang, and S. H. Jhung, *Chem. Eng. Sci.*, 2013, **93**, 91–95.

76. A. J. Sanborn, US Patent 7,420,067, 2008.

77. A. Liu, and C. C. Luckett, US Patent 7,982,059, 2011.

78. Y. Morita, S. Furusato, A. Takagaki, S. Hayashi, R. Kikuchi, and S. T. Oyama, *ChemSusChem*, 2014, **7**, 748–752.

79. Y. Román-Leshkov, M. Moliner, J. A. Labinger, and M. E. Davis, *Angew. Chem. Int. Ed.*, 2010, **49**, 8954–8957.

80. G. R. Akien, L. Qi, and I. T. Horváth, *Chem. Commun.*, 2012, **48**, 5850–5852.

81. K. Nakajima, R. Noma, M. Kitano, and M. Hara, *J. Mol. Catal. A: Chem.*, 2014, **388–389**, 100–105.

82. M. Shiramizu and F. D. Toste, *Chem. Eur. J.*, 2011, **17**, 12452–12457.

83. C. L. Williams, C.-C. Chang, P. Do, N. Nikbin, S. Caratzoulas, D. G. Vlachos, R. F. Lobo, W. Fan, and P. J. Dauenhauer, *ACS Catal.*, 2012, **2**, 935–939.

84. Y. Y. Gorbanev, S. K. Klitgaard, J. M. Woodley, C. H. Christensen, and A. Riisager, *ChemSusChem*, 2009, **2**, 672–675.

85. S. E. Davis, L. R. Houk, E. C. Tamargo, A. K. Datye, and R. J. Davis, *Catal. Today*, 2011, **160**, 55–60.

86. A. A. Rosatella, S. P. Simeonov, R. F. M. Frade, and C. A. M. Afonso, *Green Chem.*, 2011, **13**, 754–793.

87. J. J. Bozell, L. Moens, D. C. Elliott, Y. Wang, G. G. Neuenscwander, S. W. Fitzpatrick, R. J. Bilski, and J. L. Jarnefeld, *Resour. Conserv. Recycl.*, 2000, **28**, 227–239.

88. R. M. West, Z. Y. Liu, M. Peter, and J. A. Dumesic, *ChemSusChem*, 2008, **1**, 417–424.

89. C. N. Hamelinck, G. van Hooijdonk, and A. P. C. Faaij, *Biomass Bioenergy*, 2005, **28**, 384–410.

90. M. Balat, *Energy Convers. Manag.*, 2011, **52**, 858–875.

91. W. L. Faith, *Ind. Eng. Chem.*, 1945, **37**, 9–11.

92. S. M. Hick, C. Griebel, D. T. Restrepo, J. H. Truitt, E. J. Buker, C. Bylda, and R. G. Blair, *Green Chem.*, 2010, **12**, 468–474.

93. N. Meine, R. Rinaldi, and F. Schüth, *ChemSusChem*, 2012, **5**, 1449–1454.

94. A. Shrotri, L. K. Lambert, A. Tanksale, and J. Beltramini, *Green Chem.*, 2013, **15**, 2761–2768.

95. J. Hilgert, N. Meine, R. Rinaldi, and F. Schüth, *Energy Environ. Sci.*, 2013, **6**, 92–96.

96. A. Shrotri, H. Kobayashi, A. Tanksale, A. Fukuoka, and J. Beltramini, *ChemCatChem*, 2014, **6**, 1349–1356.

97. Y. Ogasawara, S. Itagaki, K. Yamaguchi, and N. Mizuno, *ChemSusChem*, 2011, **4**, 519–525.

98. K. Shimizu, H. Furukawa, N. Kobayashi, Y. Itaya, and A. Satsuma, *Green Chem.*, 2009, **11**, 1627–1632.

99. L. P. Walker and D. B. Wilson, *Bioresour. Technol.*, 1991, **36**, 3–14.

100. J. Medve, J. Ståhlberg, and F. Tjerneld, *Appl. Biochem. Biotechnol.*, 1997, **66**, 39–56.

101. G. Davies and B. Henrissat, *Structure*, 1995, **3**, 853–859.

102. J. D. McCarter and G. S. Withers, *Curr. Opin. Struct. Biol.*, 1994, **4**, 885–892.

103. G. H. Emert, and P. J. Blotkamp, US Patent 4,220,721, 1980.

104. J. Woodward, US Patent 4,840,904, 1989.

105. A. Garcia, S. Oh, and C. R. Engler, *Biotechnol. Bioeng.*, 1989, **33**, 321–326.

106. S. B. Hartono, S. Z. Qiao, J. Liu, K. Jack, B. P. Ladewig, Z. Hao, and G. Q. M. Lu, *J. Phys. Chem. C*, 2010, **114**, 8353–8362.

107. R. H.-Y. Chang, J. Jang, and K. C.-W. Wu, *Green Chem.*, 2011, **13**, 2844–2850.

108. C. Divne, J. Ståhlberg, T. T. Teeri, and T. A. Jones, *J. Mol. Biol.*, 1998, **275**, 309–325.

109. M. Sasaki, B. Kabyemela, R. Malaluan, S. Hirose, N. Takeda, T. Adschiri, and K. Arai, *J. Supercrit. Fluids*, 1998, **13**, 261–268.

110. M. Sasaki, M. Furukawa, K. Minami, T. Adschiri, and K. Arai, *Ind. Eng. Chem. Res.*, 2002, **41**, 6642–6649.

111. T. Harada, Y. Tokai, A. Kimura, S. Ikeda, and M. Matsumura, *RSC Adv.*, 2014, **4**, 26838–26842.

112. C. Li and Z. K. Zhao, *Adv. Synth. Catal.*, 2007, **349**, 1847–1850.

113. R. Rinaldi, R. Palkovits, and F. Schüth, *Angew. Chem. Int. Ed.*, 2008, **47**, 8047–8050.

114. R. Rinaldi, N. Meine, J. vom Stein, R. Palkovits, and F. Schüth, *ChemSusChem*, 2010, **3**, 266–276.

115. C. Zhang, Z. Fu, Y. C. Liu, B. Dai, Y. Zou, X. Gong, Y. Wang, X. Deng, H. Wu, Q. Xu, K. R. Steven, and D. Yin, *Green Chem.*, 2012, **14**, 1928–1934.

116. S. Suganuma, K. Nakajima, M. Kitano, D. Yamaguchi, H. Kato, and S. Hayashi, *J. Am. Chem. Soc.*, 2008, **130**, 12787–12793.

117. A. Onda, T. Ochi, and K. Yanagisawa, *Green Chem.*, 2008, **10**, 1033–1037.

118. S. Van de Vyver, L. Peng, J. Geboers, H. Schepers, F. de Clippel, C. J. Gommes, B. Goderis, P. A. Jacobs, and B. F. Sels, *Green Chem.*, 2010, **12**, 1560–1563.

119. J. Pang, A. Wang, M. Zheng, and T. Zhang, *Chem. Commun.*, 2010, **46**, 6935–6937.

120. D. Lai, L. Deng, J. Li, B. Liao, Q. Guo, and Y. Fu, *ChemSusChem*, 2011, **4**, 55–58.

121. A. Takagaki, M. Nishimura, S. Nishimura, and K. Ebitani, *Chem. Lett.*, 2011, **40**, 1195–1197.

122. L. Shuai and X. Pan, *Energy Environ. Sci.*, 2012, **5**, 6889–6894.

123. H. Kobayashi, T. Komanoya, K. Hara, and A. Fukuoka, *ChemSusChem*, 2010, **3**, 440–443.

124. X. Zhao, J. Wang, C. Chen, Y. Huang, A. Wang, and T. Zhang, *Chem. Commun.*, 2014, **50**, 3439–3442.

125. D. Yamaguchi, M. Kitano, S. Suganuma, K. Nakajima, H. Kato, and M. Hara, *J. Phys. Chem. C*, 2009, **113**, 3181–3188.

126. K. Fukuhara, K. Nakajima, M. Kitano, H. Kato, S. Hayashi, and M. Hara, *ChemSusChem*, 2011, **4**, 778–784.

127. X. Mo, D. E. López, K. Suwannakarn, Y. Liu, E. Lotero, J. G. Goodwin Jr., and C. Lu, *J. Catal.*, 2008, **254**, 332–338.

128. M. Kitano, D. Yamaguchi, S. Suganuma, K. Nakajima, H. Kato, S. Hayashi, and M. Hara, *Langmuir*, 2009, **25**, 5068–5075.

129. K. Nakajima and M. Hara, *ACS Catal.*, 2012, **2**, 1296–1304.

130. M. Hara, *J. Phys. Chem. C*, 2009, **113**, 3181–3188.

131. A. Onda, T. Ochi, and K. Yanagisawa, *Top. Catal.*, 2009, **52**, 801–807.

132. D. Lai, L. Deng, Q. Guo, and Y. Fu, *Energy Environ. Sci.*, 2011, **4**, 3552–3557.

133. R. B. Merrifield, *J. Am. Chem. Soc.*, 1963, **85**, 2149–2154.

134. T. Komanoya, H. Kobayashi, K. Hara, W.-J. Chun, and A. Fukuoka, *Appl. Catal. A Gen.*, 2011, **407**, 188–194.

135. C. Loerbroks, R. Rinaldi, and W. Thiel, *Chem. Eur. J.*, 2013, **19**, 16282–16294.

136. P.-W. Chung, A. Charmot, O. A. Olatunji-Ojo, K. A. Durkin, and A. Katz, *ACS Catal.*, 2013, **4**, 302–310.

137. O. M. Gazit, A. Charmot, and A. Katz, *Chem. Commun.*, 2011, **47**, 376–378.

138. O. M. Gazit and A. Katz, *Langmuir*, 2011, **28**, 431–437.

139. O. M. Gazit and A. Katz, *J. Am. Chem. Soc.*, 2013, **135**, 4398–4402.

140. A. A. Balandin, N. A. Vasyunina, G. S. Barysheva, S. V Chepigo, and M. M. Dubinin, *Bull. Acad. Sci. USSR, Div. Chem. Sci.*, 1957, **6**, 403–404.

141. A. Fukuoka and P. L. Dhepe, *Angew. Chem. Int. Ed.*, 2006, **45**, 5161–5163.

142. C. Luo, S. Wang, and H. Liu, *Angew. Chem. Int. Ed.*, 2007, **46**, 7636–7639.

143. H. Kobayashi, Y. Ito, T. Komanoya, Y. Hosaka, P. L. Dhepe, K. Kasai, K. Hara, and A. Fukuoka, *Green Chem.*, 2011, **13**, 326–333.

144. J. Geboers, S. Van de Vyver, K. Carpentier, P. Jacobs, and B. Sels, *Green Chem.*, 2011, **13**, 2167–2174.

145. L.-N. Ding, A.-Q. Wang, M.-Y. Zheng, and T. Zhang, *ChemSusChem*, 2010, **3**, 818–821.

146. P. Yang, H. Kobayashi, K. Hara, and A. Fukuoka, *ChemSusChem*, 2012, **5**, 920–926.

147. S. de Vyver, J. Geboers, M. Dusselier, H. Schepers, T. Vosch, L. Zhang, G. V. Tendeloo, P. A. Jacobs, and B. F. Sels, *ChemSusChem*, 2010, **3**, 698–701.

148. S. de Vyver, J. Geboers, W. Schutyser, M. Dusselier, P. Eloy, E. Dornez, J. W. Seo, C. M. Courtin, E. M. Gaigneaux, P. A. Jacobs, and B. F. Sels, *ChemSusChem*, 2012, **5**, 1549–1558.

149. J. Pang, A. Wang, M. Zheng, Y. Zhang, Y. Huang, X. Chen, and T. Zhang, *Green Chem.*, 2012, **14**, 614–617.

150. A. Shrotri, A. Tanksale, J. N. Beltramini, H. Gurav, and S. V. Chilukuri, *Catal. Sci. Technol.*, 2012, **2**, 1852–1858.

151. H. Kobayashi, H. Matsuhashi, T. Komanoya, K. Hara, and A. Fukuoka, *Chem. Commun.*, 2011, **47**, 2366–2368.

152. T. Komanoya, H. Kobayashi, K. Hara, W.-J. Chun, and A. Fukuoka, *ChemCatChem*, 2014, **6**, 230–236.

153. A. A. Balandin, N. A. Vasunina, S. V Chepigo and G. S. Barysheva, *Dokl. Akad. Nauk SSSR*, 1959, **128**, 941–944.

154. H. Kobayashi, Y. Hosaka, K. Hara, B. Feng, Y. Hirosaki, and A. Fukuoka, *Green Chem.*, 2014, **16**, 637–644.

155. L. Negahdar, J. U. Oltmanns, S. Palkovits, and R. Palkovits, *Appl. Catal. B: Environ.*, 2014, **147**, 677–683.

156. P. Jacobs and H. Hinnekens, EP Patent 0,329,923, 1989.

157. S. Deguchi, K. Tsujii, and K. Horikoshi, *Chem. Commun.*, 2006, 3293–3295.

158. H. Fukuhara, F. Matsunaga, M. Yasuhara, S. Araki, T. Isaka, US Patent 5,227,563, 1993.

159. V. Jollet, F. Chambon, F. Rataboul, A. Cabiac, C. Pinel, E. Guillon, and N. Essayem, *Green Chem.*, 2009, **11**, 2052–2060.

160. V. Jollet, F. Chambon, F. Rataboul, A. Cabiac, C. Pinel, E. Guillon, and N. Essayem, *Top. Catal.*, 2010, **53**, 1254–1257.

161. M. Liu, W. Deng, Q. Zhang, Y. Wang, and Y. Wang, *Chem. Commun.*, 2011, **47**, 9717–9719.

162. R. M. Ravenelle, F. Z. Diallo, J. C. Crittenden, and C. Sievers, *ChemCatChem*, 2012, **4**, 492–494.

163. N. Yan, C. Zhao, C. Luo, P. J. Dyson, H. Liu, and Y. Kou, *J. Am. Chem. Soc.*, 2006, **128**, 8714–8715.

164. F. H. Sweeton, R. E. Mesmer, and C. F. Baes Jr., *J. Solution Chem.*, 1974, **3**, 191–214.

165. W. L. Marshall, *J. Phys. Chem. Ref. Data*, 1981, **10**, 295–304.

166. R. Palkovits, K. Tajvidi, A. M. Ruppert, and J. Procelewska, *Chem. Commun.*, 2011, **47**, 576–578.

167. P.-W. Chung, A. Charmot, O. M. Gazit, and A. Katz, *Langmuir*, 2012, **28**, 15222–15232.

168. T. Komanoya, H. Kobayashi, K. Hara, W.-J. Chun, and A. Fukuoka, *J. Energy Chem.*, 2013, **22**, 290–295.

169. B. A. Stankiewicz, D. E. G. Briggs, R. P. Evershed, M. B. Flannery, and M. Wuttke, *Science*, 1997, **276**, 1541–1543.

170. J. Sugiyama, C. Boisset, M. Hashimoto, and T. Watanabe, *J. Mol. Biol.*, 1999, **286**, 247–255.

171. M.-K. Jang, B.-G. Kong, Y.-I. Jeong, C. H. Lee, and J.-W. Nah, *J. Polym. Sci. Part A Polym. Chem.*, 2004, **42**, 3423–3432.

172. E. Khor and L. Y. Lim, *Biomaterials*, 2003, **24**, 2339–2349.

173. R. Bloch and M. M. Burger, *Biochem. Biophys. Res. Commun.*, 1974, **58**, 13–19.

174. B. Krajewska, *Enzyme Microb. Technol.*, 2004, **35**, 126–139.

175. R. J. White, M. Antonietti, and M.-M. Titirici, *J. Mater. Chem.*, 2009, **19**, 8645–8650.

176. R. L. Lavall, O. B. G. Assis, and S. P. Campana-Filho, *Bioresour. Technol.*, 2007, **98**, 2465–2472.

177. Y. S. Nakagawa, Y. Oyama, N. Kon, M. Nikaido, K. Tanno, J. Kogawa, S. Inomata, A. Masui, A. Yamamura, M. Kawaguchi, Y. Matahira, and K. Totani, *Carbohydr. Polym.*, 2011, **83**, 1843–1849.

178. M. Osada, C. Miura, Y. S. Nakagawa, M. Kaihara, M. Nikaido, and K. Totani, *Carbohydr. Polym.*, 2012, **88**, 308–312.

179. M. Osada, C. Miura, Y. S. Nakagawa, M. Kaihara, M. Nikaido, and K. Totani, *Carbohydr. Polym.*, 2013, **92**, 1573–1578.

180. A. Grigorian, L. Araujo, N. N. Naidu, D. J. Place, B. Choudhury, and M. Demetriou, *J. Biol. Chem.* , 2011, **286** , 40133–40141.

181. S. Salvatore, R. Heuschkel, S. Tomlin, S. E. Davies, S. Edwards, J. A. Walker-Smith, I. French, and S. H. Murch, *Aliment. Pharmacol. Ther.*, 2000, **14**, 1567–1579.

182. L. I. Álvarez-Añorve, M. L. Calcagno, and J. Plumbridge, *J. Bacteriol.* , 2005, **187**, 2974–2982.

183. A. R. Shikhman, K. Kuhn, N. Alaaeddine, and M. Lotz, *J. Immunol.* , 2001, **166**, 5155–5160.

184. H. Sashiwa, S. Fujishima, N. Yamano, N. Kawasaki, A. Nakayama, E. Muraki, K. Hiraga, K. Oda, and S. Aiba, *Carbohydr. Res.*, 2002, **337**, 761–763.

185. K. M. Vårum, M. H. Ottøy, and O. Smidsrød, *Carbohydr. Polym.*, 2001, **46**, 89–98.

186. A. Einbu and K. M. Vårum, *Biomacromolecules*, 2007, **8**, 309–314.

187. K. W. Omari, L. Dodot, and F. M. Kerton, *ChemSusChem*, 2012, **5**, 1767–1772.

188. M. W. Drover, K. W. Omari, J. N. Murphy, and F. M. Kerton, *RSC Adv.*, 2012, **2**, 4642–4644.

189. M. Osada, K. Kikuta, K. Yoshida, K. Totani, M. Ogata, and T. Usui, *Green Chem.*, 2013, **15**, 2960–2966.

190. M. Osada, K. Kikuta, K. Yoshida, K. Totani, M. Ogata, and T. Usui, *RSC Adv.*, 2014, **4**, 33651–33657.

191. Y. Ohmi, S. Nishimura, and K. Ebitani, *ChemSusChem*, 2013, **6**, 2259–2262.

192. F. D. Bobbink, J. Zhang, Y. Pierson, X. Chen, and N. Yan, *Green Chem.*, in press, DOI: 10.1039/C4GC01631A.

193. X. Chen, S. L. Chew, F. M. Kerton, and N. Yan, *Green Chem.*, 2014, **16**, 2204–2212.

194. Y. Pierson, X. Chen, F. D. Bobbink, J. Zhang, and N. Yan, *ACS Sustainable Chem. Eng.*, 2014, **2**, 2081–2089.

Chapter 2

Hydrolysis of Cellulose to Glucose Using Carbon Catalysts

High-yielding one-pot production of glucose from cellulose has been achieved by using alkali-activated carbon K26 as a catalyst bearing weak acid sites. The hydrolysis of solid cellulose by solid catalysts is limited due to low physical contact between the substrate and the catalyst, but a new ball-milling pre-treatment, ball-milling cellulose and carbon together (named mix-milling), has drastically improved the hydrolysis rate. As a result, 90% yield and 97% selectivity of water-soluble glucans have been obtained by K26 at 453 K for 20 min. Microscopy, model reactions, and kinetic studies have shown that the mix-milling pre-treatment selectively accelerates solid-solid reaction (cellulose to water-soluble oligomers), but does not liquid-solid reaction (oligomers to glucose). Hence, a trace amount of HCl (0.012 wt%) is used to depolymerize oligomers to glucose and as high as 88% yield of glucose with 90% selectivity has been achieved. The mix-milling pre-treatment is also effective for the hydrolysis of cellulose/hemicellulose in bagasse kraft pulp to hexoses/pentoses.

2.1. Introduction

Cellulose is a potential and attractive alternative to petrol to reduce emission of greenhouse gases as the biomass is an abundant, non-edible, and renewable carbon source.[1–6] The monomer of cellulose, glucose, is a platform chemical for the production of a variety of useful chemicals such as polymers, medicines, surfactants, gasoline, and diesel fuels (Section 1.2.3).[7–9] In addition, cello-oligosaccharides are health-promoting foods that improve bowel functions.[10] Accordingly, the reaction route of cellulose to glucose and oligosaccharides (Figure 2.1) will be a mainstream in the next-generation biorefinery, which will substitute current processes using food biomass; however, realizing this vision has been hampered by the recalcitrance of cellulose and various practical difficulties as described in Chapter 1.

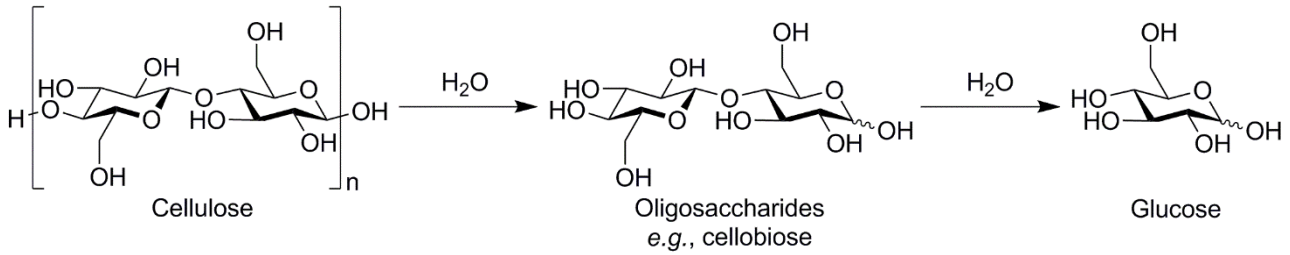


Figure 2.1. Hydrolysis of cellulose to glucose *via* oligosaccharides.

The hydrolysis of cellulose has been performed with various solid catalysts as heterogeneous catalysts are advantageous over homogeneous ones in terms of easy separation from products.[6,11–13] In the previous work, it was found that unmodified mesoporous carbon CMK-3 catalyzed the hydrolysis of cellulose.[14,15] Fukuoka *et al.* has proposed that the active sites of CMK-3 are weakly acidic groups.[15] Hence, it is noteworthy that CMK-3 is contrasting to strong acids represented by sulfonated carbons[16,17] that have been widely studied in hydrolysis of cellulose. Sulfonated catalysts possibly suffer from the leaching of SO_3H groups in hot-compressed water,[18] whereas weakly acidic carbons such as CMK-3 are highly hydrothermally stable. Furthermore, salts derived from raw biomass easily deactivate strong acids by ion exchange; in contrast, weak acids potentially preserve their catalytic activities even in the presence of salts.[19,20] These great advantages of weakly acidic carbons may breakthrough the barrier of practical hydrolysis of cellulosic

biomass. However, the highest glucose yield obtained by CMK-3 was only 16%, and the synthesis of CMK-3 was complicated in the practical perspective. Hence, in this chapter, the author has aimed the high-yielding synthesis of glucose from cellulose and real cellulosic biomass using more common carbon materials.

2.2. Experimental

2.2.1. Reagents

Microcrystalline cellulose	Column chromatography grade, 102331, Merck
Bagasse kraft pulp	Harvested in Okinawa Prefecture, composition determined by the established method (see Section 2.2.4):[21] cellulose (59 wt%), hemicellulose [27 wt% (xylan 25 wt%, arabinan (2 wt%)], and lignin (9 wt%), Showa Denko
K26	Alkali-activated carbon (not for sale), Showa Denko
K20	Alkali-activated carbon (not for sale), Showa Denko
MSP20	Alkali-activated carbon, Kansai Coke & Chemicals
BA50	Steam-activated carbon, Ajinomoto Fine Techno
SX Ultra	Steam-activated carbon, Norit, denoted as SX
Vulcan XC72	Carbon black, Cabot, denoted as XC72
Black Pearls 2000	Carbon black, Cabot, denoted as BP2000
Pluronic P123	Triblock copolymer, $HO(CH_2CH_2O)_{20}(CH_2CH(CH_3)O)_{70}(CH_2CH_2O)_{20}H$, Sigma-Aldrich
Tetraethyl orthosilicate	>99.0%, Sigma-Aldrich, denoted as TEOS
Ethanol	Special grade, Wako Pure Chemical Industries
Sulfuric acid	96–98%, super special grade, Wako Pure Chemical Industries
Sucrose	Special grade, Wako Pure Chemical Industries
Hydrofluoric acid	46–48%, special grade, Wako Pure Chemical Industries
Calcium gluconate	Special grade, Wako Pure Chemical Industries

Amberlyst 70	Sulfonic acid cation exchange resin, Organo
JRC-Z5-90H	Proton-type MFI zeolite, Si/Al ratio = 45, Catalysis Society of Japan, denoted as H-MFI
JRC-Z-HM90	Proton-type MOR zeolite, Si/Al ratio = 45, Catalysis Society of Japan, denoted as H-MOR
Q-6	Amorphous silica, Fuji Silysia Chemical, denoted as SiO_2
Silica-alumina	Grade 135, Sigma-Aldrich, denoted as SiO_2-Al_2O_3
JRC-TIO-4(2)	Titania, Catalysis Society of Japan, denoted as TiO_2
Hydrochloric acid	35–37%, special grade, Wako Pure Chemical Industries
Acetic acid	>99.7%, special grade, Wako Pure Chemical Industries
Sodium acetate	Special grade, Wako Pure Chemical Industries
Sodium chloride	Special grade, Wako Pure Chemical Industries
Benzoic acid	Special grade, Wako Pure Chemical Industries
Cellohexaose	>95%, Seikagaku Biobusiness
Cellopentaose	>95%, Seikagaku Biobusiness
Cellotetraose	>97%, Seikagaku Biobusiness
Cellotriose	>97%, Seikagaku Biobusiness
D(+)-Cellobiose	Special grade, Kanto Chemical
D(+)-Glucose	Special grade, Kanto Chemical
D(+)-Mannose	Special grade, Wako Pure Chemical Industries
D(–)-Fructose	Special grade, Kanto Chemical
1,6-Anhydro-β-D-glucopyranose	99%, Wako Pure Chemical Industries, denoted as levoglucosan
5-Hydroxymethylfurfural	99%, Sigma-Aldrich, denoted as 5-HMF
Furfural	>98.0%, Tokyo Chemical Industry
Xylobiose	Biochemical grade, Wako Pure Chemical Industries
D(+)-Xylose	Special grade, Wako Pure Chemical Industries
D(–)-Arabinose	Special grade, Wako Pure Chemical Industries

Sodium sulfide	Special grade, Wako Pure Chemical Industries
Distilled water	Wako Pure Chemical Industries
Distilled water	For HPLC, Wako Pure Chemical Industries
Acetonitrile	For HPLC, Wako Pure Chemical Industries
Milli-Q water	Prepared by an ultrapure H_2O production system (Sartorius, arium 611UF)
Lithium chloride	Special grade, Wako Pure Chemical Industries
N,*N*-Dimethylacetamide	Special grade, Wako Pure Chemical Industries, denoted as DMAc
Methanol	Special grade, Wako Pure Chemical Industries
Calcium carbonate	Special grade, Wako Pure Chemical Industries
Sodium hydrogen carbonate	Special grade, Wako Pure Chemical Industries
Sodium carbonate solution	For volumetric analysis, 0.05 M, Wako Pure Chemical Industries
Sodium hydroxide solution	For volumetric analysis, 0.05 M, Wako Pure Chemical Industries
Hydrochloric acid solution	For volumetric analysis, 0.05 M, Wako Pure Chemical Industries
Methyl orange	Special grade, Wako Pure Chemical Industries
Nitrogen gas	Alpha gas 2, Air Liquide Kogyo Gas
Oxygen gas	Alpha gas 2, Air Liquide Kogyo Gas
Argon gas	Alpha gas 2, Air Liquide Kogyo Gas

2.2.2. Synthesis of mesoporous carbon CMK-3

Mesoporous carbon CMK-3 was synthesized by following the literature.[22] Pluronic P123 (12 g) was completely dissolved in a HCl aqueous solution (1.6 M, 450 g) at 308 K, and subsequently TEOS (26 g) was added dropwise into the solution over *ca.* 3 min under vigorous stirring using a magnetic stir bar. The agitation was further continued for 15 min at 308 K. The sample was aged at 308 K for 24 h and then at 373 K for 24 h without stirring in an oven. During stirring and aging, the lid of vessel was kept closed. The resulting solid and liquid were separated by suction filtration using a Buchner funnel (filter paper 4A, hard type) and a filtering flask with ethanol as an antiform. The solid was washed with H_2O (1.5 L) and was dried

at 373 K overnight in an oven. The resulting powder was calcined in an electric furnace (Yamato, FO610) at 833 K for 8 h, for which the ramping rate of temperature was 10 K min^{-1}. After the calcination, white powder (mesoporous silica SBA-15) of 6.7 g was obtained.

Synthesized SBA-15 (2.0 g) was dispersed in a sucrose solution [including sucrose (2.5 g), H_2SO_4 (0.29 g), and H_2O (10 mL)], and the suspension was stirred at room temperature for 1 h to impregnate sucrose into the pores of SBA-15. After the filtration, the powder was dried at 373 K for 6 h and then at 433 K for 6 h. The powder was crashed on a mortar and was again dispersed in a sucrose solution [containing sucrose (1.6 g), H_2SO_4 (0.19 g), and H_2O (10 mL)]. After filtration and drying under the same conditions described above, the powder was heated to 1173 K by 2.4 K min^{-1}, and then the temperature was kept for 6 h in a horizontal quartz tube [inner diameter ø30 mm, temperature was controlled by an electric furnace (AZ ONE, TMF-300N)] under N_2 flow (10 mL min^{-1}) to carbonize impregnated sucrose. The carbon/SBA-15 composite was dispersed in an HF aqueous solution (10 wt%, 100 g), and the suspension was stirred at room temperature for 4 h to dissolve the SBA-15 template. After filtration using a Buchner funnel (filter paper 4A) and a filtering flask with a calcium gluconate solution to quench HF, washing with H_2O repeatedly, and drying in an oven at 373 K overnight, black powder (mesoporous carbon CMK-3) of 1.2 g was obtained.

2.2.3. Analysis of oxygenated functional groups on carbons

Carboxylic acids, lactones, and phenolic groups on carbons were quantified by the Boehm titration[23] as follows. 0.5 g of carbon was dispersed in a base solution (50 mM, 20 mL, containing $NaHCO_3$, Na_2CO_3, or NaOH). The suspension was stirred at 600 rpm at 298 K for 24 h under Ar, and the liquid and solid were separated by quantitative filter paper (5A, quantitative) to remove carbon. Twice of a stoichiometric amount of HCl solution (50 mM) against base used was added to a portion of the filtrate (5 mL). After sonication under 500 hPa of reduced pressure for 5 min to remove CO_2 dissolving in the solution, back-titration was conducted using NaOH solution (50 mM) with methyl orange as an indicator.

2.2.4. Analysis of components in bagasse kraft pulp

The weight ratio of cellulose, hemicellulose (xylan and arabinan), and lignin in bagasse kraft pulp was

determined by following the established method.[24] 300 mg of bagasse kraft pulp was dispersed in a 3 mL of H_2SO_4 solution (72 wt%), and the suspension was stirred at 303 K for 1 h. After adding 84 mL of H_2O, the mixture was reacted at 394 K for 1 h in a hastelloy C22 high-pressure reactor (OM Lab-Tech, MMJ-100, 100 mL, Figure 2.2). The solid and liquid phases were separated by filtration, and then $CaCO_3$ was added to the liquid phase to quench H_2SO_4 to be pH 7. The pH should be kept $\leq$7 to prevent sugars from decomposing. The resulting solution was analyzed by high-performance liquid chromatography (HPLC, the conditions are shown below) to determine the amounts of glucose, xylose, and arabinose, corresponding to cellulose, xylan, and arabinan, respectively. The solid was dried in an oven at 378 K overnight and then was calcined in an electric furnace (Denken-Highdental, KDF-S90) at 848 K for 24 h under air. The amount of lignin was determined from weight decrease by the calcination.

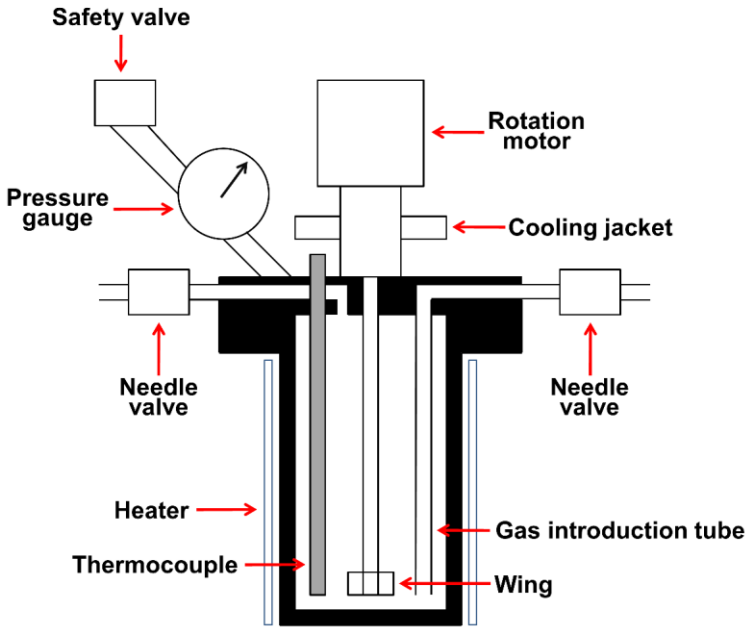


Figure 2.2. Diagram of the hastelloy C22 high-pressure reactor.

2.2.5. Ball-milling and mix-milling pre-treatment of cellulose

Microcrystalline cellulose (10 g) was ball-milled in the presence of ZrO_2 balls (ø1.0 cm, 1 kg) in a ceramic pot (0.9 L) at 60 rpm for 96 h or in the presence of Al_2O_3 balls (ø1.5 cm, 2 kg) in a ceramic pot (3.6 L) at 60 rpm for 48 h. Mix-milling of cellulose and solid catalyst was carried out in the same type of pot in the

presence of Al_2O_3 balls. Microcrystalline cellulose (10 g) and solid catalyst (1.54 g) (S/C ratio based on weight = 6.5) were added into the pot and were milled together at 60 rpm for 48 h. The amount of catalyst was reduced to 1.46 g for the mix-milling of cellobiose (S/C = 6.8).

Ball-milled samples were analyzed by XRD (Rigaku MiniFlex, Cu Kα), ^{13}C cross polarization/magic angle spinning NMR (^{13}C CP/MAS NMR, Bruker, MSL-300, 75 MHz, MAS frequency 8 kHz), laser diffraction (Nikkiso, Microtrac MT3300EXII), optical microscope (KEYENCE, VHX-5000), and SEM (JEOL, JSM-6360LA). The viscometry was conducted at 303 K using an Ubbelohde viscometer (No. 0C) by following the reported procedure.[25] A 200 mg of cellulose sample was dispersed in 100 mL of Milli-Q H_2O, and the suspension was stirred at room temperature overnight. The liquid phase was removed by centrifugation and decantation. The remaining solid was dispersed in 100 mL of CH_3OH, and the suspension was stirred for 30 min at room temperature. After removing solvent by centrifugation and decantation, the solid was immersed in 50 mL of DMAc for 30 min at room temperature, and this procedure was repeated three times. Then, the resulting solid was dissolved in 9 wt% LiCl/DMAc.[26] This solution was used for the viscometry.

2.2.6. Catalytic reactions

The hydrolysis of cellulose was conducted in the hastelloy C22 high-pressure reactor. Ball-milled cellulose (324 mg), catalyst (50 mg), and H_2O (40 mL) were charged into the reactor. For the hydrolysis of mix-milled samples, 374 mg of the sample [containing cellulose (324 mg) and catalyst (50 mg)] and H_2O (40 mL) were used. The reactor was heated to 503 K in 18 min and then cooled to 323 K by blowing air after the reaction for 22 min (named *rapid heating-cooling condition*, Figure 2.3). The suspension was separated by centrifugation and decantation. The products in the aqueous phase were analyzed by HPLC [Shimadzu LC10-AT*VP* with refractive index (RI) and ultraviolet (UV, 210 nm) detectors] with a SUGAR SH1011 column (Shodex, ø8 mm × 300 mm, mobile phase: H_2O at 0.5 mL min^{-1}, 323 K), a Rezex RPM-Monosaccharide Pb++ column (Phenomenex, ø7.8 mm × 300 mm, mobile phase: H_2O at 0.6 mL min^{-1}, 343 K), and a TSKgel Amide-80 HR column [Tosoh, ø4.6 mm × 250 mm, mobile phase: CH_3CN/H_2O (6/4) at 0.8 mL min^{-1}, 303 K]. An absolute calibration method was used for calculation of product yields (eq. 2.1).

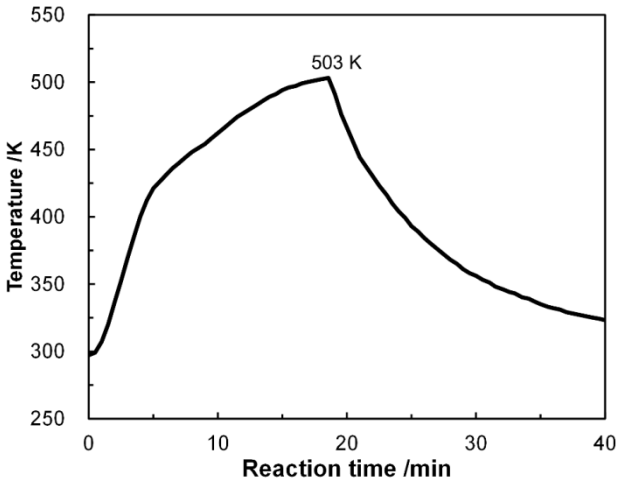


Figure 2.3. Temperature profile under the rapid heating-cooling condition.

$$(\text{Yield}/\%) = \frac{CF_{\text{HPLC}} \times A_{\text{HPLC}} \times V}{\frac{M_{\text{cellulose}}}{162.13}} \times \frac{n}{6} \times 100 \qquad (2.1)$$

where CF_{HPLC} (unit: M count^{-1}) is calibration factor, A_{HPLC} (count) is peak area in HPLC chart, V (L) is volume of reaction solution, $M_{\text{cellulose}}$ (g) is mass of cellulose charged, and n is carbon number in a product.

The products were identified by HPLC and liquid chromatography/mass spectroscopy [LC/MS, Thermo Fischer Scientific, LCQ Fleet, atmospheric pressure chemical ionization (APCI), the conditions are the same as those of HPLC]. The conversion of cellulose was determined based on the weight difference of the solid part before and after reaction (eq. 2.2).

$$(\text{Conversion}/\%) = \frac{M_{\text{residue}} - M_{\text{catalyst}}}{M_{\text{cellulose}}} \times 100 \qquad (2.2)$$

where M_{residue} (unit: g) is mass of dried residue and M_{catalyst} (g) is mass of catalyst charged.

The amount of organic carbons in a reaction solution was quantified by measurement of total organic carbon (TOC, Shimadzu TOC-V_{CSN}) to determine conversion (eq. 2.3) when catalyst was partially dissolved in H_2O after the reaction (see Section 2.3.2).

$$(\text{Conversion}/\%) = \frac{CF_{\text{TOC}} \times A_{\text{TOC}}}{M_{\text{cellulose}} \times \frac{72.06}{162.13}} \times 100 \qquad (2.3)$$

where CF_{TOC} (unit: gram-carbon count^{-1}) is calibration factor and A_{TOC} (count) is peak area in TOC measurement.

The hydrolysis of mix-milled samples at a lower temperature (≤423 K) was carried out in a pressure-resistant glass tube (Ace Glass, 15 mL). 94 mg of mix-milled sample [containing cellulose (81 mg) and catalyst (13 mg)] and H_2O (10 mL) were charged into the tube. The tube was immersed in an oil bath at a certain temperature for a designated length of time. The product analysis was performed using the same procedure described above.

The hydrolysis of cellobiose was conducted in the hastelloy C22 high-pressure reactor. Cellobiose (342 mg), catalyst (50 mg), and H_2O (40 mL) were charged into the reactor. The temperature was raised to 463 K in 11 min, and then the reactor was rapidly cooled to 323 K by blowing air. The product yield and conversion were determined by HPLC (*vide supra*).

2.2.7. Reuse experiment of mix-milled cellulose

Microcrystalline cellulose (10 g) and K26 (1.54 g) were ball-milled together in the presence of Al_2O_3 balls (ø1.5 cm, 2 kg) in a ceramic pot (3.6 L) at 60 rpm for 48 h. The recovered sample and a 0.012 wt% HCl solution (40 mL) were charged into the hastelloy C22 high-pressure reactor. The temperature was firstly raised to 473 K and was maintained for 2 min. Then, the reactor was cooled down to 423 K by blowing air and the mixture was further reacted for 60 min at the temperature. After cooling down to room temperature, the solid and liquid phases were separated by centrifugation and decantation. The solid phase was washed with H_2O repeatedly to extract physisorbed products, for which total volume of H_2O used was *ca*. 160 mL. The resulting solid was dried under vacuum overnight at 353 K. The liquid phase and washing solvent were mixed and analyzed by HPLC (*vide supra*). In the next run, the dried solid was mix-milled with fresh cellulose, the amount of which was the same as that of converted cellulose in the previous run.

2.3. Results and discussion

2.3.1. Screening of carbon catalysts for hydrolysis of cellulose

Several carbons were tested in the hydrolysis of individually ball-milled cellulose in H_2O under the rapid heating-cooling condition (Figure 2.3), and it was found that their catalytic activities strongly depended on their nature (Table 2.1). The most active catalyst, alkali-activated carbon K26, afforded 60% conversion of cellulose and 36% yield of glucose (entry 2). This glucose yield was obviously higher than that in a control experiment without catalysts (4.6%, entry 1). The other products were water-soluble oligosaccharides (2.5%, DP = mainly 2−6), fructose (2.7%), mannose (2.6%), and by-products (16%). K26 was reusable up to four times with almost no loss of activity. Alkali-activated carbon K20 showed similar catalytic activity to K26, and gave 59% conversion of cellulose and 35% yield of glucose (entry 3). Another alkali-activated carbon MSP20, steam-activated carbon BA50, and mesoporous carbon CMK-3 were less active than K26 and K20 (entries 4–6). Other carbons, steam-activated carbon SX, carbon black BP2000, and carbon black XC72 were almost inactive (entries 7–9). Consequently, K26, which can be synthesized in a bulk-scale in industry, showed a significantly higher catalytic activity than that of CMK-3, and thus K26 was mainly used for further study.

Table 2.1. Hydrolysis of individually ball-milled cellulose by carbon catalysts.[a]

Entry	Catalyst	Conv. /%	Yield based on carbon /%						
			Glucan		By-product				
			Glc[b]	Olg[c]	Frc[d]	Man[e]	Lev[f]	HMF[g]	Others[h]
1	None	28	4.6	15	0.5	0.6	0.2	1.8	5.3
2	K26	60	36	2.5	2.7	2.6	2.1	3.4	11
3	K20	59	35	1.7	1.9	1.3	2.7	2.9	14
4	MSP20	50	26	6.3	1.7	1.6	1.6	2.1	11
5	BA50	57	17	20	1.0	1.0	0.9	3.5	14
6	CMK-3	52	12	25	0.9	0.8	0.7	2.5	10
7	SX	38	8.1	20	0.6	0.9	0.4	1.4	6.6
8	BP2000	37	6.4	12	0.5	0.5	0.3	1.8	16
9	XC72	35	5.8	19	0.6	0.9	0.2	1.9	6.6

[a]Conditions: individually ball-milled cellulose (0.9 L-pot) 324 mg, catalyst (not milled) 50 mg, H_2O 40 mL, 503 K, <1 min (rapid heating-cooling condition). Cellulose was ball-milled without catalyst. [b]Glucose. [c]Water-soluble oligosaccharides (DP = mainly 2–6). [d]Fructose. [e]Mannose. [f]Levoglucosan. [g]5-Hydroxymethylfurfural. [h](Conversion) – (total yield of the characterized products).

Next, the amounts of carboxylic acids, lactones, and phenolic groups as oxygenated functional groups (denoted as OFGs, hereafter) on carbons were quantified by the Boehm titration[23] (Table 2.2). The highly active catalysts such as K26 and K20 contain a large number of OFGs (entries 10 and 11), and less active catalysts do lower amounts of OFGs (entries 12–16). The total amount of OFGs on carbons positively correlates with catalytic activity for glucose production from cellulose (Figure 2.4), indicating that weakly acidic OFGs may be active sites. However, this trend would also include the influence of physical properties of each carbon material, and the detailed functions of OFGs are discussed in Chapter 3. The author further confirmed that the hydrolysis activity did not result from the catalysis of sulfonic groups. The content of sulfur in K26 was less than 0.01%, corresponding to only 10^{-5}% in the whole reaction mixture. Even 10^{-4}% H_2SO_4 did not promote the hydrolysis of cellulose (see Table 2.3, entry 17). The author further conducted control experiments to evaluate acidity of active sites. K26 was treated with AcOH/AcONa (pH 4.0), NaCl (pH 7.0), $NaHCO_3$ (pH 8.3), and NaOH (pH 12.6) to neutralize corresponding acidic sites on K26 and the treated carbons were subjected to the hydrolysis of individually ball-milled cellulose (Figure 2.5). The acetate buffer treatment did not influence the catalytic activity of K26, indicating that no strong acid is working as a predominant active site. Similarly, K26 has resisted an actual salt NaCl; K26 possibly maintains its catalytic activity even in the presence of salts. The $NaHCO_3$-treated K26 still produces glucose in 13% yield, but exposure to NaOH completely deactivates K26 due to neutralization of all acidic groups. Hence, the hydrolytic activity of K26 may be ascribed to weakly acidic groups such as carboxylic acids and phenolic groups. These results also suggest that weak acids are advantageous over strong acids owing to the resistance to salts derived from raw biomass since strong acids easily cause ion exchange to be deactivated in an acetate buffer.[19,20]

Table 2.2. Amounts of oxygenated functional groups on carbon.[a]

Entry	Carbon	Oxygenated functional groups /μmol g^{-1}				Conv.[b] /%	Glucose yield[b] /%
		Carboxylic acids	Lactones	Phenolic groups	Total		
10	K26	270	310	310	880	60	36
11	K20	420	270	320	1010	59	35
12	MSP20	65	110	280	450	50	26
13	CMK-3	140	97	180	410	52	12
14	SX	80	49	34	160	38	8.1
15	BP2000	61	12	88	160	37	6.4
16	XC72	26	49	0	75	35	5.8

[a]Determined by the Boehm titration.[23] [b]Reaction conditions: individually ball-milled cellulose (0.9 L-pot) 324 mg, catalyst (not milled) 50 mg, H_2O 40 mL, 503 K, <1 min (rapid heating-cooling condition).

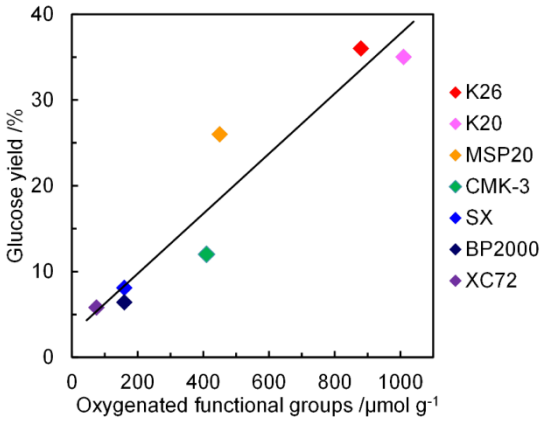


Figure 2.4. Correlation between the amount of OFGs and catalytic activity of carbons.

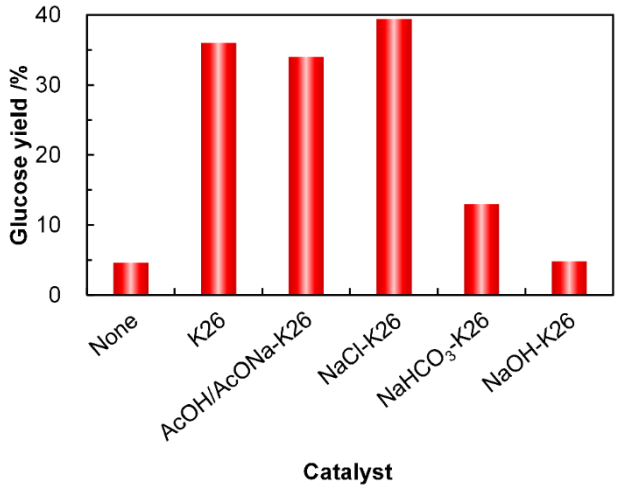


Figure 2.5. Hydrolysis of individually milled cellulose by base-treated K26. Conditions: individually milled cellulose (0.9 L-pot) 324 mg, catalyst 50 mg, H_2O 40 mL, 503 K, <1 min (rapid heating-cooling condition).

The author has checked whether the most active catalyst K26 works as a *solid catalyst* in the hydrolysis of cellulose. The pH value of an aqueous dispersion of K26 was 4.9 because of weakly acidic OFGs. This result does not indicate the formation of soluble acids from K26 because the pH of the solution returns to 5.8 after separation of K26 using a polytetrafluoroethylene (PTFE) membrane. For comparison, 10 μM H_2SO_4 (pH 4.7) and 50 μM CH_3COOH (pH 4.6) were used in the hydrolysis of individually ball-milled cellulose, resulting in no enhancement of conversion or yield at all (Table 2.3, entries 17 and 18). As it is known that the hydrolysis by H_3O^+ is negligible at pH higher than 4,[27] the promotion of the hydrolysis by K26 is not ascribed to the buffering effect releasing H_3O^+ in the suspended state. Moreover, an aqueous mixture of K26 was subjected to the reaction conditions at 503 K and filtered to remove the K26. The filtrate was used for the hydrolysis of cellulose; however, the reaction was not accelerated (entry 19). In addition, soluble acidic by-products formed from cellulose during the hydrolysis reaction degraded only 11% of the cellulose, subtracting the conversion of cellulose in the blank experiment (28%, entry 1) from that in this reaction (39%, entry 20). Therefore, soluble compounds would not be major active species in the hydrolysis of cellulose by K26. The author has also investigated whether or not cellulose is hydrolyzed as a *solid substrate*. The ball-milled cellulose did not contain a considerable amount of soluble oligomers (only 0.3%) verified by the extraction with 40 mL of boiling water, and the ball-milled cellulose had a high DP (640). The influence of solubility of cellulose in H_2O was also estimated. If the slightly soluble portion of cellulose (*ca.* 2×10^{-3} wt% at ambient temperature)[28] corresponded to the reaction performance, the hydrolysis rate should be controlled by the saturated solubility of cellulose, giving a constant concentration of dissolved cellulose. However, the rate increased almost linearly with increasing concentration of solid cellulose (Table 2.4 and Figure 2.6). Although the possibility of soluble active species or partial dissolution of the substrate is not completely excluded, these results suggest that *solid* K26 hydrolyzes *solid* cellulose in addition to the hydrolysis by hot-compressed water[27] and small amounts of acids derived from cellulose. Hence, both carbon and cellulose behave as solids in the hydrolysis. In solid-solid reactions, a collision between a solid substrate and a solid catalyst is limited and this hampers reaction proceeding. In other words, solid catalyst would unsatisfactorily show their performances during the reaction because of loose contact with substrate.

Table 2.3. Control experiments on hydrolysis of individually ball-milled cellulose.[a]

Entry	Solvent	Conv. /%	Yield based on carbon /%						
			Glucan		By-product				
			Glc[b]	Olg[c]	Frc[d]	Man[e]	Lev[f]	HMF[g]	Others[h]
1	H_2O	28	4.6	15	0.5	0.6	0.2	1.8	5.3
17	10 μM H_2SO_4[i]	29	4.3	17	0.8	0.8	0.2	1.9	3.9
18	50 μM CH_3COOH[j]	26	3.8	17	0.8	0.8	0.2	2.0	1.9
19	Filtrate of used K26[k]	22	3.1	13	0.5	0.6	0.1	1.4	2.9
20	Filtrate of used K26 and cellulose[l]	39	n.d.[m]	n.d.[m]	n.d.[m]	n.d.[m]	n.d.[m]	n.d.[m]	n.d.[m]

[a]Conditions: individually ball-milled cellulose (0.9 L-pot) 324 mg, solvent *ca.* 40 mL, 503 K, <1 min (rapid heating-cooling condition). Cellulose was ball-milled without catalyst. [b]Glucose. [c]Water-soluble oligosaccharides (DP = mainly 2–6). [d]Fructose. [e]Mannose. [f]Levoglucosan. [g]5-Hydroxymethylfurfural. [h](Conversion) – (total yield of the characterized products). [i]pH 4.7. [j]pH 4.6. [k]The filtrate of K26 aqueous mixture subjected to the rapid heating-cooling condition was used as the solvent instead of distilled water. [l]The filtrate of the mixture of the cellulose hydrolysis by K26 (Table 2.1, entry 2) was used as the solvent instead of distilled water. [m]Determination was impossible because products in the primary reaction (Table 2.1, entry 2) were contained, and they underwent the degradation during this reaction.

Table 2.4. Effect of cellulose concentration on hydrolysis by K26.[a]

Entry	Concentration of ball-milled cellulose /g L^{-1}	Conv. /%	Conv. rate[b] /g L^{-1} h^{-1}	Yield based on carbon /%						
				Glucan		By-product				
				Glc[c]	Olg[d]	Frc[e]	Man[f]	Lev[g]	HMF[h]	Others[i]
21	8.1	72	8.7	40	1.4	2.1	1.8	2.8	5.4	19
22	16	66	16	40	1.5	1.7	1.3	2.5	6.3	13
23	24	66	24	39	1.7	1.4	1.2	2.6	7.0	13
24	40	58	35	38	2.1	1.3	1.2	2.2	6.7	7.2

[a]Conditions: K26 50 mg, H_2O 40 mL, 508 K, <1 min (rapid heating-cooling condition). Cellulose was ball-milled without catalyst in a 0.9 L pot. [b]Conversion rate of cellulose based on the total reaction time (40 min, see Figure 2.3). [c]Glucose. [d]Water-soluble oligosaccharides (DP = mainly 2–6). [e]Fructose. [f]Mannose. [g]Levoglucosan. [h]5-Hydroxymethylfurfural. [i](Conversion) – (total yield of the characterized products).

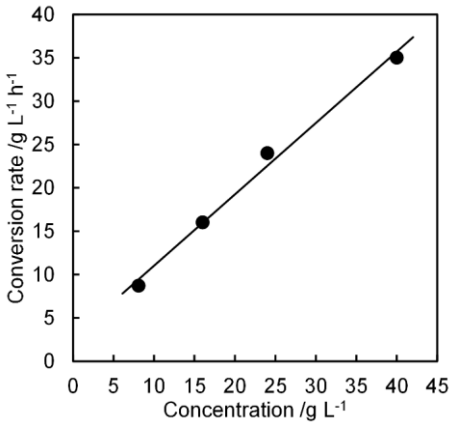


Figure 2.6. Correlation between cellulose concentration and conversion rate.

2.3.2. High-yielding production of glucose from cellulose

In the previous section, K26 provided glucose in 36% yield from individually ball-milled cellulose (Table 2.1, entry 2), but the yield needs to be improved. The hydrolysis of cellulose by carbon catalyst takes place at their interface, namely a solid-solid reaction. Limited contact between a solid substrate and a solid catalyst is an obstacle in this type of reaction, and the author therefore employed a new pre-treatment method named *mix-milling*, ball-milling cellulose and catalyst together, to make tight contact (Figure 2.7).

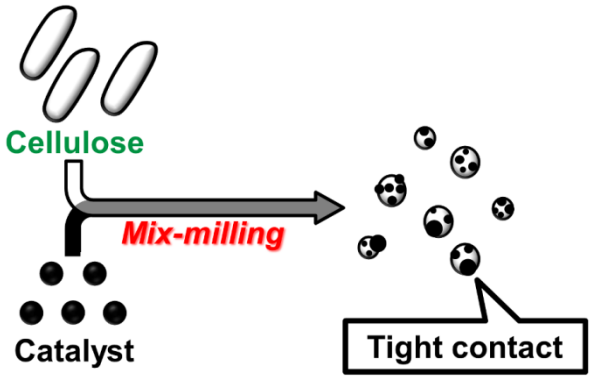


Figure 2.7. Diagram of mix-milling.

The activities and properties of various solid catalysts including carbons and other acid catalysts were studied in the hydrolysis of cellulose at 453 K for 20 min after the mix-milling treatment. As control experiments, the hydrolysis of ball-milled cellulose without catalyst gave a poor reaction result (7.9% yield of glucans, Table 2.5, entry 25), and all the catalysts tested in this study provided low yields of the products without mix-milling as expected (entries 26–34). The results of the hydrolysis of mix-milled cellulose are also shown in Table 2.5 (entries 35–43). An alkali-activated carbon K26 produced water-soluble glucans in 90% yield [glucose (20%) and oligosaccharides (70%)] with 97% selectivity (entry 35). The other products were fructose (0.6%), mannose (0.7%), levoglucosan (0.7%), 5-HMF (1.0%), and unidentified compounds (0.1%). The solid containing the catalyst K26 was easily separated by filtration after the reaction (Figure 2.8). Other carbons, BA50 and SX, produced glucans in 34% and 22% yields, respectively (entries 36 and 37), and they were less active than K26 due to lower amounts of weakly acidic groups. Amberlyst 70 gave

Table 2.5. Hydrolysis of cellulose by various solid catalysts.[a]

Entry	Catalyst	Pre-treatment	Conv. /%	Yield based on carbon /%						
				Glucan		By-product				
				Glc[b]	Olg[c]	Frc[d]	Man[e]	Lev[f]	HMF[g]	Others[h]
25	None	Individual[l]	12	1.3	6.6	0.2	0.2	<0.1	0.2	3.4
26	K26	Individual	18	2.9	10	0.5	0.4	0.1	<0.1	3.7
27	BA50	Individual[l]	20	2.4	8.6	0.2	0.3	<0.1	<0.1	8.0
28	SX	Individual[l]	16	2.3	8.0	0.3	0.3	<0.1	<0.1	4.8
29	Amberlyst 70	Individual[l]	18	6.3	8.2	0.2	0.8	0.2	0.3	2.4
30	H-MFI	Individual[l]	16	3.2	9.1	0.3	0.2	0.1	0.1	3.3
31	H-MOR	Individual[l]	17	3.8	9.6	0.3	0.3	0.1	0.2	3.0
32	SiO_2-Al_2O_3	Individual[l]	7.0	0.9	5.4	0.2	0.2	<0.1	0.2	0.1
33	SiO_2	Individual[l]	12	2.1	8.3	0.3	0.4	<0.1	0.2	1.1
34	TiO_2	Individual[l]	14	2.3	9.7	0.4	0.4	0.1	0.3	0.2
35	K26	Mix[m]	93	20	70	0.6	0.7	0.7	1.0	<1[o]
36	BA50	Mix[m]	35	6.7	27	0.7	0.7	0.2	0.2	0.2
37	SX	Mix[m]	24	4.2	18	0.8	0.5	0.1	0.3	0.1
38	Amberlyst 70	Mix[m]	>99	82	1.9	0.5	1.4	2.6	2.8	8.8
39	H-MFI	Mix[m]	19	4.0	11	0.4	0.3	0.1	0.2	3.2
40	H-MOR	Mix[m]	21	4.9	11	0.4	0.3	0.2	0.5	4.0
41	SiO_2-Al_2O_3	Mix[m]	6.8	0.9	4.8	0.2	0.2	<0.1	0.2	0.5
42	SiO_2	Mix[m]	16	3.4	11	0.3	0.3	0.1	0.3	0.1
43	TiO_2	Mix[m]	13	1.6	7.1	0.5	0.3	<0.1	0.4	2.6
44	K26, HCl[j]	Mix[m]	98	88	2.7	1.5	1.5	3.0	1.7	<1[o]
45	K26, H_2SO_4[k]	Mix[m]	95	69	8.6	0.7	1.3	2.2	1.8	11
46	HCl[j]	Mix[m]	39	27	3.9	1.8	1.8	1.0	1.6	1.8
47	K26, HCl[j]	Individual[n]	40	30	4.3	1.3	1.3	1.1	0.7	0.7
48[i]	K26	Mix[m]	97	72	2.8	1.4	1.5	1.4	4.9	13

[a]Conditions: cellulose 324 mg, catalyst 50 mg, H_2O 40 mL, 453 K, 20 min. For hydrolysis of mix-milled cellulose, 374 mg of sample (containing cellulose 324 mg and catalyst 50 mg) was used. [b]Glucose. [c]Water-soluble oligosaccharides (DP = mainly 2–6). [d]Fructose. [e]Mannose. [f]Levoglucosan. [g]5-Hydroxymethylfurfural. [h](Conversion) – (total yield of the characterized products). [i]Conditions: mix-milled cellulose 94 mg (containing cellulose 81 mg and K26 13 mg), H_2O 10 mL, 418 K, 24 h. [j]Hydrolysis was conducted in a 0.012 wt% HCl solution (pH 2.5) instead of H_2O. [k]Hydrolysis was conducted in a 0.018 wt% H_2SO_4 solution (pH 2.5) instead of H_2O. [l]Cellulose was ball-milled without catalyst in a 3.6 L pot, and catalyst was not ball-milled. [m]Cellulose and catalyst were ball-milled together. [n]Cellulose and K26 were separately ball-milled. [o]The total yield of others was not correctly determined because of high conversion.

the highest glucose yield (entry 38, 82%). In this case, mechanocatalytic hydrolysis occurred during the milling process owing to the strong acidity of the resin. After ball-milling cellulose and Amberlyst 70 together, the author found that >99% of cellulose was solubilized as various kinds of oligomers[29] in H_2O at room temperature. Moreover, Amberlyst 70 was completely degraded after the hydrolysis reaction; Amberlyst 70 was not recovered by centrifugation at 4600*g* (4.5×10^4 m s^{-2}) or filtration using a PTFE

membrane (0.1 μm mesh) and the color of the filtrate was brown (Figure 2.9). Since the Tyndall effect was hardly observed, Amberlyst 70 presumably dissolved in H_2O during the reaction, which was contrasting to the behavior of K26 described above (Figure 2.8). The other catalysts tested (H-MFI, H-MOR, SiO_2-Al_2O_3, SiO_2, and TiO_2) were almost inactive (entries 39–43), and these catalysts except TiO_2 partially dissolved in H_2O during the reaction (Figure 2.10).

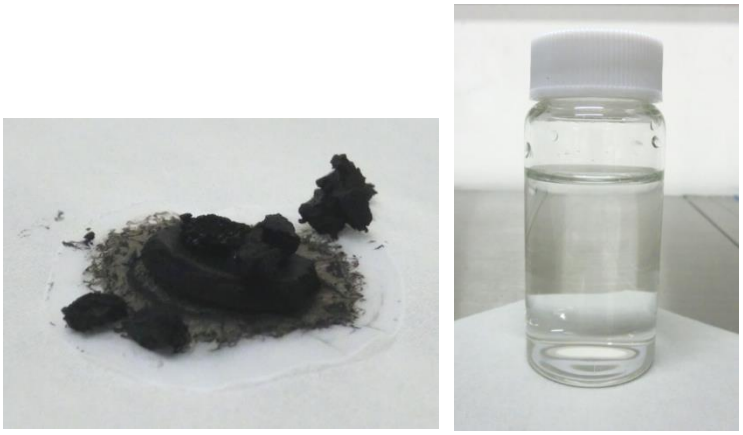


Figure 2.8. Solid residue (left) and product cocktail (right) after the hydrolysis of mix-milled cellulose containing K26. The solid and liquid phases were separated with a PTFE membrane (0.1 μm mesh).



Figure 2.9. Reaction mixture after the hydrolysis of mix-milled cellulose containing Amberlyst 70. No solids were obtained after the reaction. The solution has been irradiated with a green laser from right side of the bottle, but the Tyndall effect is hardly observed, showing that the solution is homogeneous and does not contain colloids.

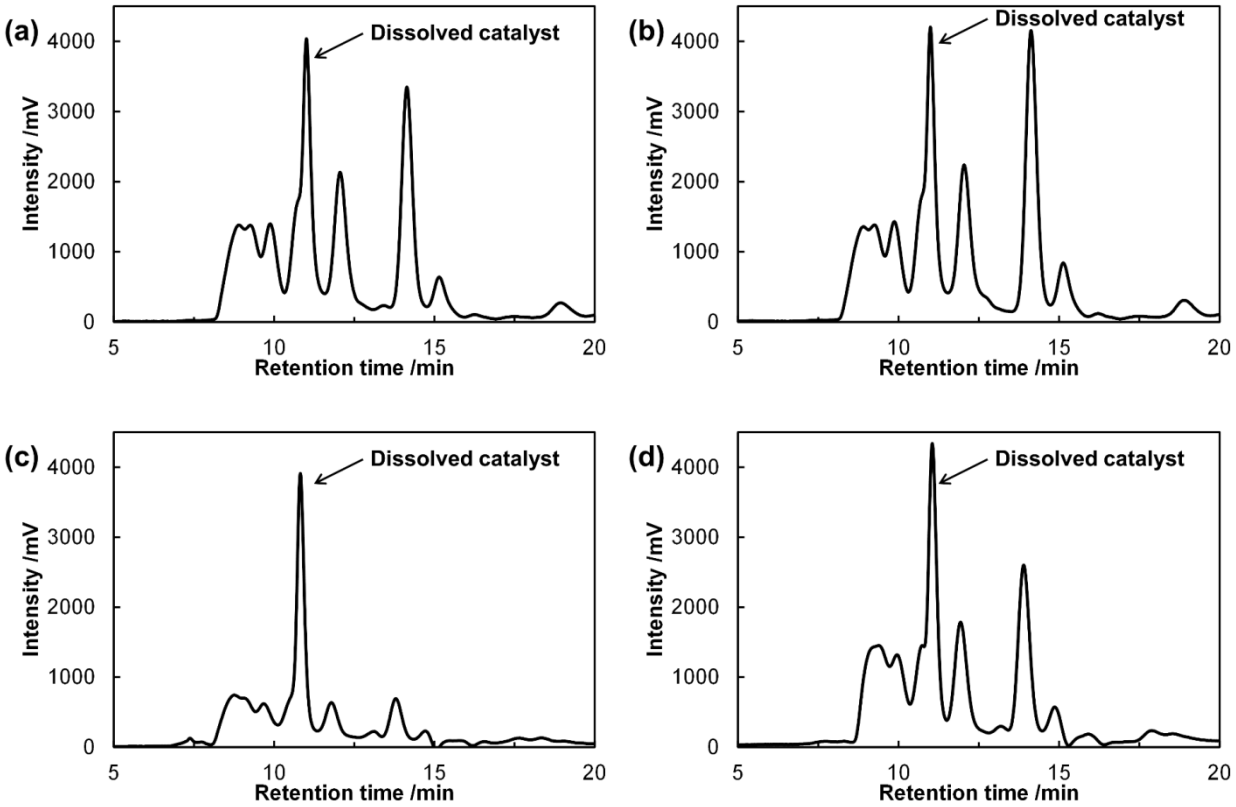


Figure 2.10. HPLC charts for the hydrolysis of mix-milled cellulose containing (a) H-MFI, (b) H-MOR, (c) SiO_2-Al_2O_3, and (d) SiO_2. Column: Rezex RPM Monosaccharide Pb++, detector: RI.

The correlation between the crystallinity of cellulose and the results of respective catalytic reactions was studied because the decomposition of the crystalline structure of cellulose by milling treatment improves the reactivity of cellulose as described in Section 1.2.2. The results of XRD measurements showed no peak for crystalline cellulose for all the milled samples (Figure 2.11), indicating that cellulose was similarly in the amorphous form in these samples. Hence, the deference in catalytic performance is not ascribed to crystallinity of cellulose but activity of catalyst. Again, K26 is the most active catalyst, except for soluble Amberlyst 70, for the hydrolysis of cellulose using the mix-milling pre-treatment.

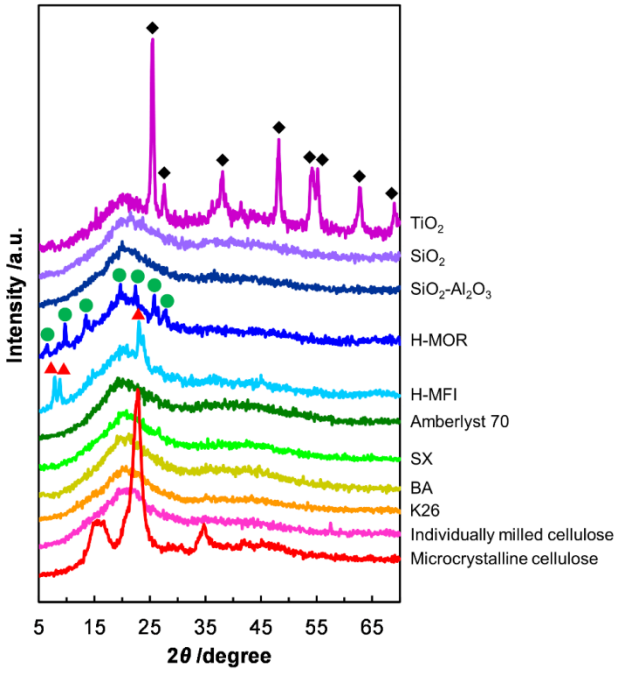


Figure 2.11. XRD patterns of mix-milled samples containing cellulose and solid catalysts. The peaks marked with red triangles (▲), green circles (●), and black diamonds (♦) are from H-MFI, H-MOR, and TiO_2, respectively.

The mix-milled cellulose containing K26 gave glucose and water-soluble oligosaccharides in 20% and 70% yields, respectively (Table 2.5, entry 35). In order to improve glucose yield by accelerating depolymerization of oligosaccharides to glucose, a 0.012% HCl aqueous solution (pH 2.5) was utilized as a solvent instead of H_2O. This trace HCl neither corrodes common stainless steel reactors nor has a negative economic impact because of very low concentration and low price (0.07–0.1 USD kg^{-1} as concentrated HCl in 2014 according to ICIS).[30,31] The hydrolysis of mix-milled cellulose using K26 was conducted in the trace HCl solution at 453 K for designated reaction times (Figure 2.12). In the initial stage of the reaction (≤2 min), water-soluble oligomers were produced prior to the formation of glucose. Subsequently, the yield of glucose increased up to 88% at 20 min and the selectivity of glucose based on cellulose conversion (98%) was 90% (Table 2.5, entry 44). This is the best result achieved in this work and one of the highest yields of glucose ever obtained in any methods. The yield of humins was at most 2% under the conditions as the recovered solid after the reaction was only 1.4%. After 20 min, the yield of glucose decreased because of the

degradation. Although H_2SO_4 (0.018 wt%, pH 2.5) was also used as a solvent due to its lower price (0.05 USD kg^{-1})[32] and less corrosive property than those of HCl, it was not as effective as HCl at the same pH (entry 45). This result is due to the negative effect of SO_4^{2-} on the hydrolysis reaction (Table 2.6); SO_4^{2-} may prevent the activation of glycosidic bonds by forming chelate. Next, the author focused on HCl, and control experiments were conducted to evaluate the contributions of HCl, K26, and mix-milling pre-treatment. Hydrolysis of individually ball-milled cellulose by HCl provided 27% yield of glucose and 39% conversion (Table 2.5, entry 46). The yield of oligomers was only 3.9%, showing the quick transformation of oligomers to glucose by HCl. Accordingly, HCl works for the hydrolysis of cellulose and oligomers, and the further improvement from entry 46 to 44 is accounted for the hydrolysis by K26. Besides, the hydrolysis of individually ball-milled cellulose by individually ball-milled K26 in the trace HCl gave a similar yield of glucose (30%) and a conversion (40%, entry 47) to those of entry 46 (yield 27%, conversion 39%), indicating that the hydrolysis by K26 without the mix-milling pre-treatment was almost negligible owing to the limited collision. Clearly, the mix-milling treatment is essential for high yield and selectivity of glucose.

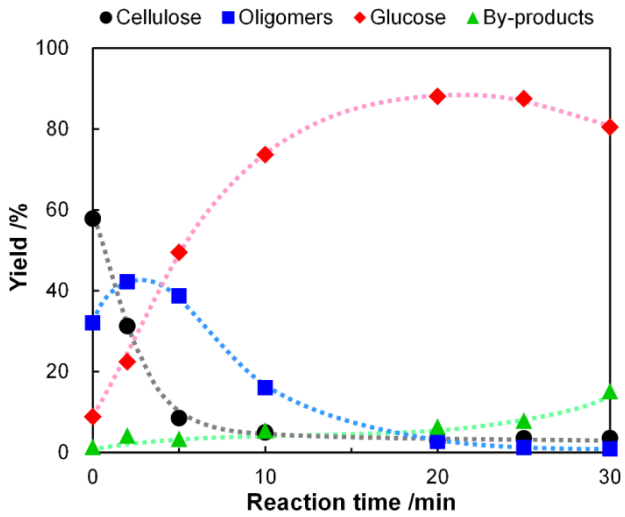


Figure 2.12. Time course of hydrolysis of mix-milled cellulose containing K26 in a 0.012 wt% HCl solution at 453 K.

Table 2.6. Effect of salts on the hydrolysis of cellulose.[a]

Entry	Salt	Conv. /%	Yield based on carbon /%						
			Glucan		By-product				
			Glc[b]	Olg[c]	Frc[d]	Man[e]	Lev[f]	HMF[g]	Others[h]
1	None	28	4.6	15	0.5	0.6	0.2	1.8	4.8
49	3.2 mM NaCl	15	1.7	5.6	0.4	0.7	0.1	1.0	1.2
50	1.6 mM Na_2SO_4	6.7	0.3	2.3	0.1	0.1	0.4	0.2	3.4

[a]Conditions: individually ball-milled cellulose 324 mg (0.9 L-pot), salt solution 40 mL, 503 K, <1 min (rapid heating-cooling condition). [b]Glucose. [c]Water-soluble oligosaccharides (DP = mainly 2–6). [d]Fructose. [e]Mannose. [f]Levoglucosan. [g]5-Hydroxymethylfurfural. [h](Conversion) – (total yield of the characterized products).

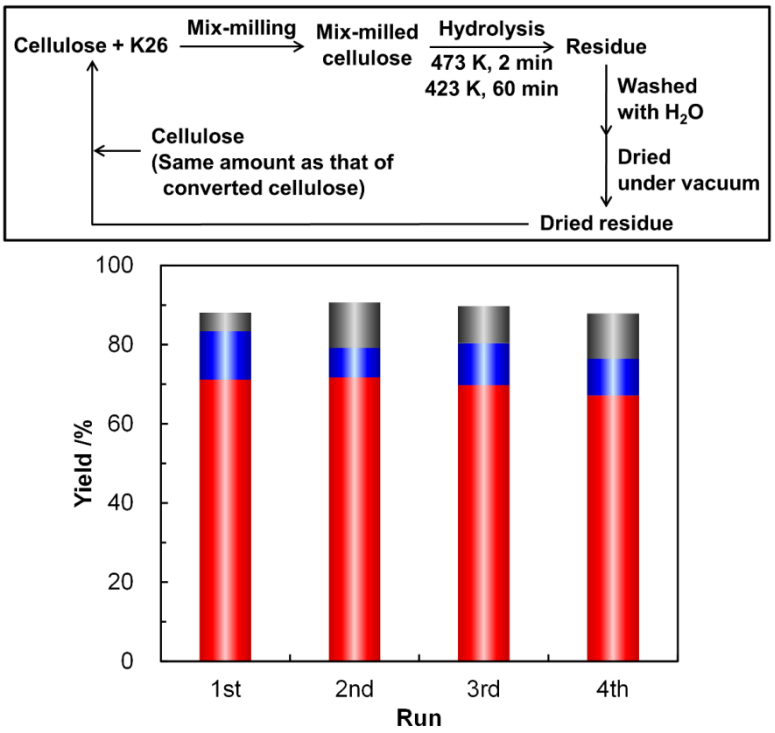


Figure 2.13. Reuse experiments of mix-milled K26 for the hydrolysis of cellulose (200 g L^{-1}) in a 0.012 wt% HCl solution (40 mL). First, 473 K for 2 min, then 423 K for 60 min. Red bar = glucose, blue bar = oligosaccharides, and grey bar = by-products.

The durability of K26 in this system was evaluated in reuse tests (Figure 2.13). In this case, a high concentration of the mix-milled sample (cellulose: 200 g L^{-1}, K26: 31 g L^{-1}) was used in the hydrolysis. The used K26 and unreacted cellulose were recovered, milled again with fresh cellulose, used for the hydrolysis reactions in 0.012 wt% HCl; the reuse experiments were repeated for three times (total four runs). The

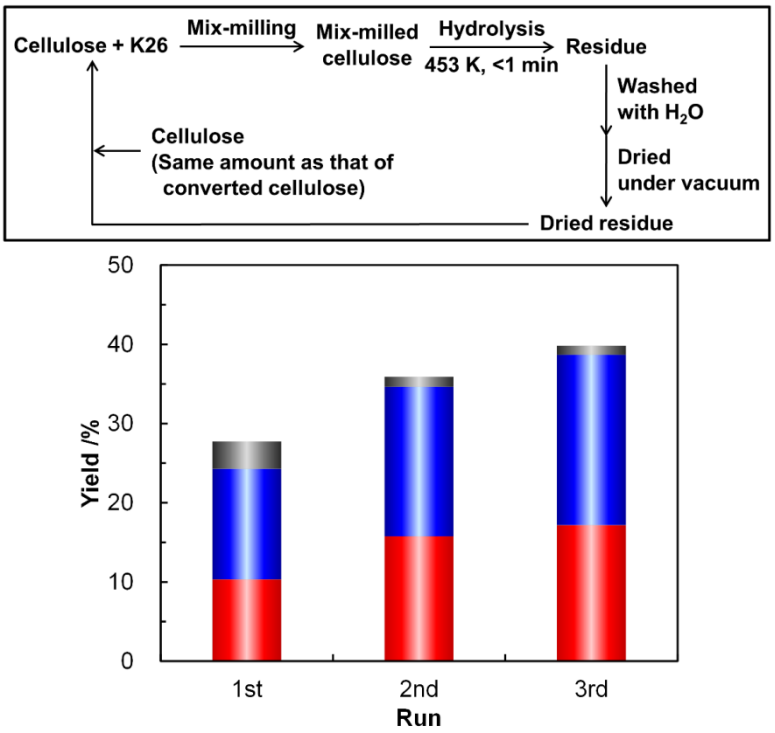


Figure 2.14. Reuse experiments of mix-milled K26 for the hydrolysis of cellulose (200 g L^{-1}) in a 0.012 wt% HCl solution (40 mL) at 453 K for <1 min (rapid heating-cooling condition). Red bar = glucose, blue bar = oligosaccharides, and grey bar = by-products.

additive amount of fresh cellulose was just equivalent to that consumed in the previous run, keeping a constant amount of cellulose in each run. Conversion of cellulose was 88−91%, and glucose was obtained in 71%, 72%, 70%, and 67% yields in the reuse experiments with its concentrations of 13 to 14 wt% (Figure 2.13). Although these glucose yields were lower than that in the standard conditions (88% at 8.1 g L^{-1}, Table 2.6, entry 44), the high concentration of glucose clears the practical demand (10 wt%) to avoid energy-consuming condensation of product. Another reuse experiments at lower cellulose conversion were performed (Figure 2.14), in which yields of products and cellulose conversion gradually increased. This trend is reasonable as the residual solid cellulose has partially undergone hydrolysis to decrease DP in the previous run; this remaining part should be relatively easily converted to soluble products in the subsequent run. These results in both high and low conversions show that the degradation rate of cellulose does not decrease during the reactions. Hence, K26 is fairly stable in the mix-milling as well as in the presence of HCl

and high concentrations of products.

Toward practical applications, the author demonstrated the saccharification of bagasse kraft pulp as a real biomass substrate by an inexpensive steam-activated carbon BA50, which showed catalytic activity in cellulose conversion (Table 2.5, entry 36). The pulp contained cellulose (59 wt%), hemicellulose [xylan (25 wt%) and arabinan (2 wt%)], and lignin (9 wt%). At first, one-pot hydrolysis of both cellulose and hemicellulose in bagasse kraft pulp was performed in a 0.012 wt% HCl solution for 2 min at various temperatures (Figure 2.15). The yields of xylose and arabinose based on the amount of hemicellulose in the pulp were 89% and 5.2% at 473 K, respectively. In this case, glucose yield based on the amount of cellulose in bagasse kraft pulp was only 32%. The glucose yield increased up to 72% with increasing the reaction temperature to 493 K, whereas the xylose yield decreased to 45% due to the degradation. Hence, high-yielding production of both hexoses and pentoses is difficult in one-pot reaction. Xylan hemicellulose is known as a more reactive substrate than cellulose due to the lack of an OH group at C6, which would make cellulose more chemically stable by forming hydrogen bonds (Figure 2.16).[33] Indeed, xylobiose (the minimum model of xylan hemicellulose) was five times more reactive for the hydrolysis than cellobiose (that of cellulose) under the same reaction conditions (443 K, 10 min, Figure 2.17).

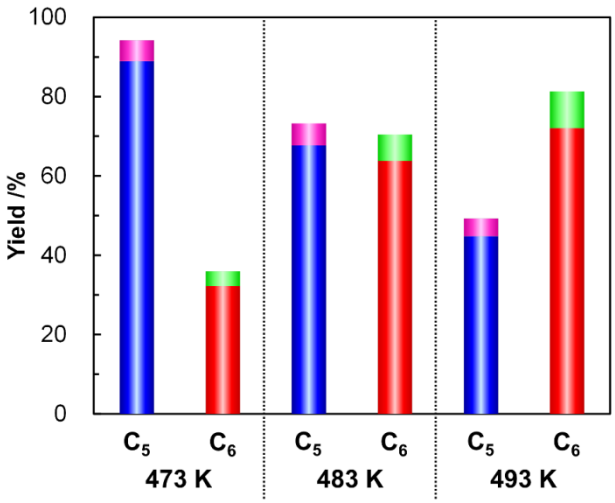


Figure 2.15. One-pot hydrolysis of both cellulose/hemicellulose in bagasse kraft pulp at various temperatures for 2 min. Blue bar = xylose, pink = arabinose, red = glucose, and green = fructose and mannose.

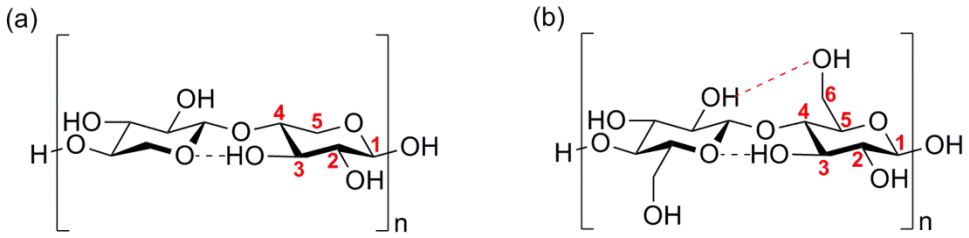


Figure 2.16. Structure of (a) xylan and (b) cellulose. The hydrogen bond at OH group coordinating to C6 (red line) would make cellulose less reactive.

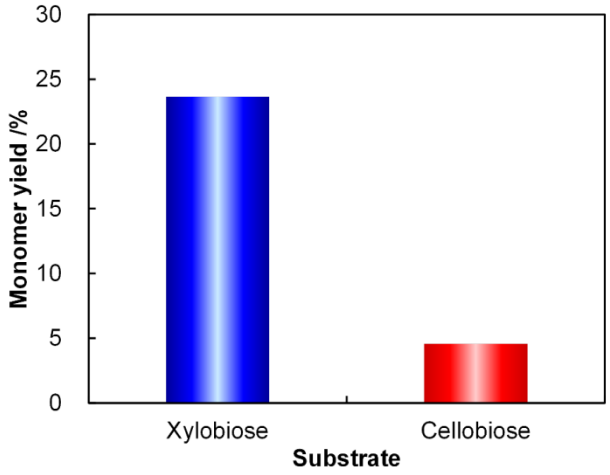


Figure 2.17. Hydrolysis of xylobiose (model of xylan) and cellobiose (that of cellulose) by K26 at 443 K for 10 min. Blue bar = xylose and red = glucose.

Taking account of the different reactivity of hemicellulose and cellulose, a cascade reaction was applied to the reaction; the mix-milled sample was subjected to the reaction at 453 K for 1 min and subsequently at 483 K for 2 min (Figure 2.18). In the first step, the hydrolysis of hemicellulose was preferred to that of cellulose due to higher reactivity of hemicellulose, and the major products were pentoses, namely xylose (69%) and arabinose (6.7%). It is noteworthy that the yield of hexoses was only 1.9% in this step. In contrast, glucose (74%) and other hexoses [fructose (2.5%) and mannose (1.5%)] from cellulose were mainly produced in the second step. The yields of xylose and arabinose were only 15% and 1.4%, respectively. This separate production of sugars will be advantageous for their further use. The total yields of sugars in this two-step reaction were 76% for glucose, 4.0% for other hexoses, 84% for xylose, and 8.1% for arabinose.

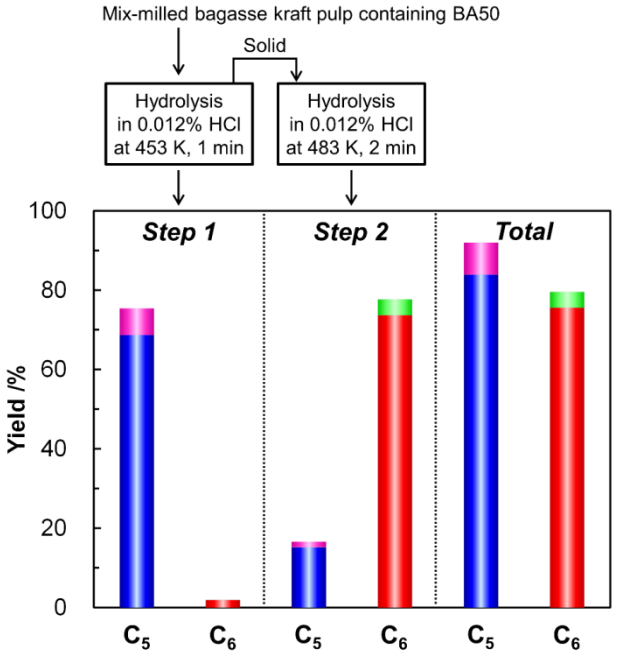


Figure 2.18. Two-step depolymerization of cellulose/hemicellulose in bagasse kraft pulp to hexoses/pentoses. Blue bar = xylose, pink = arabinose, red = glucose, and green = fructose and mannose.

2.3.3. Effect of mix-milling pre-treatment

In order to clarify the effect of the mix-milling pre-treatment, individually ball-milled cellulose and the mix-milled cellulose containing K26 were analyzed by microscope (optical microscope and SEM). Optical microscopic images are shown in Figure 2.19. The particles of individually ball-milled cellulose are clear or white and their diameter is *ca.* 10 μm (Figure 2.19a). Individually ball-milled K26 has black small particles (≤1 μm) (Figure 2.19b). The particle size of mix-milled cellulose containing K26 is similar to that of individually ball-milled cellulose, whereas the surface color is black (Figure 2.19c). The particle size distributions of both individually ball-milled and mix-milled celluloses determined by laser diffraction are also almost the same (37–40 μm, Figure 2.20). These results suggest that small K26 particles are attached to the surface of large cellulose particles. SEM image of the mix-milled cellulose sample (Figure 2.19d) also shows that there are small particles on a large particle. Hence, cellulose and K26 in the mix-milled sample would have a good contact.

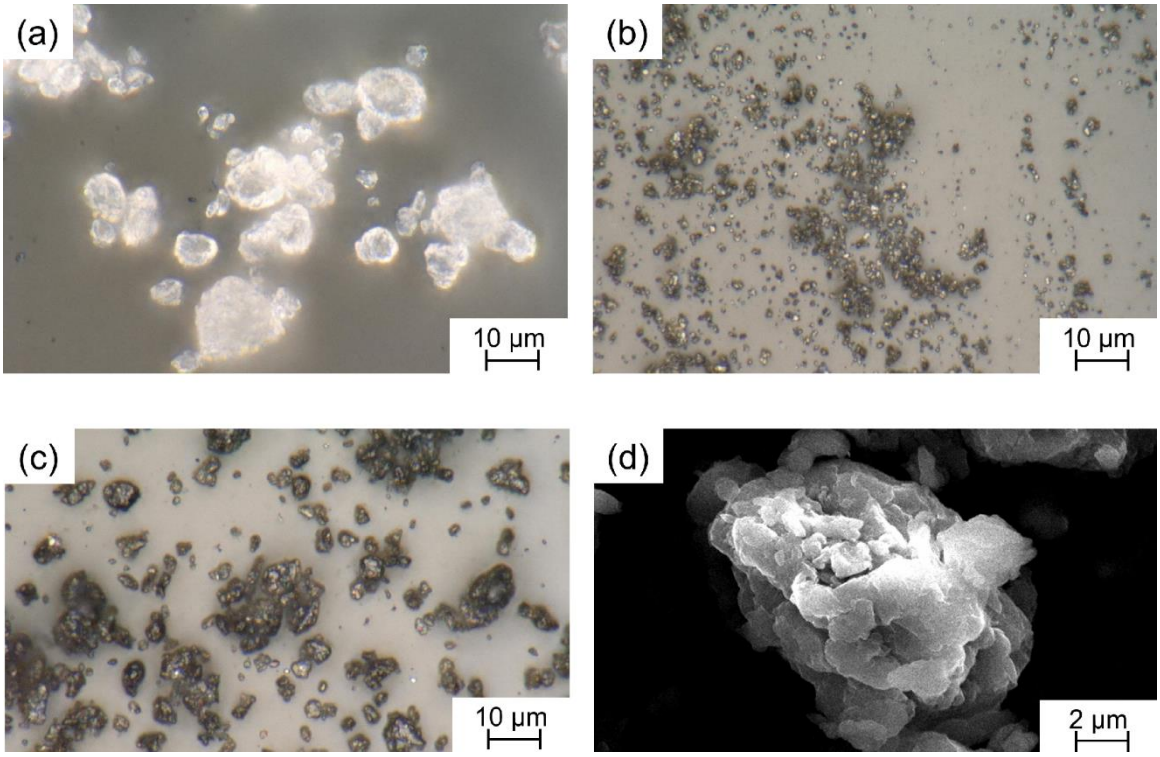


Figure 2.19. Microscopic images of cellulose samples. Optical microscopic images of (a) individually ball-milled cellulose, (b) individually ball-milled K26, and (c) mix-milled cellulose containing K26 and (d) SEM image of the mix-milled cellulose sample.

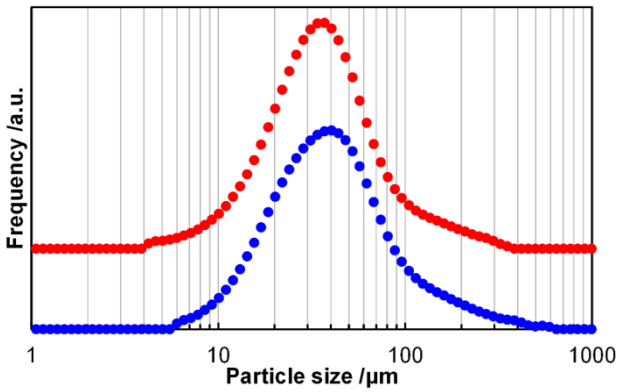


Figure 2.20. Particle size distributions of the mix-milled cellulose containing K26 (red) and simple mixture of individually ball-milled cellulose and individually ball-milled K26 (blue), which were observed by laser diffraction.

The author further analyzed the mix-milled cellulose containing K26 by ^{13}C CP/MAS NMR and viscometry to investigate its chemical properties. As well as XRD measurement (Figure 2.11), ^{13}C CP/MAS NMR indicated that both individually ball-milled and mix-milled cellulose samples were in amorphous form (Figure 2.21). The *CrI* values determined from the C4 signals based on eq. 1.2 for both samples were less than 5%. The DP of mix-milled cellulose was determined 690 by viscometry with 9 wt% LiCl/DMAc at 303 K and the Mark-Houwink-Sakurada equation (eq. 2.4).[26]

$$[\eta] = KM_w^a \qquad (2.4)$$

in which $[\eta]$ (dL g^{-1}) and M_w are intrinsic viscosity and weight-average molecular weight, respectively. The values of K and a when using 9 wt% LiCl/DMAc at 303 K have been reported 1.278×10^{-3} dL g^{-1} and 1.19 in a reference.[26] Intrinsic viscosity is determined from eq. 2.5 and experimental data (Figure 2.22).

$$[\eta] = \lim_{c \to 0} \frac{\frac{t}{t_0} - 1}{c} \qquad (2.5)$$

where c (unit: g dL^{-1}) is concentration of solution, t (s) is flow time of solution in viscometer, and t_0 (s) is flow time of solvent (in this study, 9 wt% LiCl/DMAc).

H_2SO_4[29,34] and Amberlyst 70 (*vide supra*) hydrolyzed cellulose during the milling process, but K26 did not; the DP of mix-milled cellulose (690) was as high as half of that of microcrystalline cellulose (1240) and the value was similar to that of individually milled cellulose (640). Thus, the difference in the catalytic performance between individually ball-milled cellulose (Table 2.5, entry 26) and mix-milled cellulose (Table 2.5, entry 35) is not ascribed to the nature of cellulose but to the hydrolytic activities of the catalyst and the contact between the catalyst and cellulose.

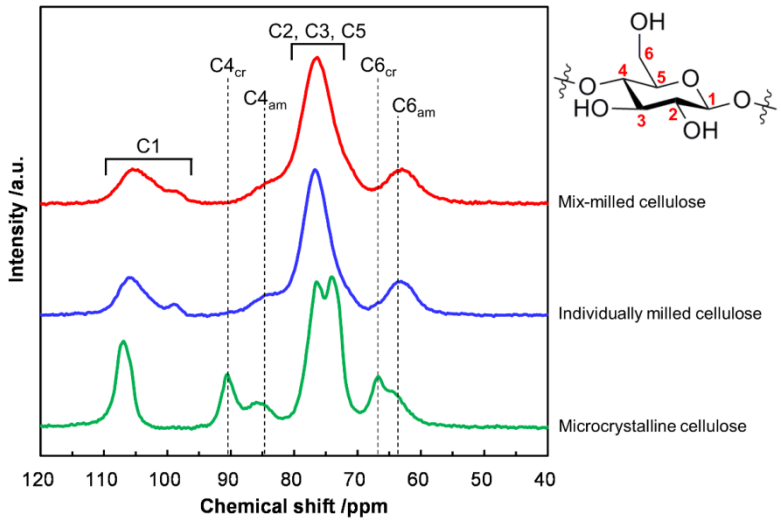


Figure 2.21. ^{13}C CP/MAS NMR spectra of mix-milled cellulose containing K26 and individually ball-milled cellulose. $C4_{cr}$ and $C6_{cr}$ show the chemical shifts of C4 and C6 in crystalline cellulose and $C4_{am}$ and $C6_{am}$ represent those in amorphous one.

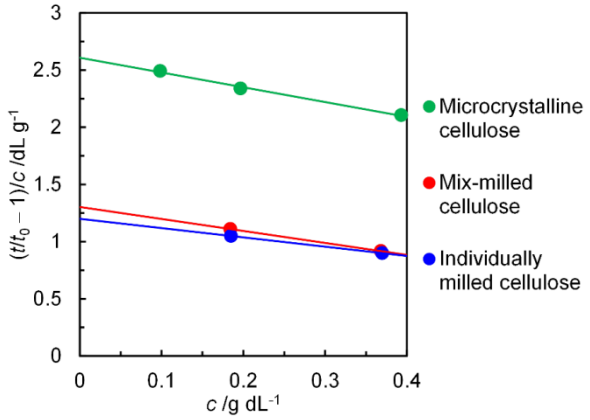


Figure 2.22. Plots of $(t/t_0 - 1)/c$ against c. In the figure, the intercept is corresponding to $[\eta]$.

Next, the roles of mix-milling were evaluated in model reactions using soluble catalysts or substrates. If the major role of mix-milling pre-treatment is improvement of the solid-solid contact, then the promotional effect of mix-milling will disappear in these cases since use of a soluble substrate or catalyst gives a liquid-solid reaction. Therefore, the author carried out the mix-milling and hydrolysis for two types of substrate-catalyst combinations: (i) cellobiose (water-soluble substrate) and K26 (insoluble catalyst) and (ii) cellulose (insoluble substrate) and benzoic acid (soluble catalyst). The author chose benzoic acid as a soluble

catalyst because this compound is a typical model for the active sites of weakly-acidic carbons (see Section 3.3.2). Note that a typical soluble catalyst H_2SO_4 is not suitable for this solid-solid mixing because H_2SO_4 itself is liquid and furthermore this strong acid depolymerizes cellulose during the mix-milling treatment.[29,34] For the combination (i), the hydrolysis of cellobiose by K26 was performed with or without the mix-milling pre-treatment. As expected, the reactions provided almost the same yields of glucose (Table 2.7, entries 51 and 52). In both cases, *ca.* 90% of cellobiose dissolved in H_2O at room temperature, and the remaining part (*ca.* 10%) adsorbed onto K26 (see Section 3.3.3). Therefore, the contact between K26 and cellobiose in both cases were the same during the hydrolysis reaction. Likewise, the combination (ii) indicated no positive effect of mix-milling, in which almost no difference in product yields was observed with or without mix-milling (entries 53 and 54). Benzoic acid completely dissolved in H_2O at the reaction temperature. In contrast, the mix-milling pre-treatment drastically enhanced the hydrolysis with the combination of cellulose and K26; the yield of glucans (glucose and oligomers) was increased by a factor of seven, from 13% to 90% (entries 35 and 55). Mix-milling pre-treatment accelerates solid-solid reactions but not liquid-solid ones. These results indicate that the predominant role of the mix-milling is to improve solid-solid contacts.

A kinetic study of the hydrolysis of cellulose was conducted to quantitatively estimate the effect of mix-milling, in which 418 K was selected to accurately determine the kinetic parameters under the steady state. Figure 2.23 shows the time course of the depolymerization of mix-milled cellulose containing K26.

Table 2.7. Effect of solubility of substrate and catalyst on hydrolysis after the mix-milling pre-treatment.

Entry	Pre-treatment	Substrate	Catalyst	Conv. /%	Yield based on carbon /%	
					Glc[a]	Olg[b]
51[c]	Only K26 was milled.	Cellobiose	K26	12[f]	9.0	–
52[c]	Mix-milling	Cellobiose	K26	14[f]	11	–
53[d]	Only cellulose was milled.	Cellulose	Benzoic acid	17	3.4	9.8
54[d]	Mix-milling	Cellulose	Benzoic acid	13	2.7	8.7
55[e]	Individual milling	Cellulose	K26	18	2.9	10
35[e]	Mix-milling	Cellulose	K26	93	20	70

[a]Glucose. [b]Water-soluble oligosaccharides (DP = mainly 2–6). [c]Cellobiose 342 mg, K26 50 mg, H_2O 40 mL, 463 K, <1 min (rapid heating-cooling condition). [d]Cellulose 324 mg, benzoic acid 50 mg, H_2O 40 mL, 453 K, 20 min. [e]Cellulose 324 mg, K26 50 mg, H_2O 40 mL, 453 K, 20 min. [f]Conversion of cellobiose was calculated from the total amount of recovered and adsorbed cellobiose. For the estimation of adsorbed amount of cellobiose, the adsorption equilibrium constant and adsorption capacity[35] were used.

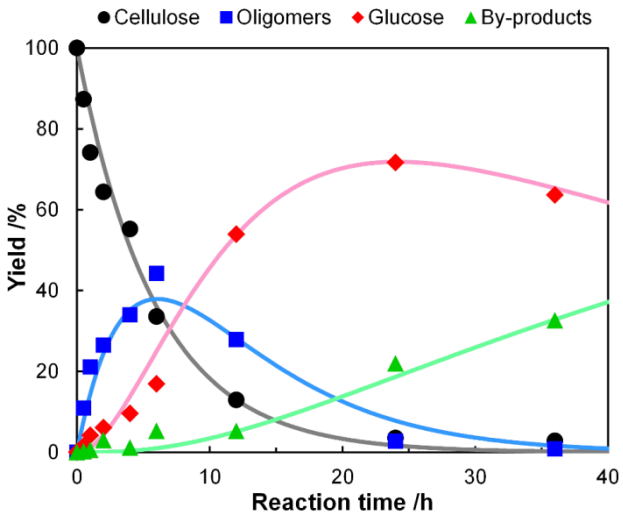


Figure 2.23. Time course of hydrolysis of mix-milled cellulose containing K26 at 418 K. The dots show the experimental data and the lines are the results of kinetic simulations based on eqs. 2.11–2.14.

The amount of cellulose (black circles) decreased, whereas that of soluble oligosaccharides (blue squares) increased in the initial period. The yield of oligomers was maximized at 6 h (44%) and then gradually decreased as the oligomers were intermediates to glucose in this reaction. With regard to glucose, a small amount of glucose (red diamonds) was simultaneously produced with the oligosaccharides from cellulose, but glucose mainly formed after the oligosaccharides accumulated. The yield of glucose reached 72% at 24 h with 97% conversion of cellulose and 74% selectivity (Table 2.5, entry 48). The yield of glucose started to decrease after 24 h due to the decomposition, as by-products (green triangles) increased. Accordingly, the hydrolysis of cellulose predominantly consists of three steps as shown in eq. 2.6,[36] for which first-order dependence on substrates were hypothesized as reported elsewhere.[37–39]

$$\text{Cellulose} \xrightarrow{k_1} \text{Oligomers} \xrightarrow{k_2} \text{Glucose} \xrightarrow{k_3} \text{By-products} \qquad (2.6)$$

where k_1, k_2, and k_3 (unit: h^{-1}) are pseudo first-order rate constants of respective steps.

The reaction rate for each step was represented as eqs. 2.7–2.10.

$$\frac{\mathrm{d}[\mathrm{Cellulose}]}{\mathrm{d}t} = -k_1[\mathrm{Cellulose}] \qquad (2.7)$$

$$\frac{\mathrm{d}[\mathrm{Oligomers}]}{\mathrm{d}t} = k_1[\mathrm{Cellulose}] - k_2[\mathrm{Oligomers}] \qquad (2.8)$$

$$\frac{\mathrm{d}[\mathrm{Glucose}]}{\mathrm{d}t} = k_2[\mathrm{Oligomers}] - k_3[\mathrm{Glucose}] \qquad (2.9)$$

$$\frac{\mathrm{d}[\mathrm{By\text{-}products}]}{\mathrm{d}t} = k_3[\mathrm{Glucose}] \qquad (2.10)$$

where [Cellulose], [Oligomers], [Glucose], and [By-products] (unit: M) are concentrations of respective compounds and t (h) is time. The integration of these formulae gives eqs. 2.11–2.14.

$$[\mathrm{Cellulose}] = [\mathrm{Cellulose}]_0 \mathrm{e}^{-k_1 t} \qquad (2.11)$$

$$[\mathrm{Oligomers}] = [\mathrm{Cellulose}]_0 \frac{k_1}{k_2 - k_1}\left(\mathrm{e}^{-k_1 t} - \mathrm{e}^{-k_2 t}\right) \qquad (2.12)$$

$$[\mathrm{Glucose}] = [\mathrm{Cellulose}]_0 \frac{k_1 k_2}{k_2 - k_1}\left\{\frac{1}{k_3 - k_1}\left(\mathrm{e}^{-k_1 t} - \mathrm{e}^{-k_3 t}\right) + \frac{1}{k_3 - k_2}\left(\mathrm{e}^{-k_3 t} - \mathrm{e}^{-k_2 t}\right)\right\} \qquad (2.13)$$

$$[\mathrm{By\text{-}products}] = [\mathrm{Cellulose}]_0 - [\mathrm{Cellulose}] - [\mathrm{Oligomers}] - [\mathrm{Glucose}] \qquad (2.14)$$

where $[\mathrm{Cellulose}]_0$ (unit: M) is initial concentration of cellulose and $k_1 \neq k_2 \neq k_3$.

Four lines in Figure 2.23 represent curve fitting using eqs. 2.11–2.14, which have reproduced the experimental data. The determined rate constants from the curve fitting were k_1 = 0.17 h^{-1}, k_2 = 0.16 h^{-1}, and k_3 = 0.017 h^{-1}. The rate constant of hydrolysis of cellulose to soluble oligosaccharides was as high as that of oligosaccharides to glucose (k_1/k_2 = 1.1). It is surprising that k_1/k_2 exceeds 1 as the rate-determining step of the hydrolysis of cellulose to glucose is generally the first step,[36] suggesting that the conversion of solid cellulose to soluble oligomers is selectively accelerated by the mix-milling. In addition, high k_1/k_3 (10) and k_2/k_3 (9.4) ratios provide a good yield of glucose because the decomposition of glucose is relatively slow.

The hydrolysis of individually ball-milled cellulose by K26 at 418 K was also performed to highlight the effect of mix-milling. Note that the reactivity itself of individually ball-milled cellulose should be similar to that of mix-milled cellulose, as their polymerization degrees determined by viscometry (640–690), median

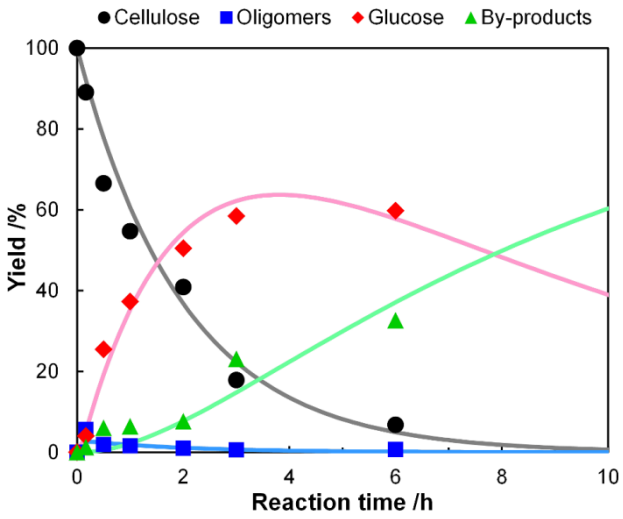


Figure 2.24. Time course of hydrolysis of individually ball-milled cellulose by H_2SO_4 (50 mM) at 418 K. The dots show the experimental data and the lines are the results of kinetic simulations based on eqs. 2.11–2.14.

particle diameters (37–40 μm), and *CrI*s (<5%) are almost the same (*vide supra*). Since the hydrolysis reaction was slow in this case, the products were analyzed by a sampling method to improve the accuracy. The formation of oligomers, subsequent production of glucose and successive decomposition of glucose were observed in this reaction. Therefore, the same curve fitting was applied to this reaction, which provided rate constants of k_1 = 0.013 h^{-1}, k_2 = 0.16 h^{-1}, and k_3 = 0.017 h^{-1}. k_1 was 13-fold decreased by changing the pre-treatment from mix-milling to individual milling, while the values of k_2 and k_3 were similar regardless of the pre-treatment methods. As a result, the ratio of k_1/k_2 was as small as 0.018, showing that the hydrolysis of cellulose to soluble oligomers was the rate-determining step. Consequently, the author has quantitatively revealed that the mix-milling selectively and drastically increases k_1 in the solid-solid reaction.

A typical soluble acid H_2SO_4 was also tested as a catalyst for the hydrolysis of individually ball-milled cellulose in order to compare solid-solid and solid-liquid reactions (Figure 2.24). The concentration of H_2SO_4 was set at 50 mM (0.49%) as a usual value for the diluted H_2SO_4 processes.[9,11,40] The rate constants obtained by a curve fitting were k_1 = 0.5 h^{-1}, k_2 = 17 h^{-1}, and k_3 = 0.12 h^{-1}. The first step is slow (k_1/k_2 = 0.029), indicating that the hydrolysis of cellulose to soluble oligosaccharides is the rate-determining step for the

production of glucose. This result is reasonable as the hydrolysis of cellulose is significantly more difficult than that of soluble oligomers.[36] Therefore, the high ratio of k_1/k_2 for the hydrolysis using K26 and mix-milling is specific to this reaction, and the author concludes that the solid-solid contact created by mix-milling can selectively accelerate the solid-solid reaction.

2.4. Conclusions

Simple carbon materials catalyze hydrolysis of cellulose, and the catalytic activity correlates with the amounts of weakly acidic groups. It is demonstrated that such weak acid catalysts can survive in the presence of buffer and salt potentially derived from real biomass. However, the loose contact between the solid substrate and solid catalyst limits the yield of glucose at most 36% even when using the most active catalyst, an alkali-activated carbon K26. This obstacle has been overcome by a new pre-treatment method, namely mix-milling cellulose and K26 to make tight contact. The hydrolysis of mix-milled cellulose provides a 72% yield of glucose in pure water and an 88% yield with 90% selectivity in 0.012% HCl, which are one of the highest glucose yields ever reported. The mix-milling pre-treatment is also effective for the depolymerization of cellulose/hemicellulose in bagasse kraft pulp, resulting in 80% and 92% yields of hexoses and pentoses, respectively. Characterization of mix-milled cellulose, a series of model reactions, and kinetic studies show that the hydrolysis of insoluble cellulose to soluble oligomers over a carbon catalyst is selectively and drastically accelerated owing to tight contact between solid cellulose and solid K26 created by the mix-milling pre-treatment.

Recently, it has been reported that the mix-milling pre-treatment is also effective for hydrolytic hydrogenation of cellulose to sorbitol by carbon-supported metal catalysts since the first step is the same hydrolysis of insoluble cellulose to water-soluble oligomers.[41,42] Mix-milling is a promising method to overcome a fundamental problem of solid-solid reactions, namely loose contact between solids, by making tight contact. This pre-treatment method would be applicable to other reactions, *e.g.*, oxidation of diesel soot particulates by solid catalysts.[24]

References

1. R. Rinaldi and F. Schüth, *Energy Environ. Sci.*, 2009, **2**, 610–626.
2. D. M. Alonso, J. Q. Bond, and J. A. Dumesic, *Green Chem.*, 2010, **12**, 1493–1513.
3. P. Gallezot, *Chem. Soc. Rev.*, 2012, **41**, 1538–1558.
4. C. O. Tuck, E. Pérez, I. T. Horváth, R. A. Sheldon, and M. Poliakoff, *Science*, 2012, **337**, 695–699.
5. M. Besson, P. Gallezot, and C. Pinel, *Chem. Rev.*, 2013, **114**, 1827–1870.
6. M. Yabushita, H. Kobayashi, and A. Fukuoka, *Appl. Catal. B: Environ.*, 2014, **145**, 1–9.
7. J. C. Serrano-Ruiz, R. M. West, and J. A. Dumesic, *Annu. Rev. Chem. Biomol. Eng.*, 2010, **1**, 79–100.
8. G. W. Huber, S. Iborra, and A. Corma, *Chem. Rev.*, 2006, **106**, 4044–4098.
9. H. Kobayashi and A. Fukuoka, *Green Chem.*, 2013, **15**, 1740–1763.
10. O. Akpinar, R. J. McGorrin, and M. H. Penner, *J. Agric. Food Chem.*, 2004, **52**, 4144–4148.
11. R. Rinaldi and F. Schüth, *ChemSusChem*, 2009, **2**, 1096–1107.
12. H. Kobayashi, H. Ohta, and A. Fukuoka, *Catal. Sci. Technol.*, 2012, **2**, 869–883.
13. F. Schüth, R. Rinaldi, N. Meine, M. Käldström, J. Hilgert, and M. D. K. Rechulski, *Catal. Today*, 2014, **234**, 24–30.
14. H. Kobayashi, T. Komanoya, K. Hara, and A. Fukuoka, *ChemSusChem*, 2010, **3**, 440–443.
15. T. Komanoya, H. Kobayashi, K. Hara, W.-J. Chun, and A. Fukuoka, *Appl. Catal. A: Gen.*, 2011, **407**, 188–194.
16. S. Suganuma, K. Nakajima, M. Kitano, D. Yamaguchi, H. Kato, S. Hayashi, and M. Hara, *J. Am. Chem. Soc.*, 2008, **130**, 12787–12793.
17. A. Onda, T. Ochi, and K. Yanagisawa, *Green Chem.*, 2008, **10**, 1033–1037.
18. X. Mo, D. E. López, K. Suwannakarn, Y. Liu, E. Lotero, J. G. Goodwin Jr., and C. Lu, *J. Catal.*, 2008, **254**, 332–338.
19. P.-W. Chung, A. Charmot, O. A. Olatunji-Ojo, K. A. Durkin, and A. Katz, *ACS Catal.*, 2013, **4**, 302–310.
20. A. Charmot, P.-W. Chung, and A. Katz, *ACS Sustainable Chem. Eng.*, 2014, **2**, 2866–2872.

21. A. Sluiter, B. Hames, R. Ruiz, C. Scarlata, J. Sluiter, D. Templeton, and D. Crocker, *Technical Report NREL/TP-510-42618*, 2011, http://www.nrel.gov/biomass/pdfs/42618.pdf (accessed Nov. 20, 2014).
22. S. Jun, S. H. Joo, R. Ryoo, M. Kruk, M. Jaroniec, Z. Liu, T. Ohsuna, and O. Terasaki, *J. Am. Chem. Soc.*, 2000, **122**, 10712–10713.
23. H. P. Boehm, *Carbon*, 1994, **32**, 759–769.
24. B. R. Stanmore, J. F. Brilhac, and P. Gilot, *Carbon*, 2001, **39**, 2247–2268.
25. M. Strlic, J. Kolenc, J. Kolar, and B. Pihlar, *J. Chromatogr. A*, 2002, **964**, 47–54.
26. C. L. McCormick, P. A. Callais, and B. H. Hutchinson, *Macromolecules*, 1985, **18**, 2394–2401.
27. O. Bobleter, *Prog. Polym. Sci.*, 1994, **19**, 797–841.
28. J. Strachan, *Nature*, 1938, **141**, 332–333.
29. A. Shrotri, L. K. Lambert, A. Tanksale, and J. Beltramini, *Green Chem.*, 2013, **15**, 2761–2768.
30. J. Geboers, S. Van de Vyver, K. Carpentier, P. Jacobs, and B. Sels, *Chem. Commun.*, 2011, **47**, 5590–5592.
31. ICIS, "Hydrochloric acid Prices, markets & analysis," http://www.icis.com/chemicals/hydrochloric-acid/ (accessed Nov. 20, 2014).
32. Nexant, "Sulfur/Sulfuric Acid Market Analysis," http://yosemite.epa.gov/oa/eab_web_docket.nsf/Filings%20By%20Appeal%20Number/EFAE40E5FFEFBBF785257A2A0047AC45/$File/Exhibit%2052m%20to%20Revised%20Petition%20for%20Review%20...12.52m.pdf (accessed Nov. 20, 2014).
33. Y. Maréchal and H. Chanzy, *J. Mol. Struct.*, 2000, **523**, 183–196.
34. N. Meine, R. Rinaldi, and F. Schüth, *ChemSusChem*, 2012, **5**, 1449–1454.
35. M. Yabushita, H. Kobayashi, J. Hasegawa, K. Hara, and A. Fukuoka, *ChemSusChem*, 2014, **7**, 1443–1450.
36. N. Abatzoglov, J. Bouchard, E. Chornet, and R. P. Overend, *Can. J. Chem. Eng.*, 1986, **64**, 781–786.
37. J. F. Saeman, *Ind. Eng. Chem.*, 1945, **37**, 43–52.
38. M. Sasaki, B. Kabyemela, R. Malaluan, S. Hirose, N. Takeda, T. Adschiri, and K. Arai, *J. Supercrit. Fluids*, 1998, **13**, 261–268.

39. H. Kobayashi, Y. Ito, T. Komanoya, Y. Hosaka, P. L. Dhepe, K. Kasai, K. Hara, and A. Fukuoka, *Green Chem.*, 2011, **13**, 326–333.

40. W. L. Faith, *Ind. Eng. Chem.*, 1945, **37**, 9–11.

41. T. Komanoya, H. Kobayashi, K. Hara, W.-J. Chun, and A. Fukuoka, *ChemCatChem*, 2014, **6**, 230–236.

42. Y. Liao, Q. Liu, T. Wang, J. Long, Q. Zhang, L. Ma, Y. Liu, and Y. Li, *Energy Fuels*, 2014, **28**, 5778–5784.

Chapter 3

Mechanistic Study of Cellulose Hydrolysis by Carbon Catalysts

The structure-activity correlation by carbon catalysts for hydrolysis of glycosidic bonds in cellulosic molecules has been investigated. The characterization of carbon materials by titration and infrared spectroscopy indicates that hydrophilic functionalities contribute to catalytic activity; especially, vicinal oxygenated functional groups as in salicylic acid and phthalic acid show high catalytic performance due to increase of frequency factor but not to decrease of activation energy. One of the functional groups forms a hydrogen bond with a hydroxyl group of the substrate and another group gains an opportunity to activate and hydrolyze a glycosidic bond. In addition, it is found that hydrophobic surface of carbon plays important roles for adsorption process of cellulosic molecules, and this function increases the possibility to hydrolyze the substrate. Finally, the author proposes reaction mechanism for cellulose hydrolysis by carbon catalyst.

3.1. Introduction

In Chapter 2, the author has conducted the screening of carbon catalysts for cellulose hydrolysis and found that catalytic activity strongly depended on their nature. The preliminary study has represented that the amount of weakly acidic sites detected by the Boehm titration[1] positively correlates with catalytic activity for glucose production from cellulose (Figure 2.4). Surprisingly, K26 similarly accelerated the hydrolysis of cellulose even after acetate buffer and NaCl treatment (pH 4 and 7); weak acids are major active sites for the reaction. However, the detailed structure of active sites and their catalytic mechanisms have still remained unclear, which should be clarified for catalytic science and for designing highly active carbon catalysts. Hence, the first objective of this chapter is to reveal the roles of weak acids on carbon catalysts by structural characterization, model reactions, kinetics, and thermodynamics.

The author has so far focused on the cleavage of glycosidic bonds itself. Meanwhile, in heterogeneous catalysis, adsorption of substrates on catalyst surface is also essential for starting and accelerating reactions.[2,3] In the literatures, cellulosic molecules immobilized through ether bonds on SiO_2 and Al_2O_3 are easily hydrolyzed by surface OH groups (with pK_a in the range of 7), whereas these oxides are inactive for the hydrolysis of *free* cellulose dispersed in H_2O.[4–6] The hydrolysis of glycosidic bonds by weakly acidic groups is surprising since acids with a pK_a value larger than –3 are usually inactive for the hydrolysis.[7] Therefore, it is evident that even weak acids can hydrolyze cellulose by strongly interacting with it, and so the adsorption of cellulosic molecules could be involved in the high performances of carbon-based catalysts (Figure 3.1). Herein, the author has investigated both thermodynamics and computational calculations to understand the adsorption process.

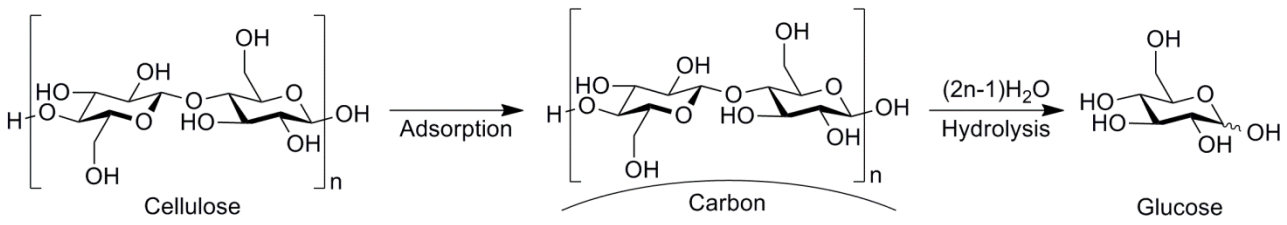


Figure 3.1. Scheme of cellulose conversion by carbon catalysts *via* adsorption.

3.2. Experimental

3.2.1. Reagents

Microcrystalline cellulose	Column chromatography grade, 102331, Merck
D(+)-Cellobiose	Special grade, Kanto Chemical
K26	Alkali-activated carbon (not for sale), Showa Denko
ZTC	Zeolite-templated carbon,[8] electrolytically oxidized, Prof. Kyotani's group in Tohoku University
Phenol	Special grade, Kanto Chemical
Benzoic acid	Special grade, Wako Pure Chemical Industries
Salicylic acid	Special grade, Wako Pure Chemical Industries
m-Hydroxybenzoic acid	First grade, Wako Pure Chemical Industries
p-Hydroxybenzoic acid	First grade, Wako Pure Chemical Industries
4-Trifluoromethylsalicylic acid	Special grade, Wako Pure Chemical Industries
Phthalic acid	Special grade, Wako Pure Chemical Industries
o-Chlorobenzoic acid	Special grade, Wako Pure Chemical Industries
o-Trifluoromethylbenzoic acid	First grade, Wako Pure Chemical Industries
Catechol	>99.0%, Tokyo Chemical Industry
3,4-Dihydrocoumarin	Special grade, Wako Pure Chemical Industries
Isochroman-1-one	97%, Wako Pure Chemical Industries
Cellohexaose	>95%, Seikagaku Biobusiness
Cellopentaose	>95%, Seikagaku Biobusiness
Cellotetraose	>97%, Seikagaku Biobusiness
Cellotriose	>97%, Seikagaku Biobusiness
D(+)-Glucose	Special grade, Kanto Chemical
D(+)-Mannose	Special grade, Wako Pure Chemical Industries
D(–)-Fructose	Special grade, Kanto Chemical
1,6-Anhydro-β-D-glucopyranose	99%, Wako Pure Chemical Industries, denoted as levoglucosan

5-Hydroxymethylfurfural	99%, Sigma-Aldrich, denoted as 5-HMF
Furfural	>98.0%, Tokyo Chemical Industry
Distilled water	Wako Pure Chemical Industries
Dimethyl sulfoxide	Special grade, Wako Pure Chemical Industries, denoted as DMSO
Distilled water	For HPLC, Wako Pure Chemical Industries
Deuterated dimethyl sulfoxide	For NMR, Acros Organics, denoted as DMSO-d_6
Sodium hydrogen carbonate	Special grade, Wako Pure Chemical Industries
Sodium carbonate solution	0.05 M, for volumetric analysis, Wako Pure Chemical Industries
Sodium hydroxide solution	0.05 M, for volumetric analysis, Wako Pure Chemical Industries
Hydrochloric acid solution	0.05 M, for volumetric analysis, Wako Pure Chemical Industries
Methyl orange	Special grade, Wako Pure Chemical Industries
Cyclohexane	Special grade, Wako Pure Chemical Industries
Helium gas	Alpha gas 1, Air Liquide Kogyo Gas
Helium gas	99.9999%, Hokkaido Air Water, used for N_2 adsorption-desorption measurement
Nitrogen gas	Alpha gas 2, Air Liquide Kogyo Gas
Nitrogen gas	99.999%, Hokkaido Air Water, used for N_2 adsorption-desorption measurement
Argon gas	Alpha gas 2, Air Liquide Kogyo Gas

3.2.2. Heat-treatment of alkali-activated carbon K26

Alkali-activated carbon K26 was heat-treated under He flow to partially remove surface functional groups[9] in a fixed-bed flow reactor (Figure 3.2) at various temperatures. K26 (2.00 g) was charged into a quartz tube, and the tube was set in an electric furnace (Asahi Rika, ARF-30K). The heater was controlled by a thyristor (Shimaden, PAC-15C, cycle calculation zero voltage switching) equipped with a program controller (Shimaden, FP93) and a thermocouple (Chino, type K, JIS class 1, ø1.6 mm) set aside of the sample. Temperature of the sample was monitored by another thermocouple attached in a bottom dimple of the

reactor. The difference in temperatures for the two thermocouples was less than 3 K in the experiments. Temperature of the heater was increased to 393 K by 10 K min^{-1} and maintained for 1 h to remove physisorbed H_2O under He flow (10 mL min^{-1}, kept by a needle bulb [Kojima Instruments (Kofloc), Variable Secondary Pressure Flow Controller Model 2203]). Then, the reactor was heated to a designated temperature (673, 873, 1073, and 1273 K) under He flow (10 mL min^{-1}), and K26 was treated at the temperature for 2 h under He flow (3 mL min^{-1}). The samples treated at the temperatures were denoted as K26-673 (recovery 1.82 g), K26-873 (1.79 g), K26-1073 (1.73 g), and K26-1273 (1.72 g).

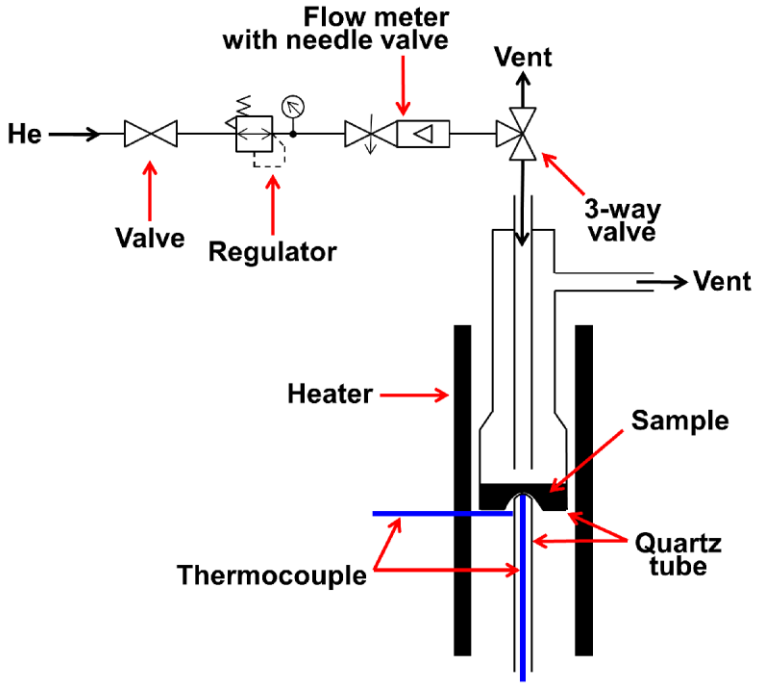


Figure 3.2. Diagram of the fixed-bed flow reactor.

3.2.3. Characterization of carbon materials

Carbon materials were characterized by several physicochemical methods. The specific surface area of samples based on the Brunauer-Emmett-Teller (BET) theory was determined by N_2 adsorption-desorption measurements (BEL Japan, BELSORP-mini) at 77 K after drying at 393 K for 4 h under vacuum (<10 Pa). For micropore analysis, an automated apparatus (BEL Japan, BELSORP-max, equipped with a turbo-molecular pump) was employed, and the isotherm was recorded from 1×10^{-8} to 0.997 of relative

pressure at 77 K. This instrument can detect ≥0.4 nm of micropores using N_2 as an adsorbate.[10] The specific external surface area was determined from the *t*-plot method based on a standard isotherm for carbon and distribution of pore diameter was estimated from a nonlocal density functional theory (NLDFT) calculation (slit model of carbon black, atomic diameter of adsorbent: 0.142 nm, distribution function: no assumption). The secondary particle size of carbon materials was analyzed in H_2O by laser diffraction (Nikkiso, Microtrac MT3300EXII).

The qualitative analysis of surface functional groups was conducted by diffuse reflectance infrared Fourier transform [DRIFT, PerkinElmer, Spectrum 100, mercury-cadmium-telluride (MCT) detector] spectroscopy. The amounts of carboxylic acids, lactones, and phenolic groups on carbons were quantified by the Boehm titration[1] with the same procedure as Section 2.2.3.

The framework of carbon was analyzed by ^{13}C CP/MAS-TOSS NMR (JEOL, JNM-ECX400, 100 MHz, MAS frequency 5 kHz, TOSS: total suppression of sidebands), Raman spectroscopy [Renishaw inVia Raman microscope, Nd:YAG laser using second harmonic generation (532 nm, YAG: yttrium-aluminium-garnet)], and XRD (Rigaku, Ultima IV, Cu Kα). The average size of graphene sheet in carbon was estimated using Raman spectroscopy and the Knight formula for 532 nm of laser (eq. 3.1).[11,12]

$$L_a = 2.4 \times 10^{-10} \lambda^4 \left(\frac{I_G}{I_D} \right) \quad (3.1)$$

where L_a (unit: nm) is average size of graphene sheet, λ (nm) is wavelength of laser, I_D is intensity of D-band, and I_G is intensity of G-band observed by Raman spectroscopy.

The hydrophobicity was evaluated by cyclohexane adsorption under saturated vapor pressure at 298 K.

3.2.4. Ball-milling pre-treatment and hydrolysis of cellulose

Microcrystalline cellulose (10 g) was ball-milled in the presence of ZrO_2 balls (ø1.0 cm, 1 kg) in a ceramic pot (0.9 L) at 60 rpm for 96 h. The hydrolysis of cellulose was conducted by the same manner described in Section 2.2.6.

3.2.5. Hydrolysis of cellobiose by aromatic compounds

Cellobiose (342 mg) and aromatic compound in aqueous solution (0.5 mM, 40 mL) were charged into a hastelloy C22 high-pressure reactor (OM Lab-Tech, MMJ-100, 100 mL, Figure 2.2). The temperature was increased to 443 K for *ca.* 10 min, maintained for 10 min, and decreased to room temperature. After the reaction, products in solution were analyzed by HPLC (see Section 2.2.6).

3.2.6. Adsorption of cellulosic molecules

K26 (25 mg) or ball-milled cellulose (500 mg) was dispersed in an aqueous solution of cellobiose (20 mL). The suspension was stirred at 600 rpm at a designated temperature until adsorption reaching equilibrium (>1 h), after which the mixture was filtered through a polyvinylidene difluoride (PVDF) 0.20 μm mesh membrane maintained at the same temperature. The liquid phase obtained was immediately analyzed by HPLC with a Rezex RPM-Monosaccharide Pb++ column (Phenomenex, ø7.8 mm × 300 mm, mobile phase: H_2O at 0.6 mL min^{-1}, 343 K). The amount of cellobiose detected by HPLC was determined by an absolute calibration method, and the resulting data were applied to calculate the amount of cellobiose adsorbed on carbon material. The amount of carbon used in these experiments was changed to 100 mg when studying the adsorption of glucose and to 12.5 mg when using cellotriose in order to improve accuracy.

Adsorption experiment at 413 K was performed in the hastelloy-C22 high-pressure reactor into which He was introduced through a nozzle at 2 MPa (Figure 3.3). Another nozzle was equipped with a PTFE membrane (0.10 μm mesh) on the inlet and a needle bulb at the outlet. After reaching adsorption equilibrium, the solution was ejected by applying pressure of He, in which the outlet was cooled. The first 5 mL fraction was discarded and the subsequent 5 mL of solution was used for the analysis.

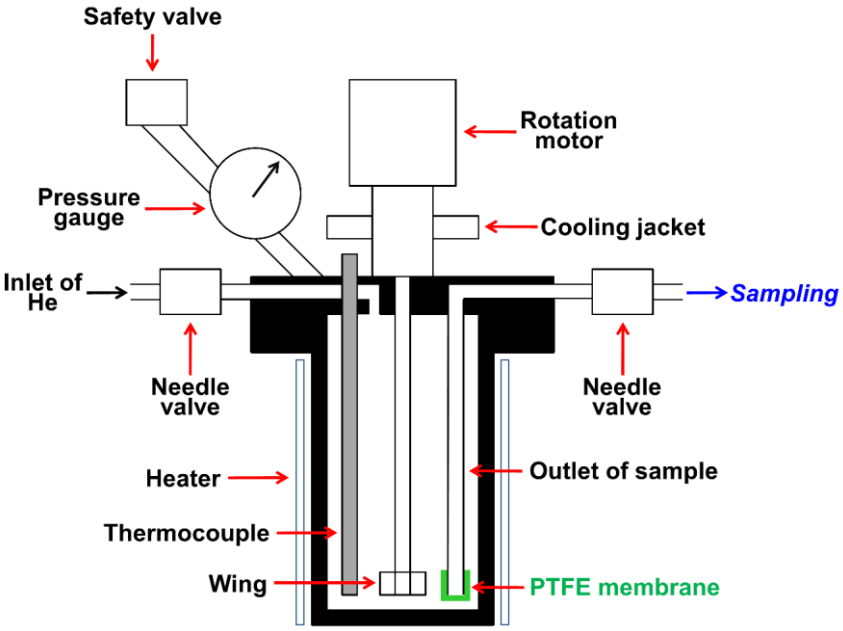


Figure 3.3. Diagram of an apparatus for the adsorption experiment at 413 K. During the experiment, 2 MPa of He was charged in the apparatus.

3.2.7. Computational modeling of adsorption state

The adsorption structures of cellobiose on carbon were calculated by using the Gaussian 09 program, which employed a model carbon based on quadruple-layered graphene sheets. The author and co-workers adopted two kinds of carbon sheets, A and B, which involved 24 and 19 six-membered rings, respectively. Sheets A and B were stacked in an alternating fashion and cellobiose was adsorbed on sheet A (see Figure 3.19). The structure of the overall system was optimized by density functional theory (DFT) calculations using the Becke 3-parameter Lee-Yang-Parr (B3LYP) function with the 6-31G* basis set.[13–15] Dispersion interactions were also included in an empirical manner by using Grimme's D3 damping function.[16] The solvation effect was taken into account by using the self-consistent reaction field (SCRF) method with a polarized continuum model[17] and the dielectric constant of bulk H_2O was included.

3.3. Results and discussion

3.3.1. Contributions of oxygenated functional groups on carbons for hydrolysis of cellulose

Hydrolysis of cellulose by various carbons indicated that the activity correlated with the amount of weakly acidic groups (Section 2.3.1); however, it is necessary to consider the influence of physical structures of respective carbons. To accurately elucidate the contributions of OFGs for the hydrolytic activity by minimizing the structural effect, K26 was heat-treated[9] under He flow at 673 to 1273 K. This treatment may provide structurally-similar carbons bearing decreased amounts of OFGs. Figure 3.4a depicts hydrolytic activities of the heat-treated K26 samples for the hydrolysis of individually ball-milled cellulose against heat-treatment temperature. For evaluating the activities, conversion and glucose yield obtained in the blank reaction without catalysts were subtracted from those of the catalytic reactions, and ΔConversion and ΔGlucose are defined as follows (eqs. 3.2 and 3.3):

$$\begin{aligned}\Delta\text{Conversion} = &(\text{conversion in the catalytic reaction}) \\ &- (\text{conversion in the control experiment without catalysts, 28\%})\end{aligned} \quad (3.2)$$

$$\begin{aligned}\Delta\text{Glucose} = &(\text{yield of glucose in the catalytic reaction}) \\ &- (\text{yield of glucose in the control experiment without catalysts, 4.6\%})\end{aligned} \quad (3.3)$$

Both ΔConversion and ΔGlucose gradually decreased when elevating the heat-treatment temperature, suggesting the decomposition of active sites of K26 in the heat-treatment. Then, the specific amounts of OFGs of heat-treated K26 samples were determined by the Boehm titration[1] (Figure 3.4b). The amount of carboxylic acids first decreased at *ca.* 673 K, followed by the reduction of lactones. Phenolic groups were slightly more stable than lactones, which was consistent with previous results.[9] The elimination of OFGs was also checked by DRIFT (Figures 3.5). In DRIFT spectra, the peak intensity at 1738 cm^{-1} derived from C=O decreased with increasing heat-treatment temperature, indicating the elimination of carboxylic acids, ketones, and lactones. This peak disappeared by heat-treatment at 1073 K and 1273 K since most of C=O groups decomposed. Although the intensities of the peaks due to O–H and C–O vibrations at 1241 cm^{-1}, 1403 cm^{-1}, and 3523 cm^{-1} also diminished, they still presented even after the heat-treatment at 1273 K.

Hence, OFGs such as alcohols, phenols, and ethers are thermally more stable than carboxylic acids and others. These DRIFT observations agreed well with the results of the titration. Thus, it was concluded that the weakly acidic OFGs were removed in the temperature range of the deactivation of K26.

Morphological change by the heat-treatment was also checked by N_2 adsorption-desorption and laser diffraction measurements. The heat-treated K26 samples provided type I isotherms, indicating similar microporous structures (Figure 3.6). The BET specific surface area decreased from 2270 m^2 g^{-1} to 1730 m^2 g^{-1} along with the decrease of the pore volume from 1.00 cm^3 g^{-1} to 0.75 cm^3 g^{-1} when increasing the heat-treatment temperature (Table 3.1). The distributions of particle diameters were maintained even after the heat-treatment (Figure 3.7), providing almost constant median particle diameters (12–13 μm) (Table 3.1). It is not probable that these small morphological changes of K26 in the heat-treatment are the origin of the deactivation of K26. Instead, the author proposes that the catalytic activity correlates with the specific amounts of OFGs. Since the amounts of respective OFGs are similarly decreased in the heat-treatment, the remaining subject is to clarify the contribution of respective oxygenated groups.

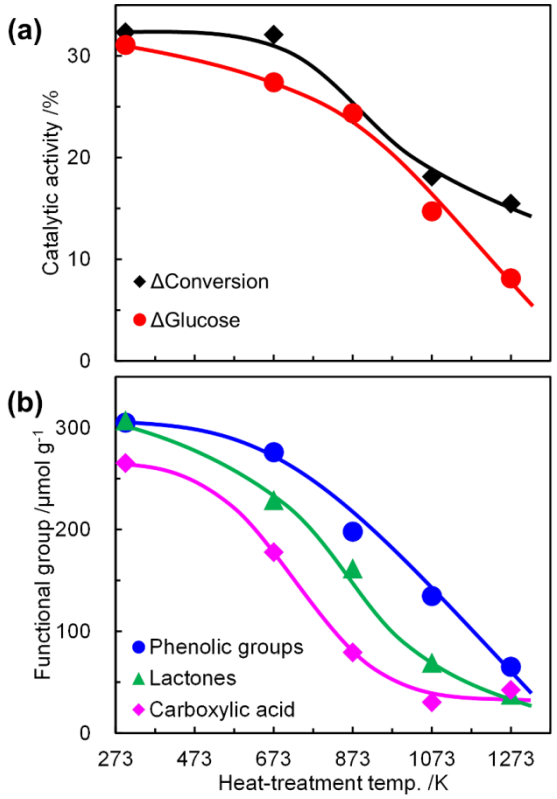


Figure 3.4. (a) Hydrolysis of cellulose by heat-treated K26 catalysts and (b) the specific amounts of OFGs. Definitions of ΔConversion and ΔGlucose are described as eqs. 3.2 and 3.3.

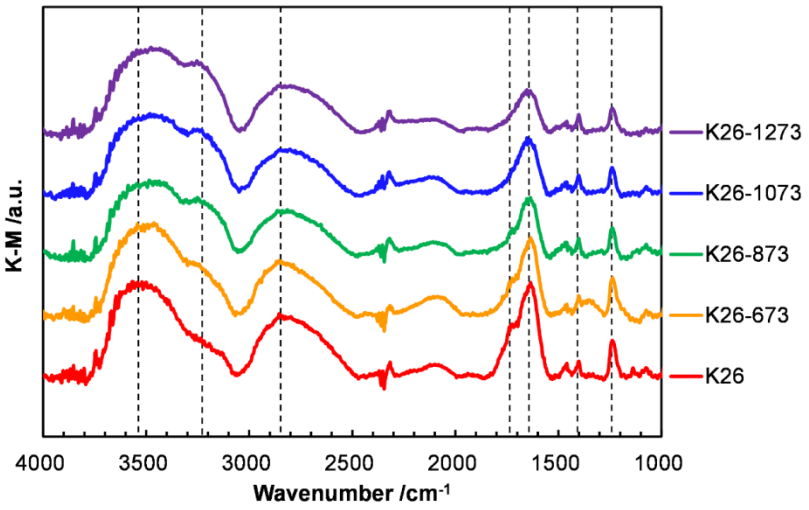


Figure 3.5. DRIFT spectra of heat-treated K26 samples. Assignments (cm^{-1}): 3523 [ν(O–H), ν(OH–O)], 3227 [ν(C–H, aliphatic and aromatic)], 2841 [ν(C–H, aliphatic)], 1738 [ν(C=O)], 1637 [ν(C=C, aliphatic and aromatic)], 1403 [δ(C–H, aliphatic), δ(O–H, carboxyl), γ(O–H, hydroxyl and phenol)], 1241 [ν(C–O)].

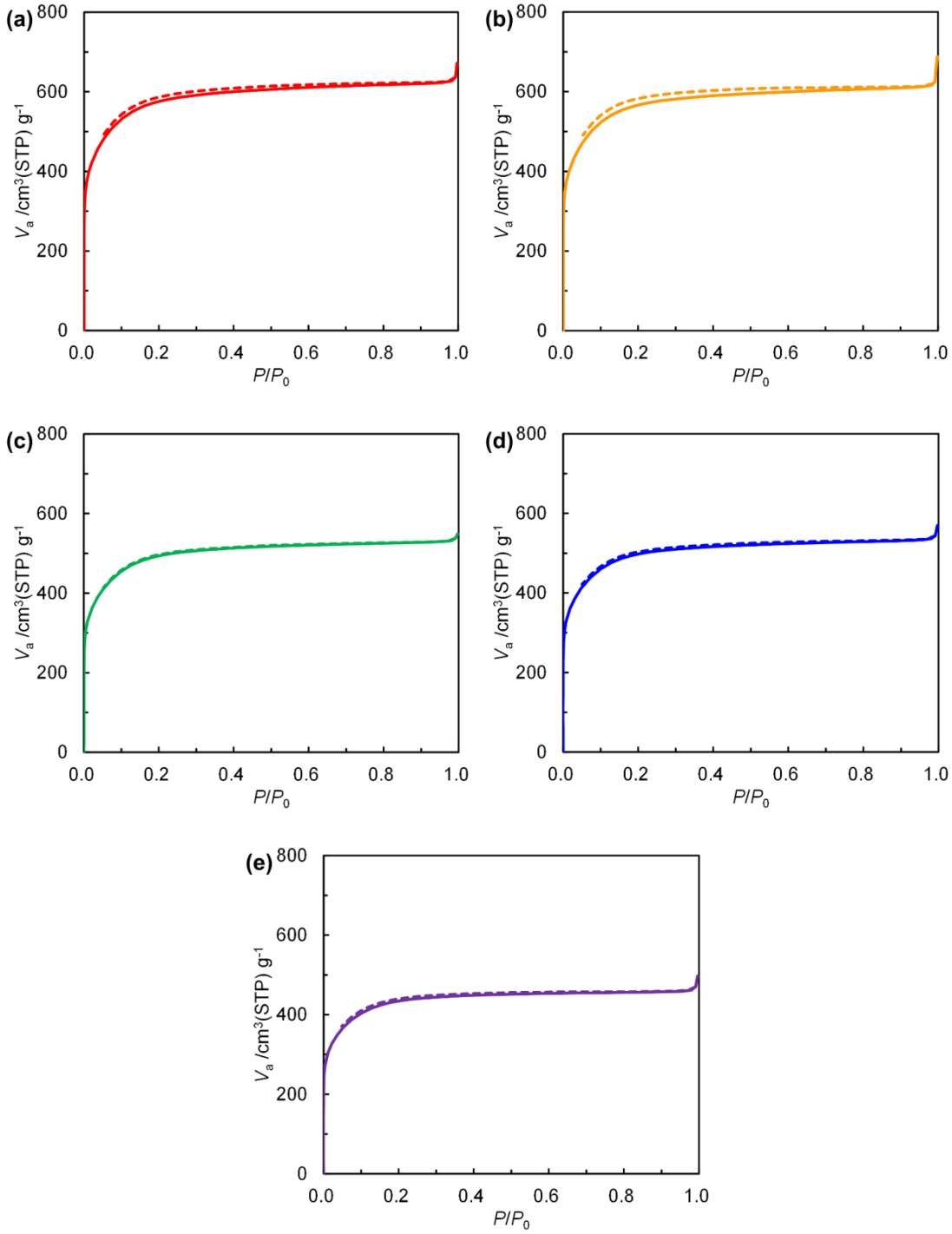


Figure 3.6. N_2 adsorption-desorption isotherms for heat-treated K26 samples at 77 K: (a) non-treated K26, (b) K26-673, (c) K26-873, (d) K26-1073, and (e) K26-1273. Solid lines show adsorption isotherms, and dashed lines represent desorption isotherms.

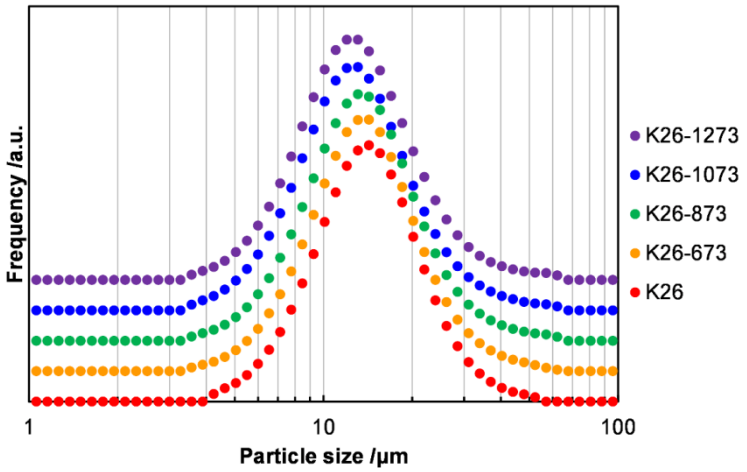


Figure 3.7. Particle size distributions of heat-treated K26 samples in H_2O. Baselines are shifted to show respective distributions.

Table 3.1. Morphological properties of heat-treated K26 samples.

Entry	Heat-treatment temp. /K	BET specific surface area /m^2 g^{-1}	Total pore volume /cm^3 g^{-1}	Median particle diameter /μm
1	None	2270	1.00	13
2	673	2240	0.99	13
3	873	1970	0.86	13
4	1073	1980	0.86	12
5	1273	1730	0.75	12

3.3.2. Hydrolysis of cellobiose by aromatic compounds as model reactions

The roles of carboxylic acids and phenols on K26 were studied in model reactions, in which aromatic compounds were used as molecular catalysts and cellobiose as a substrate (Figure 3.8) by quantitatively evaluating the hydrolytic activities at 443 K in H_2O (Table 3.2). TOF for glucose production was calculated from eq. 3.4.

$$\mathrm{TOF} = \frac{(\text{mole of glucose produced in the catalytic reaction}) - (\text{mole of glucose produced without catalyst})}{2 \times (\text{mole of catalyst}) \times (\text{reaction time})} \quad (3.4)$$

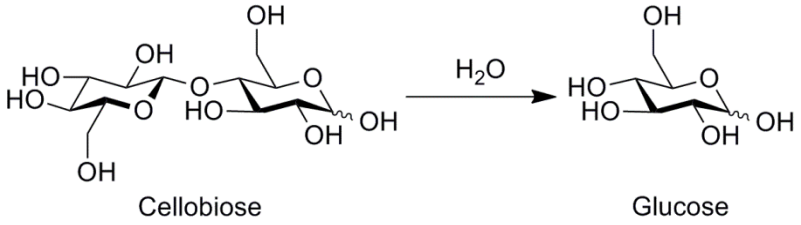
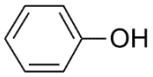
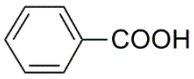
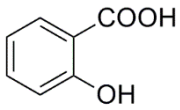
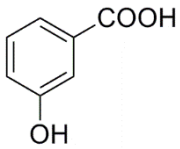
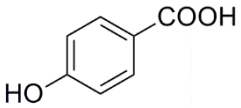
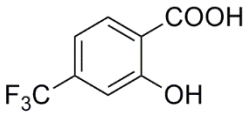
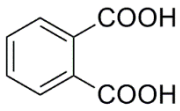
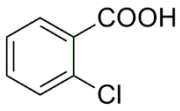
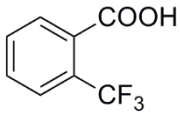
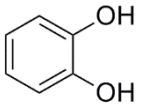
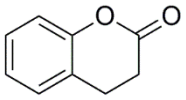
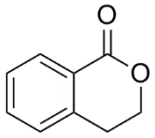


Figure 3.8. Hydrolysis of cellobiose to glucose.

Phenol (pK_a = 10) and benzoic acid (pK_a = 4.2) showed low activities (TOF = 0 h^{-1} and 4.5 h^{-1}, respectively, entries 6 and 7). *o*-Hydroxybenzoic acid (salicylic acid, pK_a = 3.0) bearing both a carboxylic acid and a phenolic group gave a TOF as high as 28 h^{-1} (entry 8); however, *m*- and *p*-hydroxybenzoic acids (pK_a = 4.1 and 4.6, respectively) were nearly inactive (TOF = 5.7 h^{-1} and 2.4 h^{-1}, entries 9 and 10). These results imply that one or both of acidity and ortho positioning of some specific groups relate to catalytic activity in the hydrolysis of cellobiose. Therefore, the effect of pK_a was evaluated using 4-trifluoromethylsalicylic acids (pK_a = 2.5). This compound provided a very high TOF of 46 h^{-1} (entry 11), showing that a stronger acid is more active for this reaction, as expected. Next, ortho-substituted benzoic acids were tested for evaluating influence of the vicinal group. Benzene-1,2-dicarboxylic acid (phthalic acid, pK_a = 3.0, TOF = 32 h^{-1}, entry 12) was as effective as salicylic acid. In contrast, *o*-chlorobenzoic acid (pK_a = 2.9, TOF = 17 h^{-1}, entry 13) was less active than salicylic acid regardless of their similar acidities. *o*-Trifluoromethylbenzoic acid (pK_a = 2.6, entry 14) gave a higher TOF (21 h^{-1}) than that of *o*-chlorobenzoic acid due to the stronger acidity, but its catalytic performance was still less than that of salicylic acid. Hence, the catalytic activity also depends on the structure of acids as salicylic acid and phthalic acid were rather more active than that expected from their pK_a values. This suggests the synergy between neighboring OH/COOH as well as COOH/COOH in the hydrolysis of glycosidic bonds. In a related study, Capon has reported that the hydrolysis of a glycosidic bond is dramatically accelerated by an intramolecular adjacent carboxylic acid, while opposite-side one does not work.[18] Taking account this fact, it is speculated that OH and COOH groups might interact with cellobiose, and then another COOH attacks glycosidic bonds (Figure 3.9). 1,2-Dihydroxybenzene (catechol, pK_a = 9.5) and lactones, 3,4-dihydrocoumarin and isochroman-1-one, were inactive for the reaction due to low acidity (entries 15–17).

Table 3.2. Hydrolysis of cellobiose by aromatic compounds.[a]

Entry	Aromatic compound	pK_a[b]	TOF[c] /h^{-1}	E_a[d] /kJ mol^{-1}	A[e] /10^{12} M^{-1} s^{-1}	k_H[f] /s^{-1}
6		10	0	n.d.[g]	n.d.[g]	43
7		4.2	4.5	111[h]	1.1[h]	41
8		3.0	28	118	37	190
9		4.1	5.7	115[h]	3.2[h]	30
10		4.6	2.4	115[h]	2.6[h]	30
11		2.5	46	n.d.[g]	n.d.[g]	–[i]
12		3.0	32	120	73	250
13		2.9	17	108	2.0	23
14		2.6	21	n.d.[g]	n.d.[g]	13
15		9.5	0	n.d.[g]	n.d.[g]	–[j]
16		n.d.[g]	0	n.d.[g]	n.d.[g]	0
17		n.d.[g]	0	n.d.[g]	n.d.[g]	0

[a]Conditions: cellobiose 342 mg, 0.5 mM aromatic compound solution 40 mL, 443 K, 10 min. [b]The pK_a values were cited from a reference.[19] [c]TOF for glucose production calculated from eq. 3.4. [d]Activation energy. [e]Frequency factor. [f]Rate constant of proton-exchange determined from a peak at 6.32 ppm in ^{1}H NMR spectrum. [g]No data. [h]1.5 mM of aromatic compound solution was used for accurate evaluation of the parameters. [i]k_H was not determined since the peak at 6.32 ppm was significantly broadened. [j]k_H was not accurately determined due to tailing of the peak at 6.58 ppm derived from catechol.

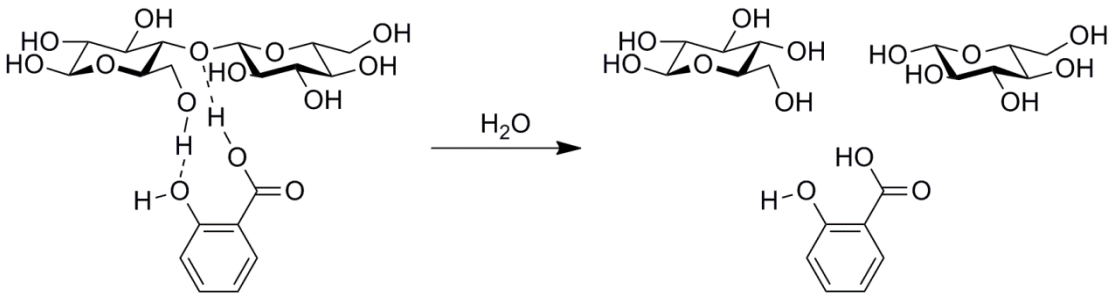


Figure 3.9. Proposed reaction mechanism by vicinal functional groups. The detailed mechanism is depicted in Figure 3.25.

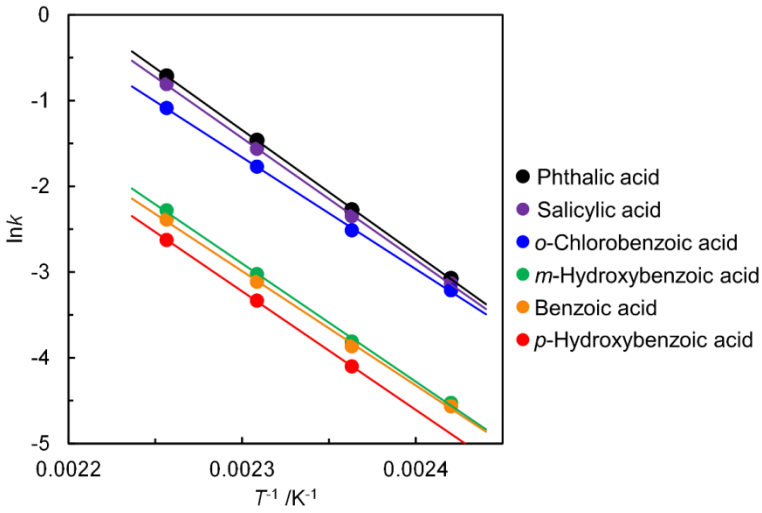


Figure 3.10. Arrhenius plots for cellobiose hydrolysis by aromatic compounds.

In the kinetic study of this reaction, the author assumed the second-order kinetics (eq. 3.5), and the Arrhenius equation was employed to clarify the origin of high catalytic activities of salicylic acid and phthalic acid over other compounds (Figure 3.10 and eq. 3.6).

$$\frac{d[\text{Glucose}]}{dt} = k[\text{Cellobiose}][\text{Aromatic compound}] \qquad (3.5)$$

where [Glucose], [Cellobiose], and [Aromatic compound] (unit: M^{-1}) are concentrations of glucose, cellobiose, and Aromatic compounds, respectively. t (s^{-1}) is reaction time.

$$k = A\exp\left(-\frac{E_a}{RT}\right) \qquad (3.6)$$

where k (unit: $M^{-1}\ s^{-1}$) is a rate constant based on eq. 3.5, A ($M^{-1}\ s^{-1}$) is a frequency factor, E_a (J mol^{-1}) is activation energy, R (J K^{-1} mol^{-1}) is the gas constant, and T (K) is reaction temperature.

The apparent E_a and A for the hydrolysis of cellobiose by aromatic compounds are summarized in Table 3.2. The E_a of salicylic acid and phthalic acid were 118 kJ mol^{-1} and 120 kJ mol^{-1}, respectively (entries 8 and 12), and other less active catalysts showed similar or rather lower E_a (108–115 kJ mol^{-1}, entries 7, 9, 10, and 13). In contrast, A of salicylic acid and phthalic acid (3.7×10^{13} s^{-1} and 7.3×10^{13} s^{-1}) were one-order of magnitude larger than those of other compounds ($1.1 \times 10^{12} \sim 3.2 \times 10^{12}$ s^{-1}). Thus, it is concluded that the vicinal OH/COOH and COOH/COOH accelerate the hydrolysis of glycosidic bonds not by decreasing E_a but by increasing A. It is more clearly suggested that one OH or COOH group interacts with cellobiose,[20,21] which increases the chance of glycosidic bond cleavage by an adjacent carboxylic acid. To confirm this interaction, ^{1}H NMR measurement of cellobiose was conducted in the presence of various aromatic molecules in DMSO-d_6 (Figure 3.11). Note that the signals derived from protons of hydroxyl groups can be detected in DMSO-d_6. Both hydroxyl and CH groups of cellobiose provided sharp peaks without aromatic compounds (black line). They were significantly broadened by adding salicylic acid (orange), phthalic acid (blue), and catechol (purple) due to fast proton-exchanges between cellobiose and the aromatic compounds, indicating formation of hydrogen bonds.[22,23] The rate of proton-exchange for each case was determined using a 6.32 ppm signal derived from a hydroxyl group coordinating to C1' at a reducing end of cellobiose (depicted in Figure 3.11) and eq. 3.7,[24,25] since this peak was isolated from other peaks of cellobiose. Proton-exchange rate constants (k_H) were 180 s^{-1} for salicylic acid and 240 s^{-1} for phthalic acid as represented in Table 3.2. Unfortunately, k_H for catechol was not accurately determined since the signal at 6.32 ppm partially overlapped with another signal at 6.58 ppm derived from catechol.

$$k_H = \pi(v_{aromatic} - v_{cellobiose}) \qquad (3.7)$$

where k_H (unit: s^{-1}) is rate constant of proton-exchange, $v_{aromatic}$ (s^{-1}) is half-value width of a peak for a mixture of cellobiose and aromatics, and $v_{cellobiose}$ (4.20 s^{-1}) is a half-value width of a peak for only cellobiose.

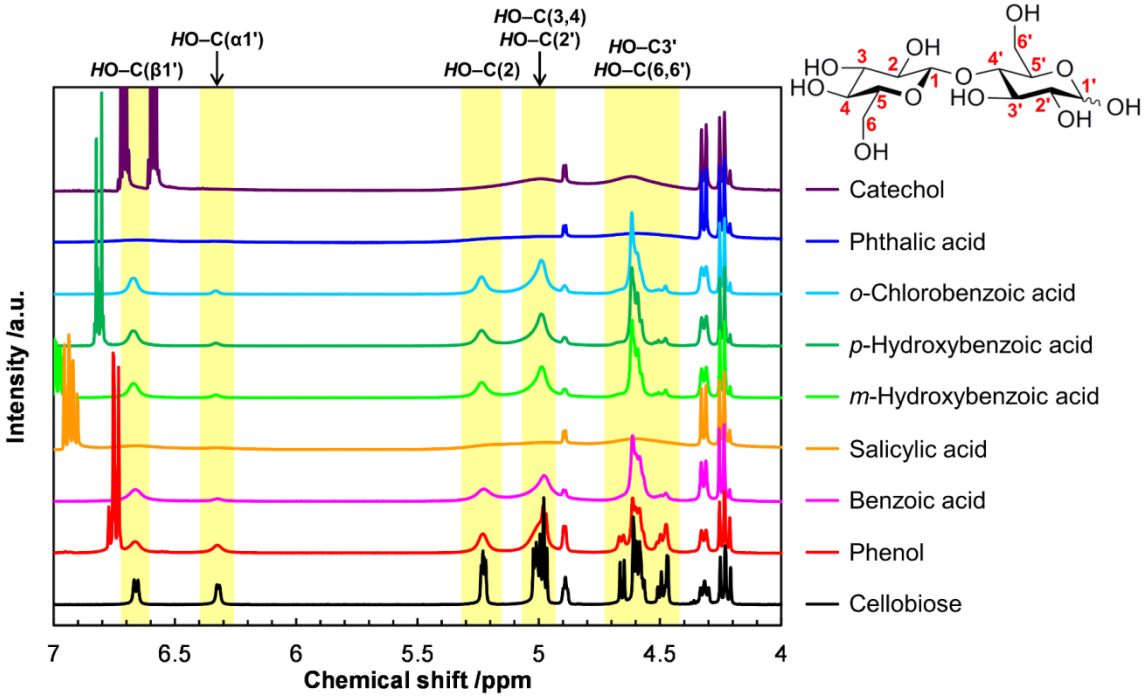


Figure 3.11. ^{1}H NMR spectra of a mixture of cellobiose and aromatic compounds in DMSO-d_6. The peaks in yellow areas are derived from hydroxyl groups of cellobiose. Cellobiose 58 mM, aromatic compound 58 mM. The assignments of hydroxyl groups shown in the figure are based on references.[23,26]

Substituted benzenes bearing no vicinal OH/COOH or COOH/COOH groups, such as *o*-chlorobenzoic acid, only slightly broadened the OH peaks of cellobiose, and the rates of proton-exchange were one-order of magnitude lower than those of salicylic acid and phthalic acid (Table 3.2). This result shows that the fast proton exchange is not due to high acidity but specific to vicinal COOH/OH and COOH/COOH. Hence, it is shown that these vicinal OFGs uniquely interact with cellobiose with hydrogen bonds and subsequently exchange protons with the substrate.[22,23] Owing to the better interaction, the substrate has a larger chance to undergo activation and hydrolysis.

Table 3.3. Hydrolysis of cellulose by salicylic acid and phthalic acid.[a]

Entry	Catalyst	Conv. /%	Yield based on carbon /%						
			Glucan		By-product				
			Glc[b]	Olg[c]	Frc[d]	Man[e]	Lev[f]	HMF[g]	Others[h]
18	None	28	4.6	15	0.5	0.6	0.2	1.8	5.3
19	Salicylic acid	37	11	19	1.1	1.0	0.6	3.2	0.9
20	Phthalic acid	39	13	20	0.9	0.8	0.7	3.1	0.9
21	K26	60	36	2.5	2.7	2.6	2.1	3.4	11

[a]Conditions: individually ball-milled cellulose (0.9 L-pot) 324 mg, catalyst 14 μmol based on the amount of carboxylic acids, H_2O 40 mL, 503 K, <1 min (rapid heating-cooling condition). [b]Glucose. [c]Water-soluble oligosaccharides (DP = mainly 2–6). [d]Fructose. [e]Mannose. [f]Levoglucosan. [g]5-Hydroxymethylfurfural. [h](Conversion) – (total yield of the characterized products).

The author further investigated catalytic activities of salicylic acid and phthalic acid to compare with that of carbon catalyst K26 and employed the acids for cellulose hydrolysis (Table 3.3). For the reaction, the amount of carboxylic acids included in catalysts was the same. Both salicylic acid and phthalic acid promoted the hydrolysis and afforded 11% and 13% yields of glucose, respectively (entries 19 and 20). However, their activities were obviously lower than that of K26 (36% yield, entry 21). These results indicate that K26 has other functions for cellulose hydrolysis in addition to oxygenated functionalities.

3.3.3. Adsorption of cellulosic molecules onto alkali-activated carbon K26

With regard to the higher activity of alkali-activated carbon K26 than model organic acids, carbons may have functions for the adsorption process in addition to those for the hydrolytic step (Figure 3.1). In Section 3.1, the author has already mentioned that the adsorption process of substrates on catalyst surface is crucial for heterogeneous catalysis to draw the potential. Indeed, Katz *et al.* has revealed that weakly acidic surface OH groups on SiO_2 ($pK_a \sim 7$) and Al_2O_3 can hydrolyze cellulosic molecules only when the substrate strongly interacts with the surface, covalently bonded in this specific case.[4–6] Consequently, it is necessary to study the adsorption of cellulosic molecules on K26 to understand the origin of high activities of carbon catalysts, for which glucose and short β-1,4-glucans were used as models of cellulosic molecules in this work.

Insight into structure of carbon surface is essential to evaluate the adsorption nature, and the author further characterized K26 by ^{13}C CP/MAS-TOSS NMR and Raman spectroscopy. A single peak at 131 ppm

in the NMR spectrum (Figure 3.12) is derived from aromatic carbon atoms,[27] indicating that the framework of K26 is primarily composed of aromatic rings. The Raman spectrum of K26 (Figure 3.13) represents both a G-band (1586 cm^{-1}) and a D-band (1343 cm^{-1}) in an intensity ratio (I_G/I_D) of 1.1. Therefore, an average size of graphene sheet of K26 is calculated to be 21 nm using the ratio and the Knight formula[11] (eq. 3.1).

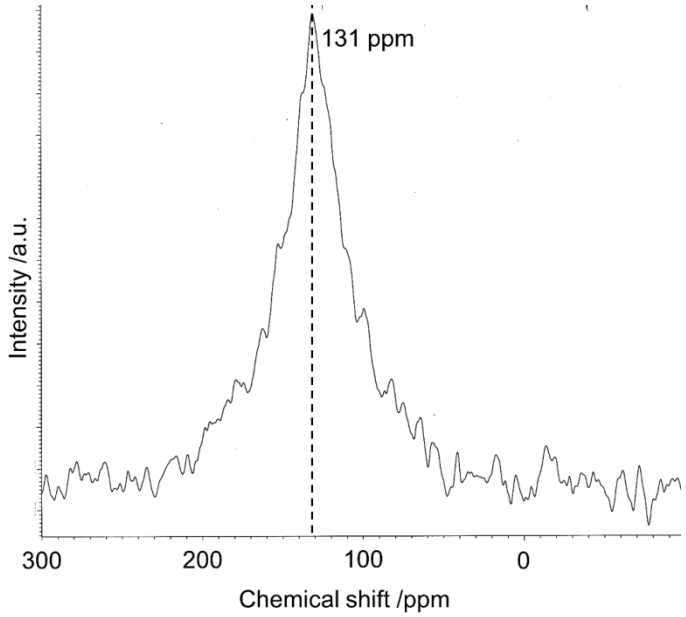


Figure 3.12. ^{13}C CP/MAS-TOSS NMR spectrum of K26. The peak at 131 ppm is assigned to aromatic carbon atoms.[27]

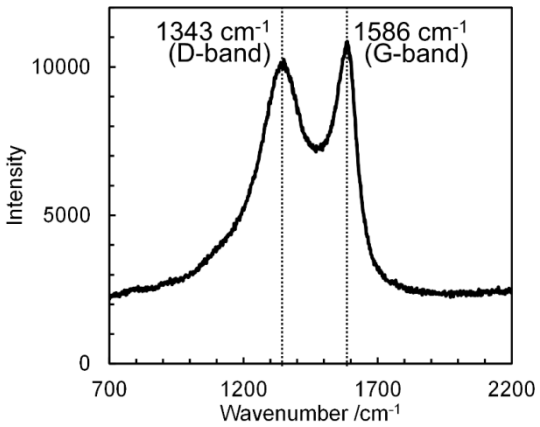


Figure 3.13. Raman spectrum of K26.

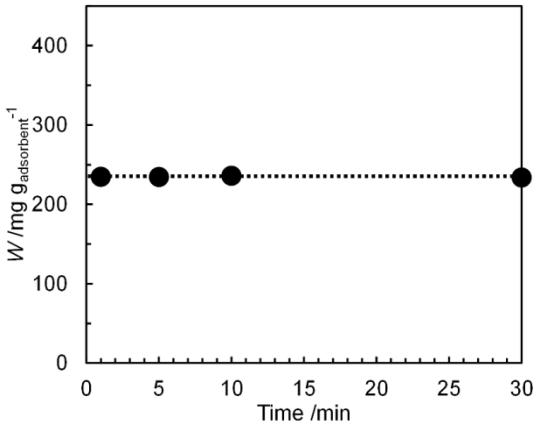


Figure 3.14. Time course of cellobiose adsorption on K26 at 296 K. *W* in the figure represents specific adsorption amount. K26 25 mg, cellobiose 6.8 mg (an initial concentration of 1 mM), H_2O 20 mL.

Time course of cellobiose adsorption on K26 was measured at 296 K (Figure 3.14). 235 mg $g_{adsorbent}^{-1}$ of cellobiose adsorbed onto K26 in 1 min (the shortest time for reliable experiments), thus showing that cellulosic molecules indeed interacted with carbon surface. The adsorption amounts of cellobiose were constant in increasing the time to 30 min, indicating that the adsorption is rapidly equilibrated within 1 min.

Next, various concentrations of cellobiose were adsorbed onto K26 in H_2O at 296 K to determine the adsorption parameters (Figure 3.15a, red line). The adsorption amount increased with increasing concentration from 0 to 4 mM and eventually reached a plateau at 4–6 mM. Accordingly, this isotherm is categorized as type I, which implies the Langmuir adsorption. A linear line (determination coefficient R^2 = 0.999) was successfully obtained in a Langmuir plot (Figure 3.15b, red line), giving an adsorption equilibrium constant (K_{ads}) of 5660 M^{-1} and an adsorption capacity (W_{max}) of 412 mg $g_{adsorbent}^{-1}$ (Table 3.4, entry 26) using the Langmuir formulae (eqs. 3.8 and 3.9). The author has ascertained that any multilayer adsorption of cellobiose is negligible within this concentration range (0–6 mM, see below). Previous reports also showed similar isotherms for the adsorption of glucans on carbons and these were also assigned to be of Langmuir type.[28,29] Monolayer coverage is predominant in the regions of isotherms associated with increasing adsorption, even when multilayer adsorption occurs.[30] Hence, it is concluded that cellobiose strongly adsorbs on K26 in a Langmuir-type adsorption. Accordingly, the W_{max} means that cellobiose, having a cross section of 0.9 nm^2 per one molecule, occupies a specific surface area of 650 m^2 g^{-1} on K26 associated

with the adsorption. This calculation suggests that cellobiose penetrates the micropores of K26 because the occupied surface area is seven times greater than the specific external surface area of the K26 sample (88 m^2 g^{-1}). The cellobiose molecule has dimensions of 1.1 nm × 0.7 nm × 0.4 nm (Figure 3.16), whereas K26 has non-uniform pores with an average diameter of 0.7 nm. Accordingly, the average pore diameter is similar to the minimal cross section that a cellobiose molecule requires for penetration (0.7 nm × 0.4 nm). Although the hydrated radius of cellobiose in H_2O is larger than the molecular size itself, the hydrated H_2O molecules are partially removed during the adsorption process (see below) and H_2O molecules can be dynamically rearranged. Hence, the author proposes that a portion of the internal surface of the carbon (*ca.* 2200 m^2) accepts cellobiose molecules.

$$\frac{C}{W} = \frac{C}{W_{\max}} + \frac{1}{K_{\text{ads}} W_{\max}} \qquad (3.8)$$

$$K_{\text{ads}} = \frac{\theta}{[\text{adsorbate}](1-\theta)} \qquad (3.9)$$

where C (unit: M) is concentation of β-glucan, W (mg $g_{adsorbent}^{-1}$) is specific adsorption amount, W_{max} (mg $g_{adsorbent}^{-1}$) is adsorption capacity, and K_{ads} (M^{-1}) is equilibrium constant defined by eq. 3.9, in which θ is coverage.

Table 3.4. Langmuir parameters for the adsorption of glucose and cello-oligosaccharides onto K26 at various temperatures.

Entry	Adsorbate	T /K	W_{max}[a] /mg $g_{adsorbent}^{-1}$	K_{ads}[b] /M^{-1}
22	Glucose	296	95.2	220
23	Glucose	306	85.5	208
24	Glucose	320	76.3	172
25	Glucose	330	69.0	157
26	Cellobiose	296	412	5660
27	Cellobiose	306	404	4660
28	Cellobiose	320	387	3410
29	Cellobiose	330	360	3130
30	Cellotriose	296	527	181,000
31	Cellotriose	306	517	135,000
32	Cellotriose	320	501	95,800
33	Cellotriose	330	485	77,500

[a]Adsorption capacity of substrate. [b]Adsorption equilibrium constant.

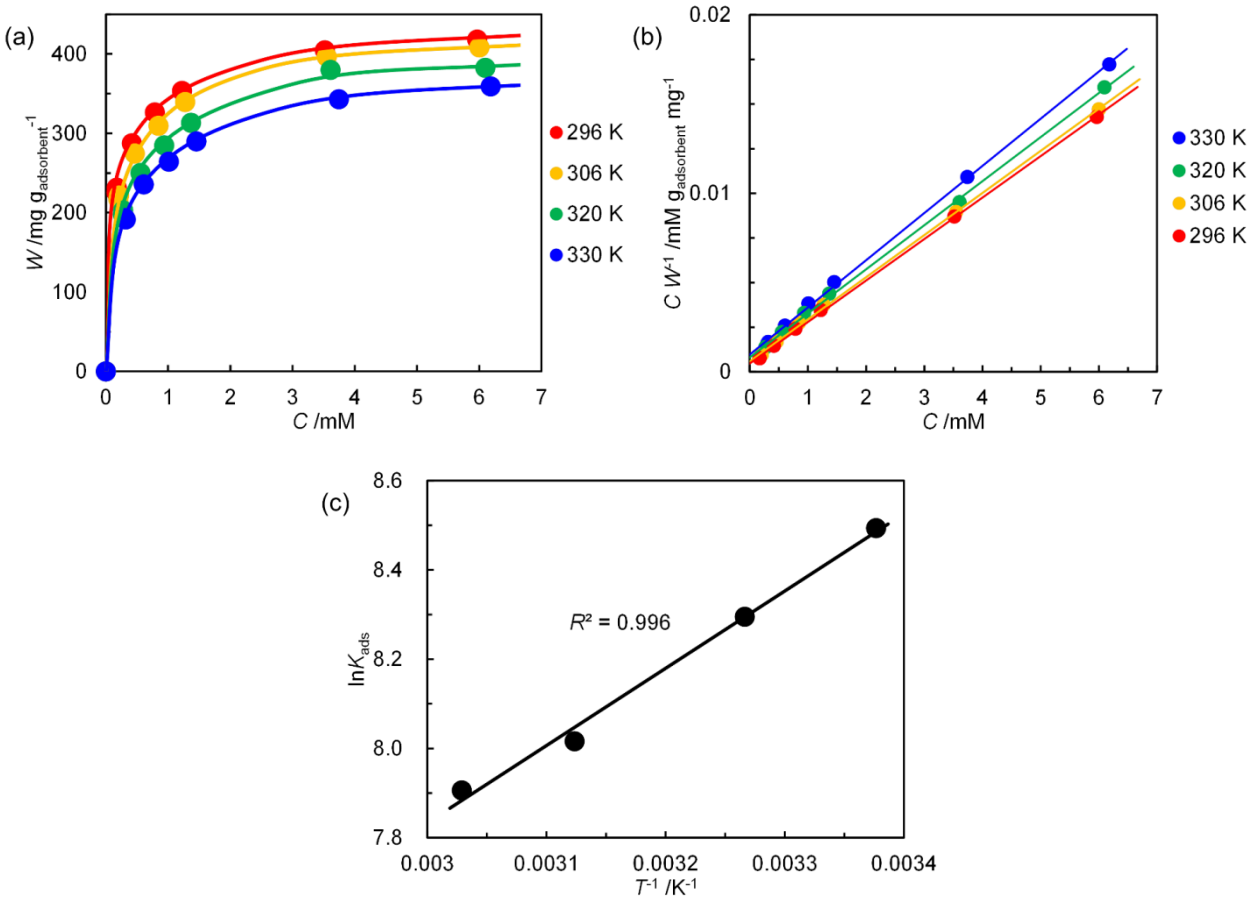


Figure 3.15. Adsorption of cellobiose on K26: (a) isotherms, (b) Langmuir plots, and (c) a van't Hoff plot.

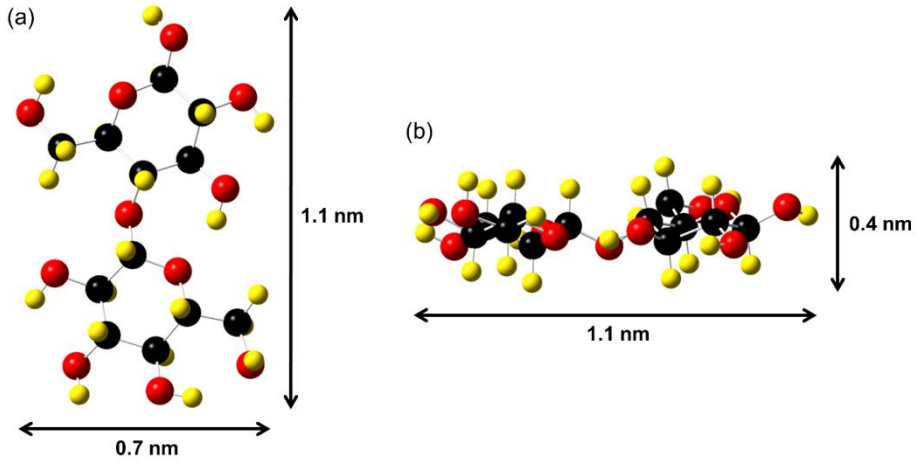


Figure 3.16. Molecular size of cellobiose: (a) top view and (b) side view. Black = carbon atoms, red = oxygen atoms, and yellow = hydrogen atoms. The DFT calculation at the B3LYP/6-31G* level optimized the structure of a cellobiose molecule.

Cellobiose was adsorbed on K26 at various temperatures to determine adsorption thermodynamics. All the experiments at the temperatures provided Langmuir-type adsorptions (Figure 3.15a and 3.15b), and adsorption parameters were determined as summarized in Table 3.4. K_{ads} was reduced from 5660 to 3130 M^{-1} upon increasing the adsorption temperature from 296 to 330 K; this indicates exothermic adsorption. In addition, the Gibbs energy of adsorption ($\Delta G°_{ads}$) always takes a negative value (exergonic), for example, –21.3 kJ mol^{-1} at 296 K based on eq. 3.10 and K_{ads}, showing that adsorption spontaneously occurs.

$$\Delta G^{\circ}_{ads} = -RT\ln K_{ads} \qquad (3.10)$$

W_{max} also slightly decreased from 412 to 360 mg $g_{adsorbent}^{-1}$ as the temperature was elevated (Table 3.4, entries 26–29). A minimal decline in adsorption capacity is common in elevating temperature and is due to an increase in the adsorption cross-sectional area.[31,32] The observed W_{max} reduction is not related to structural degradation of K26; W_{max} changes reversibly as a function of temperature and both the specific surface area (2270 m^2 g^{-1}) and XRD patterns (broad peaks at 22° and 44°, Figure 3.17) of K26 in H_2O are unchanged even at 453 K.

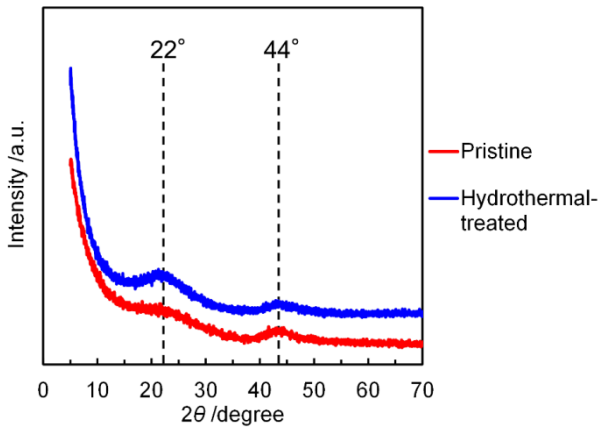


Figure 3.17. XRD patterns of pristine K26 (red) and hydrothermal-treated K26 (blue).

Table 3.5. Adsorption enthalpy and entropy changes for glucose and cello-oligosaccharides on K26.

Entry	Adsorbate	$\Delta H°_{ads}$ /kJ mol^{-1}	$\Delta S°_{ads}$ /J K^{-1} mol^{-1}
34	Glucose	–8.4 ± 1.2	+16.5 ± 3.8
35	Cellobiose	–14.1 ± 1.9	+23.5 ± 3.4
36	Cellotriose	–20.2 ± 0.8	+32.2 ± 3.3

The van't Hoff equation was employed to determine changes of adsorption enthalpy ($\Delta H°_{ads}$ in J mol^{-1}) and entropy ($\Delta S°_{ads}$ in J K^{-1} mol^{-1}; eqs. 3.11 and 3.12). A plot of $\ln K_{ads}$ against $1/T$ (Figure 3.15c) showed good linearity (R^2 = 0.996) because of negligible heat capacity differences. From eq. 3.12, $\Delta H°_{ads}$ and $\Delta S°_{ads}$ were determined to be –14.1 ± 1.9 kJ mol^{-1} and +23.5 ± 3.4 J K^{-1} mol^{-1}, respectively (Table 3.5, entry 35). Accordingly, it is revealed that the adsorption of cellobiose onto K26 is favored by the accompanying changes in both enthalpy and entropy.

$$\frac{\mathrm{d}\ln K_{\mathrm{ads}}}{\mathrm{d}\left(\frac{1}{T}\right)} = -\frac{\Delta H^{\circ}_{\mathrm{ads}}}{R} \qquad (3.11)$$

$$\ln K_{\mathrm{ads}} = -\frac{\Delta H^{\circ}_{\mathrm{ads}}}{R}\frac{1}{T} + \frac{\Delta S^{\circ}_{\mathrm{ads}}}{R} \qquad (3.12)$$

The cause of this strong adsorption was studied by control experiments and computations. Two possible driving forces have been proposed for the adsorption of glucans onto carbon materials so far: (i) hydrogen bonds between OH groups of glucans and OFGs on carbon[20,21,28] and (ii) van der Waals forces with CH–π hydrogen bonds between CH groups in axial planes of the glucose units and aromatic rings of the carbon structure.[29] As a means of examining the former hypothesis, the adsorption experiments of cellobiose onto the heat-treated K26 samples were conducted at 296 K (Figure 3.18). The total concentration of OFGs on the carbon determined by the Boehm titration[1] was reduced from 880 μmol g^{-1} (in pristine K26) to 440 μmol g^{-1} (K26-873) and 150 μmol g^{-1} (K26-1273, Table 3.6); however, these carbons had similar W_{max} values (412, 432, and 342 mg $g_{adsorbent}^{-1}$ for K26, K26-873, and K26-1273, respectively). In addition, K26 and K26-1273 had almost the same adsorption capacity when normalizing the capacity by the surface area (0.181 and 0.198

mg $m_{adsorbent}^{-2}$). Specific surface area roughly correlates with the number of aromatic hydrophobic sites because the surface area occupied by OFGs is 3% at most and the framework of K26 is primarily composed of aromatic carbon atoms (Figure 3.12). A hydrophobic probe cyclohexane was used for confirmation of this approximation, and cyclohexane was adsorbed on the K26 samples in the same fashion (0.301, 0.314, and 0.273 mg $m_{adsorbent}^{-2}$ for K26, K26-873, and K26-1273, respectively). Moreover, similar K_{ads} values were also obtained (5290–5690 M^{-1}) that were independent of variations in the OFG concentrations for the adsorption of cellobiose. These results indicate that interactions between hydrophobic groups dominate in the adsorption of cellobiose on carbons. It is known that cellulases adsorb on cellulose through carbohydrate binding sites that consist of hydrophobic aromatic amino acid residues;[33] this resembles the hydrophobic adsorption on carbons.

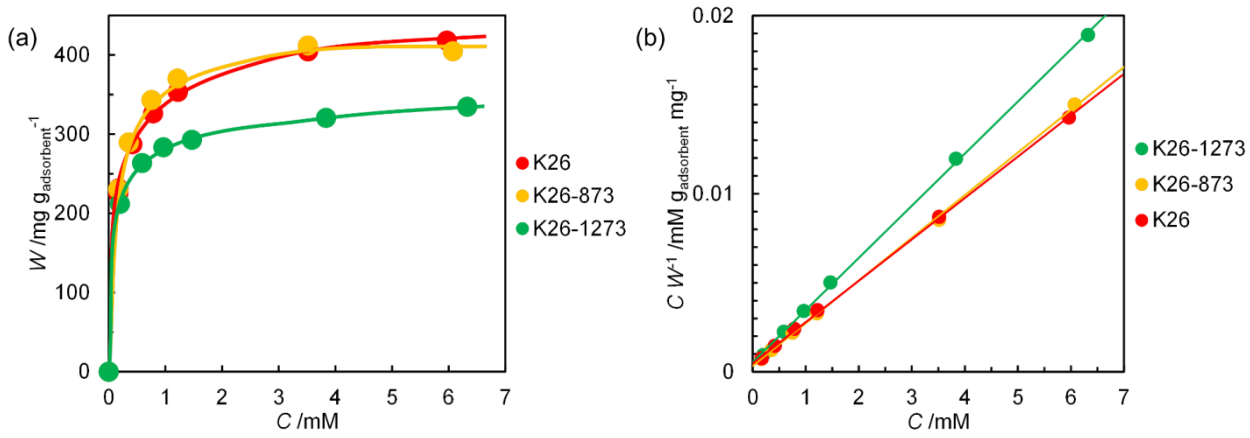


Figure 3.18. Adsorption of cellobiose on heat-treated K26: (a) isotherms and (b) Langmuir plots.

Table 3.6. Oxygenated functionality concentrations and Langmuir parameters for cellobiose adsorption on heat-treated K26.

Entry	Adsorbent	OFGs[a] /μmol g^{-1}	SSA[b] /$m_{adsorbent}^2$ g^{-1}	W_{max}[c] /mg $g_{adsorbent}^{-1}$	W_{max}/SSA[d] /mg $m_{adsorbent}^{-2}$	K_{ads}[e] /M^{-1}
37	K26	880	2270	412	0.181	5660
38	K26-873	440	1970	432	0.219	5690
39	K26-1273	150	1730	342	0.198	5290

[a]Total specific amount of OFGs determined by the Boehm titration.[1] [b]BET specific surface area. [c]Adsorption capacity. [d]Adsorption capacity divided by BET specific surface area. [e]Adsorption equilibrium constant.

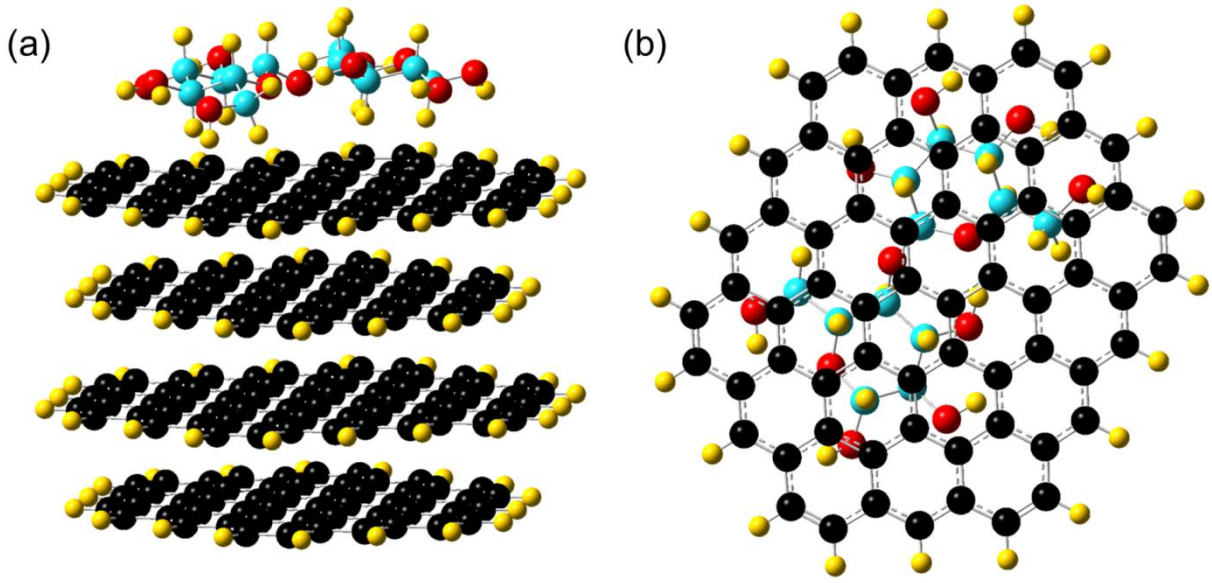


Figure 3.19. Optimized adsorption orientation of cellobiose onto carbon by DFT calculations: (a) side view and (b) top view. In the top view, three graphene layers are omitted to assist in viewing of the structure. Black = graphene carbon atoms, blue = cellobiose carbon atoms, red = oxygen atoms, and yellow = hydrogen atoms.

To allow the hydrophobic adsorption, interactions between CH groups of cellobiose and π electrons of the K26 graphene sheets (CH–π hydrogen bonding) are sufficient and the calculated value of $\Delta H°_{ads}$ per mole of CH groups (–2.8 kJ mol^{-1}) is indeed reasonable for the reported value of a CH–π hydrogen bond (–2.8 kJ mol^{-1}).[34] To further support this hypothesis, the author and co-workers investigated the behavior of a cellobiose molecule on a carbon model consisting of quadruple-layered graphene sheets through DFT calculations. The results have demonstrated that cellobiose is stabilized on the graphene sheet and adsorbs *via* the axial plane (Figure 3.19). Even when the equatorial plane of cellobiose faces the carbon in the initial placement, the cellobiose molecules spontaneously rotates and the axial planes bind on the carbon surface. As a result, the CH groups of cellobiose are directed toward the centers of the aromatic rings of carbon; thus forming CH–π hydrogen bonds. An alternative calculation, excluding van der Waals forces, has shown that the adsorption energy is –2.9 kJ mol^{-1}, which was slightly smaller than the experimental data (–14.1 kJ mol^{-1}). However, the accurate adsorption energy from the calculation including van der Waals forces, solvent

H_2O molecules, and upper orbitals of hydrogen atoms (6-31G* includes only s-orbitals for them) were not determined, because doing so would result in unfeasible computational costs. Accordingly, the conclusion led from the current results is that the computation qualitatively supports the formation of CH–π hydrogen bonds.

The positive value of $\Delta S°_{ads}$ (+23.5 J K^{-1} mol^{-1}) experimentally determined in this study is unique to the adsorption of cellobiose on carbon because adsorption of molecules generally results in a negative $\Delta S°_{ads}$ value due to reduced freedom of molecular motion on a 2D surface. For example, $\Delta S°_{ads}$ is –3.4 J K^{-1} mol^{-1} for the adsorption of cellobiose on a hydrophilic polyacrylamide surface in an aqueous phase.[35] These facts suggest that another driving force derived from the hydrophobic properties in addition to the formation of CH–π hydrogen bonds leads to the entropically favored adsorption. This second factor can be ascribed to so-called *hydrophobic interactions* between the carbon and cellobiose as described below. When using proteins/alkyl sepharose or cethyltrimethylammonium bromide/activated carbon, it is reported that adsorptions driven by hydrophobic interactions result in positive entropy changes with negligible enthalpy effects.[36,37] In an aqueous environment, the conformations and mobility of H_2O molecules surrounding substrates are restricted to maintain hydrogen-bonding networks around the apolar materials,[38] which are entropically disfavored. As a result, when hydrophobic adsorbates are loaded onto lipophilic surfaces, the H_2O molecules are unbound and gain a higher degree of freedom (Figure 3.20). The surface of carbon is hydrophobic as indicated in cyclohexane adsorption and the axial plane of cellobiose consists of CH groups. Moreover, cellobiose adsorbs on carbon through its hydrophobic plane through CH–π hydrogen bonds (see above). Similarly, a computation has shown that a protein domain Pin WW interacts with sugar molecules through its aromatic residue by hydrophobic interactions in addition to CH–π hydrogen bonds.[39] In this regard, DMSO was utilized as a solvent with hydrophobic groups for the adsorption of cellobiose on K26, but cellobiose was not adsorbed on K26 at all (Figure 3.21). DMSO medium does not cause the hydrophobic interactions of carbon and cellobiose, and this compound competes with cellobiose in adsorption by hydrophobic groups. Thus, the adsorption of cellobiose was completely inhibited. The author concludes that hydrophobic interactions are included in the adsorption of cellobiose on carbon materials in the aqueous phase, which precedes the cellulose conversion. The calculation of entropy change of cellobiose adsorption

on carbon surface based on the theoretical values is summarized in a note.[40]

The positive entropy change associated with this process assists in obtaining strong adsorption, especially at the high temperatures required for the conversion of cellulosic biomass. Specifically, the $\Delta S°_{ads}$ value of +23.5 J mol^{-1} K^{-1} increases the value of K_{ads} by a factor of 16.9 times, independent of the temperature, as shown in eq. 3.12, whereas the contribution of enthalpy is gradually reduced with increasing temperature. By using this effect, 230 mg of cellobiose can adsorb on 1 g of K26 from a 1.7 mM cellobiose solution within 0.2 h even at a relatively high temperature of 413 K. The author has also confirmed that K26 can hydrolyze cellulose into glucose over 24 h at near 413 K. Consequently, the dominant driving forces for this adsorption process at the reaction temperature are derived from hydrophobic functionalities, and consist

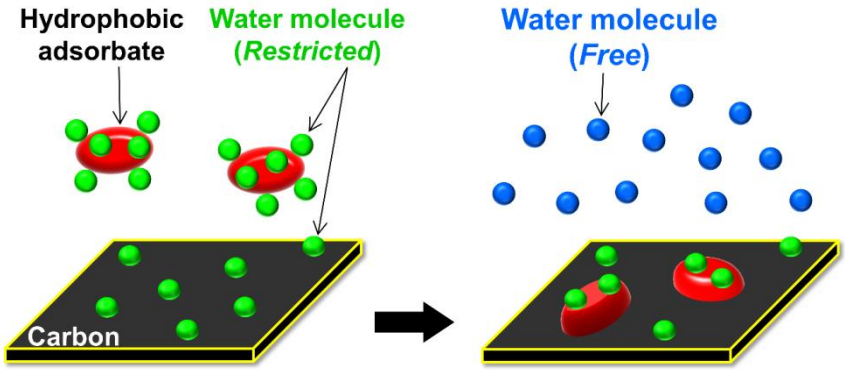


Figure 3.20. Reorientation of H_2O molecules associated with the hydrophobic adsorption, so-called *hydrophobic interaction*.

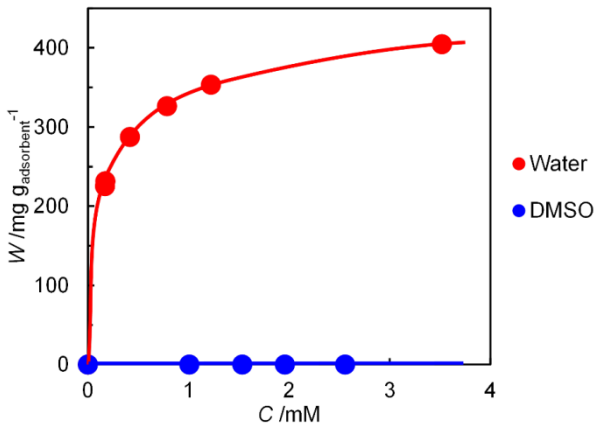


Figure 3.21. Solvent effect for adsorption of cellobiose on K26.

of CH–π hydrogen bonds and hydrophobic interactions. To date, only direct interactions between sugar molecules and the carbon have been considered, but these results show significant contribution of entropy changes derived from the rearrangement of H_2O molecules in an aqueous phase.

Adsorption experiments of glucose and cellotriose on K26 were carried out at various temperatures to study the effect of DP. The resulting isotherms, Langmuir plots, and van't Hoff plots are shown in Figures 3.22 and 3.23, and the Langmuir parameters are summarized in Table 3.4. W_{max} increased from 95.2 to 527 mg $g_{adsorbent}^{-1}$ at 296 K as the number of glucose units increased. The low adsorption capacity of glucose implies that the adsorption sites of glucose might be different from those of the oligomers. However, glucose was similarly adsorbed on both pristine K26 (12 mg $m_{adsorbent}^{-2}$ at a glucose concentration of 1.8 mM) and K26 with the OFGs removed (K26-1273, 10 mg $m_{adsorbent}^{-2}$ at the same concentration), which shows that the adsorption of glucose is not affected by hydrophilic groups but by hydrophobicity. The K_{ads} value for glucose adsorption is 220 M^{-1} at 296 K (entry 22), which is 1/25 of that obtained for cellobiose. In contrast, the K_{ads} value for cellotriose is 181,000 M^{-1} (entry 30), a value which is 32 times larger than that for cellobiose. The adsorption strength therefore greatly increases with increasing length of the cellulosic molecules. The K_{ads} values for glucose and cellotriose decrease with increasing in temperature up to 330 K (entries 22–25 and 30–33), similar to those obtained with cellobiose (entries 26–29). From these results, the adsorption enthalpy and entropy changes were determined based on the temperature dependence. The value of $\Delta H°_{ads}$ decreases in an almost linear fashion with increasing number of glucose units, as shown in Table 3.5. This is because each glucose unit has two or three CH groups in each axial plane, all of which interact with π electrons on the carbon. Similarly, $\Delta S°_{ads}$ gradually increased with increasing molecular size. As noted above, the positive value of $\Delta S°_{ads}$ is attributed to hydrophobic interactions between the sugars and the carbon, and larger β-glucans can unbind greater numbers of H_2O molecules from the lipophilic surfaces during adsorption. Hence, cellotriose gives the lowest value of $\Delta H°_{ads}$ and the highest value of $\Delta S°_{ads}$ among the three sugar compounds used in this study.

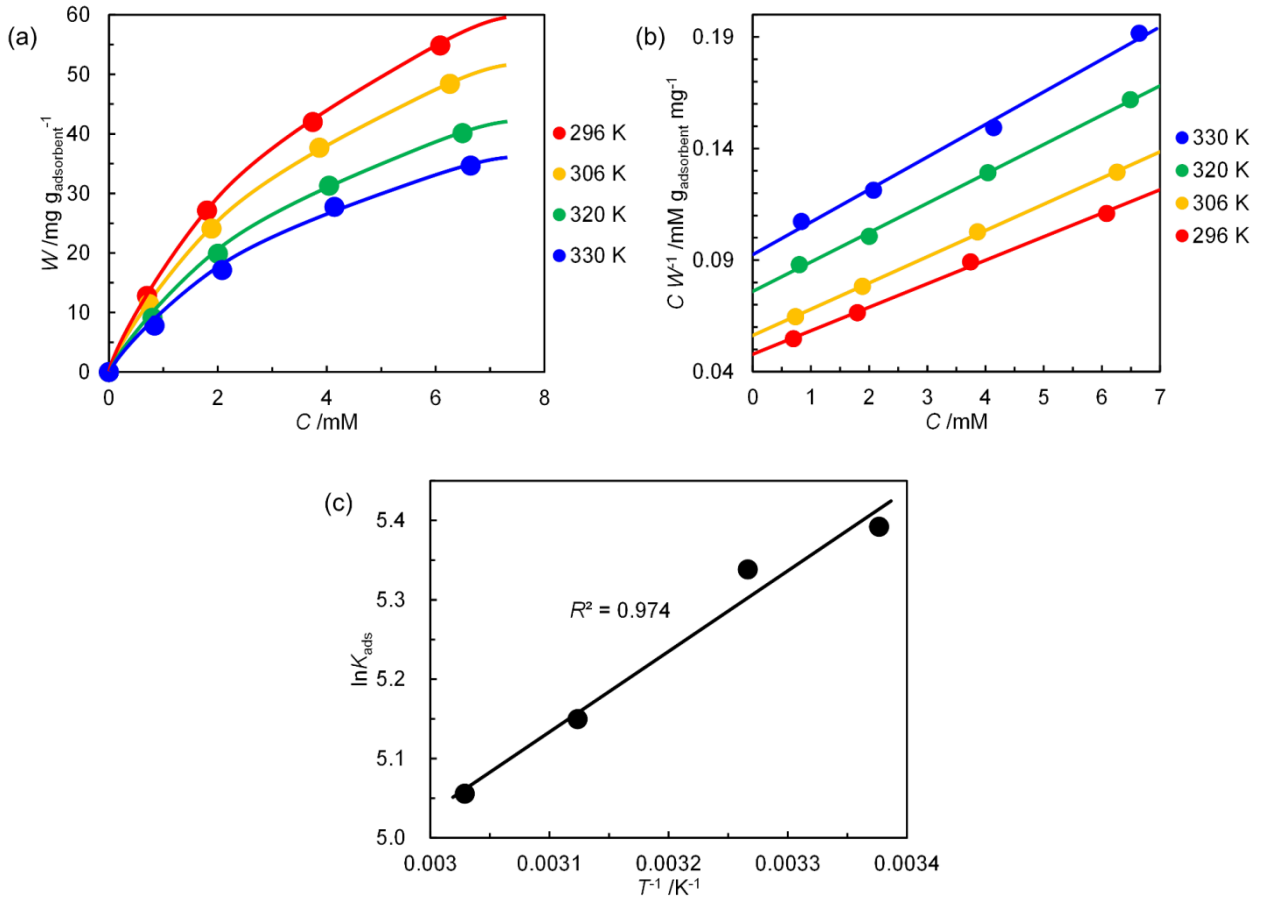


Figure 3.22. Adsorption of glucose on K26: (a) adsorption isotherms, (b) Langmuir plots, and (c) a van't Hoff plot.

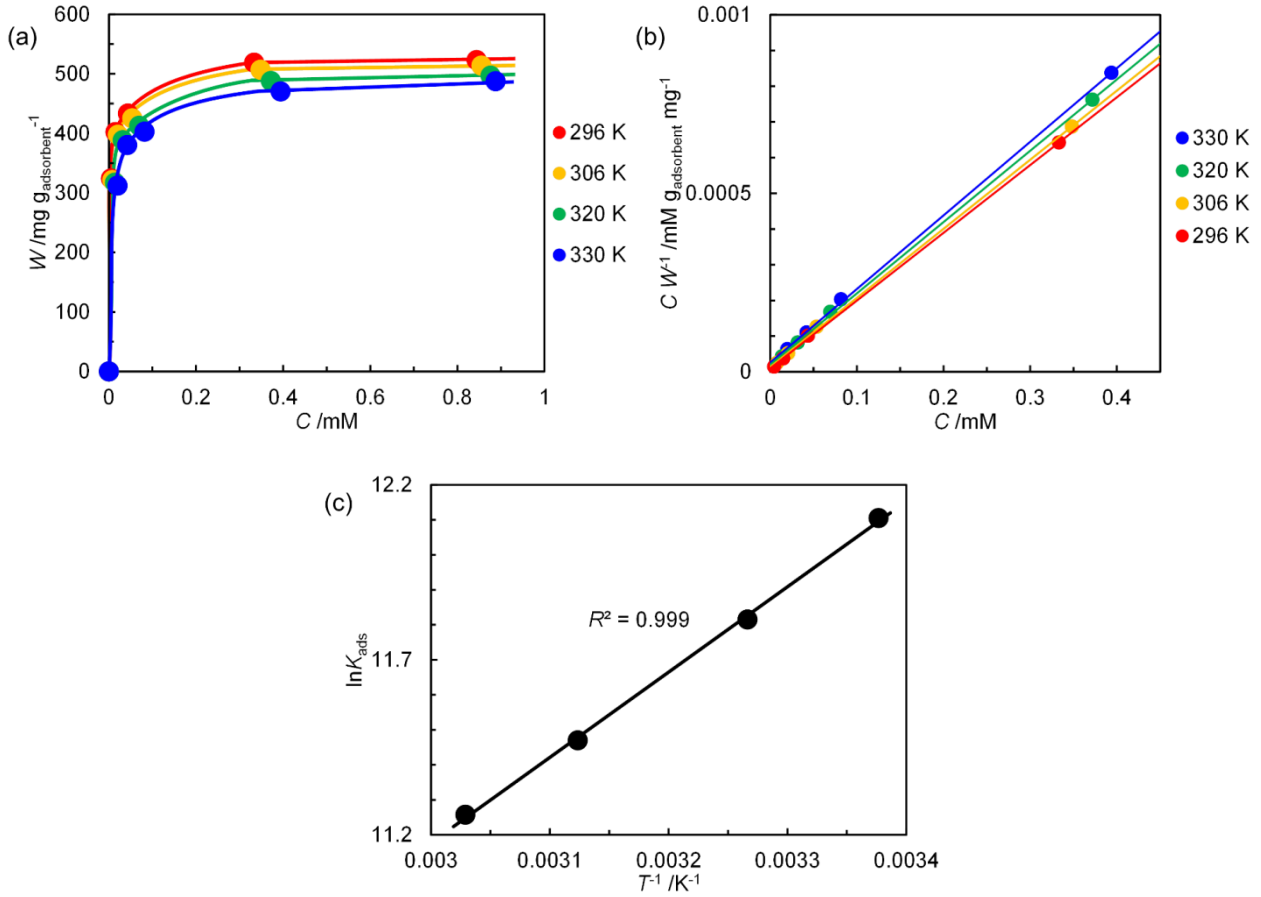


Figure 3.23. Adsorption of cellotriose on K26: (a) adsorption isotherms, (b) Langmuir plots, and (c) a van't Hoff plot.

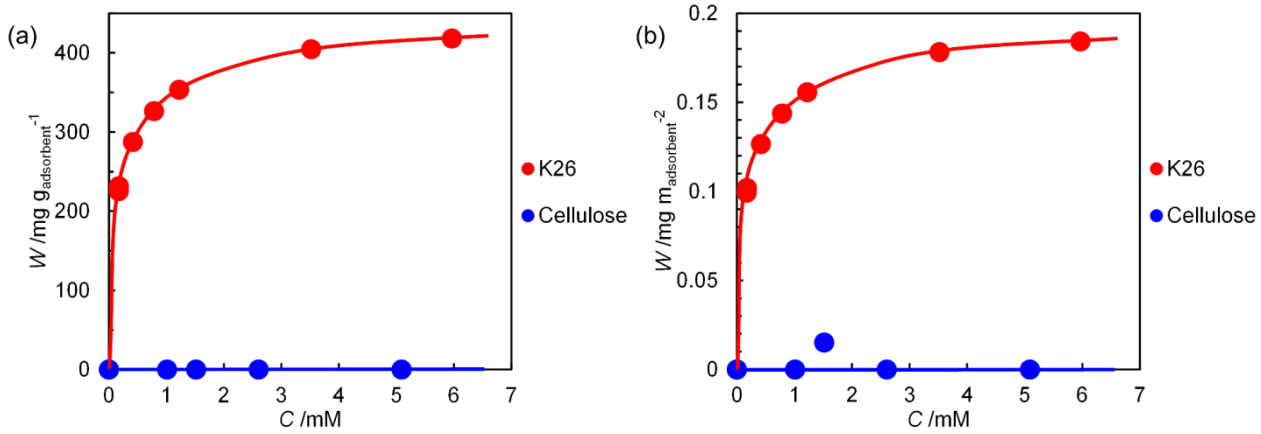


Figure 3.24. Adsorption isotherms for cellobiose on K26 (red) and cellulose (blue) standardized by (a) weight of adsorbents and (b) specific surface areas (2270 m^2 g^{-1} for K26, 1.3 m^2 g^{-1} for cellulose).

The author has elucidated the affinity of β-1,4-glucans with each other to know whether β-1,4-glucans can form multilayers during their adsorption on carbon materials. Figure 3.24a shows the adsorption isotherms of cellobiose on ball-milled cellulose and K26 at 296 K. K26 easily adsorbs cellobiose as already discussed, but almost no adsorption on ball-milled cellulose is observed. This is not due to the large specific surface area of K26 because the adsorption amount per surface area are also negligible for ball-milled cellulose within this cellobiose concentration range (<5 mM, Figure 3.24b). Similarly, cellobiose did not adsorb on crystalline cellulose at all. Cellohexaose was also tested as an adsorbate to establish that strong adsorption is not dependent on the DP. In these experiments, 333 mg of cellohexaose adsorbed on 1 g of K26 (= 0.147 mg $m_{adsorbent}^{-2}$) at a cellohexaose concentration of 0.035 mM at 296 K, whereas the same hexamer did not adsorb on ball-milled cellulose at all (<0.025 mg $m_{adsorbent}^{-2}$) under the same conditions. These results indicate that the affinity between carbons and β-1,4-glucans are significantly stronger than the attractive forces between the β-1,4-glucan molecules. The author concludes that the multilayer adsorption is negligible in this work.

To briefly conclude this section, the adsorption of β-1,4-glucans on carbon surface is driven by hydrophobic planes of both adsorbate and adsorbent, namely the formation of CH–π hydrogen bonds and hydrophobic interactions, not by hydrophilic ones. The affinity between β-1,4-glucans and carbon is enhanced by the increase of DP, suggesting that carbon can attract cellulose (long-chain β-1,4-glucan), and that produced short-chain oligomers and glucose possibly desorbs from carbon surface in the presence of long-chain oligomers during the hydrolysis of cellulose. This is why K26 is significantly more active than model catalysts (salicylic acid and phthalic acid) in the reaction. In other words, salicylic acid and phthalic acid do not have large aromatic planes, resulting in weaker affinity with substrates and lower catalytic activities than K26.

3.3.4. Proposed mechanism of cellulose hydrolysis by carbon catalysts

From the above results and discussion, the author proposes the reaction mechanism for cellulose hydrolysis by carbons as follows (Figure 3.25). The first step (i) is the adsorption of cellulosic molecules onto the

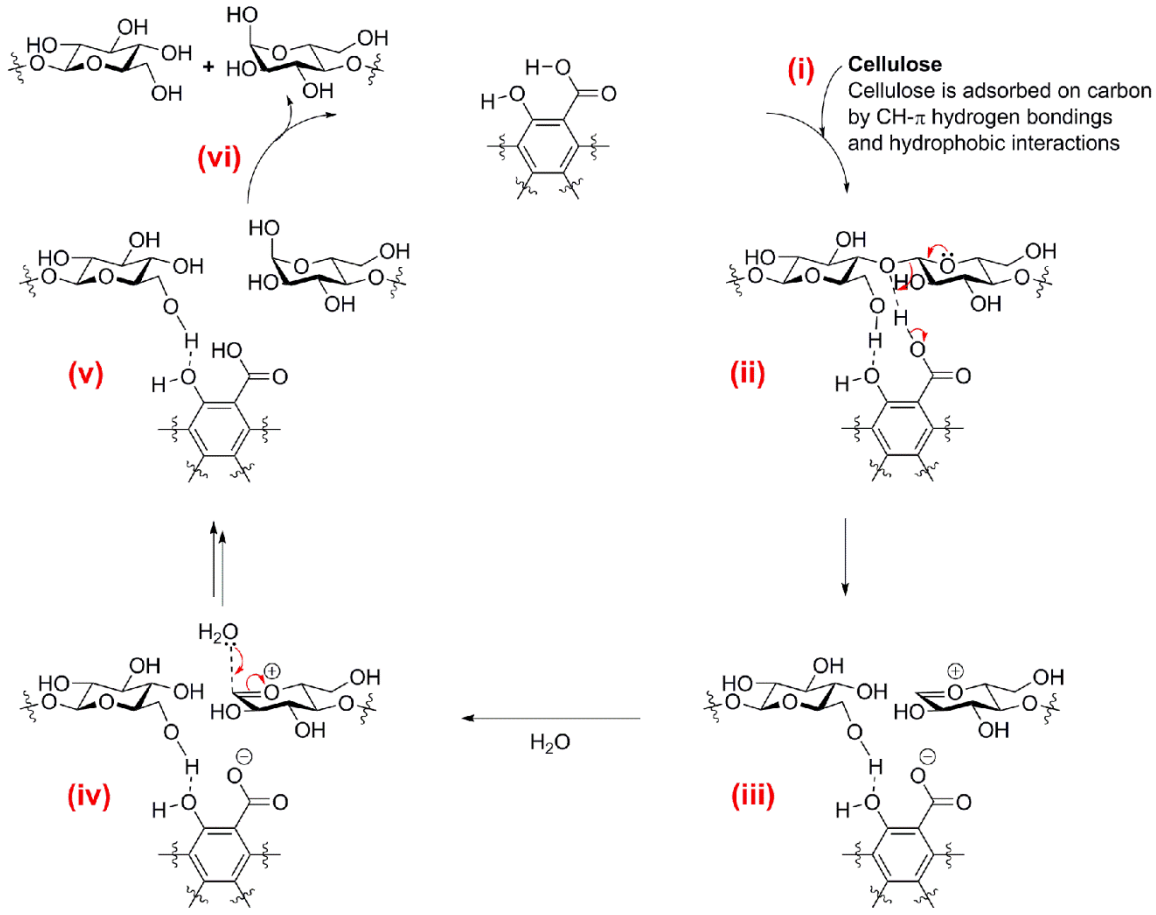


Figure 3.25. Proposed reaction mechanism of cellulose hydrolysis by carbon catalysts.

surface of carbon driven by both CH–π hydrogen bonds and hydrophobic interactions, which may help the subsequent interaction between hydrophilic functionalities. In the second step (ii), vicinal weak acids on carbon with the structure similar to salicylic acid and phthalic acid interact with the substrate through OH–O hydrogen bonds and activate a glycosidic bond. Then, in step (iii), the glycosidic bond is cleaved to form an intermediate oxocarbenium species.[41] In step (iv), a H_2O molecule readily attacks the oxocarbenium species and a hydroxyl group is produced. Subsequently, in step (v), the active site on carbon is recovered by proton transfer from the substrate to catalyst. Finally, in step (vi), the divided cellulosic molecules desorb from the carbon surface since the interaction of carbon with shorter β-1,4-glucans is weaker.

3.3.5. Hydrolysis of cellulose by zeolite-templated carbon ZTC

The mechanistic study has indicated that both OFGs and aromatic rings of carbon materials play crucial roles

for cellulose hydrolysis. Based on these facts, the author and collaborators have tried to prepare highly active carbon catalysts for cellulose hydrolysis.

It is known that zeolite-templated carbon, denoted as ZTC (Figure 3.26),[8] consists of 3D-covalented warped nanographenes with a number of edges, thus possessing an ultralarge surface area of *ca.* 4000 m^2 g^{-1}. ZTC is expected to be a good adsorbate for cellulosic molecules since the nanographenes would be good adsorption sites as discussed in Section 3.3.3. In addition, ZTC possibly contains large amounts of OFGs due to the unique structure with many edges, on which OFGs can be introduced. Indeed, Nishihara *et al.* has demonstrated the preparation of ZTC containing >10 wt% of oxygen atoms as carboxylic acids, phenolic groups, and so on.[8] The report motivated the author and collaborators to utilize oxidized ZTC in cellulose hydrolysis. An electrolytically-oxidized ZTC was employed as a catalyst for the hydrolysis of individually ball-milled cellulose at 503 K under the rapid heating-cooling condition (Table 3.7). The oxidized ZTC produced glucose in 46% yield with 70% conversion of cellulose (entry 40), and thus this material specifically showed a higher catalytic activity than other carbons tested in this work. This result clearly indicates that highly active carbon catalyst can be designed based on the mechanistic insights. Meanwhile, oxidized ZTC has given lower glucose yield (27%) in the second run, and its durability needs to be improved. Therefore, further investigations for oxidized ZTC including its characterization are necessary in future work.

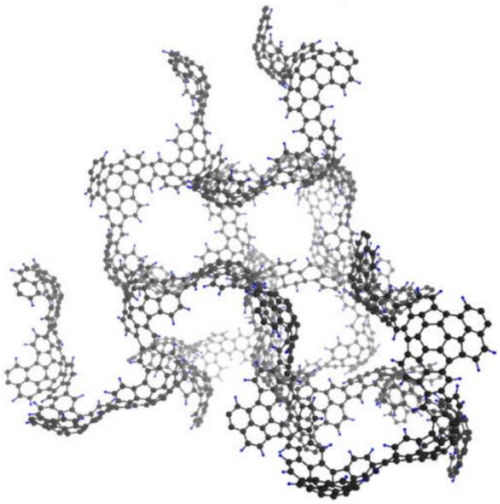


Figure 3.26. Structure of ZTC, reproduced from a reference.[8]

Table 3.7. Hydrolysis of cellulose by ZTC.[a]

Entry	Catalyst	Conv. /%	Yield based on carbon /%						
			Glucan		By-product				
			Glc[b]	Olg[c]	Frc[d]	Man[e]	Lev[f]	HMF[g]	Others[h]
18	None	28	4.6	15	0.5	0.6	0.2	1.8	5.3
40	ZTC	70	46	1.4	2.4	1.8	2.8	5.0	10
21	K26	60	36	2.5	2.7	2.6	2.1	3.4	11

[a]Conditions: individually ball-milled cellulose 324 mg (0.9 L-pot), catalyst 50 mg, H_2O 40 mL, 503 K, <1 min (rapid heating-cooling condition). Cellulose was ball-milled without catalyst. [b]Glucose. [c]Water-soluble oligosaccharides (DP = mainly 2–6). [d]Fructose. [e]Mannose. [f]Levoglucosan. [g]5-Hydroxymethylfurfural. [h](Conversion) – (total yield of the characterized products).

3.4. Conclusions

Adsorption and hydrolysis of cellulosic molecules over K26 have been investigated. Both hydrophilic and hydrophobic functions of carbon catalysts play significant roles for the hydrolysis of cellulosic molecules. The formation of CH–π hydrogen bonds and hydrophobic interactions promote the first adsorption step of the substrate onto carbon surface. Then, vicinal weak acids such as OH/COOH and COOH/COOH on carbon activate and cleave the glycosidic bonds. During the reaction, one functional group makes an OH–O hydrogen bond with a hydroxyl group of the substrate, and then another carboxylic acid hydrolyzes the glycosidic bonds. Hence, the interactions with the substrate enable carbon catalysts to hydrolyze glycosidic bonds even in the absence of strong acid sites.

References and note

1. H. P. Boehm, *Carbon*, 1994, **32**, 759–769.
2. H.-P. Lin, C.-P. Kao, C.-Y. Mou, and S.-B. Liu, *J. Phys. Chem. B*, 2000, **104**, 7885–7894.
3. H. Yang, L. Zhang, L. Zhong, Q. Yang, and C. Li, *Angew. Chem. Int. Ed.*, 2007, **46**, 6861–6865.
4. O. M. Gazit, A. Charmot, and A. Katz, *Chem. Commun.*, 2011, **47**, 376–378.
5. O. M. Gazit and A. Katz, *Langmuir*, 2012, 431–437.
6. O. M. Gazit and A. Katz, *J. Am. Chem. Soc.*, 2013, **135**, 4398–4402.
7. C. Loerbroks, R. Rinaldi, and W. Thiel, *Chem. Eur. J.*, 2013, **19**, 16282–16294.
8. H. Nishihara, Q.-H. Yang, P.-X. Hou, M. Unno, S. Yamauchi, R. Saito, J. I. Paredes, A.

Martínez-Alonso, J. M. D. Tascón, Y. Sato, M. Terauchi, and T. Kyotani, *Carbon*, 2009, **47**, 1220–1230.

9. J. L. Figueiredo, M. F. R. Pereira, M. M. A. Freitas, and J. J. M. Órfão, *Carbon*, 1999, **37**, 1379–1389.
10. S. Ishikawa, T. Murayama, S. Ohmura, M. Sadakane, and W. Ueda, *Chem. Mater.*, 2013, **25**, 2211–2219.
11. D. S. Knight and W. B. White, *J. Mater. Res.*, 1989, **4**, 385–393.
12. M. A. Pimenta, G. Dresselhaus, M. S. Dresselhaus, L. G. Cancado, A. Jorio, and R. Saito, *Phys. Chem. Chem. Phys.*, 2007, **9**, 1276–1290.
13. A. D. Becke, *J. Chem. Phys.*, 1993, **98**, 5648–5652.
14. C. Lee, W. Yang, and R. G. Parr, *Phys. Rev. B*, 1988, **37**, 785–789.
15. W. J. Hehre, R. Ditchfield, and J. A. Pople, *J. Chem. Phys.*, 1972, **56**, 2257–2261.
16. S. Grimme, J. Antony, S. Ehrlich, and H. Krieg, *J. Chem. Phys.*, 2010, **132**, 154104.
17. J. Tomasi, B. Mennucci, and R. Cammi, *Chem. Rev.*, 2005, **105**, 2999–3094.
18. B. Capon, *Tetrahedron Lett.*, 1963, **4**, 911–913.
19. W. P. Jencks and J. Regenstein, *Handb. Biochem. Mol. Biol.*, 1976, **1**, 305–352.
20. S. Suganuma, K. Nakajima, M. Kitano, D. Yamaguchi, H. Kato, S. Hayashi, and M. Hara, *J. Am. Chem. Soc.*, 2008, **130**, 12787–12793.
21. M. Kitano, D. Yamaguchi, S. Suganuma, K. Nakajima, H. Kato, S. Hayashi, and M. Hara, *Langmuir*, 2009, **25**, 5068–5075.
22. P. Qrtiz, E. Reguera, and J. Fernández-Bertrán, *J. Fluor. Chem.*, 2002, **113**, 7–12.
23. J. Zhang, H. Zhang, J. Wu, J. Zhang, J. He, and J. Xiang, *Phys. Chem. Chem. Phys.*, 2010, **12**, 1941–1947.
24. E. Liepinsh, G. Otting, and K. Wüthrich, *J. Biomol. NMR*, 1992, **2**, 447–465.
25. E. Liepinsh and G. Otting, *Magn. Reson. Med.*, 1996, **35**, 30–42.
26. B. Bernet, R. Bürli, J. Xu, and A. Vasella, *Helv. Chim. Acta*, 2002, **85**, 1800–1811.
27. I. Kögel-Knabner, *Geoderma*, 1997, **80**, 243–270.
28. S. Bui, X. Verykios, and R. Mutharasan, *Ind. Eng. Chem. Process Des. Dev.*, 1985, **24**, 1209–1213.

29. P.-W. Chung, A. Charmot, O. M. Gazit, and A. Katz, *Langmuir*, 2012, **28**, 15222–15232.

30. K. S. W. Sing, *Pure Appl. Chem.*, 1985, **57**, 603–619.

31. W. Zhu, J. M. van de Graaf, L. J. P. van den Broeke, F. Kapteijn, and J. A. Moulijn, *Ind. Eng. Chem. Res.*, 1998, **37**, 1934–1942.

32. Z. Yong, V. Mata, and A. E. Rodrigues, *Sep. Purif. Technol.*, 2002, **26**, 195–205.

33. J. Tormo, R. Lamed, A. J. Chirino, E. Morag, E. A. Bayer, Y. Shoham, and T. A. Steitz, *EMBO J.*, 1996, **15**, 5739–5751.

34. S. Tsuzuki, K. Honda, T. Uchimaru, M. Mikami, and K. Tanabe, *J. Am. Chem. Soc.*, 2000, **122**, 3746–3753.

35. W. Brown, *J. Chromatogr. A*, 1970, **52**, 273–284.

36. A. Gurses, M. Yalcin, M. Sozbilir, and C. Dogar, *Fuel Process. Technol.*, 2003, **81**, 57–66.

37. W.-Y. Chen, H.-M. Huang, C.-C. Lin, F.-Y. Lin, and Y.-C. Chan, *Langmuir*, 2003, **19**, 9395–9403.

38. R. Haselmeier, M. Holz, W. Marbach, and H. Weingaertner, *J. Phys. Chem.*, 1995, **99**, 2243–2246.

39. W. Chen, S. Enck, J. L. Price, D. L. Powers, E. T. Powers, C.-H. Wong, H. J. Dyson, and J. W. Kelly, *J. Am. Chem. Soc.*, 2013, **135**, 9877–9884.

40. The entropy change of cellobiose adsorption on carbon surface ($\Delta S°_{ads}$) can be theoretically calculated as follows. $\Delta S°_{ads}$ is divided into nine constituents (eq. 3.13).

$$\begin{aligned}\Delta S^{\circ}_{ads} = {} & \Delta S^{\circ}_{hydrophobi} \\ & + \Delta S^{\circ}_{trans}(\text{Cellobiose}) + \Delta S^{\circ}_{rot}(\text{Cellobiose}) + \Delta S^{\circ}_{vib}(\text{Cellobiose}) + \Delta S^{\circ}_{conf}(\text{Cellobiose}) \\ & + \Delta S^{\circ}_{trans}(\text{Carbon}) + \Delta S^{\circ}_{rot}(\text{Carbon}) + \Delta S^{\circ}_{vib}(\text{Carbon}) + \Delta S^{\circ}_{conf}(\text{Carbon})\end{aligned}$$

(3.13)

where $\Delta S°_{hydrophobic}$ is entropy change of hydrophobic interaction, $\Delta S°_{trans}$(Cellobiose), $\Delta S°_{rot}$(Cellobiose), $\Delta S°_{vib}$(Cellobiose), and $\Delta S°_{conf}$(Cellobiose) are entropy changes of translation, rotation, vibration, and conformation for cellobiose, respectively. $\Delta S°_{trans}$(Carbon), $\Delta S°_{rot}$(Carbon), $\Delta S°_{vib}$(Carbon), and $\Delta S°_{conf}$(Carbon) are entropy changes of translation, rotation, vibration, and conformation for carbon material.

For the calculation, the author has assumed that $\Delta S°_{trans}$(Carbon) and $\Delta S°_{rot}$(Carbon) are negligible since the size of carbon material is much larger than cellobiose (see Figures 3.13 and 3.16) and its motion would not be restricted by cellobiose adsorption. $\Delta S°_{vib}$(Cellobiose) and $\Delta S°_{vib}$(Carbon) are approximately zero because almost all kinds of molecular vibrations are in ground state *zero-point vibration* (*viz.* $S°_{vib} = 0$) at room temperature.[42] Furthermore, $\Delta S°_{conf}$(Cellobiose) and $\Delta S°_{conf}$(Carbon) would also be zero as the DFT calculation has shown that conformation of cellobiose and carbon material consisting of quadruple-layered graphene is retained during the adsorption. Hence, $\Delta S°_{hydrophobic}$, $\Delta S°_{trans}$(Cellobiose), and $\Delta S°_{rot}$(Cellobiose) values for cellobiose are necessary to determine theoretical $\Delta S°_{ads}$. First, for $\Delta S°_{hydrophobic}$, it is reported that a standard entropy of +4.2 J K^{-1} mol^{-1} increases when one water molecule are desorbed from each substrate molecule.[43] The adsorption cross-section of cellobiose is 0.7 nm × 1.1 nm as shown in Figure 3.16, indicating that 15–24 water molecules exist on axial plane of cellobiose. Since the same number of water molecules on carbon surface is also removed in the adsorption, total 30–48 water molecules gain entropies of 4.2 J K^{-1} mol^{-1}, respectively. Therefore, entropy increase by hydrophobic interaction ($\Delta S°_{hydrophobic}$) is +164 ± 37 J K^{-1} mol^{-1}. Next, $\Delta S°_{trans}$(Cellobiose) and $\Delta S°_{rot}$(Cellobiose) can be elucidated by the Sackur-Tetrode equation (eq. 3.14) and eq. 3.15, respectively.[42] The number of *1/3* shown in eq. 3.14 is derived from the restriction of molecular motion. Free molecules can move in 3D space, whereas adsorbed molecules can on 2D surface; hence, adsorbed molecules lose one of three translational degrees of freedom. The calculated value in the brackets followed by *1/3* in eq. 3.14 gives whole translational entropy, and thus the multiplication of the value by *1/3* is required to calculate translational entropy change in adsorption. For the same reason, two rotational degrees of freedom are lost on 2D surface (in 3D space, molecules have three rotational degrees of freedom), and the value of *2/3* is included in eq. 3.15. The author notes that these equations are for ideal gas, and the values are overestimated.[42]

$$\Delta S^{\circ}_{\mathrm{trans}}(\mathrm{Cellobiose}) = \frac{1}{3}\left\{ R\ln\left[\left(\frac{2\pi R}{h^2}\right)^{\frac{3}{2}} \cdot \frac{V}{N_{\mathrm{A}}} \cdot \mathrm{e}^{\frac{5}{2}}\right] + \frac{3}{2} R\ln M + \frac{3}{2} R\ln T \right\} \qquad (3.14)$$

$$\Delta S^{\circ}_{\mathrm{rot}}(\mathrm{Carbon}) = \frac{2}{3}\left\{ R\ln\left[\pi^{\frac{1}{2}}\left(\frac{8\pi^2 Re}{N_{\mathrm{A}} h^2}\right)^{\frac{3}{2}}\right] + \frac{1}{2} R\ln\left(I_{\mathrm{A}} I_{\mathrm{B}} I_{\mathrm{C}}\right) + \frac{3}{2} R\ln T \right\} \qquad (3.15)$$

where R is gas constant, h is Planck constant, V is volume of solution [in this study, V is 1×10^{-3} m^3 (= 1 L)], N_A is Avogadro constant, M (unit: kg mol^{-1}) is molecular weight, T is temperature, and I_A, I_B, and I_C are principal moments of inertia. I_A, I_B, and I_C are defined by eqs. 3.16–3.18.

$$I_{\mathrm{A}} = \frac{M}{12N_{\mathrm{A}}}\left(a^2 + b^2\right) \qquad (3.16)$$

$$I_{\mathrm{B}} = \frac{M}{12N_{\mathrm{A}}}\left(b^2 + c^2\right) \qquad (3.17)$$

$$I_{\mathrm{C}} = \frac{M}{12N_{\mathrm{A}}}\left(c^2 + a^2\right) \qquad (3.18)$$

in which a, b, and c represent the size of cellobiose molecule; a, b, and c are 0.4 nm, 0.7 nm, and 1.1 nm, respectively (Figure 3.16).

Based on eqs. 3.14 and 3.15, $\Delta S°_{\mathrm{trans}}$(Cellobiose) and $\Delta S°_{\mathrm{rot}}$(Cellobiose) at 296 K are –51.6 J K^{-1} mol^{-1} and –99.5 J K^{-1} mol^{-1}, respectively. Consequently, the whole entropy change during adsorption ($\Delta S°_{\mathrm{ads}}$) is estimated to be +12.1 ± 37 J K^{-1} mol^{-1}; the number of water molecules related to hydrophobic interaction is not determined (30–48 molecules), giving a wide range of theoretical value. This theoretical value roughly agrees with the experimental value (+23.5 ± 3.4 J K^{-1} mol^{-1}, Table 3.5).

41. T. P. Nevell and W. R. Upton, *Carbohydr. Res.*, 1976, **49**, 163–174.

42. M. Mammen, E. I. Shakhnovich, J. M. Deutch, and G. M. Whitesides, *J. Org. Chem.*, 1998, **63**, 3821–3830.

43. N. T. Southall, K. A. Dill, and A. D. J. Haymet, *J. Phys. Chem. B*, 2002, **106**, 521–533.

Chapter 4

Two-Step Depolymerization of Chitin to Monomers

Chitin, the most abundant *N*-containing biopolymer, includes both glycosidic bonds and *N*-acetyl groups and is an attractive source of useful monomers such as *N*-acetylglucosamine (GlcNAc) and 1-*O*-methyl-*N*-acetylglucosamine (MeGlcNAc). In order to synthesize the monomers in high yields, selective cleavage of glycosidic bonds in chitin without deacetylation is necessary. In this chapter, the two-step transformation of chitin to MeGlcNAc has been studied: (i) mechanical-force-assisted hydrolysis of chitin to water-soluble oligomers and (ii) methanolysis of oligomers to MeGlcNAc. In both reactions, chitin does not undergo deacetylation, and only depolymerization proceeds. As a result, MeGlcNAc has been obtained in 67% yield from chitin. Additionally, it is also shown that MeGlcNAc is easily transformed into GlcNAc in a good yield.

4.1. Introduction

Chitin (Figure 4.1) is expected to be primary feedstock for organic nitrogen compounds because chitin is the most abundant nitrogen-containing biomass consisting of a single unit, *N*-acetylglucosamine (GlcNAc).[1] GlcNAc is used as a biologically-active agent, cosmetic,[2] and potential feedstock for various kinds of chemicals (Figure 1.28),[3–7] and 1-*O*-alkyl-GlcNAc is also a promising precursor to medicines,[8] organocatalysts,[9] ligands,[10] and gelators[11] in addition to the applications of GlcNAc. Another type of monomer is a deacetylated compound glucosamine (GlcN), but the removal of the acetyl group declines physiological activity and usability.[12,13] Thus, the dissociation of glycosidic bonds of chitin with preserving the acetyl group is favorable for efficient utilization of this biomass.

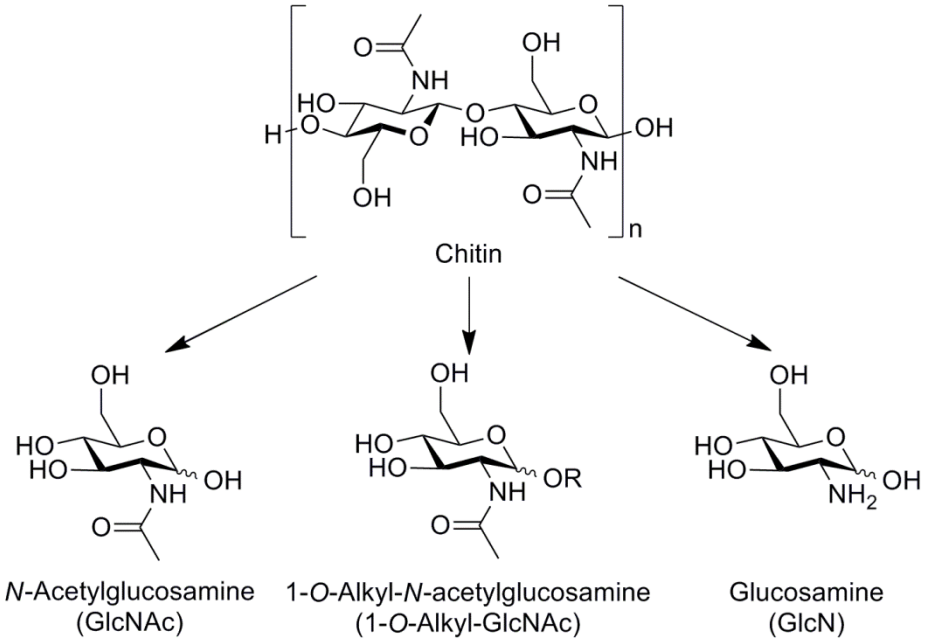


Figure 4.1. Structure of chitin and its monomers.

To date, the selective synthesis of GlcNAc from chitin has been intensively studied; however, this reaction has remained a challenge. The major difficulties are as follows. (i) Chitin is highly recalcitrant. (ii) Dissociation of glycosidic and amide bonds simultaneously takes place. (iii) GlcNAc has a hemiacetal group that easily undergoes side-reactions. Chitinase enzymes depolymerize chitin to GlcNAc in a high yield of

77% as they are extremely chemoselective and work under ambient conditions, but it takes 10 days to obtain such a high yield of GlcNAc.[14] Although 15–36 wt% concentration of HCl also can hydrolyze chitin with retaining *N*-acetyl group (*ca.* 65% yield GlcNAc), this reaction system suffers from the serious corrosive property of concentrated HCl and a huge amount of acidic waste.[2] Diluting HCl results in the removal of acetyl group and side-reactions of hemiacetal during a longer reaction time due to the slower hydrolysis of glycosidic bonds.[15,16] This issue has largely hampered to utilize the chitin monomers in the applications mentioned above.

Hence, the selective depolymerization of chitin with preserving acetyl group has been a great challenge in ocean biomass refinery. In this chapter, the author shows a new strategy for the production of valuable monomers, GlcNAc and 1-*O*-methyl-*N*-acetylglucosamine (MeGlcNAc), from chitin without deacetylation by two-step depolymerization: (i) mechanical-force-assisted hydrolysis and (ii) methanolysis. In the reported works for polymer degradation, it has been demonstrated that mechanical force cleaves connecting points of polymers since polymers can receive the macro-scale power as tensile stress.[17] Thus, mechanical conversion of chitin is expected to provide selective dissociation of glycosidic bonds connecting GlcNAc units rather than that of amide bonds hanging on the units, giving chitin oligomers. The oligomers are water-soluble and significantly more reactive than the original recalcitrant polymer. Then, the alcoholysis of the oligomers provides a benefit of protection of reactive hemiacetal group by an alkyl group during the reaction in addition to the direct production of useful MeGlcNAc.

4.2. Experimental

4.2.1. Reagents

Chitin	First grade, Wako Pure Chemical Industries
D(+)-Cellobiose	Special grade, Kanto Chemical
D(+)-Maltose	Monohydrate, special grade, Wako Pure Chemical Industries
Sulfuric acid	96–98%, super special grade, Wako Pure Chemical Industries

Amberlyst 70	Sulfonic acid cation exchange resin, Organo
Nafion SAC-13	Silica-supported fluorinated sulfonic acid polymer, Sigma-Aldrich
K26	Alkali-activated carbon (not for sale), Showa Denko
JRC-Z-HM90	Proton-type MOR zeolite, Si/Al = 45, Catalysis Society of Japan, denoted as H-MOR
N-Acetylglucosamine	First grade, Wako Pure Chemical Industries, denoted as GlcNAc
Chitobiose	≥96%, Sigma-Aldrich
1-*O*-Methyl-α-*N*-acetylglucosamine	98%, Toronto Research Chemicals, denoted as α-MeGlcNAc
1-*O*-Methyl-β-*N*-acetylglucosamine	98%, Toronto Research Chemicals, denoted as β-MeGlcNAc
Acetic acid	>99.7%, special grade, Wako Pure Chemical Industries
Methyl acetate	First grade, Wako Pure Chemical Industries
D(+)-Glucose	Special grade, Kanto Chemical
1-*O*-Methyl-α-glucose	>98.0%, Tokyo Chemical Industry, denoted as α-MeGlc
1-*O*-Methyl-β-glucose	>98.0%, Hemihydrate, Tokyo Chemical Industry, denoted as β-MeGlc
Sorbitol	>97.0%, Tokyo Chemical Industry
Distilled water	Wako Pure Chemical Industries
Methanol	Special grade, Wako Pure Chemical Industries
Hydrochloric acid methanolic solution	0.5 M, for volumetric analysis, Wako Pure Chemical Industries
Diethyl ether	First grade, Wako Pure Chemical Industries
Acetone	Special grade, Wako Pure Chemical Industries
Distilled water	For HPLC, Wako Pure Chemical Industries
Acetonitrile	For HPLC, Wako Pure Chemical Industries
Phosphoric acid	85%, special grade, Kanto Chemical

Potassium dihydrogen phosphate solution	0.5 M, for HPLC, Wako Pure Chemical Industries
Deuterium oxide	For NMR, Acros Organics
Deuterated methanol	For NMR, Acros Organics
Maleic acid	>99%, special grade, Wako Pure Chemical Industries
Potassium bromide	Crystal block, for IR, Wako Pure Chemical Industries
Helium gas	Alpha gas 2, Air Liquide Kogyo Gas
Hydrogen gas	>99.99%, for gas chromatography (GC), generated from H_2O in an apparatus (GL Sciences, HG260)

4.2.2. Mechanocatalytic hydrolysis of chitin

Chitin (10 g) was dispersed in 25 mL of diethyl ether containing H_2SO_4 (0.59 g). After drying diethyl ether, 10 g of resulting powder was ball-milled at 80 rpm for 96 h by using Al_2O_3 balls (ø1.5 cm, 2 kg) in a 3.6 L of ceramic pot. When using solid catalyst, chitin 10 g and catalyst 1.23 g were milled together in the pot. For planetary ball-milling (Fritsch, Pulverisette 6), 4.9 g of H_2SO_4-impregnated chitin was treated at 500 rpm for 6 h in the presence of Al_2O_3 balls (ø5.0 mm, 100 g) in a 250 mL of Al_2O_3 pot, in which milling was stopped every 15 min for 15 min to decrease temperature in the pot.

The solubility of the chitin samples was determined as follows. The chitin sample (430 mg, containing 406 mg of chitin and 24 mg of H_2SO_4) was added into 40 mL of H_2O. After stirring and sonication, the suspension was filtered with a PTFE membrane (0.1 μm mesh). The solid phase was dried in an oven at 383 K overnight, and the solubility was calculated from the difference between the amount of chitin used and that of dried residue. The water-soluble oligomers were analyzed by LC/MS (Thermo Fischer Scientific, LCQ Fleet, APCI, the conditions were the same as those of HPLC described below). The mass spectra are depicted as Figure 4.A.1 in Appendices, by which GlcNAc, chitobiose, and chitotriose have been identified (Figure 4.2). Chitin samples themselves were also characterized by XRD (Rigaku, Ultima IV, Cu Kα).

***GlcNAc*.** LC/MS (*m*/*z*): $[M + H]^+$ calculated for $[C_8H_{15}NO_6 + H]^+$, 222; found, 222.

***Chitobiose*.** LC/MS (*m*/*z*): $[M + H]^+$ calculated for $[C_{16}H_{28}N_2O_{11} + H]^+$, 425; found, 425.

***Chitotriose*.** LC/MS (*m*/*z*): $[M + H]^+$ calculated for $[C_{24}H_{41}N_3O_{16} + H]^+$, 628; found, 628.

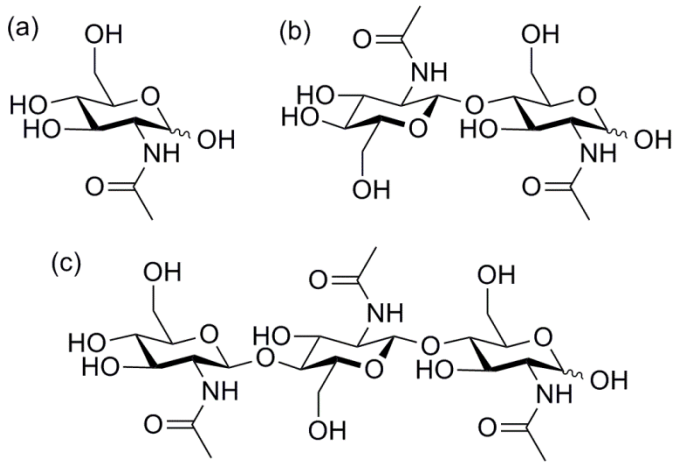


Figure 4.2. Structures of (a) GlcNAc, (b) chitobiose, and (c) chitotriose.

4.2.3. Methanolysis of chitin

Mix-milled chitin (456 mg, containing chitin 406 mg and catalyst 50 mg) or H_2SO_4-impregnated chitin (430 mg, containing 406 mg of chitin and 24 mg of H_2SO_4) and MeOH (40 mL) were charged into a SUS316 high-pressure reactor (OM-Lab Tech, MMJ-100, 100 mL, Figure 2.2). The temperature was raised to 443 K in 12 min or to 463 K in 16 min. After reaching the temperature, the reactor was rapidly cooled down to room temperature, namely rapid heating-cooling condition. After the reaction, sorbitol (182 mg, 1 mmol) was added into the solution as an internal standard. A portion of the reaction mixture (0.5 mL) was filtered by a Mini-UniPrep [Whatman, equipped with a PVDF membrane (0.2 μm mesh)], the amount of MeOAc in the liquid phase was determined by GC (Shimadzu GC-14B) with a ULBON HR-20M capillary column (Shinwa Chemical Industries, ø0.25 mm × 25 m, film thickness: 0.25 μm). The liquid and solid phases of the remaining reaction mixture (*ca.* 39.5 mL) were separated by filtration using a PTFE membrane (0.1 μm mesh). The liquid phase was analyzed by following procedure. After evaporating MeOH, the reaction products were dissolved in 40 mL of H_2O. The products in the aqueous phase were quantified by HPLC

[Shimadzu LC10-AT*VP*, RI and UV (210 nm) detectors] with a SUGAR SH1011 column (Shodex, ø8 mm × 300 mm, mobile phase: H_2O 0.5 mL min^{-1}, 323 K), a Rezex RPM-Monosaccharide Pb++ column (Phenomenex, ø8 mm × 300 mm, mobile phase: H_2O 0.6 mL min^{-1}, 343 K), and a Asahipak NH2P-50 4E column [Shodex, ø4.6 mm × 250 mm, mobile phase: CH_3CN/H_2O (7/3) 0.5 mL min^{-1}, 303 K]. For the analysis of AcOH by HPLC, a Synergi 4 μm Hydro-RP 80Å column [Phenomenex, ø4.6 mm × 250 mm, mobile phase: 40 mM potassium phosphate buffer solution (pH 2.9) 0.8 mL min^{-1}, 303 K] was used. The author also conducted LC/MS (the conditions were the same as those of HPLC), IR [PerkinElmer, Spectrum 100, deuterated triglycine sulfate (DTGS) detector, transmission mode, KBr pellet], NMR [JEOL, JNM-ECX400, ^1H 400 MHz, ^{13}C 100 MHz, including ^1H NMR, ^{13}C NMR, distortionless enhancement by polarization transfer (DEPT), ^1H–^1H correlation spectroscopy (COSY), ^{13}C–^1H heteronuclear multiple quantum coherence (HMQC), and ^{13}C–^1H heteronuclear multiple bond correlation (HMBC)], and elemental analysis to identify reaction products. The LC/MS, IR, and NMR spectra of MeGlcNAc are shown in Figures 4.A.2–4.A.6 in Appendices. Figure 4.3 represents the structure of MeGlcNAc.

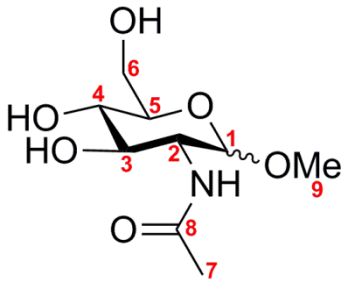


Figure 4.3. Structure of 1-*O*-methyl *N*-acetylglucosamine (MeGlcNAc).

α-MeGlcNAc. ^1H NMR (400 MHz, D_2O): δ 4.74 (d, J = 3.6 Hz, 1H, *H*–C1), 3.90 (dd, J = 11.2, 3.6 Hz, 1H, *H*–C2), 3.87 (dd, J = 12.4, 2.4 Hz, 1H, *H*–C6), 3.77 (dd, J = 12.4, 5.6 Hz, 1H, *H*–C6), 3.70 (dd, J = 10.4, 9.2 Hz, 1H, *H*–C3), 3.66 (ddd, J = 9.6, 5.6, 2.4 Hz, 1H, *H*–C5), 3.46 (dd, J = 10.0, 9.2 Hz, 1H, *H*–C4), 3.37 (s, 3H, *H*–C9), 2.02 (s, 3H, *H*–C7); ^{13}C NMR (100 MHz, D_2O): δ 175.4 (C, C8), 99.0 (CH, C1), 72.6 (CH, C5), 72.1 (CH, C3), 70.9 (CH, C4), 61.5 (CH_2, C6), 56.1 (CH_3, C9), 54.5 (CH, C2), 22.8 (CH_3, C7); LC/MS (*m*/*z*): $[M + H]^+$ calculated for $[C_9H_{17}NO_6 + H]^+$, 236; found, 236. The NMR peaks were assigned using an

authentic sample from Toronto Research Chemicals.

β-MeGlcNAc. ^{1}H NMR (400 MHz, D_2O): δ 4.43 (d, J = 8.4 Hz, 1H, *H*–C1), 3.92 (dd, J = 12.4, 2.0 Hz, 1H, *H*–C6), 3.73 (dd, J = 12.4, 5.4 Hz, *H*–C6), 3.67 (dd, J = 10.4, 8.8 Hz, *H*–C2), 3.53 (d, J = 8.0 Hz, *H*–C3), 3.49 (s, 3H, *H*–C9), 3.39–3.47 (m, 2H, *H*–C4 and *H*–C5), 2.02 (s, 3H, *H*–C7); ^{13}C NMR (100 MHz, D_2O): δ 175.7 (C, C8), 102.9 (CH, C1), 76.9 (CH, C5), 74.9 (CH, C3), 70.9 (CH, C4), 61.7 (CH_2, C6), 58.0 (CH_3, C9), 56.4 (CH, C2), 23.1 (CH_3, C7); LC/MS (m/z): $[M + H]^+$ calculated for $[C_9H_{17}NO_6 + H]^+$, 236; found, 236. The NMR peaks were assigned using an authentic sample from Toronto Research Chemicals.

MeGlcNAc (produced by methanolysis of chitin). IR (KBr pellet, cm^{-1}): 3391 [ν(O–H)], 3299 [ν(N–H, amide)], 2994 [ν(C–H, alkyl)], 2955 [ν(C–H, alkyl)], 2927 [ν(C–H, alkyl)], 1649 [ν(C=O, amide I)], 1556 [δ(N–H, amide II)]; elemental analysis (calculated, found for $C_9H_{17}NO_6$): C (45.95, 45.74), H (7.28, 7.21), N (5.96, 5.96), O (40.81, 41.10). ^{1}H NMR and DEPT peaks indicated that both α- and β-MeGlcNAc were included (Figures 4.A.3 and 4.A.4).

4.2.4. Synthesis of MeGlcNAc

MeGlcNAc was synthesized from GlcNAc by Fischer glycosidation. GlcNAc (2.5 g) and HCl/MeOH (50 mM, 40 mL) were charged into a hastelloy C22 high-pressure reactor (MMJ-100, OM-Lab Tech, 100 mL, Figure 2.2). The temperature was raised to 423 K in 10 min and then rapidly decreased to room temperature. After removing HCl/MeOH with a rotary evaporator, MeGlcNAc was recrystallized using MeOH and CH_3CN. The resulting powder was filtered and washed with acetone repeatedly. After drying under vacuum overnight, white MeGlcNAc powder of 0.97 g with *ca.* 98% of relative purity was obtained. The relative purity was determined by ^{1}H NMR (repetition time: 7.7 s) using maleic acid as an internal standard.

4.2.5. Hydrolysis of MeGlcNAc

Hydrolysis of MeGlcNAc was conducted in a pressure-resistant glass tube (Ace Glass, 15 mL). MeGlcNAc (20 mg), H-BEA (250 mg), and H_2O (5 mL) were charged into the reactor. The reactor was immersed in an oil bath at 423 K for 12 min. The liquid and solid phases were separated with a PVDF membrane (0.20 μm mesh), and the liquid phase was analyzed by HPLC under the same conditions described above.

4.3. Results and discussion

4.3.1. Mechanocatalytic depolymerization of chitin

The new strategy in this work is based on two reactions: the first is mechanocatalytic depolymerization of chitin to oligomers (Figure 4.4).

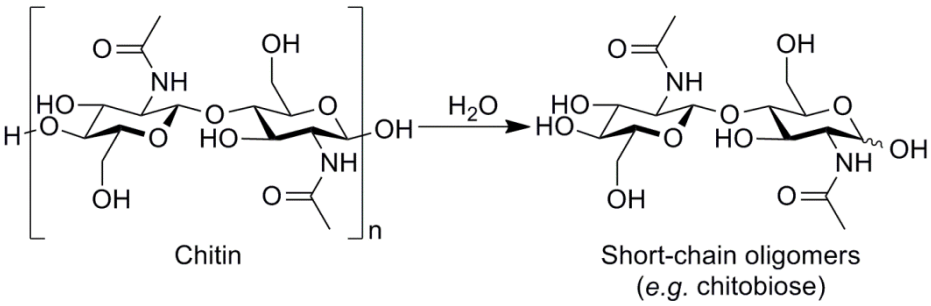


Figure 4.4. Hydrolysis of chitin to short-chain oligomers.

At first, solid catalysts were tested for the first step since heterogeneous catalysts are advantageous over homogenous ones in their ease of separation and reusability. Thus, chitin and solid catalysts were milled together at 80 rpm for 96 h. Amberlyst 70 gives *ca.* 88% of solubility of chitin, indicating the proceeding of mechanocatalytic hydrolysis. However, Amberlyst 70 itself is also dissolved in H_2O, similar to Figure 2.9. Amberlyst 70 therefore does not have advantages as a heterogeneous catalyst described above. Chitin was not dissolved in H_2O by using other solids such as Nafion SAC-13, alkali-activated carbon K26, and H-MOR. Hence, the solid catalysts tested in this work are not effective for the reaction.

Next, the author conducted ball-milling of H_2SO_4-impregnated chitin as a mechanocatalytic reaction (Table 4.1). *Ca.* 97% of chitin was solubilized in H_2O after the milling (entry 1), indicating the formation of oligomers having low DP during the process.[18–20] Indeed, a combination of LC/MS and LC/RI determined three compounds, *i.e.*, GlcNAc (18% yield), chitobiose (19%), and chitotriose (23%) (structures: Figure 4.2, LC/MS spectra: Figure 4.A.1 in Appendices). The LC/MS analysis also represented *m*/*z* of 813 (corresponding to mono-dehydrated tetramer with H^+), 1016 (mono-dehydrated pentamer with H^+), 1219 (mono-dehydrated hexamer with H^+), and 1422 (mono-dehydrated heptamer with H^+). These products are

included in *Others* shown in Table 4.1. These oligomers are useful as antitumor, immunoenhancing, and antimicrobial agents.[21] The author also confirmed no formation of AcOH by HPLC; thus, acetyl groups of chitin were completely preserved during the depolymerization. Accordingly, the ball-milling of chitin with H_2SO_4 selectively produced chitin oligomers. In contrast, the ball-milling of chitin without H_2SO_4 gave no water-soluble oligomers (<0.1%, entry 4), but just formed amorphous chitin (XRD, Figure 4.5).[23] In addition, chitin impregnated with H_2SO_4 caused very limited solubilization in 96 h in the absence of ball-milling (entry 5). Hence, both mechanical force and H_2SO_4 catalyst are necessary for the depolymerization of chitin, indicating mechanocatalytic reaction.

The milling time was as long as 96 h when using a conventional rolling pot-mill as described above; however, the use of planetary ball-milling at 500 rpm shortened it to 6 h to solubilize chitin in >99% in the experiments (entry 2). A bulk-scale milling (attritor) used in industry possesses similar efficiency to planetary milling, suggesting that large-scale mechanocatalytic reactions would be completed within a reasonable time.

Table 4.1. Mechanocatalytic hydrolysis of chitin in the presence of H_2SO_4.[a]

Entry	Catalyst	Treatment	Solubility /%	Yield /%		
				GlcNAc	Chitobiose + chitotriose[b]	Others[c]
1	H_2SO_4	Mix[d]	97	18	42	37
2	H_2SO_4	Mix[e]	>99	4.7	19	75
3	None	None[f]	<0.1	<0.1	<0.1	<0.1
4	None	Individual[g]	<0.1	<0.1	<0.1	<0.1
5	H_2SO_4	Impregnated[h]	2.0	0.3	0.3	1.4

[a]Chitin 406 mg, H_2SO_4 24 mg, MeOH 40 mL, 443 K (rapid heating-cooling condition). [b]Total yield of chitobiose and chitotriose. [c]Water-soluble oligomers (DP ≥ 3) and unidentified products. [d]H_2SO_4-impregnated chitin was ball-milled in a 3.6 L pot. [e]H_2SO_4-impregnated chitin was planetary ball-milled. [f]Chitin was not ball-milled. [g]Chitin was ball-milled without H_2SO_4 in a 3.6 L pot. [h]H_2SO_4-impregnated chitin was left for 96 h without ball-milling.

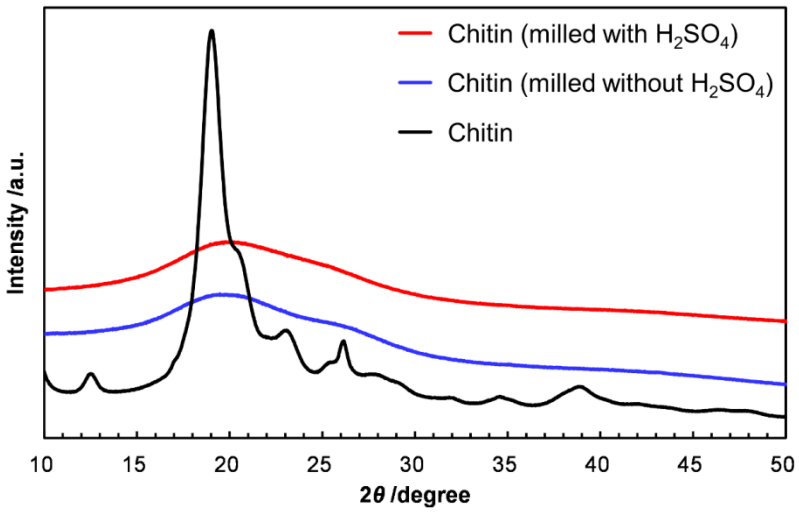


Figure 4.5. XRD patterns of chitin samples. The sharp peak at 19.8° is derived from the crystalline structure of chitin.[22] After ball-milling with/without H_2SO_4, amorphous chitin was formed.

4.3.2. Methanolysis of chitin oligomers

The second step is alcoholysis of produced oligomers to 1-*O*-alkyl GlcNAc. In this work, the author conducted the depolymerization of oligomers in MeOH, namely methanolysis, to produce 1-*O*-methyl GlcNAc (denoted as MeGlcNAc) (Figure 4.6).

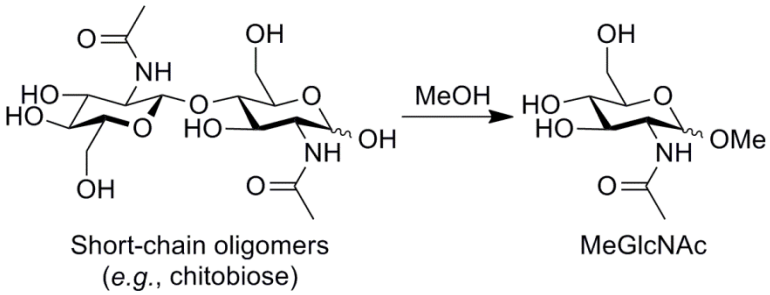


Figure 4.6. Methanolysis of short-chain oligomers to MeGlcNAc.

Table 4.2 represents the results of methanolysis of chitin oligomers and control experiments performed at 443 K in MeOH solvent. 63% yield (overall yield based on original chitin) of MeGlcNAc is obtained by Amberlyst 70 (entry 6), but Amberlyst 70 is not recovered after the reaction as described in Section 4.3.1.

Other solids are almost inactive (entries 7–9). At this moment, the author concludes that solid acids tested in this study are not applicable to chitin conversion.

In contrast, the reaction of the ball-milled sample containing chitin oligomers and H_2SO_4 provided the highest yield of MeGlcNAc (67%, entry 10), which was identified by IR spectroscopy, various NMR techniques, LC/MS, and elemental analysis (see Section 4.2.3 and Figures 4.A.2–4.A.6 in Appendices). A ratio of α- to β-anomers of MeGlcNAc was 6.3 in the product, which is discussed below. Turnover number (TON) for MeGlcNAc production based on H_2SO_4 is 4.8. The yield of humins was only 6.6 wt% based on the weight of chitin used. A trace amount of MeOAc (0.59%) was observed by GC, indicating almost no progress of deacetylation during the methanolysis. The catalyst for the methanolysis is the H_2SO_4 contained in the milled sample, corresponding to a concentration of 0.075 wt% in MeOH in this case. The chitin oligomers produced by planetary ball-milling was also useful for the production of MeGlcNAc (67% yield, entry 11). Contrastingly, individually ball-milled chitin in an amorphous form gave only a 6.4% yield of MeGlcNAc in 0.075% H_2SO_4/MeOH (entry 15). Amorphous chitin is significantly less reactive than soluble chitin oligomers. The absence of ball-milling or H_2SO_4 further reduced the yield of MeGlcNAc to 0–1.3% (entries 12–14). These results clearly show that the mechanocatalytic depolymerization of chitin prior to methanolysis is essential for the high-yielding synthesis of MeGlcNAc.

Very recently, Yan *et al.* demonstrated that the alcoholysis of chitin in ethylene glycol was possible in the presence of 8% H_2SO_4, but the major product was a deacetylated compound, 1-*O*-(2-hydroxyethyl)-2-amino-2-deoxyglucopyranoside (HADP, Figure 4.7), with 24% yield (TON = 0.22) due to harsh conditions required for the direct depolymerization of robust chitin.[23] In contrast, the combination of mechanocatalysis and alcoholysis in this study successfully preserved acetyl group, giving MeGlcNAc in 67% yield using only 0.075% H_2SO_4 with a higher TON (4.8). Thus, this new methodology makes the chitin depolymerization feasible for utilizing the produced monomers in a variety of applications.

Table 4.2. Methanolysis of chitin.[a]

Entry	Catalyst	First-step	MeGlcNAc /%
6	Amberlyst 70	Mix[c]	63
7	Nafion SAC-13	Mix[c]	0.2
8	K26	Mix[c]	1.1
9	H-MOR	Mix[c]	0.2
10	H_2SO_4	Mix[d]	67
11[b]	H_2SO_4	Mix[e]	67
12	None	None[f]	0.0
13	H_2SO_4	None[g]	1.4
14	None	Individual[h]	0.0
15	H_2SO_4	Individual[i]	6.4

[a]Chitin 406 mg, solid catalyst 50 mg or H_2SO_4 24 mg, MeOH 40 mL, 443 K (rapid heating-cooling condition). [b]The methanolysis was conducted under rapid heating-cooling condition, in which target temperature was 463 K. [c]Chitin and solid catalyst were ball-milled together in a 3.6 L pot. [d]H_2SO_4-impregnated chitin was ball-milled in a 3.6 L pot. [e]H_2SO_4-impregnated chitin was planetary ball-milled. [f]Chitin was not ball-milled. [g]Chitin was not ball-milled. During the methanolysis, H_2SO_4 was added. [h]Chitin was ball-milled without H_2SO_4 in a 3.6 L pot. [i]Chitin was ball-milled without H_2SO_4 in a 3.6 L pot. In the second step (methanolysis), H_2SO_4 was added.

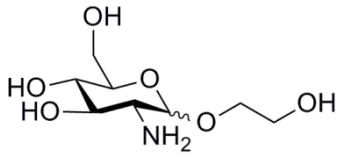


Figure 4.7. Structure of 1-*O*-(2-hydroxyethyl)-2-amino-2-deoxyglucopyranoside (HADP).

Next, stereoselectivity of the produced MeGlcNAc (α/β = 6.3) is discussed from the viewpoint of reaction mechanism. The solvolysis of glycosidic bonds generally takes place by an S_N1 mechanism *via* oxocarbenium intermediates except for enzymatic hydrolysis.[24] The intermediate could undergo both front- and back-side attacks by a nucleophile, which produces a mixture of α- and β-anomers. Nonetheless, the produced MeGlcNAc was mainly α-isomer as described above, showing an inversion of stereochemistry of chitin (= β-1,4-glycosidic bond). This result implies that the nucleophile, MeOH, probably attacks oxocarbenium species from back-side before the leaving group (counterpart of chitin oligomer) diffuses outside of solvent cage owing to the very high concentration of MeOH (19 M at 443 K, Figure 4.8).[25–27] An anomeric effect is also considered, but probably this is not the reason as such inversion occurs in similar methanolysis reactions using both maltose (α-1,4-glycosidic bond) and cellobiose (β-1,4-glycosidic bond)

(Table 4.3). The methanolysis of α-1,4-glycosidic bond mainly gave β-anomer as a major product (entry 16), and that of β-1,4-glycosidic bond did α-anomer (entry 17). The selective production of one anomer, α-MeGlcNAc, may be favorable for its further applications.

MeGlcNAc is a potential precursor to GlcNAc (Figure 4.9); the hydrolysis of MeGlcNAc to GlcNAc by H-BEA zeolite catalyst afforded a 60% yield of GlcNAc. This result gives the application of MeGlcNAc, since the utilization of GlcNAc has also been widely studied.[2]

Table 4.3. Methanolysis of disaccharides.[a]

Entry	Substrate	α-MeGlc /%	β-MeGlc /%
16[b]	Maltose	12	23
17[c]	Cellobiose	16	6.2

[a]Substrate 342 mg, 0.5 mM HCl/MeOH 40 mL. MeGlc = 1-*O*-Methylglucose. [b]493 K, <1 min (rapid heating-cooling condition). [c]473 K, <1 min (rapid heating-cooling condition).

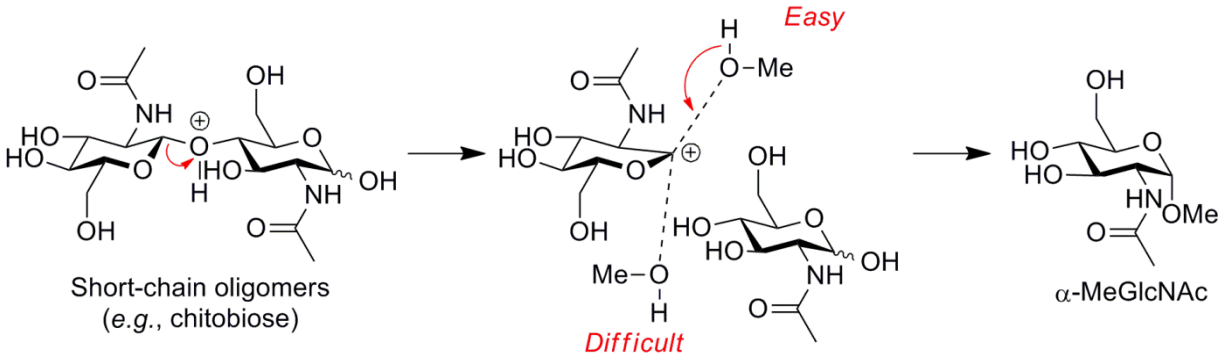


Figure 4.8. Proposed reaction mechanism of methanolysis of chitin oligomers. Front-side attack of MeOH is hampered by the leaving group.

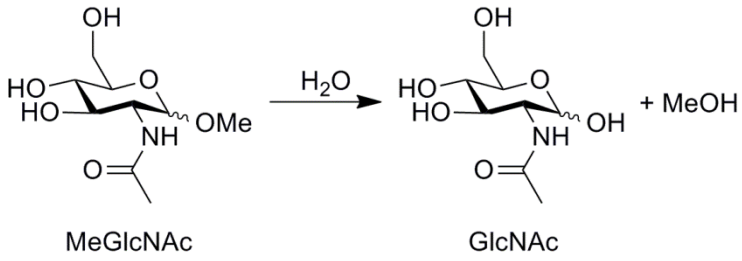


Figure 4.9. Hydrolysis of MeGlcNAc to GlcNAc.

4.4. Conclusions

A two-step depolymerization of chitin has been conducted to synthesize MeGlcNAc. In the first mechanocatalytic hydrolysis step, chitin is transformed into water-soluble oligomers with low DP. In the second step, the oligomers provide a 67% yield of MeGlcNAc by methanolysis in 0.075% H_2SO_4/MeOH, as the oligomers are remarkably more reactive than even amorphous chitin. The substrates undergo almost no deacetylation during the both reactions, and thus the good-yielding production of MeGlcNAc from chitin has been achieved. MeGlcNAc is easily converted to GlcNAc in 60% yield.

This new system has overcome the issues in previous systems such as a long reaction time and a huge amount of acidic waste. The author believes that the two-step depolymerization system has the potential for utilizing various polymers effectively.

Appendices: raw data for LC/MS, IR, and NMR

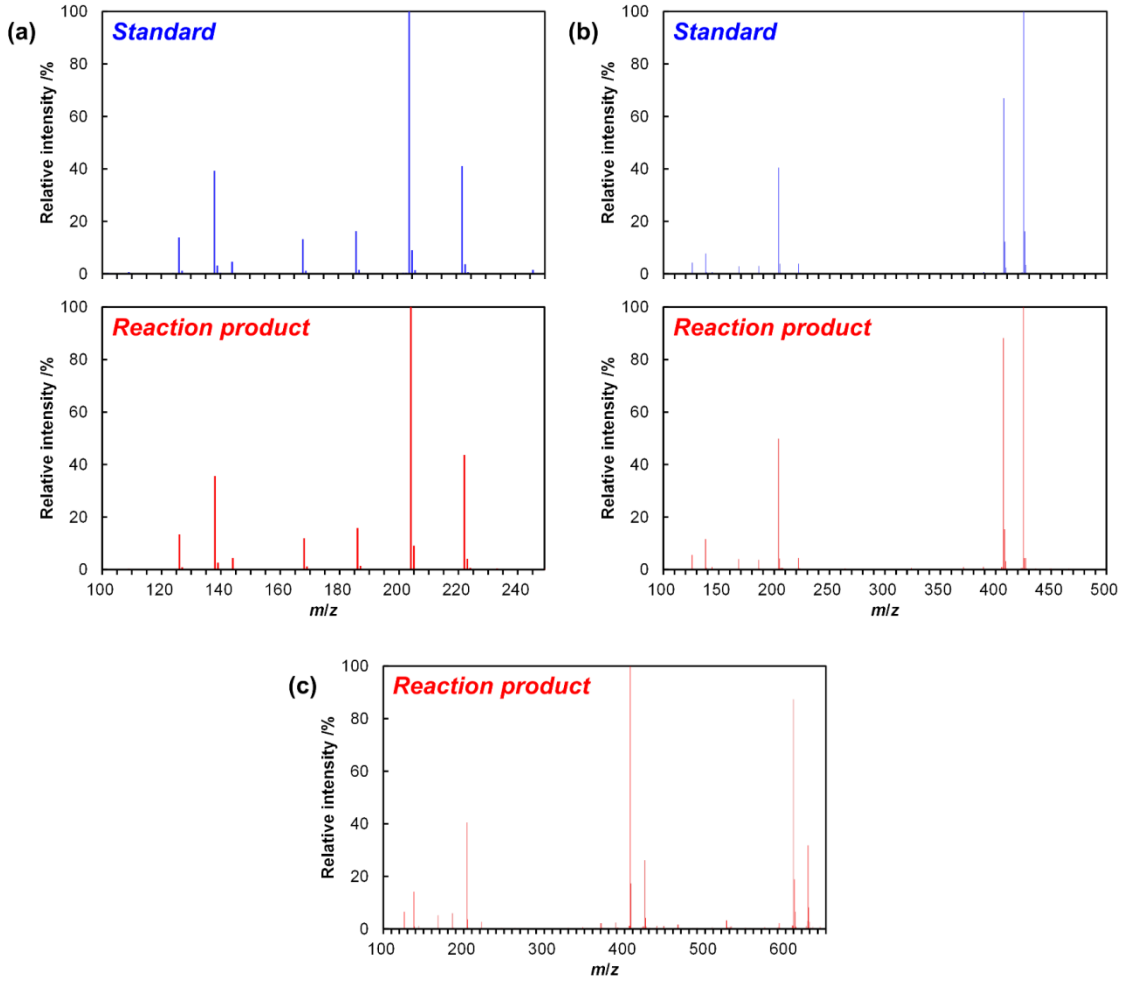


Figure 4.A.1. LC/MS spectra of reaction products of mechanocatalytic hydrolysis. (a) GlcNAc, (b) chitobiose, and (c) chitotriose. The spectra were recorded in positive ion mode.

GlcNAc (M = $C_8H_{15}NO_6$): 138 ($[M + H - CH_8O_4]^+$), 204 ($[M + H - H_2O]^+$), 222 ($[M + H]^+$).

Chitobiose (M = $C_{16}H_{28}N_2O_{11}$): 204 ($[M + H - C_8H_{15}NO_6]^+$), 407 ($[M + H - H_2O]^+$), 425 ($[M + H)^+$).

Chitotriose (M = $C_{24}H_{41}N_3O_{16}$): 204 ($[M + H - C_{16}H_{28}N_2O_{11}]^+$), 407 ($[M + H - C_8H_{15}NO_6]^+$), 610 ($[M + H - H_2O]^+$), 628 ($[M + H]^+$).

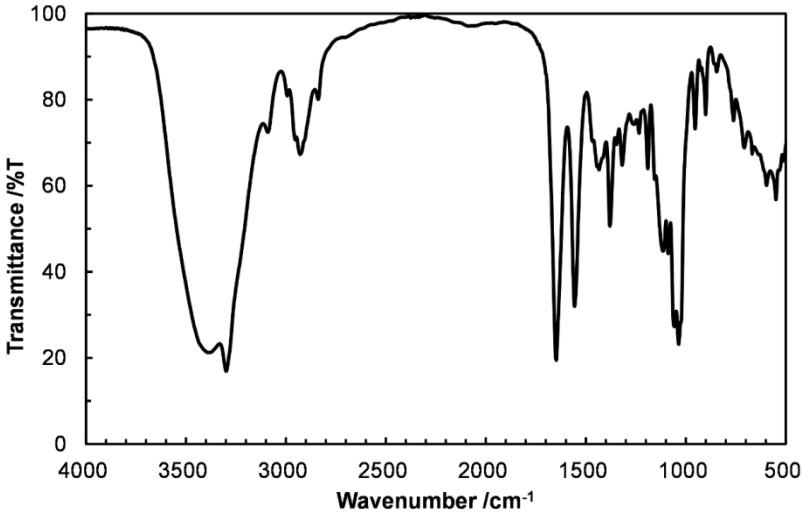


Figure 4.A.2. IR spectrum of MeGlcNAc produced from chitin. The assignments are shown in Section 4.2.3.

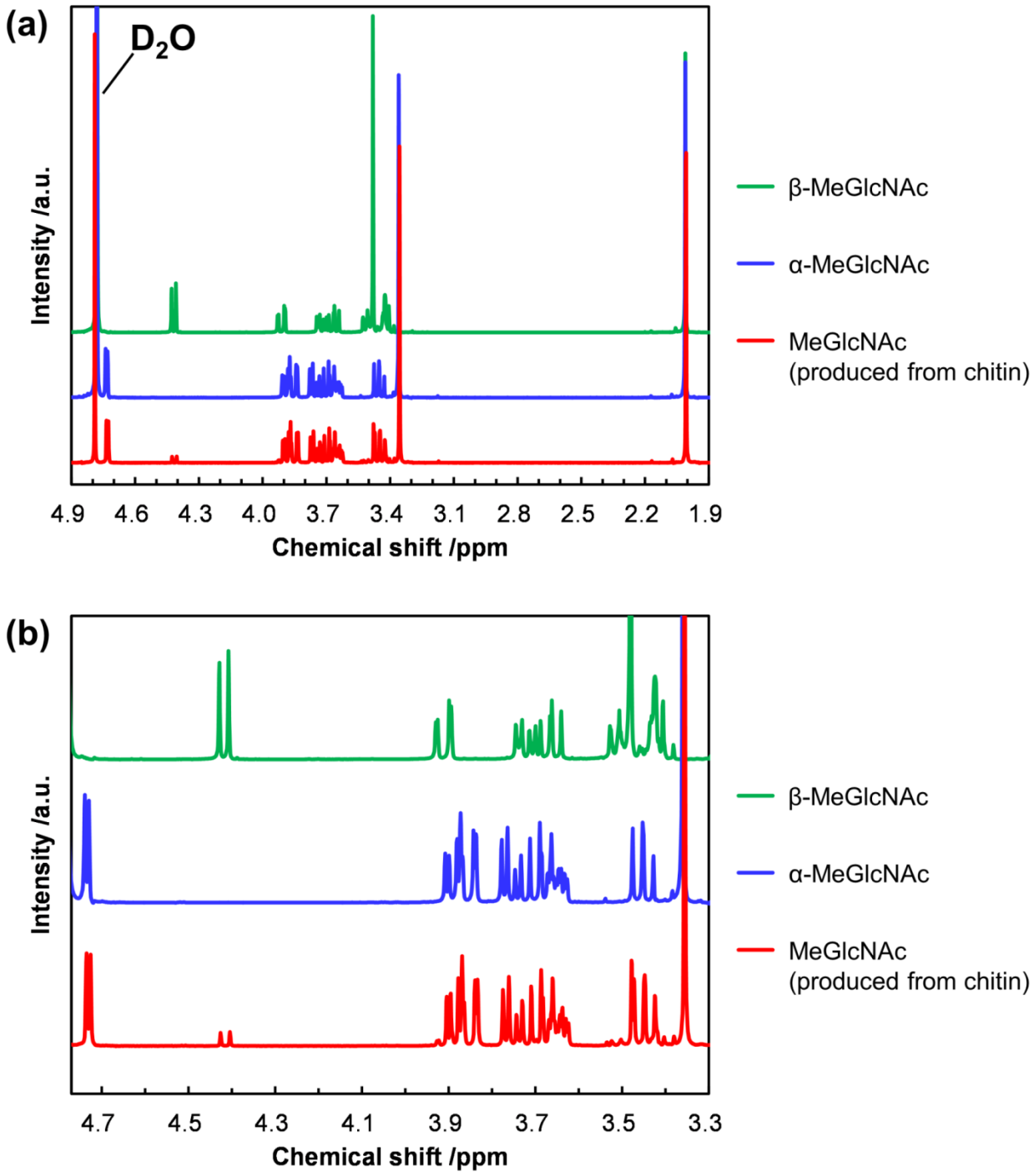


Figure 4.A.3. ^{1}H NMR spectra of MeGlcNAc produced from chitin: (a) 1.9–4.9 ppm and (b) 3.3–4.77 ppm.

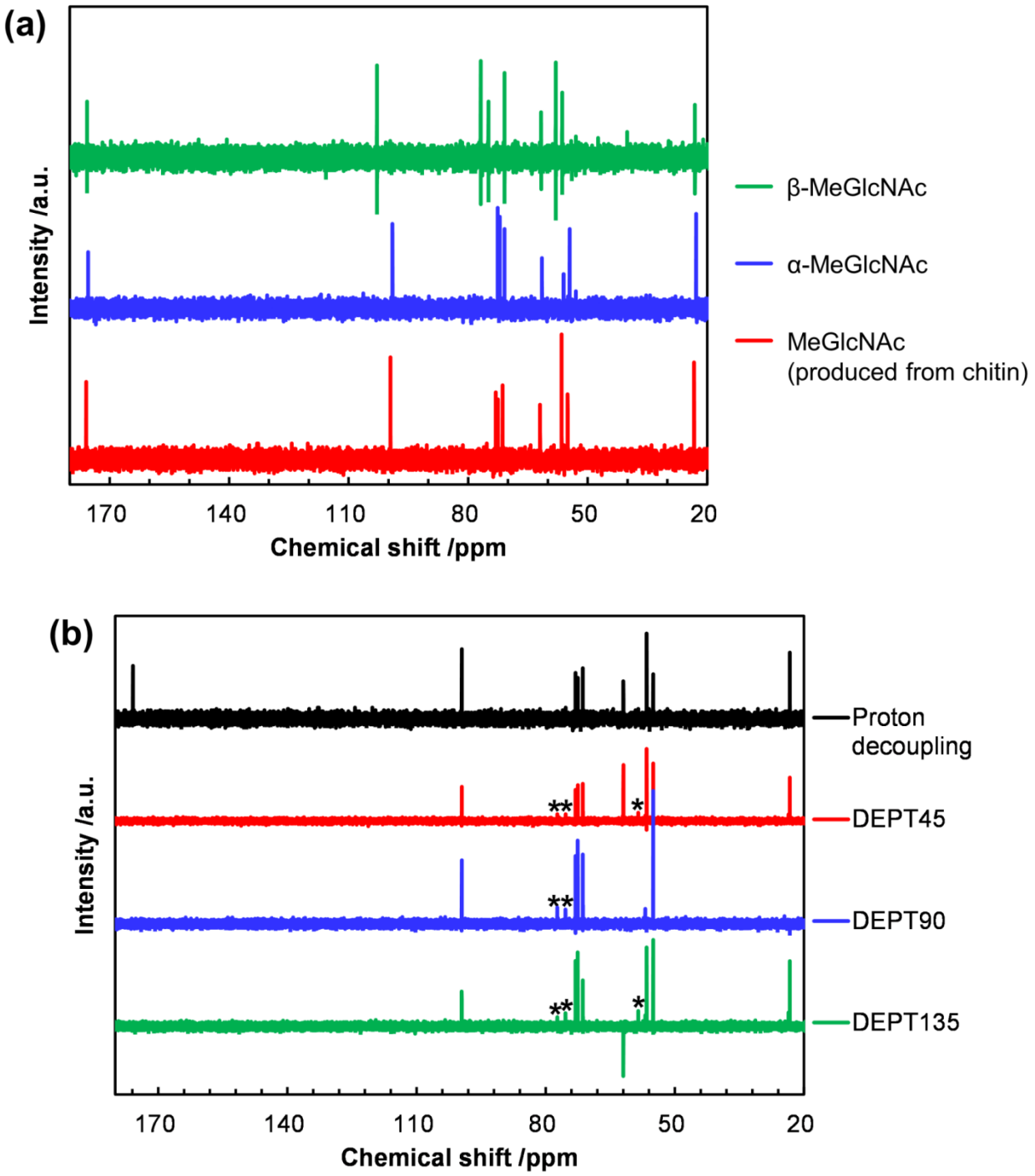


Figure 4.A.4. ^{13}C NMR spectra of MeGlcNAc produced from chitin. (a) Proton-decoupled ^{13}C NMR (comparison with authentic samples) and (b) proton-decoupled ^{13}C NMR and DEPT. The marked peaks (*) are derived from β-MeGlcNAc.

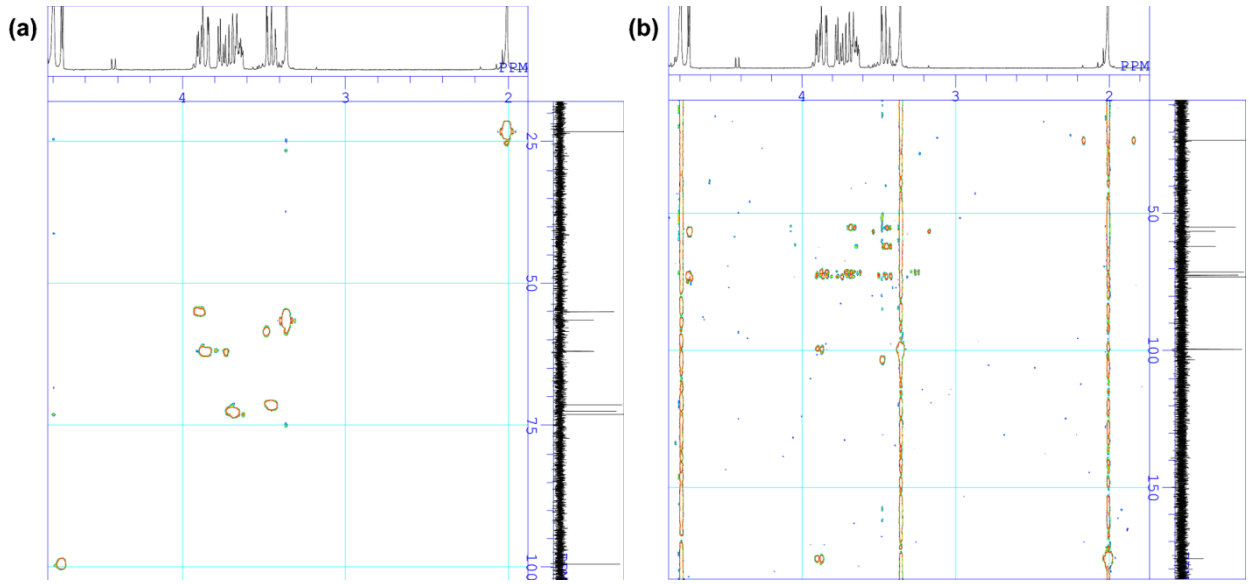


Figure 4.A.5. 2D NMR of MeGlcNAc produced from chitin. (a) ^{13}C–^{1}H HMQC (horizontal axis: ^{1}H, vertical axis: ^{13}C) and (b) ^{13}C–^{1}H HMBC (horizontal axis: ^{1}H, vertical axis: ^{13}C).

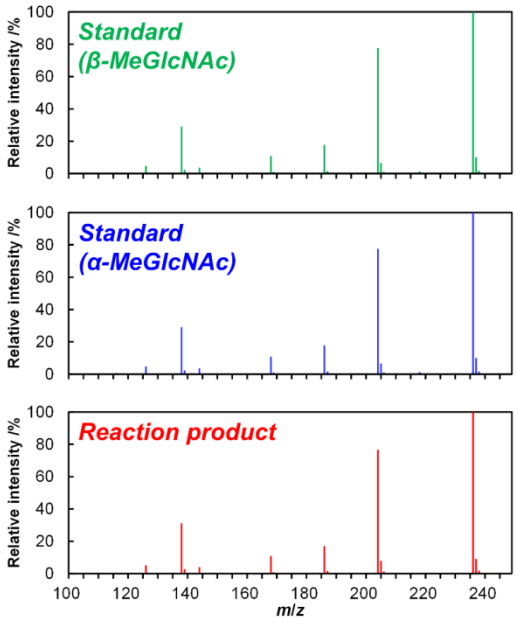


Figure 4.A.6. LC/MS spectra of MeGlcNAc. The spectra were recorded in positive ion mode.

α-MeGlcNAc (M = $C_9H_{17}NO_6$): 138 ($[M + H – C_2H_{10}O_4]^+$), 204 ($[M + H – CH_3OH]^+$), 236 ($[M + H]^+$).

β-MeGlcNAc (M = $C_9H_{17}NO_6$): 138 ($[M + H – C_2H_{10}O_4]^+$), 204 ($[M + H – CH_3OH]^+$), 236 ($[M + H]^+$).

MeGlcNAc (reaction product, $C_9H_{17}NO_6$): 138 ($[M + H – C_2H_{10}O_4]^+$), 204 ($[M + H – CH_3OH]^+$), 236 ($[M + H]^+$).

References

1. X. Chen and N. Yan, *Catal. Surv. Asia*, 2014, **18**, 164–176.
2. J.-K. Chen, C.-R. Shen, and C.-L. Liu, *Mar. Drugs*, 2010, **8**, 2493–2516.
3. K. W. Omari, L. Dodot, and F. M. Kerton, *ChemSusChem*, 2012, **5**, 1767–1772.
4. Y. Wang, C. M. Pedersen, T. Deng, Y. Qiao, and X. Hou, *Bioresour. Technol.*, 2013, **143**, 384–390.
5. M. Osada, K. Kikuta, K. Yoshida, K. Totani, M. Ogata, and T. Usui, *Green Chem.*, 2013, **15**, 2960–2966.
6. Y. Ohmi, S. Nishimura, and K. Ebitani, *ChemSusChem*, 2013, **6**, 2259–2262.
7. X. Chen, S. L. Chew, F. M. Kerton, and N. Yan, *Green Chem.*, 2014, **16**, 2204–2212.
8. T. M. Gloster, W. F. Zandberg, J. E. Heinonen, D. L. Shen, L. Deng, and D. J. Vocadlo, *Nat. Chem. Biol.*, 2011, **7**, 174–181.
9. J. Agarwal and R. K. Peddinti, *Eur. J. Org. Chem.*, 2012, **2012**, 6390–6406.
10. T. V RajanBabu, T. A. Ayers, G. A. Halliday, K. K. You, and J. C. Calabrese, *J. Org. Chem.*, 1997, **62**, 6012–6028.
11. N. Goyal, S. Cheuk, and G. Wang, *Tetrahedron*, 2010, **66**, 5962–5971.
12. A. R. Shikhman, K. Kuhn, N. Alaaeddine, and M. Lotz, *J. Immunol.*, 2001, **166**, 5155–5160.
13. L. I. Álvarez-Añorve, M. L. Calcagno, and J. Plumbridge, *J. Bacteriol.*, 2005, **187**, 2974–2982.
14. H. Sashiwa, S. Fujishima, N. Yamano, N. Kawasaki, A. Nakayama, E. Muraki, K. Hiraga, K. Oda, and S. Aiba, *Carbohydr. Res.*, 2002, **337**, 761–763.
15. K. M. Vårum, M. H. Ottøy, and O. Smidsrød, *Carbohydr. Polym.*, 2001, **46**, 89–98.
16. A. Einbu and K. M. Vårum, *Biomacromolecules*, 2007, **8**, 309–314.
17. D. A. Davis, A. Hamilton, J. Yang, L. D. Cremar, D. Van Gough, S. L. Potisek, M. T. Ong, P. V Braun, T. J. Martinez, S. R. White, J. S. Moore, and N. R. Sottos, *Nature*, 2009, **459**, 68–72.
18. N. Meine, R. Rinaldi, and F. Schüth, *ChemSusChem*, 2012, **5**, 1449–1454.
19. A. Shrotri, L. K. Lambert, A. Tanksale, and J. Beltramini, *Green Chem.*, 2013, **15**, 2761–2768.
20. A. Shrotri, H. Kobayashi, A. Tanksale, A. Fukuoka, and J. Beltramini, *ChemCatChem*, 2014, **6**, 1349–1356.

21. F. Shahidi, J. K. V. Arachchi, and Y.-J. Jeon, *Trends Food Sci. Technol.*, 1999, **10**, 37–51.

22. M. Osada, C. Miura, Y. S. Nakagawa, M. Kaihara, M. Nikaido, and K. Totani, *Carbohydr. Polym.*, 2013, **92**, 1573–1578.

23. Y. Pierson, X. Chen, F. D. Bobbink, J. Zhang, and N. Yan, *ACS Sustainable Chem. Eng.*, 2014, **2**, 2081–2089.

24. J. M. Stubbs and D. Marx, *J. Am. Chem. Soc.*, 2003, **125**, 10960–10962.

25. S. Winstein, E. Clippinger, A. H. Fainberg, R. Heck, and G. C. Robinson, *J. Am. Chem. Soc.*, 1956, **78**, 328–335.

26. R. D. Goodwin, *J. Phys. Chem. Ref. Data*, 1987, **16**, 799–892.

27. J. Chan, A. Tang, and A. J. Bennet, *J. Am. Chem. Soc.*, 2012, **134**, 1212–1220.

Chapter 5

Dehydration of Sorbitol to 1,4-Sorbitan by Acid Catalysts

1,4-Sorbitan is produced from biomass *via* sorbitol and is a precursor to environmentally benign surfactants. Acid catalysts can convert sorbitol to 1,4-sorbitan; however, further dehydration of 1,4-sorbitan to isosorbide readily occurs, making the selective synthesis of 1,4-sorbitan difficult. In this work, the author has at first studied the dehydration of sorbitol to 1,4-sorbitan using solid acids. Although sulfated zirconia affords 1,4-sorbitan in good yield and selectivity, but it is found that leached acids from the solid promote the reaction. The author has therefore investigated the catalysis of H_2SO_4 instead of solid acids to be the basis of designing selective dehydration catalysts. The results have shown that both thermodynamics and kinetics play significant roles to determine the yield of 1,4-sorbitan. H_2SO_4 preferentially forms an adduct with sorbitol over 1,4-sorbitan, and thus the subsequent dehydration of 1,4-sorbitan is inhibited in the presence of sorbitol.

5.1. Introduction

In Chapter 2, the high-yielding one-pot synthesis of glucose from cellulose was achieved by using carbon catalysts and mix-milling pre-treatment. Thus, in this chapter, the author deals with the conversion of glucose to useful chemicals. Glucose is hydrogenated over Raney Ni or supported Ru catalysts under H_2 pressure to form sorbitol,[1–4] which has been already established in chemical industries. Additionally the direct synthesis of sorbitol from cellulose has been achieved in laboratories since 2006.[5–7] Many kinds of chemicals can be synthesized from sorbitol such as medicines, plastics, surfactants, and fuels (Figure 1.13),[7–9] and the dehydrated compounds of sorbitol, 1,4-anhydrosorbitol (1,4-sorbitan) and 1,4:3,6-dianhydrosorbitol (isosorbide) (Figure 5.1), are platform chemicals for the synthesis of valuable compounds. In particular, 1,4-sorbitan is a raw material for various environmentally benign surfactants[10] [*e.g.*, fatty acid esters (Span) and polysorbates (Tween)] that have been used in the production of insecticides, cosmetics, and soft templates for material synthesis.[9] Sorbitan esters are also used as emulsifying agents in food and pharmaceutical industries owing to their low-toxicity.[11] The annual demand of sorbitan-derived surfactants is more than 10,000 tons worldwide. Thus, the efficient synthesis of 1,4-sorbitan from sorbitol is a challenge.

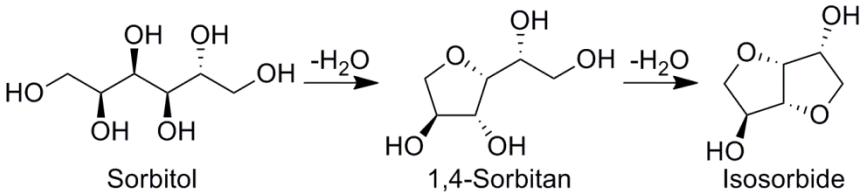


Figure 5.1. Dehydration of sorbitol.

1,4-Sorbitan is produced by the dehydration of sorbitol using acid catalysts or hot-compressed water in a laboratory scale, in which 1,4-sorbitan readily undergoes further dehydration to form isosorbide.[12–25] This hampers the selective and high-yielding synthesis of 1,4-sorbitan from sorbitol. Currently, H_2SO_4 is used as a catalyst for sorbitol dehydration in industry, since this low-price acid gives 1,4-sorbitan in a relatively high yield (58%).[12,13,16] Although it is preferable to use heterogeneous catalysts owing to the good separability, reusability, and no corrosivity, further improvement is necessary for replacing H_2SO_4. Herein, the first

purpose of this chapter is selective production of 1,4-sorbitan from sorbitol by using solid acids. Additionally, the second objective is revealing origin of high selectivity of catalysts through mechanistic study since it is useful and helpful to design more active catalysts.

5.2. Experimental

5.2.1. Reagents

D(+)-Sorbitol	>97.0%, Tokyo Chemical Industry
Sulfuric acid	96–98%, super special grade, Wako Pure Chemical Industries
JRC-ZRO-2	Zirconium(IV) hydroxide, $ZrO_{1.1}(OH)_{1.8}$, Catalysis Society of Japan
Ammonium sulfate	Special grade, Wako Pure Chemical Industries
Amberlyst 70	Sulfonic acid cation exchange resin, Organo
Nafion SAC-13	Silica-supported fluorinated sulfonic acid polymer, Sigma-Aldrich
CBV 780	Proton-type FAU zeolite, Si/Al = 40, Zeolyst, denoted as H-FAU
JRC-Z5-90H	Proton-type MFI zeolite, Si/Al = 45, Catalysis Society of Japan, denoted as H-MFI
JRC-Z-HM90	Proton-type MOR zeolite, Si/Al = 45, Catalysis Society of Japan, denoted as H-MOR
Silica-alumina	Grade 135, Sigma-Aldrich, denoted as SiO_2-Al_2O_3
1,4-Anhydrosorbitol	97%, Toronto Research Chemicals, denoted as 1,4-sorbitan
D-1,4:3,6-Dianhydrosorbitol	>98.0%, Tokyo Chemical Industry, denoted as isosorbide
1,5-Anhydrosorbitol	Toronto Research Chemicals, denoted as 1,5-sorbitan
1,5-Anhydromannitol	Toronto Research Chemicals, denoted as 1,5-mannitan
2,5-Anhydromannitol	Sigma-Aldrich, denoted as 2,5-mannitan
Distilled water	Wako Pure Chemical Industries
Diethyl ether	First grade, Wako Pure Chemical Industries
Dimethyl sulfoxide	Special grade, Wako Pure Chemical Industries, denoted as DMSO
Distilled water	For HPLC, Wako Pure Chemical Industries

Sodium hydrogen carbonate	Special grade, Wako Pure Chemical Industries
Sodium carbonate	Special grade, Wako Pure Chemical Industries
Deuterium oxide	For NMR, Acros Organics
Deuterated dimethyl sulfoxide	For NMR, Acros Organics, denoted as DMSO-d_6
Deuterated methanol	For NMR, Acros Organics

5.2.2. Preparation of sulfated zirconia

Sulfated zirconia denoted as SZ was prepared as follows.[26] 0.5 g of $ZrO_{1.1}(OH)_{1.8}$ was dispersed in 10 mL of H_2O in an eggplant flask (100 mL). Then, 0.52 M $(NH_4)_2SO_4$ aq. (10 mL, corresponding to 18 wt% S in the catalyst) was added dropwise to the mixture over *ca.* 2 min with stirring by hand in an ultrasonic generator. After drying the mixture under vacuum for ≥18 h and crashing on an Al_2O_3 mortar, the resulting white solid was heated to 773 K in 6 h and calcined at the temperature for 4 h under air in an electric furnace (Denken-Highdental, KDF-S90). Finally, SZ (0.60 g) was obtained. Similarly, ZrO_2 was prepared by the calcination of $ZrO_{1.1}(OH)_{1.8}$ under the above conditions.

The content of sulfur in SZ was determined to be 20 wt% by energy dispersive X-ray spectroscopy (EDX, Shimadzu, EDX-720) and thermal analysis,[27] which was consistent with the initial amount of sulfur in the catalyst preparation (18 wt%).

5.2.3. Dehydration of sorbitol

The dehydration reaction was conducted without solvent in an eggplant flask (50 mL). Sorbitol 182 mg (1 mmol) and solid acid 50 mg were charged into the flask, and thus S/C was 3.6. The flask was immersed in an oil bath at 403 K; however, the actual temperature of reaction mixture was *ca.* 400 K. After the reaction, 20 mL of H_2O was added to the mixture at room temperature to extract products, and the water-soluble compounds were analyzed by HPLC [Shimadzu LC10-AT*VP*, RI and UV (210 nm) detectors] with a SUGAR SH1011 column (Shodex, ø8 mm × 300 mm, mobile phase: H_2O 0.5 mL min^{-1}, 323 K) and a Rezex RPM-Monosaccharide Pb++ column (Phenomenex, ø7.8 mm × 300 mm, mobile phase: H_2O 0.6 mL min^{-1},

343 K). Yields of products and amount of unreacted sorbitol were determined by an absolute calibration method.

The reuse experiment for SZ was conducted as follows. The dehydration reaction was performed in the same manner as described above. After the reaction, 20 mL of DMSO was added to extract the products, and then the suspension was filtered with a PTFE membrane (0.1 μm mesh). The residue was repeatedly washed with diethyl ether and then dried in an oven at 383 K. The resulting powder was used for the next reaction, in which S/C was kept at 3.6. Note that H_2O is not a useful extractant for this experiment since *liquid water* causes leaching of acid species on SZ, unlike the *water vapor* formed during the reaction of sorbitol.

The amount of SO_4^{2-} leached from the catalysts was determined as follows. Soluble components were extracted with DMSO after the reaction and the DMSO solution was analyzed by ion chromatography (Dionex, ICS-3000, conductivity detector) with an IonPac AS12A column [Dionex, ø4 mm × 200 mm, mobile phase: $NaHCO_3$ (2.7 mM) / Na_2CO_3 (0.3 mM) buffer 1.5 mL min^{-1}, 308 K].

For dehydration of sorbitol by H_2SO_4, at first H_2SO_4 was impregnated on sorbitol. H_2SO_4 (13 mg) was dissolved in 10 mL of diethyl ether, and then sorbitol (3.64 g) was dispersed in the solution. By removing diethyl ether under vacuum (<1 Pa) at room temperature, H_2SO_4-impregnated sorbitol was obtained. In the dehydration reaction shown above, the H_2SO_4-impregnated sorbitol (containing sorbitol 1 mmol and H_2SO_4 6.5 μmol) was charged into the flask.

5.2.4. Product identification

The products were identified by means of NMR [JEOL, JNM-ECX400 (^{1}H 400 MHz, ^{13}C 100 MHz) and JNM-ECX600 (^{1}H 600 MHz, ^{13}C 150 MHz)] with various measurement methods: ^{1}H NMR, proton-decoupled ^{13}C NMR, DEPT, ^{1}H–^{1}H COSY, ^{13}C–^{1}H HMQC, and ^{13}C–^{1}H HMBC (Figures 5.A.1–5.A.8 in Appendices). LC/MS (Thermo Fisher Scientific, LCQ Fleet, APCI, Figures 5.A.9–5.A.11) was used under the same conditions as those of HPLC shown above. Structures of the identified products [*i.e.*, 1,4-sorbitan, isosorbide, 2,5-anhydromannitol (2,5-mannitan), and 2,5-anhydroiditol (2,5-iditan)] are represented in Figure 5.2. Mono-anhydrohexitols, denoted as *AH1* and *AH2*, were also observed by HPLC (Figure 5.A.12). Although 2,5-iditan and *AH1* were not separated by HPLC, they were distinguished by NMR methods.

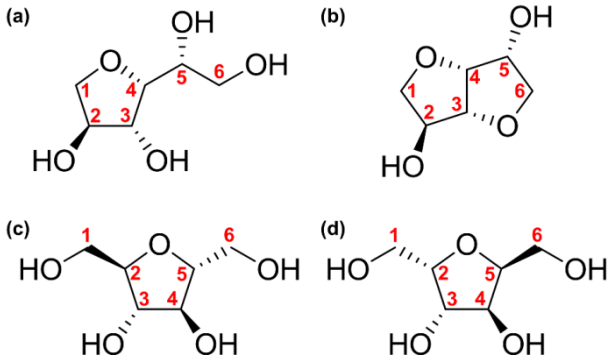


Figure 5.2. Structures of identified products: (a) 1,4-sorbitan, (b) isosorbide, (c) 2,5-mannitan, and (d) 2,5-iditan.

1,4-Sorbitan: ^{1}H NMR (400 MHz, D_2O): δ 4.27 (1H, d, J = 4.0 Hz, *H*–C2), 4.21 (1H, d, J = 2.8 Hz, *H*–C3), 4.13 (1H, dd, J = 10, 4.0 Hz, *H*–C1), 3.90 (1H, dd, J = 8.8, 2.8 Hz, *H*–C4), 3.85 (1H, ddd, J = 8.8, 6.0, 2.8 Hz, *H*–C5), 3.78 (1H, dd, J = 12, 2.8 Hz, *H*–C6), 3.70 (1H, d, J = 10 Hz, *H*–C1), 3.61 (1H, dd, J = 12, 6.0 Hz, *H*–C6). ^{13}C NMR (100 MHz, D_2O): δ 80.6 (CH, C4), 77.1 (CH, C2), 76.6 (CH, C3), 74.1 (CH_2, C1), 69.8 (CH, C5), 64.5 (CH_2, C6). The assignment of the ^{13}C NMR peaks is based on a reference.[28] C1 and C6 were distinguished by means of ^{1}H NMR in a DMSO-d_6 solvent. In DMSO-d_6, the peaks for the proton at C6 are observed as *ddd* due to coupling with one proton of the hydroxyl group in addition to two aliphatic protons, whereas the peaks of proton at C1 are in a *dd* form. This compound clearly has a five-membered ring since the peak of C4 is correlated with the peaks of protons coordinating to C1, C2, C3, C5, and C6 in the HMBC spectrum (Figure 5.A.2c). LC/MS $[M + H]^+$ calculated 165, found 165 (reaction product), found 165 (commercial standard); $[M - H]^-$ calculated 163, found 163 (reaction product), found 163 (commercial standard).

Isosorbide: ^{1}H NMR (400 MHz, D_2O): δ 4.64 (1H, dd, J = 5.2, 4.4 Hz, *H*–C4), 4.49 (1H, d, J = 4.4 Hz, *H*–C3), 4.39 (1H, ddd, J = 7.0, 7.0, 5.2 Hz, *H*–C5), 4.32 (1H, d, J = 3.2 Hz, *H*–C2), 3.89–3.96 (2H, *H*–C1 and *H*–C6), 3.87 (1H, dd, J = 10.4, 3.2 Hz, *H*–C1), 3.49 (1H, dd, J = 9.0, 7.2 Hz, *H*–C6). ^{13}C NMR (150 MHz, D_2O): δ 88.5 (CH, C3), 82.6 (CH, C4), 76.6 (CH, C2), 76.3 (CH_2, C1), 73.0 (CH, C5), 72.3 (CH_2, C6). The assignment of the ^{13}C NMR peaks is based on a reference.[28] Some of the ^{1}H NMR peaks at 3.89–3.96 and 3.87 ppm were overlapped with the peaks of *AH1* (Figure 5.A.7a). The ^{13}C NMR and DEPT peaks of

isosorbide in Figure 5.A.7b could not be distinguished from noise due to its low concentration.

2,5-Mannitan: ^{1}H NMR (400 MHz, D_2O): δ 4.03 (2H, dd, J = 5.2, 2.0 Hz, *H*–C3 and *H*–C4), 3.83–3.90 (2H, m, *H*–C2 and *H*–C5), 3.75 (2H, dd, J = 12, 3.2 Hz, *H*–C1 and *H*–C6), 3.66 (2H, dd, J = 12, 5.6 Hz, *H*–C1 and *H*–C6). ^{13}C NMR (100 MHz, D_2O): δ 83.0 (CH, C2 and C5), 77.1 (CH, C3 and C4), 61.9 (CH_2, C1 and C6). The assignment of the ^{13}C NMR peaks is based on a reference.[28] LC/MS $[M + H]^+$ calculated 165, found 165 (reaction product), found 165 (commercial standard); $[M – H]^-$ calculated 163, found 163 (reaction product), found 163 (commercial standard).

2,5-Iditan: ^{1}H NMR (600 MHz, D_2O): δ 4.21–4.25 (4H, *H*–C2, *H*–C3, *H*–C4 and *H*–C5), 3.80 (2H, dd, J = 11.4, 4.8 Hz, *H*–C1 and *H*–C6), 3.73 (2H, dd, J = 11.4, 7.2 Hz, *H*–C1 and *H*–C6). ^{13}C NMR (150 MHz, D_2O): δ 81.3 (CH, C3 and C4), 77.5 (CH, C2 and C5), 61.0 (CH_2, C1 and C6). The ^{1}H NMR peaks at 4.21–4.25, 3.80, and 3.73 ppm were overlapped with those of *AH1* (Figure 5.A.7a). The assignment of the ^{13}C NMR peaks is based on a reference.[28] LC/MS for reaction product $[M + H]^+$ calculated 165, found 165; $[M – H]^-$ calculated 163, found 163.

Mono-anhydrohexitol (AH1): ^{1}H NMR (600 MHz, D_2O): δ 4.29 (1H, d, J = 4.2 Hz), 4.15 (1H, dd, J = 10.5, 4.2 Hz), 3.92 (1H, dd, J = 9.0, 2.4 Hz), 3.88 (1H, ddd, J = 9.0, 6.0, 3.0 Hz), 3.64 (1H, dd, J = 12, 6.0 Hz). ^{13}C NMR (150 MHz, D_2O): δ 80.7 (CH), 77.2 (CH), 76.7 (CH), 74.3 (CH_2), 69.9 (CH), 64.6 (CH_2). Several ^{1}H NMR peaks were overlapped with those of 2,5-iditan and isosorbide (Figure 5.A.7a). The chemical shifts of the ^{1}H NMR peaks indicate that this unidentified compound is not 1,4-anhydrogalactitol (1,4-galactan).[29] LC/MS for reaction product $[M + H]^+$ found 165; $[M – H]^-$ found 163.

Mono-anhydrohexitol (AH2): LC/MS for reaction product $[M + H]^+$ found 165; $[M – H]^-$ found 163.

5.3. Results and discussion

5.3.1. Dehydration of sorbitol by acids

The author conducted the dehydration of sorbitol using a variety of acids at 403 K for 120 min without using solvents (Table 5.1). Sorbitol [melting point (m.p.) 368 K] and products, 1,4-sorbitan (m.p. 385 K) and isosorbide (m.p. 336 K), are liquids at 403 K, which enabled the author to perform the reaction under neat conditions. A control experiment in the absence of catalyst provided no conversion of sorbitol even for a long

reaction time of 180 min (entry 1), indicating that acid catalysts are necessary for the dehydration. SZ afforded 96% conversion of sorbitol, and the main product was 1,4-sorbitan with 60% yield and 62% selectivity based on the conversion of sorbitol (entry 2). The successive dehydration to isosorbide also took place (11% yield). Other products were 2,5-mannitan (3.9%, Figure 5.2), 2,5-iditan, an uncharacterized mono-anhydrohexitol (*AH1*), and another mono-anhydrohexitol (*AH2*, 1.1%). 2,5-Iditan and *AH1* overlapped in HPLC (Section 5.2.4 and Figure 5.A.12), and their total yield was 8.9%. Since the retention times of *AH1* and *AH2* in HPLC were different from those of 1,5-sorbitan and 1,5-mannitan, indicating *AH1* and *AH2* were not 1,5-sorbitan and 1,5-mannitan. Additionally, ^{1}H NMR spectrum of *AH1* suggested that this compound was not 3,6-anhydrosorbitol (3,6-sorbitan) or 1,4-galactan.[29] Several small peaks were also observed by HPLC, but their yields were lower than 1%. Since many products having similar structures could be formed in the dehydration of sorbitol, these products were identified by combining ^{1}H and ^{13}C NMR (Figures 5.A.1–5.A.8 in Appendices), LC/MS (Figures 5.A.9–5.A.11), and HPLC (Figure 5.A.12). The author also assigned their NMR signals using several techniques as summarized in Section 5.2.4.

In Table 5.1, Amberlyst 70 and Nafion SAC-13 showed high conversion of sorbitol, but the main product was isosorbide due to the subsequent dehydration of 1,4-sorbitan (entries 5 and 6). Over Nafion SAC-13, the yield of 1,4-sorbitan was at most 38% even under the optimized conditions (Figure 5.3), and it was clearly lower than that produced by SZ. The colors of these catalysts turned dark brown due to coking during the reaction. Zeolite catalysts (H-FAU, H-MFI, and H-MOR) also gave low yields of 1,4-sorbitan (≤31%, entries 7–9), and the colors of the catalysts also changed from white to brown or black during the reaction due to coke formation. Similarly, SiO_2-Al_2O_3 was inactive in this reaction (entry 10). Among the catalysts the author tested, SZ afforded the highest yield and selectivity for the production of 1,4-sorbitan from sorbitol.

Table 5.1. Dehydration of sorbitol by a variety of acids.[a]

Entry	Catalyst	Reaction time /min	Conv. /%	Yield /%				
				1,4-Sorbitan	2,5-Iditan + *AH1*[b]	Isosorbide	2,5-Mannitan	*AH2*
1	None	180	<1	0.0	0.0	0.0	0.0	0.0
2	SZ	120	96	60	8.9	11	3.9	1.1
3	SZ	120	64	40	7.4	3.8	2.9	2.8
4	ZrO_2	120	2.3	0.0	0.0	0.0	0.0	0.0
5	Amberlyst 70	120	99	1.7	0.8	63	1.6	0.2
6	Nafion SAC-13	120	>99	9.0	9.1	66	4.2	0.2
7	H-FAU	120	76	31	11	14	7.2	2.0
8	H-MFI	120	55	8.9	2.2	30	1.1	4.2
9	H-MOR	120	24	12	3.0	2.8	1.0	1.2
10	SiO_2-Al_2O_3	120	2.4	0.6	0.0	0.0	0.0	0.0
11	H_2SO_4	120	77	56	7.5	6.1	2.8	2.9

[a]Conditions: sorbitol 182 mg (1 mmol), solid acid 50 mg or H_2SO_4 1.0 μmol, 403 K. [b]Total yield of 2,5-iditan and *AH1*.

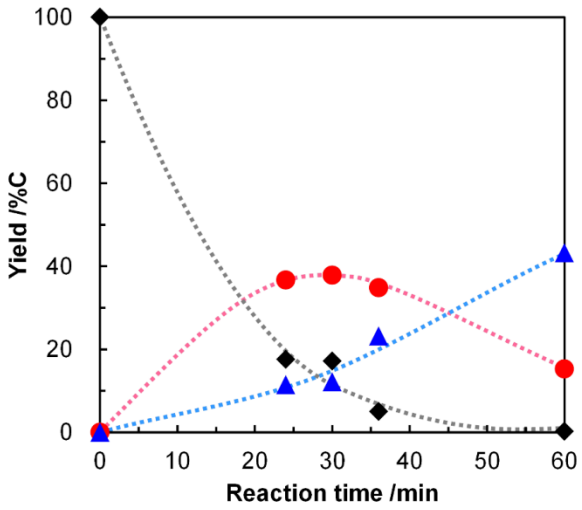


Figure 5.3. Time course for sorbitol dehydration by Nafion SAC-13 at 403 K. Legend: black diamonds (♦) = amount of unreacted sorbitol; red circles (●) = yield of 1,4-sorbitan; and blue triangles (▲) = yield of isosorbide. Reaction conditions: sorbitol 182 mg (1 mmol), Nafion SAC-13 50 mg. Each data point is the result of each batch reaction with different reaction times. Dashed lines are simply smooth lines for connecting experimental data.

Since pristine ZrO_2 does not convert sorbitol (entry 4), acid sites introduced by sulfation to ZrO_2 is responsible for the high catalytic activity of SZ. A reuse experiment of SZ was performed to evaluate the durability, resulting in a decreased yield of 1,4-sorbitan to 40% in the second run (entry 3). The leaching amount of SO_4^{2-} was determined 0.4% of SO_4^{2-} loaded on ZrO_2. As a control experiment, the equivalent amount of H_2SO_4 (1.0 μmol) was used for the dehydration of sorbitol (entry 11). Even such a small amount of H_2SO_4 has afforded 56% yield of 1,4-sorbitan with 73% selectivity, which are similar to the results by SZ. Hence, the author concludes that leached species from SZ contribute to high selective synthesis. This high selectivity by H_2SO_4 is possibly to be the basis of designing solid catalysts for selective synthesis of 1,4-sorbitan. As mentioned in Section 5.1, H_2SO_4 is currently used in an industrial process to produce 1,4-sorbitan,[12,13,16] but the origin of high selectivity of H_2SO_4 has not been clear. Hence, in the next section, the author elucidates characteristic activity of H_2SO_4.

5.3.2. Kinetic study of sorbitol dehydration by H_2SO_4

Kinetic study has been performed to uncover the origin of activity and selectivity of H_2SO_4. In this study, the author used 6.5 μmol of H_2SO_4 to increase reaction rates. Figure 5.4 shows the time course of sorbitol dehydration by 6.5 μmol of H_2SO_4 at 403 K. The amount of sorbitol decreased linearly to 7.4% in 45 min, and then the reaction rate was reduced. This behavior is typical for a pre-equilibrium reaction; the apparent reaction order changes from zeroth to first by lowering concentrations of substrate. In Figure 5.4, the yield of 1,4-sorbitan was maximized (58%) at 45 min, and only a small amount of isosorbide formed in 30 min regardless of the accumulation of 1,4-sorbitan. The yield of isosorbide then increased at an accelerated pace to reach 72% in 180 min. Since the conversion rate of 1,4-sorbitan to isosorbide increased after a large portion of sorbitol was consumed, the author can postulate that H_2SO_4 preferentially forms an adduct with sorbitol over 1,4-sorbitan. This hypothesis is quantitatively discussed as below.

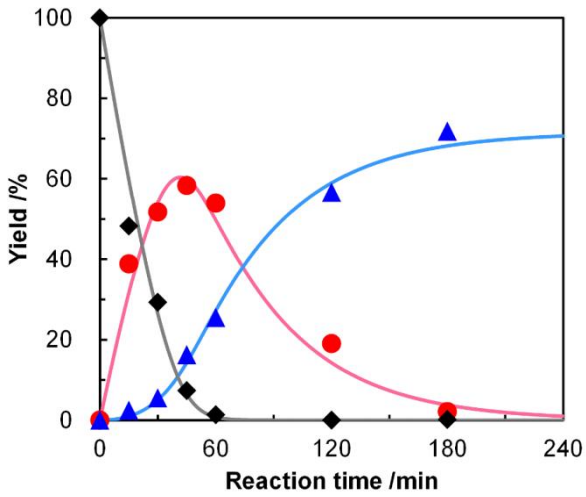


Figure 5.4. Time course of sorbitol dehydration by H_2SO_4 at 403 K. Reaction conditions: sorbitol 1 mmol, H_2SO_4 6.5 μmol. Data points show experimental results and lines are simulation curves based on eqs. 5.4–5.9. Legend: black diamonds (♦) = amount of unreacted sorbitol; red circles (●) = yield of 1,4-sorbitan; and blue triangles (▲) = yield of isosorbide.

The author simulated the time course of sorbitol dehydration by assuming the Michaelis-Menten type mechanism involving a pre-equilibrium of association and a subsequent dehydration step (see the scheme depicted in Table 5.2). k_1 and k_2 are rate constants for dehydration of sorbitol and 1,4-sorbitan, respectively, while k_3, k_4, and k_5 are those for side reactions of sorbitol, 1,4-sorbitan, and isosorbide. The rates of side reactions were estimated from the carbon balance of sorbitol, 1,4-sorbitan, and isosorbide. The equilibria of association with H_2SO_4 are assumed for sorbitol (K_1), 1,4-sorbitan (K_2), and isosorbide (K_3). The detailed kinetic equations are represented as eqs. 5.1–5.9.

$$K_1 = \frac{[\text{Sorbitol}-\text{H}_2\text{SO}_4]}{[\text{Sorbitol}]([\text{H}_2\text{SO}_4]_0 - [\text{Sorbitol}-\text{H}_2\text{SO}_4] - [\text{Sorbitan}-\text{H}_2\text{SO}_4] - [\text{Isosorbide}-\text{H}_2\text{SO}_4])} \quad (5.1)$$

$$K_2 = \frac{[\text{Sorbitan}+\text{H}_2\text{SO}_4]}{[\text{Sorbitan}]([\text{H}_2\text{SO}_4]_0 - [\text{Sorbitol}-\text{H}_2\text{SO}_4] - [\text{Sorbitan}-\text{H}_2\text{SO}_4] - [\text{Isosorbide}-\text{H}_2\text{SO}_4])} \quad (5.2)$$

$$K_3 = \frac{[\text{Isosorbide}+\text{H}_2\text{SO}_4]}{[\text{Isosorbide}]([\text{H}_2\text{SO}_4]_0 - [\text{Sorbitol}-\text{H}_2\text{SO}_4] - [\text{Sorbitan}-\text{H}_2\text{SO}_4] - [\text{Isosorbide}-\text{H}_2\text{SO}_4])} \quad (5.3)$$

where $[H_2SO_4]_0$ (unit: M) is the initial concentration of H_2SO_4. [Sorbitol], [Sorbitan], and [Isosorbide] (M) are the concentrations of sorbitol, 1,4-sorbitan, and isosorbide, respectively. [Sorbitol – H_2SO_4], [Sorbitan – H_2SO_4], and [Isosorbide – H_2SO_4] (M) are the concentrations of H_2SO_4 adducts with sorbitol, 1,4-sorbitan, and isosorbide. Accordingly,

$$[\text{Sorbitol}-\text{H}_2\text{SO}_4]=\frac{K_1[\text{Sorbitol}][\text{H}_2\text{SO}_4]_0}{1+K_1[\text{Sorbitol}]+K_2[\text{Sorbitan}]+K_3[\text{Isosorbide}]} \quad (5.4)$$

$$[\text{Sorbitan}-\text{H}_2\text{SO}_4]=\frac{K_2[\text{Sorbitan}][\text{H}_2\text{SO}_4]_0}{1+K_1[\text{Sorbitol}]+K_2[\text{Sorbitan}]+K_3[\text{Isosorbide}]} \quad (5.5)$$

$$[\text{Isosorbide}-\text{H}_2\text{SO}_4]=\frac{K_3[\text{Isosorbide}][\text{H}_2\text{SO}_4]_0}{1+K_1[\text{Sorbitol}]+K_2[\text{Sorbitan}]+K_3[\text{Isosorbide}]} \quad (5.6)$$

The reaction rates corresponding to each reactant are represented by using reaction time t (unit: min^{-1}) as

$$\frac{\text{d}[\text{Sorbitol}]}{\text{d}t}=-(k_1+k_3)[\text{Sorbitol}-\text{H}_2\text{SO}_4] \quad (5.7)$$

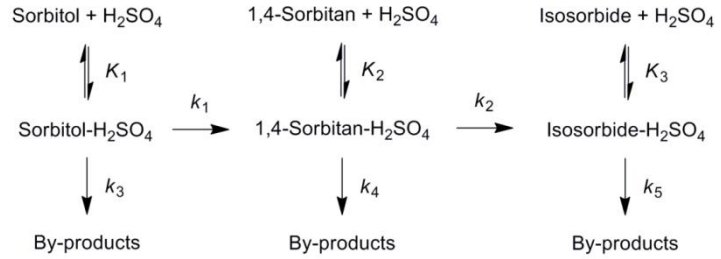
$$\frac{\text{d}[\text{Sorbitan}]}{\text{d}t}=k_1[\text{Sorbitol}-\text{H}_2\text{SO}_4]-(k_2+k_4)[\text{Sorbitan}-\text{H}_2\text{SO}_4] \quad (5.8)$$

$$\frac{\text{d}[\text{Isosorbide}]}{\text{d}t}=k_2[\text{Sorbitan}-\text{H}_2\text{SO}_4]-k_5[\text{Isosorbide}-\text{H}_2\text{SO}_4] \quad (5.9)$$

in which the volume of reaction system at 403 K is 1.32×10^{-4} L ($0.182 \text{ g} \times 0.726 \times 10^{-3}$ L g^{-1}).[31]

The simulation curve well reproduced the experimental data (dots) in Figure 5.4, giving reliable rate constants. k_1 (4.7×10^{-2} min^{-1}) is only 1.7 times larger than k_2 (2.7×10^{-2} min^{-1}) (Table 5.2). k_3 (1.1×10^{-2} min^{-1}) and k_4 (3.8×10^{-3} min^{-1}) are lower than k_1, which is consistent with the low yields of by-products such as 2,5-iditan and 2,5-mannitan. The low value of k_5 (<1.0×10^{-4} min^{-1}) indicates high stability of isosorbide under the reaction conditions.

Table 5.2 Rate constants for sorbitol dehydration by H_2SO_4 at 403 K, determined by the fitting simulations.



Rate constant /10^{-2} min^{-1}					K_1/K_2	K_1/K_3
k_1	k_2	k_3	k_4	k_5		
4.7	2.7	1.1	0.38	<0.01	4.3	4.5

Regarding the association equilibrium constants, the ratios K_1/K_2 and K_1/K_3 were estimated to be 4.3 and 4.5, respectively, from the fitting in Figure 5.4, showing that sorbitol interacts with H_2SO_4 4.3 and 4.5 times as strongly as 1,4-sorbitan and isosorbide does. If this preferential association did not occur (*e.g.*, $K_1 = K_2 = K_3$), the maximum yield of 1,4-sorbitan would become two-thirds (40%) (Figure 5.5). Note that in the absence of preferential association, recovering the original yield of 1,4-sorbitan (58%) is very difficult by controlling rate constants as follows. Yield of 1,4-sorbitan reaches 58% only when $k_1/(k_2 + k_4)$ value is greater than 3.2. However, the actual value was only 1.2, since both reactions of sorbitol and 1,4-sorbitan are similar acid-catalyzed dehydration. Hence, the large K_1/K_2 ratio effectively inhibits the association of 1,4-sorbitan with H_2SO_4 in the presence of sorbitol, which prevents the successive dehydration of 1,4-sorbitan. Takagaki *et al.* have proposed that molecular recognition is the key to selective production of 1,4-sorbitan,[32] and H_2SO_4 may selectively activate OH group at C1 of sorbitol in this study (the mechanism is discussed in Section 5.3.3). Thus, the author concludes that the preferential association is essential to achieve selective production of 1,4-sorbitan by H_2SO_4 from sorbitol.

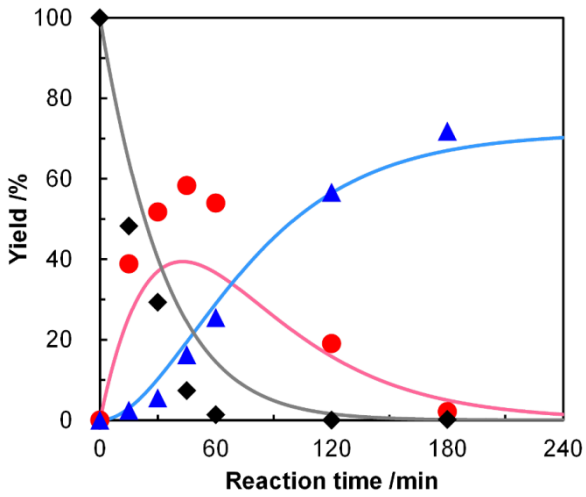


Figure 5.5. Time course of sorbitol dehydration by H_2SO_4 at 403 K. Dots show experimental results, which are the same data in Figure 5.4. Lines are simulation curves based on eqs. 5.1–5.9 with $K_1 = K_2 = K_3$. Legend: black diamonds (♦) = amount of unreacted sorbitol; red circles (●) = yield of 1,4-sorbitan; and blue triangles (▲) = yield of isosorbide. This simulation does not reproduce the experimental data, and the maximum yield of 1,4-sorbitan in the simulation is only *ca.* 40%.

For designing new catalysts based on these insights, the author speculates that the combination of Brønsted acid sites with metal cation centers may be useful. Some metal cations such as Ca^{2+} and Pb^{2+} can form chelates as applied to HPLC columns for the separation of sugar compounds. HPLC columns containing these cations retain sorbitol for a long time (*e.g.*, 45 min for a Pb^{2+} column; see Figure 5.A.12b and 5.A.12c) but does not 1,4-sorbitan (15 min under the same conditions). If H^+ is also present in the reaction system, 1,4-sorbitan may be selectively produced.

5.3.3. Reaction mechanism for dehydration of sorbitol by H_2SO_4

By considering the selective formation of 1,4-sorbitan by H_2SO_4, five types of mechanisms are possible for the dehydration of sorbitol at the 1,4-position (Figure 5.6): (1) S_N2-type attack of the secondary OH on the primary carbon,[33] (2) its S_N1-type version, (3) S_N2-type attack of the primary OH on the secondary carbon, (4) its S_N1-type version, and (5) tandem S_N2-S_N2 attacks of vicinal OH and terminal OH.[34] Among the five mechanisms, mechanism **1** is the most probable as the reaction pathway for 1,4-dehydration based on the

product distributions as described below.

H_2SO_4 gave only 1,4-sorbitan in the 1,4-dehydration of sorbitol. 1,4-Galactan, the C4 isomer of 1,4-sorbitan, was not detected in this study. In mechanism **1**, the S_N2 reaction at the primary carbon center is generally favorable with less steric hindrance with retention of the configuration of sorbitol, which is consistent with the results. In mechanism **2**, the formation of 1° carbenium ions is energetically disadvantageous and can be excluded. The S_N2 reaction at the C4 position (mechanism **3**) giving 1,4-galactan should be negligible as the product was not detected. The formation of 2° carbenium ions (mechanism **4**) can be also excluded as this pathway gives a mixture of 1,4-sorbitan and 1,4-galactan. In mechanism **5**, 1,4-sorbitan is not selectively formed as described below. If the first S_N2 reaction occurs at C4 being attacked by OH at C3 or C5, the stereochemistry of sorbitol is maintained to produce 1,4-sorbitan. However, the first S_N2 attack could also happen at OH group on C4 to the C3 (mechanism **5'**) or C5 (mechanism **5''**) positions in a similar manner to mechanism **5**, which gives 3,6-sorbitan (L-isomer) or 3,6-anhydrotalitol (3,6-talitan, L-isomer). However, these products were not observed in the experiments. Hence, the author concludes that mechanism **1** is the most probable pathway in the 1,4-dehydration of sorbitol by H_2SO_4.

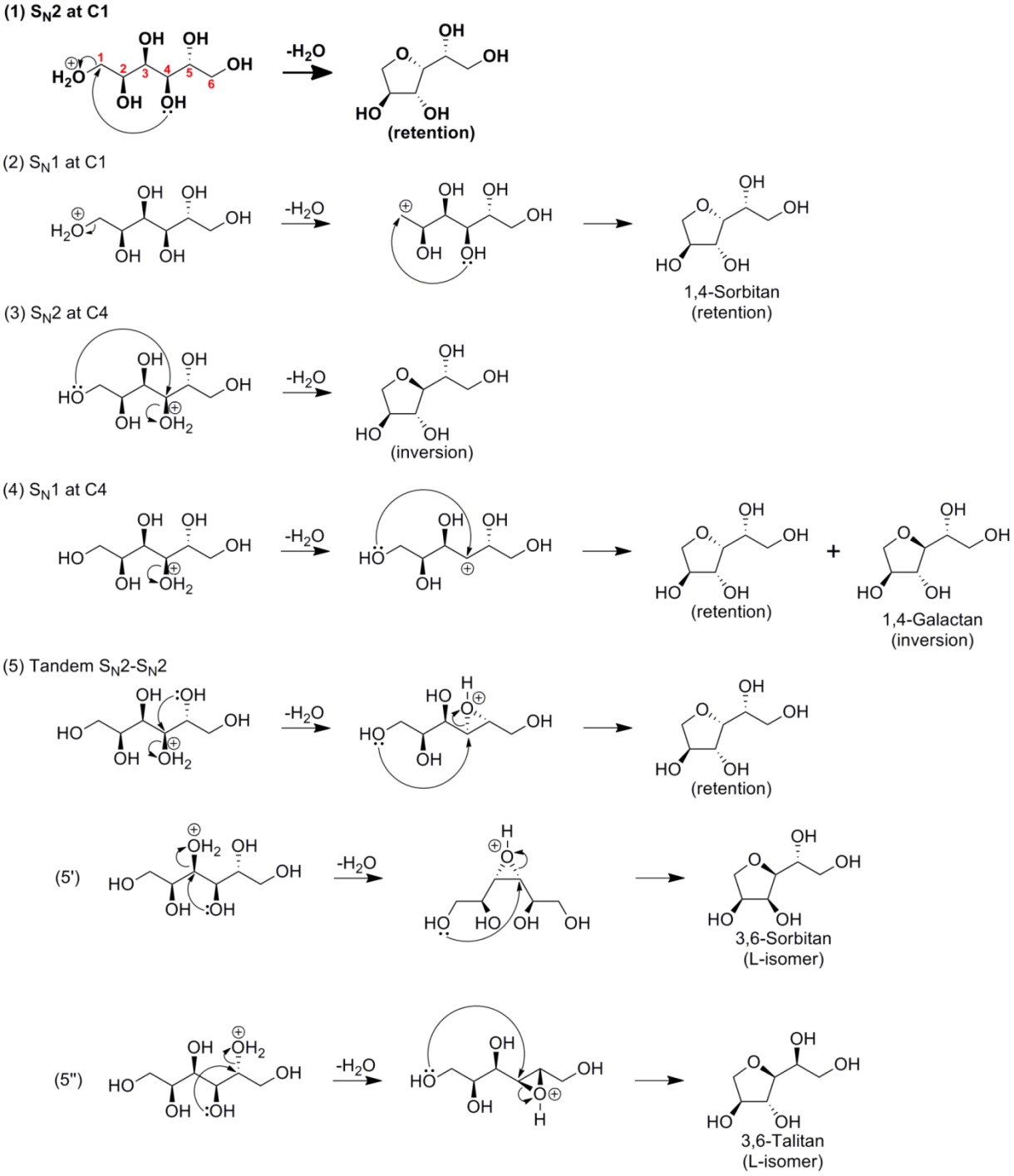


Figure 5.6. Possible reaction pathways for the 1,4-dehydration of sorbitol.

5.4. Conclusions

In sorbitol dehydration, SZ affords 1,4-sorbitan in 60% yield with 62% selectivity; however, actual active species are not acids immobilized on SZ, but leached ones. Indeed, 1.0 μmol of H_2SO_4, the amount of which is equivalent to that of leached species, gives similar yield and selectivity of 1,4-sorbitan. In other words, H_2SO_4 shows characteristic performance for selective synthesis of 1,4-sorbitan from sorbitol.

Kinetic studies of sorbitol dehydration by H_2SO_4 were conducted to understand selective catalysts. The results show that the high ratio of K_1/K_2 (4.3) contributes the good yield of 1,4-sorbitan regardless of similar rate constants of k_1/k_2 (1.7). Typically, both sorbitol and 1,4-sorbitan undergo dehydration in the presence of acids. However, the association of 1,4-sorbitan with H_2SO_4 is substantially less favored in the presence of sorbitol, and further dehydration of 1,4-sorbitan to isosorbide can be prevented. Therefore, control of association equilibrium constant (K) is effective as well as that of reaction rate (k) to maximize the yield of 1,4-sorbitan, and that this insight is useful to the design of new catalysts for the selective synthesis of anhydropolyols.

Appendices: raw data for HPLC, LC/MS, and NMR

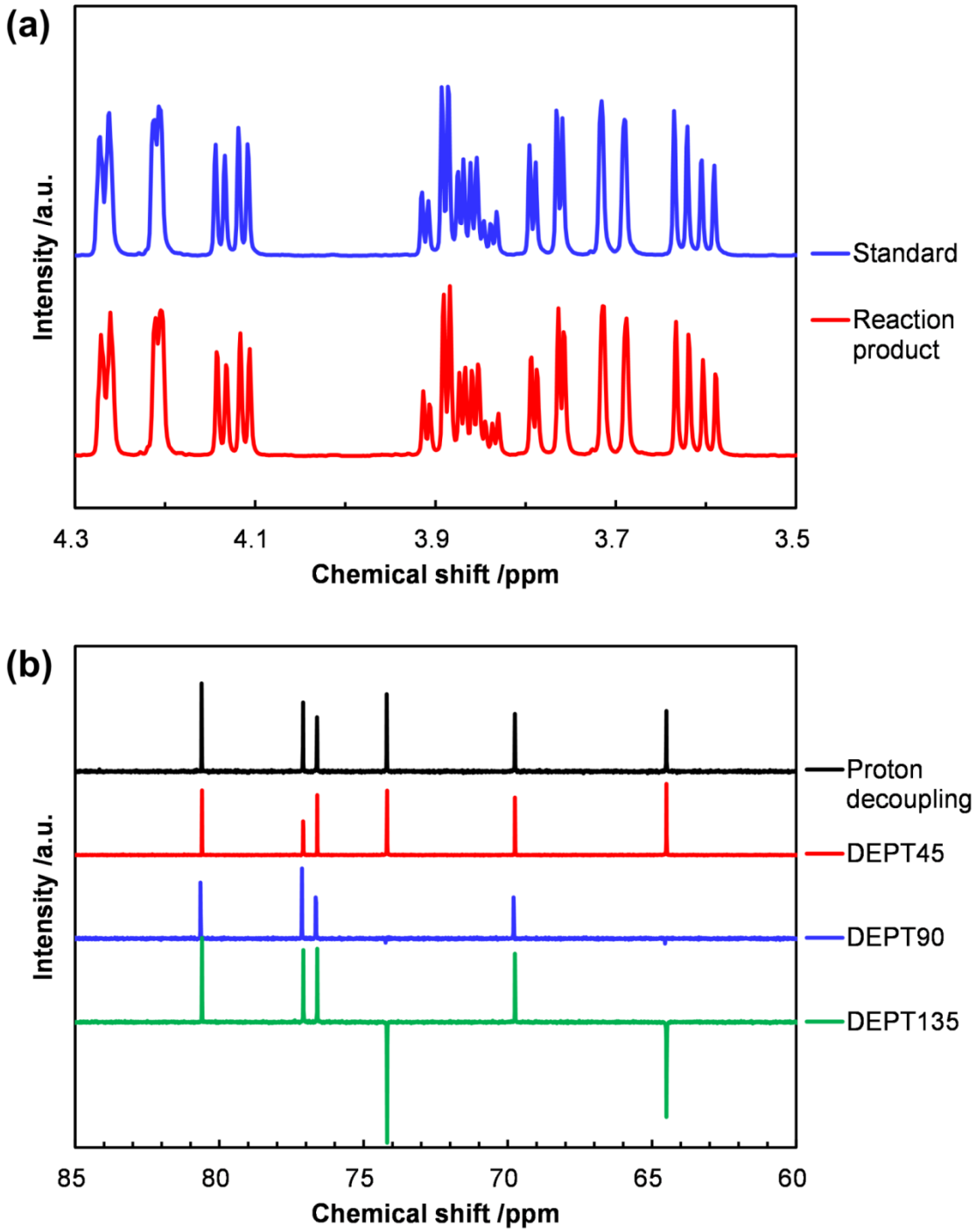


Figure 5.A.1. NMR spectra of 1,4-sorbitan: (a) ^{1}H NMR and (b) proton-decoupled ^{13}C NMR and DEPT. ^{13}C NMR spectra were recorded using a commercial standard.

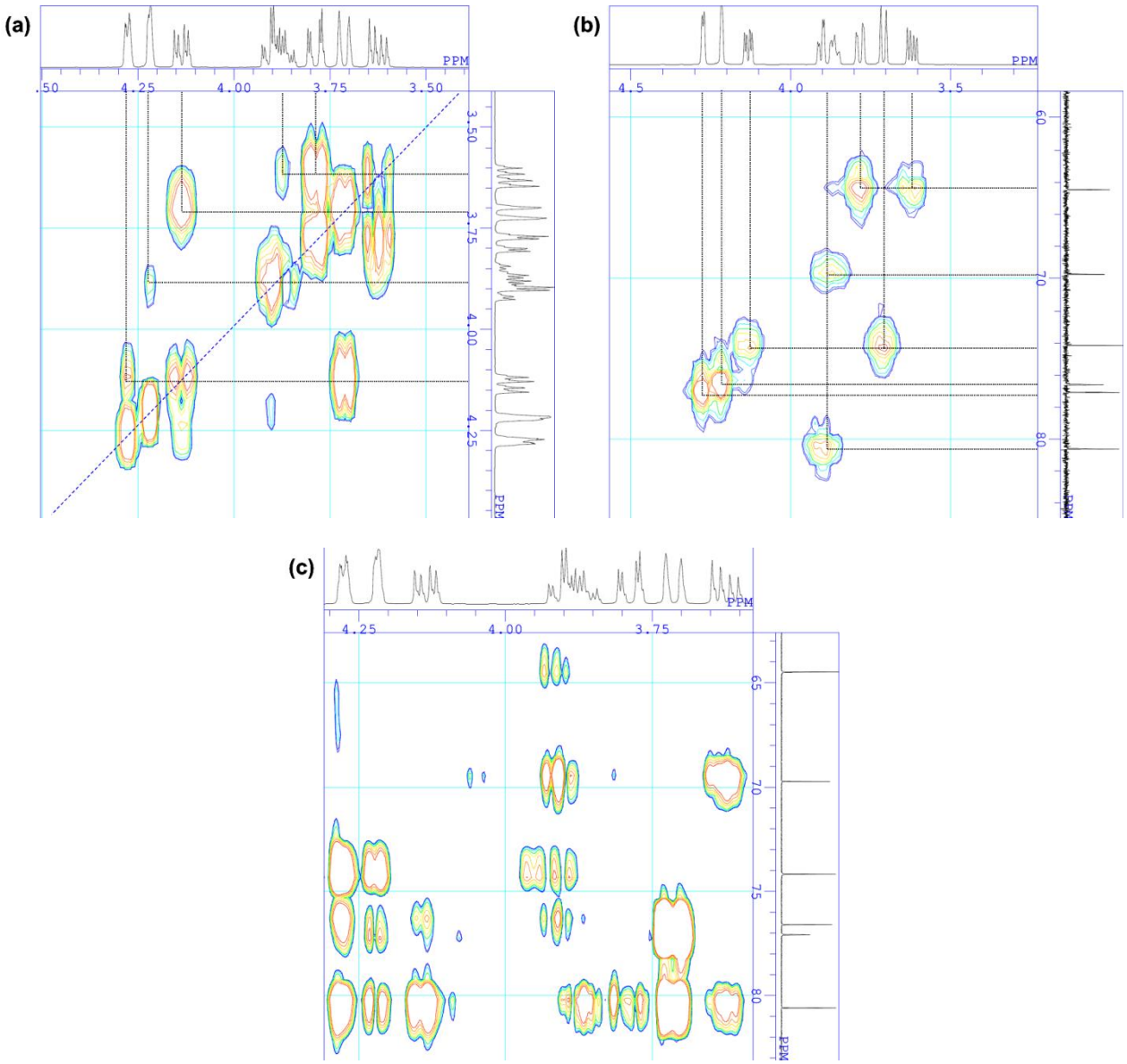


Figure 5.A.2. 2D NMR spectra of 1,4-sorbitan: (a) COSY, (b) HMQC (horizontal axis: ^{1}H; vertical axis: ^{13}C), and (c) HMBC (horizontal axis: ^{1}H; vertical axis: ^{13}C). These spectra were recorded using a commercial standard.

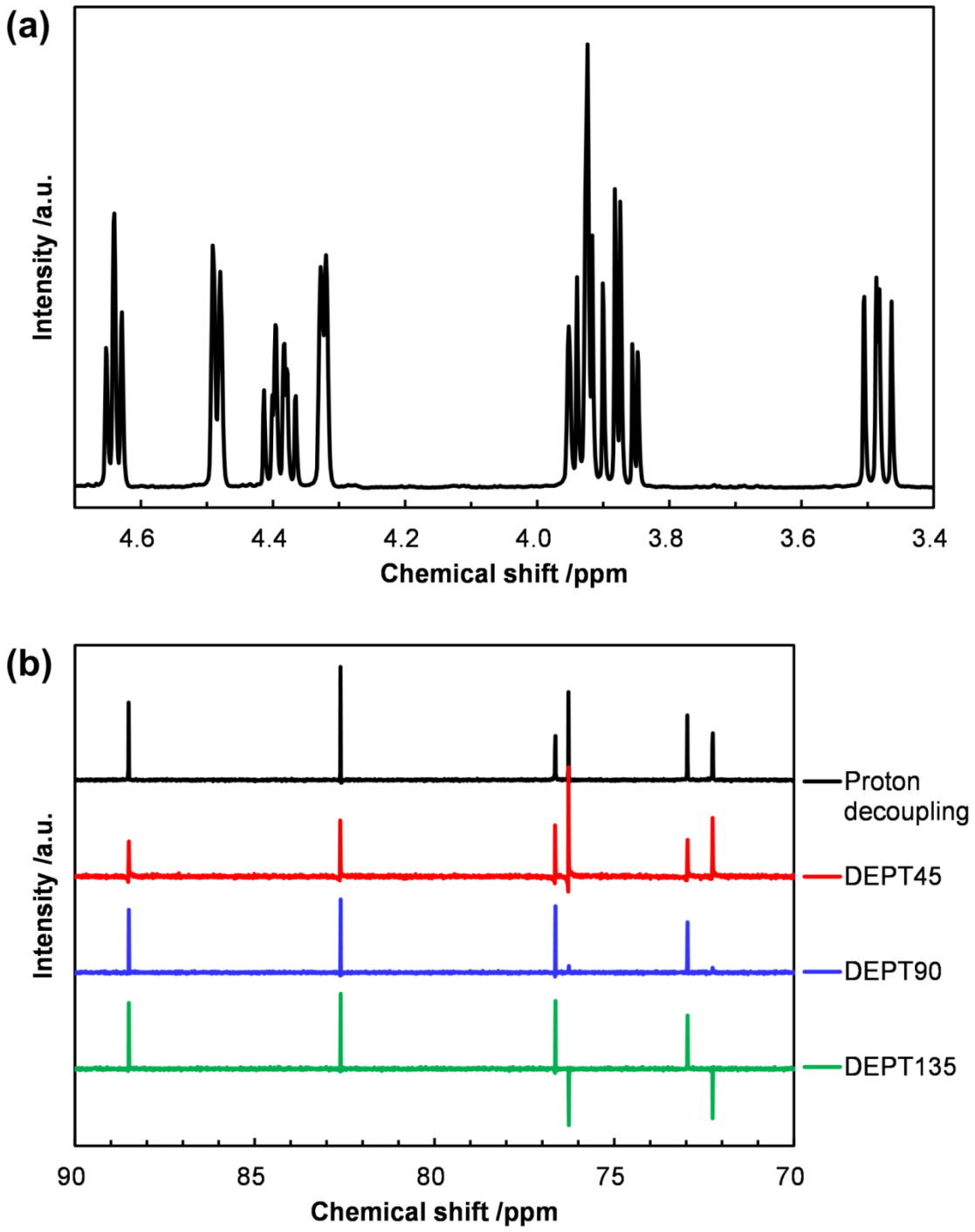


Figure 5.A.3. NMR spectra of isosorbide: (a) ^{1}H NMR and (b) proton-decoupled ^{13}C NMR and DEPT. These analyses were conducted using a commercial standard.

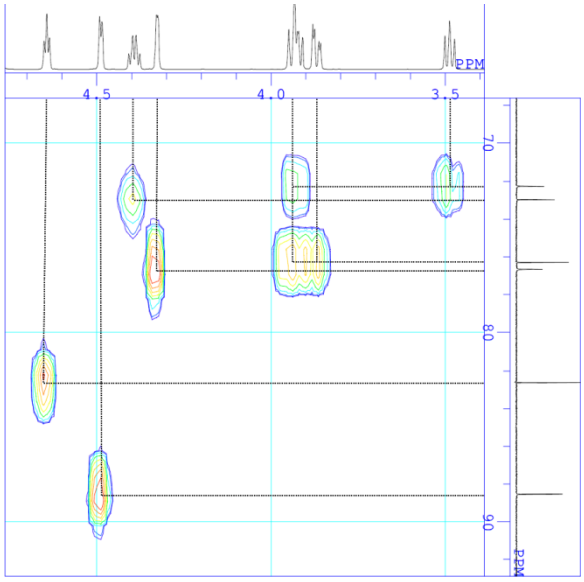


Figure 5.A.4. HMQC spectrum of isosorbide (horizontal axis: ^{1}H; vertical axis: ^{13}C). This spectrum was recorded using a commercial standard.

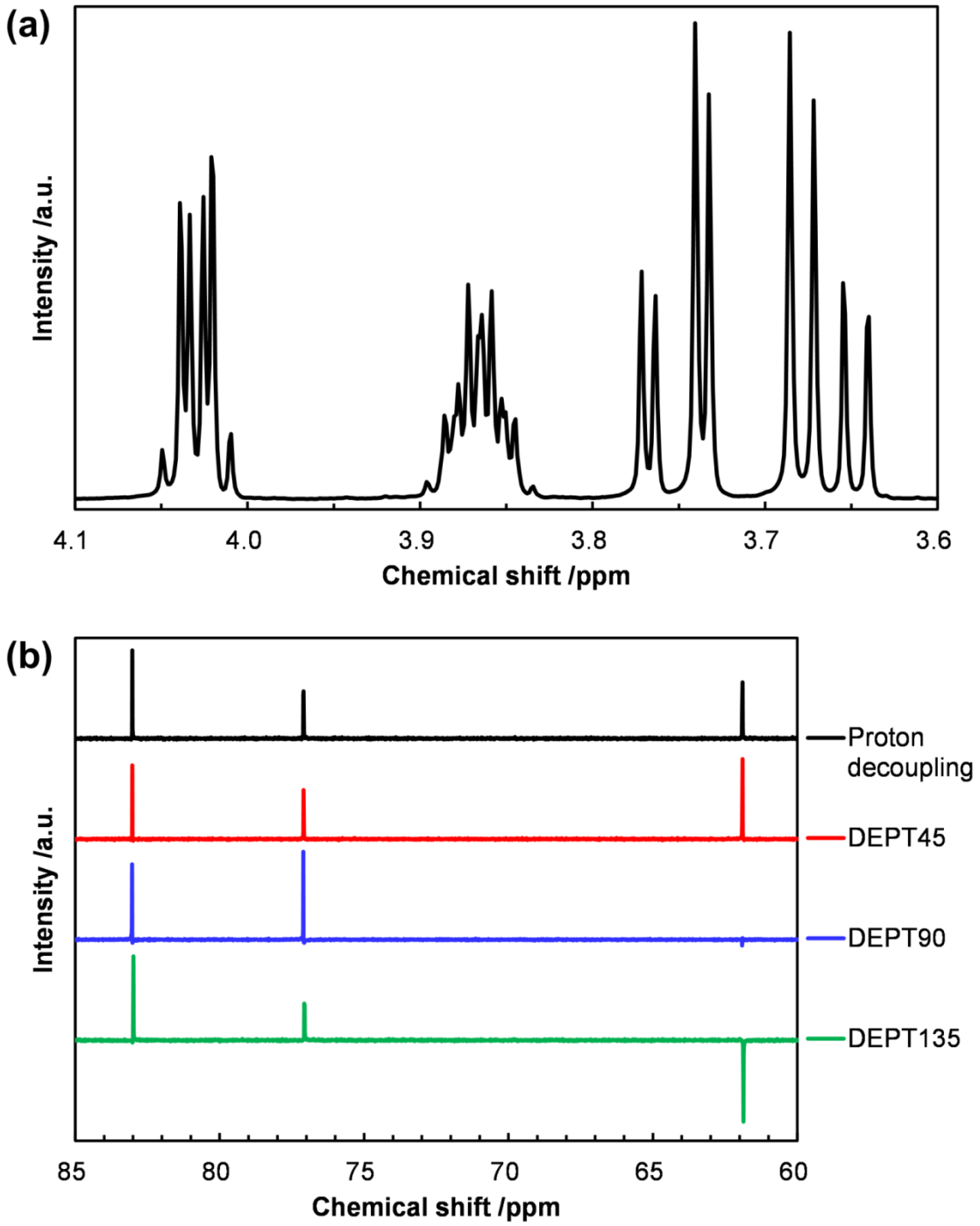


Figure 5.A.5. NMR spectra of 2,5-mannitan: (a) ^{1}H NMR and (b) proton-decoupled ^{13}C NMR and DEPT. These analyses were conducted using a commercial standard.

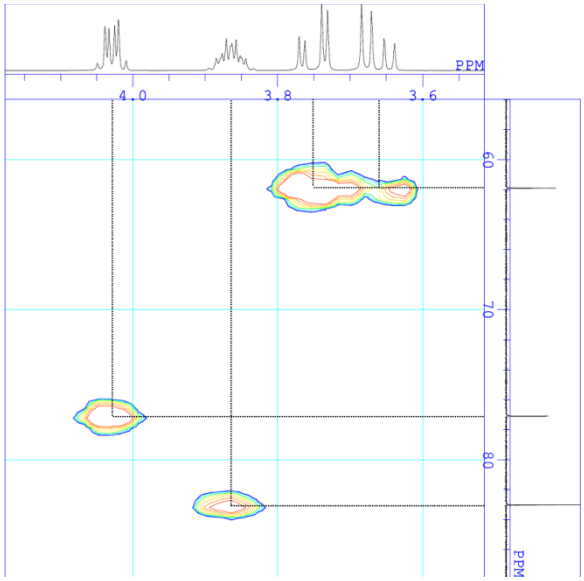


Figure 5.A.6. HMQC spectrum of 2,5-mannitan (horizontal axis: ^{1}H; vertical axis: ^{13}C). This spectrum was recorded using a commercial standard.

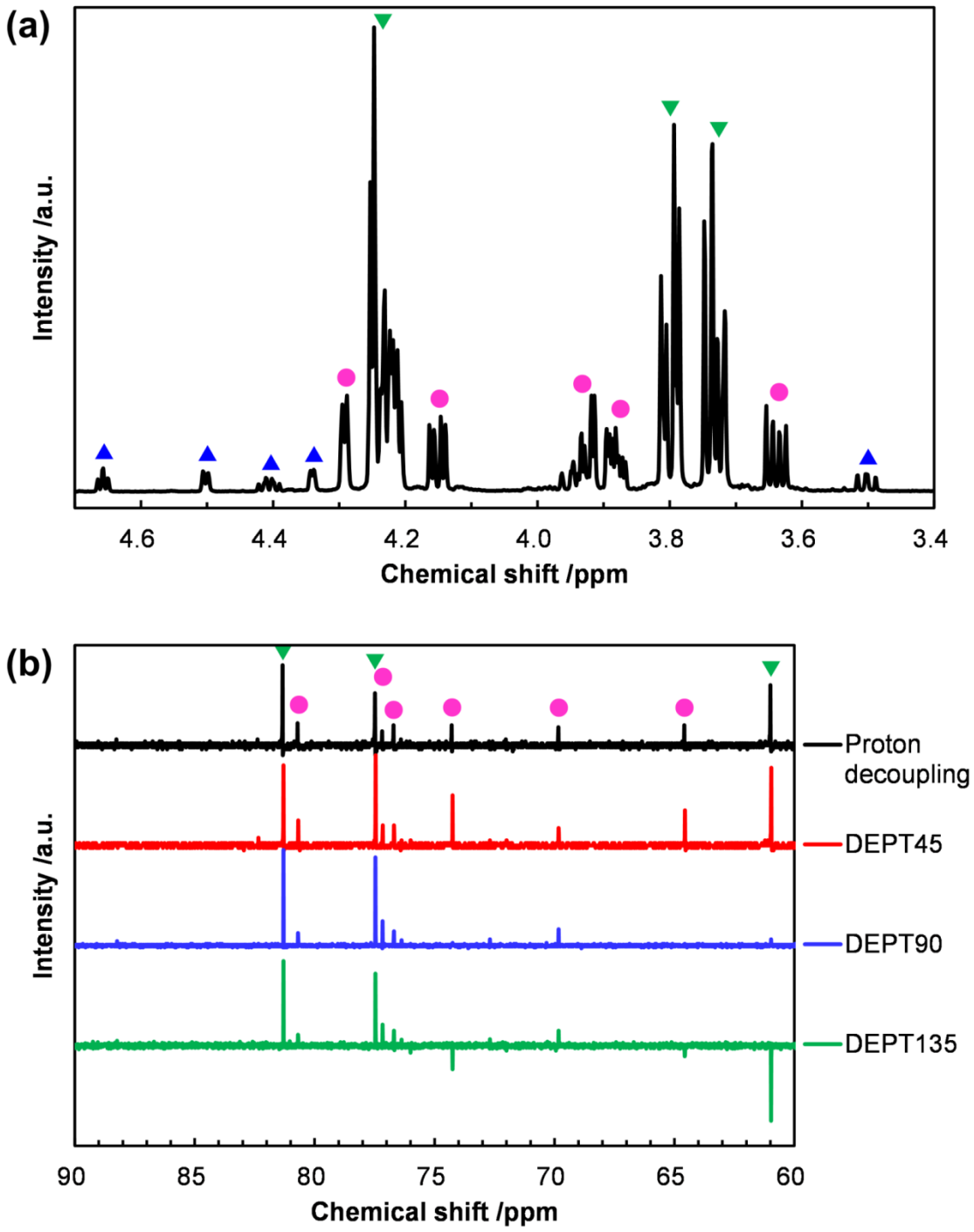


Figure 5.A.7. NMR spectra of a reaction mixture containing 2,5-iditan (▼), isosorbide (▲), and *AH1* (●): (a) ^{1}H NMR and (b) proton-decoupled ^{13}C NMR and DEPT. ^{1}H NMR peaks of isosorbide are consistent with those of a standard reagent (Figure 5.A.3a). ^{13}C NMR peaks of isosorbide could not be distinguished from noise due to its low concentration.

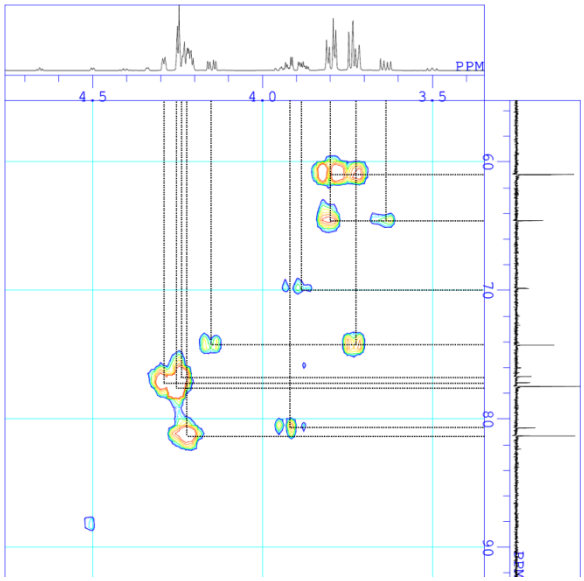


Figure 5.A.8. HMQC spectrum of a reaction mixture containing 2,5-iditan, isosorbide, and *AH1* (horizontal axis: ^{1}H; vertical axis: ^{13}C).

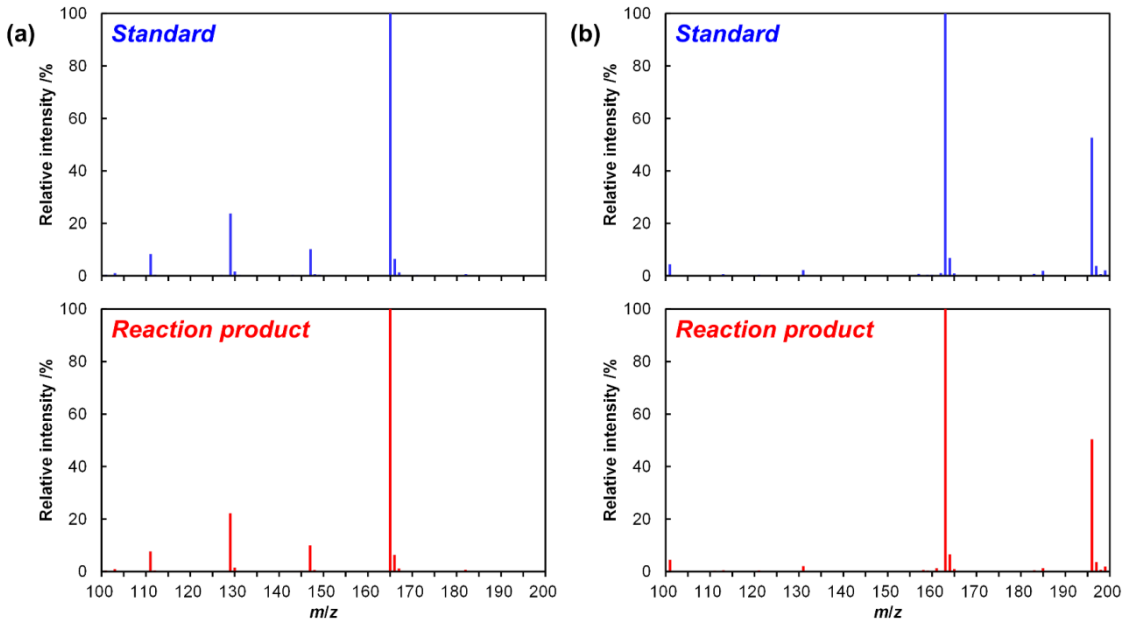


Figure 5.A.9. LC/MS spectra of 1,4-sorbitan recorded in (a) positive ion mode and (b) negative ion mode.

Positive ion mode: 111 ($[M + H - 3H_2O]^+$), 129 ($[M + H - 2H_2O]^+$), 147 ($[M + H - H_2O]^+$), 165 ($[M + H]^+$).

Negative ion mode: 163 ($[M - H]^-$), 196 ($[M + O_2]^-$).

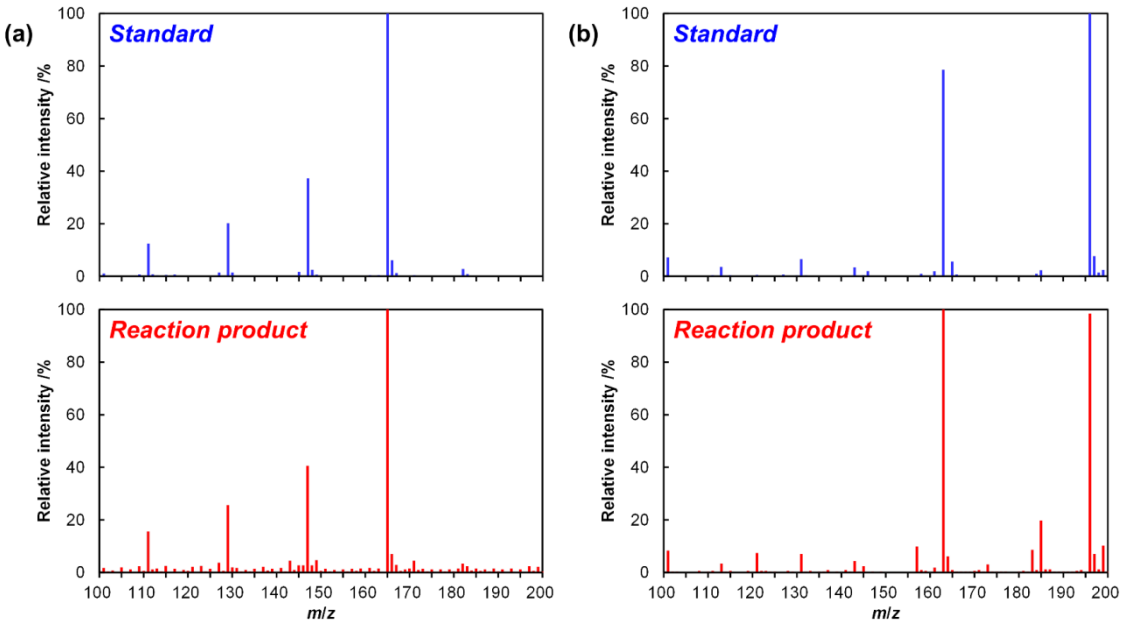


Figure 5.A.10. LC/MS spectra of 2,5-mannitan recorded in (a) positive ion mode and (b) negative ion mode. Several small peaks were observed from other products in trace amounts.

Positive ion mode: 111 ($[M + H - 3H_2O]^+$), 129 ($[M + H - 2H_2O]^+$), 147 ($[M + H - H_2O]^+$), 165 ($[M + H]^+$).

Negative ion mode: 163 ($[M - H]^-$), 196 ($[M + O_2]^-$).

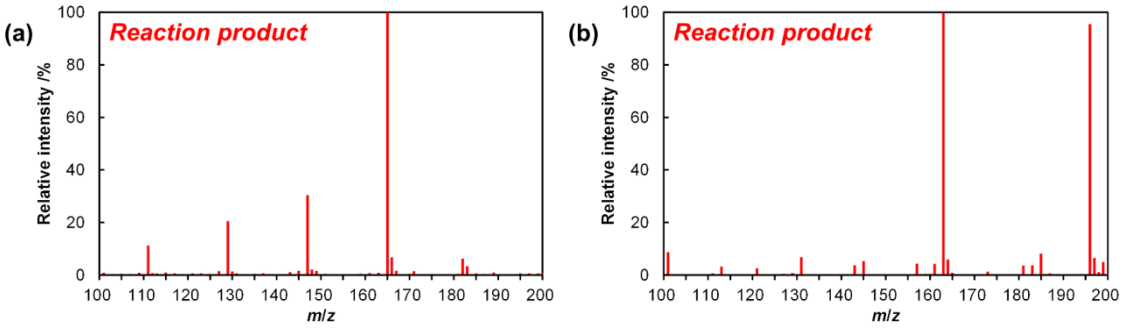


Figure 5.A.11. LC/MS spectra of a mixture of 2,5-iditan, isosorbide, and *AH1* recorded in (a) positive ion mode and (b) negative ion mode. In the positive ion mode, $[M + H]^+$ of isosorbide, calculated at 147, could not be distinguished from $[M + H - H_2O]^+$ of 2,5-iditan and *AH1*. In the negative ion mode, $[M - H]^-$ of isosorbide, calculated at 145, was not detected due to low concentration and sensitivity.

Positive ion mode: 111 ($[M + H - 3H_2O]^+$), 129 ($[M + H - 2H_2O]^+$), 147 ($[M + H - H_2O]^+$), 165 ($[M + H]^+$).

Negative ion mode: 163 ($[M - H]^-$), 196 ($[M + O_2]^-$).

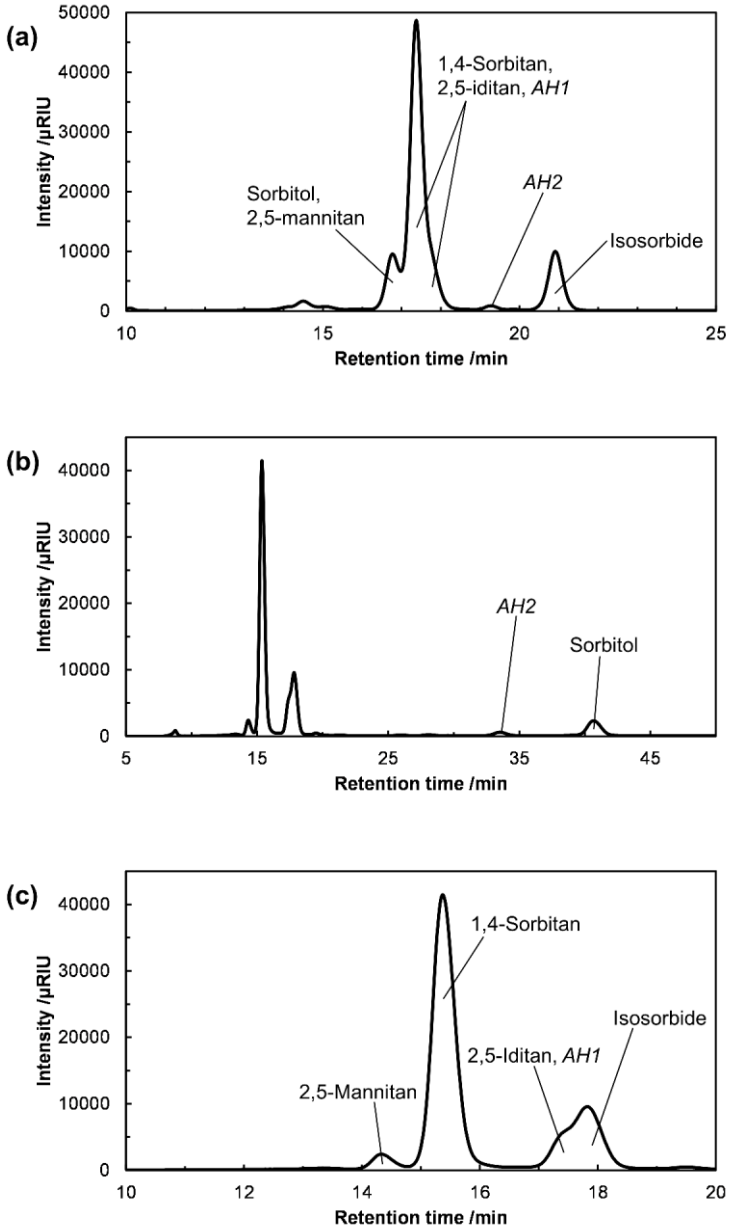


Figure 5.A.12. Typical HPLC charts for the dehydration of sorbitol by H_2SO_4: (a) SUGAR SH1011 column, (b) Rezex RPM-Monosaccharide Pb++ column, and (c) expanded view of Figure 5.A.12b.

SUGAR SH1011 column: 2,5-mannitan (16.5 min), sorbitol (16.6 min), 1,4-sorbitan, 2,5-iditan and *AH1* (17–18 min), *AH2* (19.1 min), and isosorbide (20.9 min). The retention times of 1,5-sorbitan (16.5 min) and 1,5-mannitan (18.3 min) were also checked.

Rezex RPM-Monosaccharide Pb++ column: 2,5-mannitan (14.3 min), 1,4-sorbitan (15.4 min), 2,5-iditan and *AH1* (17.5 min), isosorbide (17.8 min), *AH2* (33.5 min), and sorbitol (40.7 min). The retention times of 1,5-sorbitan (15.3 min) and 1,5-mannitan (21.8 min) were also checked.

References

1. P. Gallezot, N. Nicolaus, G. Flèche, P. Fuertes, and A. Perrard, *J. Catal.*, 1998, **180**, 51–55.
2. H. Li, W. Wang, and J. Fa Deng, *J. Catal.*, 2000, **191**, 257–260.
3. H. Li, H. Li, and J.-F. Deng, *Catal. Today*, 2002, **74**, 53–63.
4. B. W. Hoffer, E. Crezee, F. Devred, P. R. M. Mooijman, W. G. Sloof, P. J. Kooyman, A. D. van Langeveld, F. Kapteijn, and J. A. Moulijn, *Appl. Catal. A: Gen.*, 2003, **253**, 437–452.
5. A. Fukuoka and P. L. Dhepe, *Angew. Chem. Int. Ed.*, 2006, **45**, 5161–5163.
6. H. Kobayashi, H. Ohta, and A. Fukuoka, *Catal. Sci. Technol.*, 2012, **2**, 869–883.
7. M. Yabushita, H. Kobayashi, and A. Fukuoka, *Appl. Catal. B: Environ.*, 2014, **145**, 1–9.
8. T. Werpy, G. Petersen, A. Aden, J. Bozell, J. Holladay, J. White, A. Manheim, D. Elliot, L. Lasure, S. Jones, M. Gerber, K. Ibsen, L. Lumberg, and S. Kelley, "Top Value Added Chemicals From Biomass Volume I: Results of Screening for Potential Candidates from Sugars and Synthesis Gas," http://www.dtic.mil/cgi-bin/GetTRDoc?Location=U2&doc=GetTRDoc.pdf&AD=ADA436528 (accessed Nov. 20, 2014).
9. H. Kobayashi and A. Fukuoka, *Green Chem.*, 2013, **15**, 1740–1763.
10. X. Li, Y. Su, X. Zhou, and X. Mo, *Colloids Surfaces B Biointerfaces*, 2009, **69**, 221–224.
11. T. Yoshioka, B. Sternberg, and A. T. Florence, *Int. J. Pharm.*, 1994, **105**, 1–6.
12. S. Soltzberg, US Patent 2,390,395, 1945.
13. S. Soltzberg, R. M. Goepp, and W. Freudenberg, *J. Am. Chem. Soc.*, 1946, **68**, 919–921.
14. J. Defaye, A. Gadelle, and C. Pedersen, *Carbohydr. Res.*, 1990, **205**, 191–202.
15. C. Montassier, J. C. Ménézo, J. Moukolo, J. Naja, L. C. Hoang, J. Barbier, and J. P. Boitiaux, *J. Mol. Catal.*, 1991, **70**, 65–84.
16. M. A. Andrews, K. K. Bhatia, and P. J. Fagan, US Patent 6,689,892, 2004.
17. K. M. Moore, A. J. Sanborn, and P. Bloom, US Patent 7,439,352, 2008.
18. A. J. Sanborn, US Patent 7,420,067, 2008.
19. J. E. Holladay, J. Hu, X. Zhang and Y. Wang, US Patent 7,772,412, 2010.
20. J. Xia, D. Yu, Y. Hu, B. Zou, P. Sun, H. Li, and H. Huang, *Catal. Commun.*, 2011, **12**, 544–547.

21. A. Liu and C. C. Luckett, US Patent 7,982,059, 2011.

22. M. Gu, D. Yu, H. Zhang, P. Sun, and H. Huang, *Catal. Lett.*, 2009, **133**, 214–220.

23. A. Yamaguchi, N. Hiyoshi, O. Sato, and M. Shirai, *Green Chem.*, 2011, **13**, 873–881.

24. N. A. Khan, D. K. Mishra, I. Ahmed, J. W. Yoon, J.-S. Hwang, and S. H. Jhung, *Appl. Catal. A: Gen.*, 2013, **452**, 34–38.

25. I. Ahmed, N. A. Khan, D. K. Mishra, J. S. Lee, J.-S. Hwang, and S. H. Jhung, *Chem. Eng. Sci.*, 2013, **93**, 91–95.

26. B. M. Reddy and M. K. Patil, *Chem. Rev.*, 2009, **109**, 2185–2208.

27. H. Matsuhashi, H. Nakamura, T. Ishihara, S. Iwamoto, Y. Kamiya, J. Kobayashi, Y. Kubota, T. Yamada, T. Matsuda, K. Matsushita, K. Nakai, H. Nishiguchi, M. Ogura, N. Okazaki, S. Sato, K. Shimizu, T. Shishido, S. Yamazoe, T. Takeguchi, K. Tomishige, H. Yamashita, M. Niwa, and N. Katada, *Appl. Catal. A: Gen.*, 2009, **360**, 89–97.

28. K. Bock, C. Pedersen, and H. Thogersen, *Acta Chem. Scand. B*, 1981, **35**, 441–449.

29. R. Wieneke, S. Klein, A. Geyer, and E. Loos, *Carbohydr. Res.*, 2007, **342**, 2757–2765.

30. J. C. Goodwin, J. E. Hodge, and D. Weisleder, *Carbohydr. Res.*, 1980, **79**, 133–141.

31. M. Naoki, K. Ujita, and S. Kashima, *J. Phys. Chem.*, 1993, **97**, 12356–12362.

32. Y. Morita, S. Furusato, A. Takagaki, S. Hayashi, R. Kikuchi and S. T. Oyama, *ChemSusChem*, 2014, **7**, 748–752.

33. L. Došen-Mićović and Ž. Čeković, *J. Phys. Org. Chem.*, 1998, **11**, 887–894.

34. R. Barker, *J. Org. Chem.*, 1970, **35**, 461–464.

Chapter 6

General Conclusions

In this work, the author has demonstrated catalytic and mechanistic study on conversion of non-food biomass, cellulose and chitin. Therefore, in Chapter 1, the reported systems for cellulose and chitin conversions including laboratory and industrial scales are summarized and discussed to clarify the current issues in biorefinery.

The finding in Chapter 2 is that carbon materials bearing only weakly acidic sites catalyze hydrolysis of cellulose (Figure 6.1). For practical applications, the weakly acidic carbons are advantageous over reported sulfonated catalysts owing to their high hydrothermal stability and high resistance against ion exchange. Additionally, a new pre-treatment method *mix-milling* has been developed to overcome a serious issue of solid-solid reaction, namely loose contact between solids. The mix-milling makes tight contact and drastically enhances the rate of hydrolysis of solid cellulose by solid carbons. As a result, 88% yield of glucose with 90% selectivity has been achieved, and this is one of the highest yields ever reported. The mix-milling method is also applicable to hydrolysis of raw biomass, bagasse kraft pulp (Figure 6.2).

Mechanistic studies to reveal the catalysis of carbon materials for cellulose hydrolysis have been conducted in Chapter 3. The first adsorption process of cellulosic molecules on carbon surface is driven by hydrophobic functionalities, namely formation of CH–π hydrogen bonds and hydrophobic interactions. Following the adsorption, glycosidic bonds are activated and hydrolyzed by vicinal hydrophilic functional groups, the structures of which are similar to salicylic acid and phthalic acid. Based on the mechanistic insights, the author has proposed the reaction mechanism (Figure 6.3) and has also demonstrated the design of more active carbon catalysts, oxidized zeolite-templated carbon ZTC.

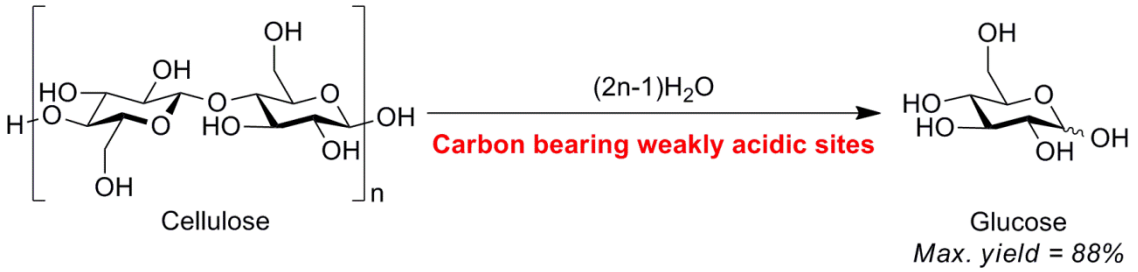


Figure 6.1. Hydrolysis of cellulose to glucose.

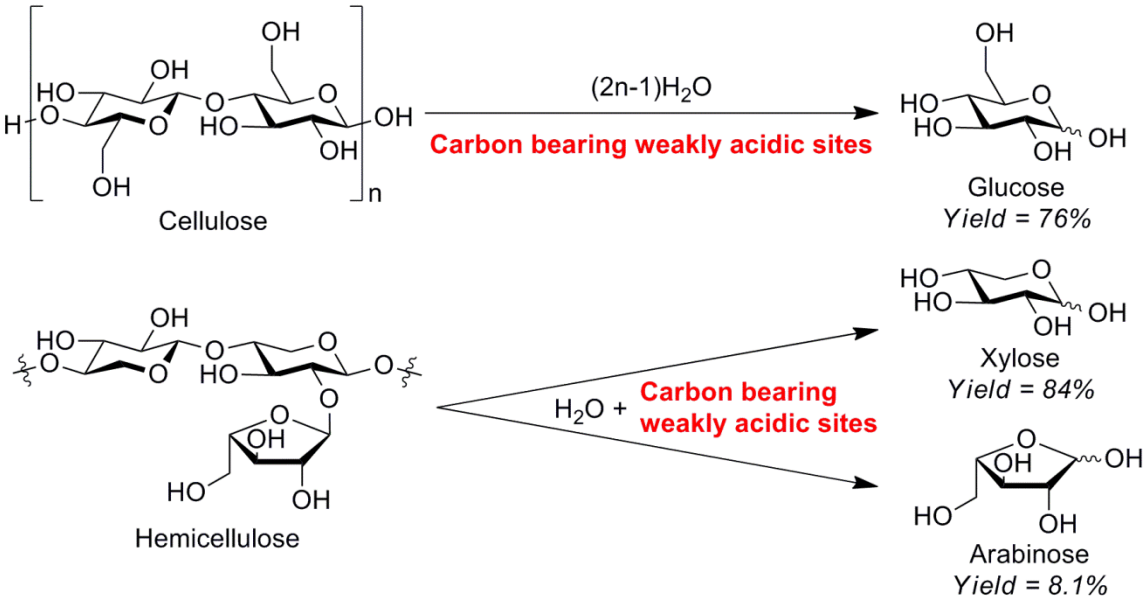


Figure 6.2. Hydrolysis of cellulose/hemicellulose in bagasse kraft pulp to sugars. Each yield is based on mole of cellulose or hemicellulose in the pulp.

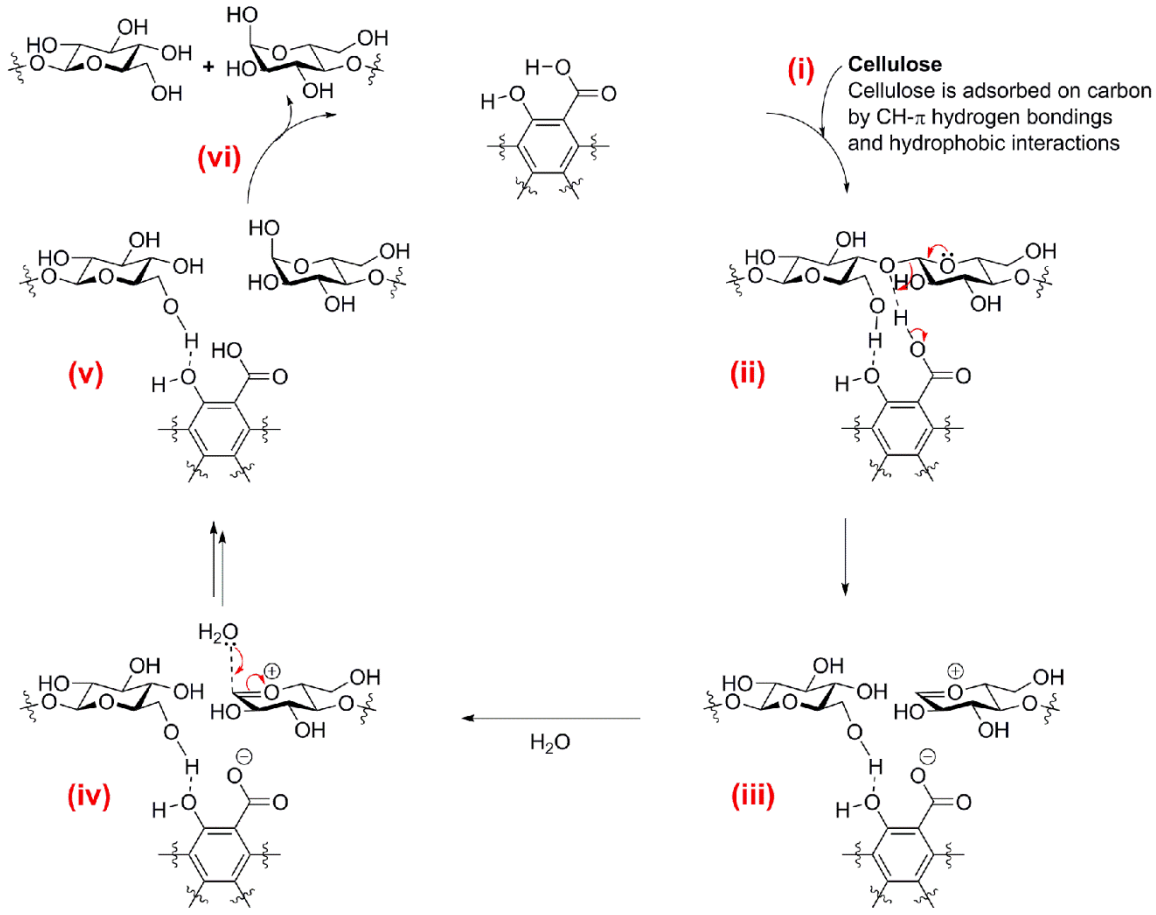


Figure 6.3. Proposed reaction mechanism of cellulose hydrolysis by carbon catalysts.

A two-step depolymerization of chitin, the most abundant biomass next to cellulose, to monomers with preserving acetyl groups was shown in Chapter 4 (Figure 6.4). Mechanical force assisted the first depolymerization step of chitin to water-soluble oligomers in the presence of H_2SO_4. The produced oligomers show high reactivity and are easily converted to 1-*O*-methyl-*N*-acetylglucosamine (MeGlcNAc, yield: 67%) in MeOH owing to their high reactivity. During these reactions, acetyl groups in the substrates are almost completely preserved.

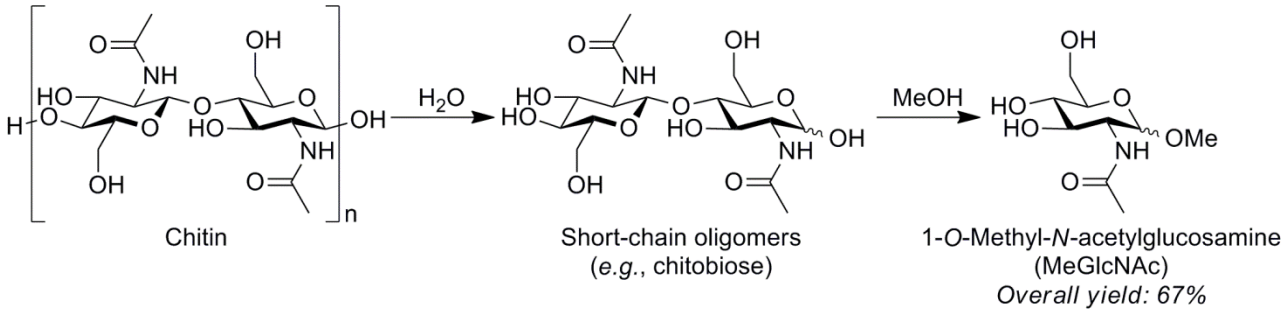


Figure 6.4. Two-step depolymerization of chitin to MeGlcNAc with preserving acetyl groups.

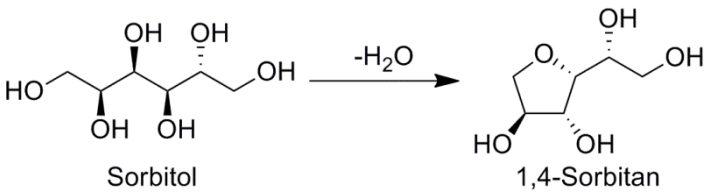


Figure 6.5. Dehydration of sorbitol to 1,4-sorbitan.

In Chapter 5, the selective dehydration of sorbitol to 1,4-sorbitan catalyzed by H_2SO_4 (Figure 6.5) has been investigated to reveal its catalysis, which is expected to be a basis of designing selective dehydration catalysts. In general, 1,4-sorbitan easily undergoes successive dehydration to isosorbide by acid catalysts. However, the transformation of 1,4-sorbitan by H_2SO_4 is hampered in the presence of sorbitol since H_2SO_4 preferentially forms a complex with sorbitol and 1,4-sorbitan. A blueprint for designing new catalysts based on the mechanistic study has been proposed.

In conclusion, the author has achieved the development of new catalytic systems to produce useful platform chemicals, glucose, MeGlcNAc, and 1,4-sorbitan from cellulose and chitin in good yields. These developed catalytic systems are promising for building up sustainable society since produced value-added chemicals are potential alternatives to petroleum in a variety of fields. Besides, the results in this work clearly show that both catalyst design and reaction engineering are effective for high-yielding production of chemicals from biomass, and this manner is useful in the next-generation biorefinery.

Nowadays, in the field of catalytic biomass transformations, a number of researchers do not focus on catalytic chemistry but on just high-yielding production of valuable chemicals by simple improvements of

known catalytic systems. This fashion limits their further applications because their characteristics and advantages are missing pieces of the puzzle. Herein, this work is different from reported ones since basic catalytic chemistry and its applications both have been studied in detail. The author strongly believes that this manner will cause paradigm shifts in biorefinery.

List of Publications

1. Papers (related to this thesis)

1.1. Original articles

1. Hirokazu Kobayashi, Mizuho Yabushita, Tasuku Komanoya, Kenji Hara, Ichiro Fujita, and Atsushi Fukuoka, "High-Yielding One-Pot Synthesis of Glucose from Cellulose Using Simple Activated Carbons and Trace Hydrochloric Acid" *ACS Catalysis*, 2013, **3**, 581–587.
2. Mizuho Yabushita, Hirokazu Kobayashi, Jun-ya Hasegawa, Kenji Hara, and Atsushi Fukuoka, "Entropically Favored Adsorption of Cellulosic Molecules onto Carbon Materials through Hydrophobic Functionalities" *ChemSusChem*, 2014, **7**, 1443–1450.
3. Mizuho Yabushita, Hirokazu Kobayashi, Kenji Hara, and Atsushi Fukuoka, "Quantitative evaluation of ball-milling effect on hydrolysis of cellulose catalysed by activated carbons" *Catalysis Science & Technology*, 2014, **4**, 2312–2317.

1.2. Review articles

1. Atsushi Fukuoka, Hirokazu Kobayashi, and Mizuho Yabushita, "High-efficient saccharification of non-food biomass by using activated carbons (Japanese title: Kasseitan wo mochi-ita hikasyoku biomass no koukouritsu touka)" *Clean Energy*, 2013, **22**, 45–48.
2. Mizuho Yabushita, Hirokazu Kobayashi, and Atsushi Fukuoka, "Catalytic transformation of cellulose into platform chemicals" *Applied Catalysis B: Environmental*, 2014, **145**, 1–9.

2. Other papers (not related to this thesis)

1. Hirokazu Kobayashi, Yukiyasu Yamakoshi, Yuto Hosaka, Mizuho Yabushita, and Atsushi Fukuoka, "Production of sugar alcohols from real biomass by supported platinum catalyst" *Catalysis Today*, 2014, **226**, 204–209.
2. Ying Shi, Yuta Nabae, Teruaki Hayakawa, Hirokazu Kobayashi, Mizuho Yabushita, Atsushi Fukuoka, and Masa-aki Kakimoto, "Synthesis and characterization of hyperbranched aromatic poly(etherketone)s functionalized with carboxylic acid terminal groups" *Polymer Journal*, 2014, **46**, 722–727.

3. International conferences (related to this thesis)

3.1. As a presenter

1. Mizuho Yabushita, Hirokazu Kobayashi, Kenji Hara, and Atsushi Fukuoka, "Catalytic Conversion of Cellulose into Renewable Chemicals" *The 3rd Hokkaido University Sustainability Weeks Research Poster Contest*, Poster, 3-11, October 26, 2011, Sapporo, Japan.
2. Mizuho Yabushita, Hirokazu Kobayashi, Kenji Hara, and Atsushi Fukuoka, "Catalytic Conversion of Cellulose into Glucose by Carbon" *15th International Congress on Catalysis 2012*, Poster, 1.07_7400, July 3, 2012, Munich, Germany.
3. Mizuho Yabushita, Hirokazu Kobayashi, Kenji Hara, and Atsushi Fukuoka, "Highly-Effective Hydrolysis of Cellulose by Carbon-Based Catalysis" *The 2nd International Conference on MEXT Project of Integrated Research on Chemical Synthesis "Molecular Functions in Complex Systems,"* Poster, P34, December 10, 2012, Nagoya, Japan.
4. Mizuho Yabushita, Hirokazu Kobayashi, Kenji Hara, and Atsushi Fukuoka, "Catalysis of Alkali-Activated Carbons in Hydrolysis of Cellulose" *The Sixteenth International Symposium on Relations between Homogeneous and Heterogeneous Catalysis*, Poster, 1P-42, August 5, 2013, Sapporo, Japan.
5. Mizuho Yabushita, Hirokazu Kobayashi, Kenji Hara, and Atsushi Fukuoka, "Hydrolysis of Cellulose Catalyzed by Alkali-Activated Carbons" *XIth European Congress on Catalysis*, Oral, S6-T6-OR-03, September 4, 2013, Lyon, France.
6. Mizuho Yabushita, Hirokazu Kobayashi, and Atsushi Fukuoka, "Selective Production of Oligosaccharides and Glucose from Cellulose by Carbon-Based Catalysts" *2nd International Congress on Catalysis for Biorefineries*, Poster, PA-15, September 24, 2013, Dalian, China, *Chinese Journal of Catalysis Best Poster Award*.
7. Mizuho Yabushita, Hirokazu Kobayashi, Kenji Hara, and Atsushi Fukuoka, "Catalysis of Oxygenated Functional Groups on Carbons for Cellulose Hydrolysis" *Frontier Chemistry Center International Symposium 2013 "Advanced Materials Science,"* Poster, P-13, December 9, 2013, Sapporo, Japan.

8. Mizuho Yabushita, Hirokazu Kobayashi, Jun-ya Hasegawa, Kenji Hara, and Atsushi Fukuoka, "Adsorption of cellulosic molecules onto carbons with positive entropy change" *International Symposium on Catalysis for Renewable Chemicals, TOCAT7 Pre-symposium*, Poster, P04, May 30, 2014, Shari, Japan.
9. Mizuho Yabushita, Hirokazu Kobayashi, Jun-ya Hasegawa, Kenji Hara, and Atsushi Fukuoka, "Entropically-Favored Adsorption of Cellulosic Molecules onto Carbon Materials by Hydrophobic Functionalities" *The Seventh Tokyo Conference on Advanced Catalytic Science and Technology*, Poster, GP2018, June 3, 2014, Kyoto, Japan.
10. Mizuho Yabushita, Hirokazu Kobayashi, Jun-ya Hasegawa, Kenji Hara, and Atsushi Fukuoka, "Adsorption of β-glucans onto carbon materials driven by hydrophobic functionalities" *France-Japan IAL International Workshop CAT&P4Bio*, Oral, 11, June 7, 2014, Kyoto, Japan.
11. Mizuho Yabushita, Hirokazu Kobayashi, Jun-ya Hasegawa, Kenji Hara, and Atsushi Fukuoka, "Adsorption mechanism of cellulosic molecules on carbons" *The 3rd Frontier Chemistry Center International Symposium "Challenges at the Frontier of Chemistry Sciences,"* Poster, P-15, June 13, 2014, Sapporo, Japan.
12. Mizuho Yabushita, Hirokazu Kobayashi, Jun-ya Hasegawa, Kenji Hara, and Atsushi Fukuoka, "Adsorption of cellulosic molecules on carbon materials driven by their hydrophobicity" *248th ACS National Meeting & Exposition*, Poster, 177, August 12, 2014, San Francisco, USA.

3.2. As a co-author

1. Hirokazu Kobayashi, Mizuho Yabushita, Kenji Hara, and Atsushi Fukuoka, "Hydrolysis of cellulose to glucose by carbon catalysts" *CRC International Symposium on Green & Sustainable Catalysis: From Theoretical and Fundamental Aspects to Catalyst Design*, Poster, P-4, January 26, 2012, Sapporo, Japan.
2. Hirokazu Kobayashi, Tasuku Komanoya, Mizuho Yabushita, Kenji Hara, and Atsushi Fukuoka, "Hydrolysis of cellulose to glucose by solid catalysts" *CAT4BIO International Conference on "Advances in Catalysis for Biomass Valorization,"* Poster, P07, July 9, 2012, Thessaloniki, Greece.

3. Atsushi Fukuoka, Hirokazu Kobayashi, and Mizuho Yabushita, "Conversion of Cellulose into Platform Chemicals by Heterogeneous Catalysis" *7th International Symposium on Acid-Base Catalysis*, Oral, OB-18, May 15, 2013, Tokyo, Japan.
4. Hirokazu Kobayashi, Mizuho Yabushita, Shogo Ito, and Atsushi Fukuoka, "Selective synthesis of sorbitan from sorbitol over sulfonated zirconia catalyst" *2nd International Congress on Catalysis for Biorefineries*, Poster, PB-19, September 24, 2013, Dalian, China.
5. Haruka Yokoyama, Mizuho Yabushita, Hirokazu Kobayashi, Shogo Ito, Kenji Hara, and Atsushi Fukuoka, "Dehydration of sorbitol to 1,4-sorbitan controlled by selective adsorption on sulfated zirconia catalyst" *International Symposium on Catalysis for Renewable Chemicals, TOCAT7 Pre-symposium*, Poster, P06, May 30, 2014, Shari, Japan.
6. Hirokazu Kobayashi, Shogo Ito, Mizuho Yabushita, Kenji Hara, and Atsushi Fukuoka, "Catalytic Conversion of Sorbitol to Sorbitan by Means of Preferencial Adsorption" *The Seventh Tokyo Conference on Advanced Catalytic Science and Technology*, Poster, GP2020, June 3, 2014, Kyoto, Japan.
7. Hirokazu Kobayashi, Mizuho Yabushita, Shogo Ito, Kenji Hara, and Atsushi Fukuoka, "Adsorption-controlled conversion of sorbitol to 1,4-sorbitan over sulfated zirconia" *248th ACS National Meeting & Exposition*, Poster, 179, August 12, 2014, San Francisco, USA.

4. International conferences (not related to this thesis, as a co-author)

1. Hiroyuki Kaiki, Mizuho Yabushita, Hirokazu Kobayashi, Kenji Hara, and Atsushi Fukuoka, "Hydrolysis of cellulose by oxygenated carbon catalysts" *The Sixteenth International Symposium on Relations between Homogeneous and Heterogeneous Catalysis*, Poster, 2P-25, August 6, 2013, Sapporo, Japan.
2. Hiroyuki Kaiki, Mizuho Yabushita, Hirokazu Kobayashi, and Atsushi Fukuoka, "Preparation and characterization of air-oxidized carbon for cellulose hydrolysis" *The 4th International Conference on MEXT Project of Integrated Research on Chemical Synthesis "Synthetic Approaches to New Chemical Functions,"* Poster, P-47, July 10, 2014, Kyoto, Japan.

3. Hiroyuki Kaiki, Kota Techikawara, Mizuho Yabushita, Hirokazu Kobayashi, Kenji Hara, and Atsushi Fukuoka, "Simple preparation method of highly active carbon catalysts for cellulose hydrolysis" *The 1st International Symposium on Catalytic Science and Technology in Sustainable Energy and Environment*, Poster, P144, October 8, 2014, Tianjin, China.
4. Haruka Yokoyama, Bo Feng, Hirokazu Kobayashi, Mizuho Yabushita, Kenji Hara, and Atsushi Fukuoka, "Dehydration of sorbitol over solid catalysts" *CRC International Symposium Novel Photocatalysts for Environmental Purification and Energy Generation*, Poster, 22, October 14, 2014, Sapporo, Japan.

5. Awards

1. Nitobe Prize in Hokkaido University, June 11, 2008.
2. Best Presentation Award in Annual Winter Meeting 2011 of Chemical Society of Japan in Hokkaido Branch, February 2, 2011.
3. Clark Prize in Hokkaido University, March 24, 2011.
4. Best Poster Award in 51th Aurora Seminar, July 25, 2011.
5. Best Poster Award in 111th Annual Meeting of Catalysis Society of Japan, March 26, 2013.
6. Chinese Journal of Catalysis Best Poster Award in 2nd International Congress on Catalysis for Biorefineries, September 25, 2013.

Acknowledgements

This work "A Study on Catalytic Conversion of Non-Food Biomass into Chemicals," supervised by Prof. Atsushi Fukuoka (Catalysis Research Center and Graduate School of Chemical Sciences and Engineering, Hokkaido University) has been conducted from April 2010 to March 2015.

First of all, I would like to show my greatest appreciation to Prof. Atsushi Fukuoka. His wide knowledge, invaluable suggestions, and warm encouragements support and motivate me at any time.

I owe my deep gratitude to all the collaborators: Mr. Makoto Saito, Mr. Ichiro Fujita, and Mr. Tadashi Yoneda (Showa Denko K.K.) for supplying alkali-activated carbons and bagasse kraft pulp, Prof. Jun-ya Hasegawa (Hokkaido University) for DFT calculations, Dr. Yukiyasu Yamakoshi (Hokkaido Research Organization Industrial Research Institute) for LC/MS, Prof. Wataru Ueda and Mr. Satoshi Ishikawa (Hokkaido University) for micropore measurements, Dr. Yasuhito Koyama (Hokkaido University) for discussion of NMR assignments, Prof. Alexander Katz and Dr. Po-Wen Chung (University of California, Berkeley) for discussion of adsorption processes in depth, Prof. Takashi Kyotani and Dr. Hirotomo Nishihara (Tohoku University) for synthesizing ZTC, Prof. Masa-aki Kakimoto and Dr. Yuta Nabae (Tokyo Institute of Technology) for preparing functionalized polymer, and Mr. Katsuhisa Ishikawa, Mr. Takahiko Hasegawa, and Mr. Tetsuzo Habu (Hokkaido University) for making up quartz-glass instruments.

For reviewing this work, Prof. Kazuki Sada, Prof. Koichiro Ishimori, Prof. Keiji Tanino, Prof. Takao Masuda, Dr. Kenji Hara, Prof. Tetsuya Taketsugu, Prof. Kei Murakoshi, Prof. Noboru Kitamura, Prof. Jun-ya Hasegawa, Prof. Masako Kato, Prof. Tamotsu Inabe, Prof. Sadamu Takeda, Prof. Kuniharu Ijiro, Prof. Yukio Hinatsu, and Prof. Junji Nishii (Hokkaido University) have given me constructive comments and suggestions.

I gratefully appreciate Dr. Kenji Hara and Dr. Hirokazu Kobayashi (Hokkaido University) for giving me a lot of enormous advices and technical helps. I also thank the previous and current members of Fukuoka's Laboratory for helps and assistances, especially Dr. Hidetoshi Ohta (Ehime University), Dr. Tasuku Komanoya (Tokyo Institute of Technology), and Dr. Abhijit Shrotri for significant discussions, and Mr. Shogo Ito (Shin-Etsu Chemical Co., Ltd.) and Mr. Kyoichi Kuroki for contributing to this work.

I would like to acknowledge my friends, Mr. Hiroyoshi Fujii, Mr. Ippei Fujisawa, Mr. Naoki Iyo, Mr. Masaru Iwakura, Mr. Tatsuya Matsunaga, Mr. Shunjiro Nagata, and Ms. Yukari Sekine who encourage each other friendly rivalry. Additionally, I am grateful to Ms. Nana Mizuki, my favorite voice actress and singer, who always cheers me up in difficult times by her wonderful, dynamic, and emotional songs.

I have received a generous support from Japan Society for the Promotion of Science (JSPS) Research Fellowship DC2 since April 2014. This work was financially supported by a Grant-in-Aid for Scientific Research (KAKENHI, 20226016), a Grant-in-Aid for Young Scientists (B) (KAKENHI, 23760734), a Grant-in-Aid for Young Scientists (A) (KAKENHI, 26709060), and a Grant-in-Aid for JSPS Fellows by JSPS, and the Japan Science and Technology Agency "Advanced Low Carbon Technology Research and Development Program" (JST-ALCA).

Finally, I would like to express my cordial appreciation to my dear family, Mr. Hiromi Yabushita, Ms. Nanae Yabushita, and Ms. Natsuki Yabushita. They have mentally supported me a lot, and there is no doubt that I have spent unforgettable times and had invaluable experiences in Hokkaido University for eight years owing to their warm encouragements and helps.

Graduate School of Chemical Sciences and Engineering, Hokkaido University
February 27, 2015

Mizuho Yabushita